Declaration

This thesis embodies 3.5 years of my life. It was composed by myself and the work contained herein is my own, and where chapters are published or submitted the authorship and contributions are noted appropriately. This thesis has not been submitted for any other degree or professional qualification.

Stewart S. R. Jamieson

Acknowledgements

Thanks to:

Nick Hulton, Hugh Sinclair, David Sugden, Erin McClymont, Magnus Hagdorn, Iain and Wendy Jamieson, Arjen Stroeven, Darrel Swift, Felix Hebeler, Jon Harbor, Jens-Ove Näslund, Andy Mackintosh, Peter Barrett, Alan Cooper, Anthony Newton, Kerry-Anne Mairs, Ross Purves, Martin Siegert, Andy Wright, Andy Shepherd, Pete Nienow, Tony Payne, Ian Rutt, Patience Cowie, Linda Kirstein, Chris Place, Steve Dowers, Alun Hubbard, Jorge Rabassa, Mike Kaplan, Christina Tsimi, Gus Wares, and all those from the School of GeoSciences, visitors to the Hutton Club and people from further afield too numerous to mention despite deserving thanks.

This work was funded by the Natural Environmental Research Council (NERC) UK, The Quaternary Research Association, The Royal Scottish Geographical Society and the Carnegie Trust for the Universities of Scotland.

"Reason not withstanding, the Universe continues unabated. Its history is terribly long and awfully difficult to understand, even in its simpler moments which are roughly speaking, the beginning and the end."

Douglas Adams.

Modelling Landscape Evolution Under Ice Sheets

Contents

List of Figures

List of Tables

Abstract

This thesis details the application of numerical modelling techniques to simulate erosion under ice sheets with the aim of better understanding the interrelationships between glacial erosion, long-term landscape evolution and ice dynamics. A model is developed that predicts patterns of basal erosion in a glaciologically sensible manner and shows that 'fluvial' landscapes can become 'glacial' systems within 100 kyrs. By simulating ice sheet growth and erosion over synthetic landscapes of varying form, amplitude and wavelength the topographic characteristics that are most critical to the evolution of ice dynamics, and to ongoing erosion are identified. The model is applied to the solution of two puzzles regarding the interaction of ice, erosion and landscape in Patagonia and Antarctica. In settings similar to Patagonia, glacial erosion is shown to be able to drive large-scale change in ice dynamics on 10^5 to 10^6 year timescales. This goes some way to explaining the behaviour of the Patagonian ice sheet since the 'Greatest Patagonian Glaciation', whereby ice extents reduce over successive glacial cycles, contradicting patterns of global ice volume. In Antarctica, the model is used to predict the pattern of long-term ice mass expansion and associated patterns of landscape evolution. For the first time, predictions tied to ice dynamics are made regarding the degree to which the Antarctic landscape has been modified by ice as it expands from local to regional ice centres and then to a continental scale ice sheet. Common themes throughout this thesis are that pre-glacial landscape geometry is a critical driver of the pattern of landscape evolution under ice, and that erosion should no longer be considered a passive component of any glacial system over timescales of 10^5 and greater.

Chapter 1 Introduction

1.1 Aim

The aim of this project is to investigate feedbacks between glacial erosion, long-term landscape evolution and ice sheet dynamics. The distribution of glacial erosion reflects the thermodynamics of an overlying ice mass as it interacts with the glacier bed. For example, warm-based, fast flowing ice can excavate deep glacial troughs, whereas areas of cold-based ice may be frozen to the bed, protecting the landscape from any significant modification. Conversely the results of this erosion - the generation of deeper, wider and more efficient ice pathways - dictates ice temperature and flow regimes. The process of glacial erosion has historically been downplayed in the context of understanding ice mass behaviour. Although geomorphology is often used to make inferences about ice dynamics, the step to determining how, on a large scale, these landscapes have themselves dictated glacier behaviour is rarely taken. Numerical models of ice sheets, glacial erosion and tectonic and hillslope processes provide the tools with which to make this step.

1.2 Rationale

Over 160 years of effort has been directed towards explaining spatial patterns of landscape evolution under ice in relation to ice sheet expansion (Agassiz, 1840; Forbes, 1843). In his Presidential address to the Geological Society, Charles Lyell (1850), when talking on the nature of glacial modification of the landscape noted that:

> *"Ignorant of glaciers and icebergs, and perhaps of ice and snow,--unable to comprehend the nature of that mysterious power which had polished the surface of rocks over wide areas, or had engraved upon them long rectilinear and parallel furrows, we should have gazed upon these markings... in stupid amazement and with feelings of despair."*

By the time of this address, small and large-scale evidence for the 'glacial hypothesis' was widespread in Scandinavia, North America, and Europe. Since the mid 19th century geologists and geomorphologists have sought to understand how ice masses modify the landscape. After all this time, interest in glacial landscape evolution continues - our comprehension of its nature still incomplete.

The motivation for this study is provided by the fact that although glacial erosion is known to affect the dynamics of glaciers over long timescales (Harbor, 1992; Kerr, 1993; MacGregor et al., 2000; Oerlemans, 1984), this important process is often neglected in interpretations of ice mass behaviour because it is often considered as passive.

Studies of ice mass behaviour are invariably hampered by the fact that that they evolve slowly, particularly in the case of ice sheets. Our understanding of their behaviour comes from a number of sources and the weight of this evidence is somewhat biased towards the northern hemisphere. Geological information records indicators pertinent to glacial behaviour including details of ice mass fluctuations (e.g. Clapperton and Sugden, 1988; Denton and Hughes, 2002), sea-level change (e.g. Denton and Hughes, 1986; Hagdorn, 2003), climate variability (e.g. DeConto and Pollard, 2003b; Raymo et al., 2006; Vimeux et al., 2002; Zachos et al., 2001) and glacial dynamics (e.g. Boulton and Clark, 1990; Roberts and Long, 2005; Stokes and Clark, 2001) and such information is often tied into a chronological framework. More recently, computers have enabled the development of numerical models consisting of generalised physical rules relating to the behaviour of ice, that can be used to simulate the growth and decay of glaciers and ice sheets over geological timescales (e.g. Hulton et al., 2002; Huybrechts, 1993; Oerlemans, 1982; Payne et al., 1989). Such models are often calibrated using available geological, and in particular, geomorphological information and have enabled a greater understanding of the controls (primarily of climatic controls) on ice sheet evolution to be reached. Models of glacial erosion have also been developed to investigate various aspects of landscape development (Anderson et al., 2006; Braun et al., 1999; Harbor, 1992; Harbor, 1995; Harbor et al., 1988; MacGregor et al., 2000; Oerlemans, 1984; Tomkin, 2003). However, the linkages between glacial erosion and the response of ice masses to self-inflicted bedrock evolution have rarely been investigated. Such an

investigation would therefore be of great value in enhancing knowledge of glacial dynamics and in advancing our ability to predict past, present and future glacial behaviour.

Furthermore, for the long-term landscape evolution and geomorphological communities, the ability to model and predict erosion under different glacial conditions will be valuable, not least because it has the potential to elucidate the degree to which an existing or palaeo-landscape has been subjected to erosion. Such a quest, for example, has been the focus of scientists with regard to the past 34 million years of landscape evolution over much of ice-covered Antarctica.

1.3 Objectives

Our current state of knowledge with regard to ice dynamics, glacial erosion and glacial geomorphology motivates us to ask the following broad questions:

- How can we determine spatial and temporal patterns of erosion under ice?
- How are ice thermodynamics affected by erosion, and vice versa?
- How effective are ice sheets as agents of landscape modification?

With this in mind, the objectives of this project are outlined below (along with the corresponding chapter of the thesis):

1. To generate ice sheet models that can predict the pattern of basal sliding in a realistic manner and to couple this to an erosion model (Chapter 2). This model will enable the investigation of the interactions between ice dynamics, glacial erosion and long-term landscape evolution. It will also provide a tool with which to predict past, present and future spatial and temporal patterns of erosion on a large scale.

2. To determine how glacial dynamics are controlled by landscape form and how this drives patterns of glacial erosion through time (Chapter 3).
3. To model the effect of erosion on ice dynamics and ice margin behaviour over 10^5 - 10^6 year timescales and to link this to conditions thought to have been experienced in Patagonia over the last 1.15 Myrs (Chapter 4).
4. To predict for the first time the pattern of long-term landscape evolution across Antarctica as ice expanded from local to continental coverage over the past 34 Myrs (Chapter 5).

1.4 Context

Before introducing the 4 specific research papers that make up this thesis, this introductory chapter will provide an outline regarding the nature of ice, erosion and modelling and the context of this research before introducing the approach used to meet the above objectives.

1.4.1 The Movement of Ice

Glaciers are essentially natural machines for transporting ice. Ice moves in three ways: 1) ice flow (creep) whereby ice deforms plastically under stress; 2) sliding (basal décollement) whereby the base of the ice mass decouples from the bed due to the presence of water; and 3) sliding can also occur or be enhanced through the deformation of the basal sediment column (Boulton, 1996a; Boulton, 1996b). Figure 1.1 illustrates the distribution of these different forms of motion throughout the ice column. This thesis will deal solely with sliding at the interface of ice and bedrock, and therefore will not treat movement by basal sediment deformation.

The aim of this thesis is to determine the role of bedrock erosion in altering the behaviour of ice sheets. The implication of not including deformable basal sediment is that erosion rates may be underestimated in some areas where such material would easily be removed. Conversely, deposition of sediment may also reduce overall rates of erosion. This is likely to effect the dynamic behaviour of the ice both in relation to

the basal traction conditions (e.g. how slippy the bed/ice interface can be) and in relation to evolving topographic states (e.g. the filling of valley floors). Furthermore, the presence of sediment at the bed will allow water to be evacuated more easily, altering the sliding behaviour of the ice. However, the impact of not including deformable sediments is not currently quantifiable. This thesis therefore ignores the contribution of deformable sediment in the experimental design, and concentrates on determining the contribution of hard bed erosion upon ice mass behaviour. However, because its importance to long-term ice mass behaviour is clear, the impacts of the assumption that no sediment column exists are considered in the concluding chapter and in the context of future work.

Ice thickness is a critical control of both creep and basal décollement because thicker ice means that steep ice surface slopes can occur. This forces driving stresses, the main control upon ice flow, to increase. Topography therefore also has a critical role to play because although the surface of an ice sheet may be relatively flat on a large scale, the variation of the basal surface means that there will be significant changes in ice thickness over space. Thicker ice also means that basal ice is more likely to reach pressure melting point, leading to the lubrication of the ice/bed interface and to decoupling. Thinner ice, conversely, can protect the subglacial topography because the ice remains cold-based. Basal ice temperature is therefore intimately linked to the occurrence of sliding (Paterson, 1994), and thus to the pattern of glacial erosion.

The temperature throughout the ice body is critical to the behaviour of the ice under stress, and therefore to the flow dynamics of ice (Glen, 1955). Cold ice is harder to deform for a given stress and therefore flows slowly whereas warm ice can deform more easily and thus is more likely to flow quickly. Furthermore, where ice flows more rapidly there is a thermal feedback whereby friction within the ice enhances the ice temperature causing the fast flow to be reinforced (Clarke, 1977; Payne and Dongelmans, 1997). This also affects the stability of ice streams (Payne and Baldwin, 2000), and therefore the amount of sliding and erosion that occurs. This is because faster flow generates heat, and thus increases the likelihood of the basal ice reaching pressure melting point.

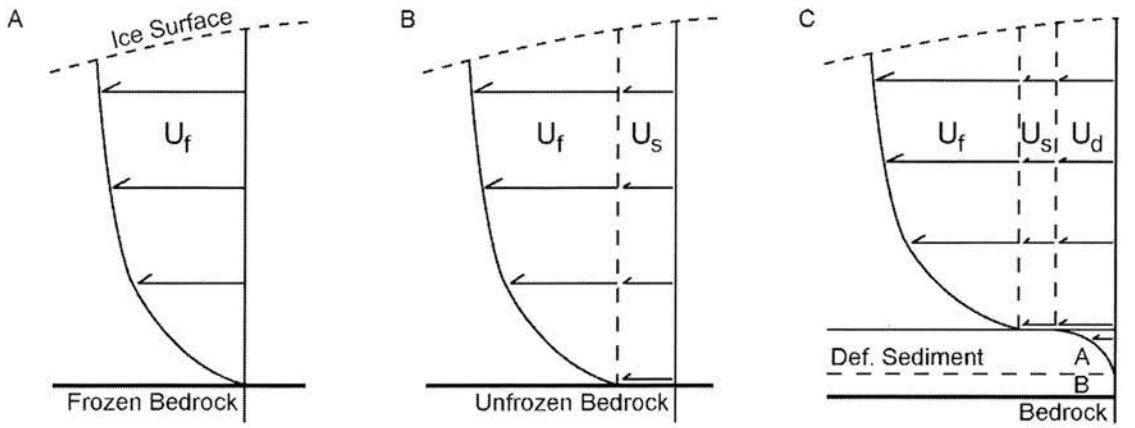

Figure 1.1: Components of ice motion

A shows the component of internal flow (Uf) generated in an ice mass that rests on a frozen bed. B illustrates the additional component of movement generated by sliding over bedrock (Us) where the basal ice is at pressure melting point. C shows that where present, deformable sediment enables an additional component of horizontal ice velocity (Ud). The occurrence of U_s is therefore the component that determines whether erosion of bedrock occurs, but the occurrence of U_f and the thermal feedbacks generated by U_f are critical in determining the pattern of U_s. After (Boulton, 1996b).

In the context of the aims of this thesis, modelling both flow and sliding are critical to determining patterns of erosion because although sliding generates the actual erosion, we need to be able to realistically model ice dynamics, and in particular the full thermal field of the ice mass, in order to determine both the pattern of erosion and the response of ice to the ongoing glacial erosion.

1.4.2 Basal Thermal Regime

Efficient glacier motion is promoted by ice that is at or near to melting point. Sliding at the bed (and thus erosion) is therefore highly sensitive to temperature at the base of the ice column. The most important factors controlling basal ice temperature are outlined here.

The temperature of ice at the surface is a function of the climate whereby heat is exchanged via conduction. Thus variations in air temperature during winter can cause a cold wave to push downwards through the upper portions of the ice column

(Paterson, 1994). Heat is also input directly at the bed via geothermal heat flux, causing warming upwards through the ice column and which may warm or melt the basal ice to allow sliding (Näslund et al., 2005; Paterson, 1994). Geothermal heat flux is generated by decaying radioactive isotopes and varies in relation to the tectonic setting of the subglacial crust. Near the glacier bed, frictional heat generated by internal shear of ice and by friction between the bed and basal ice can contribute heat on a similar scale to geothermal heat flux (Sugden and John, 1976). This heat is conducted upwards through the ice column, enhancing flow and the potential for basal melting. Ice thickness is also a strong control upon basal ice temperature because ice warms with increased overburden pressure.

The net result of the balance between the above factors is that in general, with greater depth, ice temperature profiles increase to the extent that even in polar ice masses the base can reach pressure melting point (Benn and Evans, 1998). This is bourne out by measurements in Antarctica at for example, Ice Stream B (Engelhardt et al., 1990), Law Dome (Budd et al., 1976), Byrd Station (Gow et al., 1968) and probably Vostok (Paterson, 1994).

The tendency for heat to be generated under thick ice and in zones of friction means that melting is more likely to occur where bedrock depressions are present. The consequence of this is that where fast flowing ice is generated, advection of heat can reinforce the warm basal ice temperatures as heat is transferred via flowing and deforming ice. Heat transfer by advection is very efficient in comparison to conduction (Robin, 1955) and its importance to the basal thermal regime is particularly enhanced where topography causes ice to converge, enabling higher basal ice temperatures to be generated and thus increasing the probability of the occurrence of basal melting. Higher basal temperatures will drive the deformability of basal ice up, enhancing flow. In addition, the work done in deforming the ice will generate a further heat input resulting in the reinforcement of a warm thermal regime (Paterson, 1994).

The ability of ice to reach melting point can be retarded by the depression of the melting point by charactistics such as impurities in liquid inclusions which increase the effective specific heat capacity of ice. The complex interactions between air

temperature, geothermal heat flux, ice thickness, basal topographic form and the composition of ice which all drive ice flow and sliding patterns mean that basal ice conditions are affected by past conditions and are rarely in steady state (Paterson, 1994).

1.4.3 Ice Sheet Mass Balance

The mass balance of an ice sheet is determined by the net amount of mass input (mainly through snowfall) vs. the amount of mass loss through ablation. The distribution of these changes provide information on the health and dynamics of an ice sheet but more importantly reflect the connection between the ice mass and climate. Fluctuations in climate result in variations in snowfall and in melting, which when translated through the length of the glacier will result in the expansion or contraction of an ice mass (Paterson, 1994). The elevation on the glacier or ice sheet where the net mass input is equal to the net mass loss is known as the equilibrium line altitude (ELA) which, as we will show, is coincident with the zone of maximum mass throughput and therefore is strongly linked to the zone of maximum erosion.

Air temperature decreases with increasing elevation according to the local atmospheric lapse rate. Elevated topography is therefore critical in the establishment of an ice mass (Oerlemans, 2002). Thereafter, as an ice mass expands and its surface elevation increases, more of its area will be in the accumulation zone. This can force the expansion of an ice sheet until other mechanisms can counter the growth by mass loss. Calving at marine margins is one such mechanism for losing mass rapidly in the ablation zone. As we will show (Chapter 4), changing topographic form near the margins of the ice may also provide such a mechanism.

As ice sheets grow, the zones of greatest precipitation tend to lie nearer to the ice margins because as moisture is transported from its source (oceans) and begins to travel across ice, it cools and falls. The air temperature determines whether this precipitation falls as snow, adding to the mass of the ice sheet. However, by the time they travel to the centre of an ice sheet, atmospheric currents become depleted of moisture meaning that the interior of ice masses, as noted in Antarctica at the present day, generally experience very low accumulation rates (Vaughan et al., 1999).

1.4.4 The Oscillation of Ice Masses

Ice sheets have existed repeatedly in the northern hemisphere over North America (Laurentide), Scandinavia (Fennoscandia), Greenland, Iceland and the UK. The Greenland and Icelandic ice sheets still remain at the present day. However, in the southern hemisphere, significant ice sheet growth has occurred only over Antarctica and Southern South America (Patagonia). The longevity of the Antarctic ice sheets has been debated (Sugden, 1996), but it is likely that it has been present on a continental scale since at least 15 Ma, and on a smaller scale since 34 Ma. The evolution of the Patagonian Ice Sheet is strongly linked to the state of Antarctic ice and the development of circumpolar oceanic currents, and indeed the influence of the Antarctic Ice Sheet upon climate, oceanic and atmospheric currents and sea level is global.

Only limited comprehension of how individual ice sheets oscillate over long timescales can be gained from contemporary observations of present day ice masses. Fortunately, as has long been recognised (e.g. Agassiz, 1840; Forbes, 1843), patterns of long-term ice mass fluctuations are recorded in the landscape as local and regional-scale geological and geomorphological features. Such information as ice sheet extents, timing and dynamics (e.g. Boulton, 1982; Boulton et al., 1985; Mercer, 1976; Sugden, 1978b), as well as glacio-eustatic (e.g. Fairbanks, 1989) and glacio-isostatic (e.g. Sissons, 1976) sea level change can be extracted through the interrogation of the landscapes of formerly and currently glaciated regions. Climatic information can also be extracted in relation to glacial behaviour although, as noted above, there are complications regarding the interaction of ice sheets and glacial erosion that may impact upon the interpretation of any climatic signal.

Long-term variations in the Earth's orbit are known to be the fundamental pacemaker for ice expansion and contraction (Croll, 1867; Hays et al., 1976; Imbrie et al., 1992; Milankovitch, 1941) and occur on three distinct timescales. Eccentricity (400 kyrs and 100 kyrs), obliquity (41 kyrs) and precession (19-23 kyrs) describe respectively: the Earth's orbital deviation from a circular orbit; variations between the Earth's axis of rotation and the plane of the ecliptic; and the Earth's rotation about the poles

(Figure 1.2). Figure 1.3 shows the record of Pleistocene glacial intensity and illustrates the dominance of these cycles in forcing the timings of glacial periods.

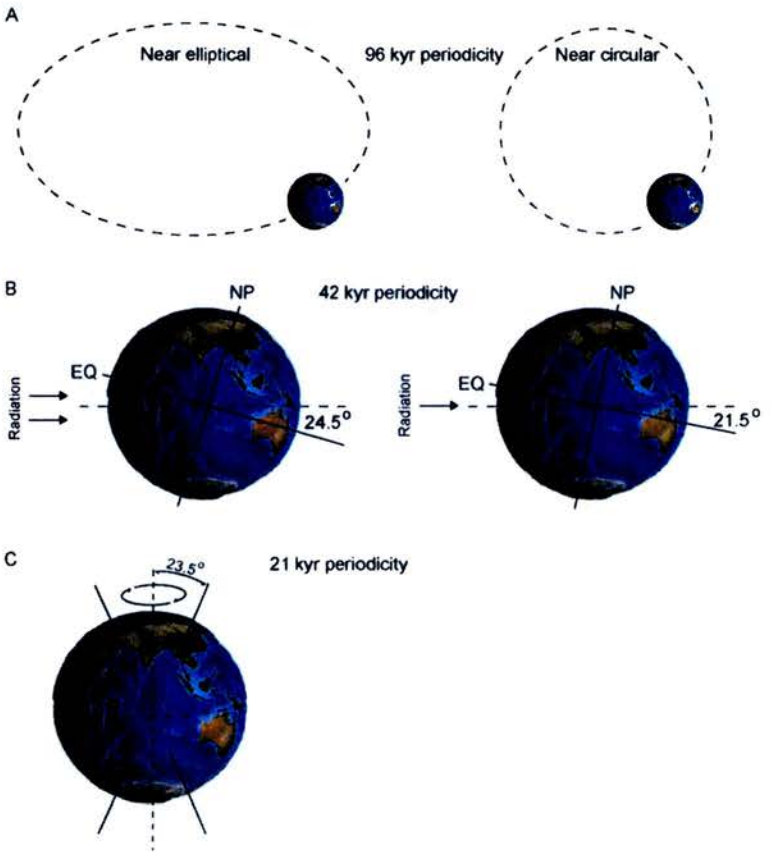

Figure 1.2: Variations in the Earth's orbit

The mode and periodicity of the 3 main components of variation in the Earth's orbit around the sun are shown. A) Eccentricity – the shape of the orbit changes due to gravitational influences. B) Obliquity – the tilt of the Earth's axis changes. C) Precession – the gravitational pull of the sun and the moon cause the Earth to 'wobble' like a spinning top. NP = North Pole, EQ = Equator.

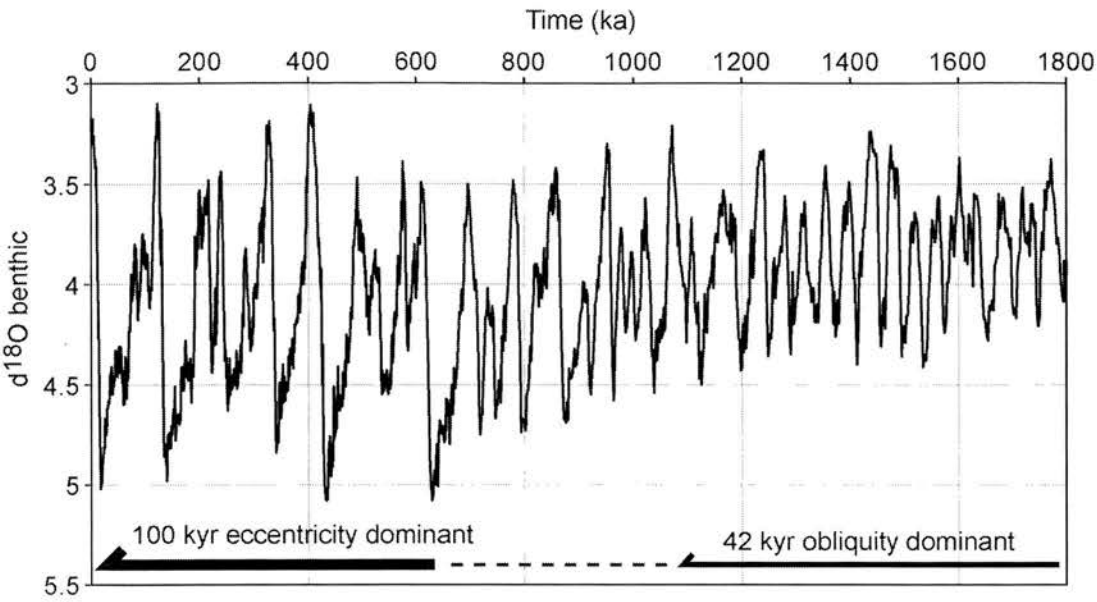

Figure 1.3: Pleistocene glacial intensity

Fluctuations in the fractionation of oxygen 18 and oxygen 16 are recorded in sea floor sediments. This benthic $\delta^{18}O$ stack (Lisiecki and Raymo, 2005) is a proxy for the intensity of glaciation over the past 1.8 Myrs. Note the shift between the dominance of the 42 kyr obliquity signal and the 100 kyr eccentricity cycles. The dotted line denotes the approximate period of transition between the two (Clark et al., 2006; McClymont and Rosell-Melé, 2005).

The Pleistocene climate is characterised by a change in the dominant orbital parameter that forces ice sheet variability from 41 kyrs, to 100 kyrs (Figure 1.3). This change is known as the Mid Pleistocence Transition (MPT). The reasons for this change are still debated, but it is thought that it began around 1.15 million years ago (Clark et al., 2006; McClymont and Rosell-Melé, 2005), and by ca. 600 ka the ice sheets were fluctuating with a cyclicity of 100 kyrs. This is concomitant with an expansion of the Scandinavian Ice Sheet in to the North Sea (Sejrup et al., 2000), and of the maximum ice extent in Patagonia – the Greatest Patagonian Glaciation (GPG - Caldenius, 1932; Singer et al., 2004). Furthermore, the Vostok (e.g. Petit et al., 1999) and EPICA Dome C (Augustin et al., 2004) ice cores and the records from the Southern Atlantic (Becquey and Gersonde, 2003) show that glacial periods have been getting colder over at least the last 440 kyrs.

There is much evidence for inter-hemispheric synchronicity in climate, and glacial chronologies in the Patagonian Andes have indeed been found to be symmetrical

with northern hemisphere chronologies (Denton et al., 1999). However, in Patagonia, although glaciations are temporally concurrent with those in the northern hemisphere, the GPG is known to precede maximum northern hemisphere ice expansion by tens of thousands of years (Mercer, 1976; Singer et al., 2004). To confuse the matter, although larger by ice volume, the 100 kyr northern hemisphere ice-sheets are less spatially extensive than their pre-MPT 41 kyr counterparts (Clark and Pollard, 1998). The linkages and feedbacks between ice-sheets in both hemispheres and between ice-sheets and climate are therefore complex. Over timescales longer than the Pleistocene, these linkages become even more difficult to determine, indicating the substantial challenges associated with unravelling the story of long-term glaciological and geomorphological evolution in regions that have undergone millions of years of glaciation e.g. 34 Myrs of Antarctic glacial history.

1.4.5 Potential Mechanisms Controlling Ice Mass Behaviour

Although the timing of ice mass expansion is most strongly determined in the long-term by orbital variations, a number of other factors, including erosion, exert control over glacial fluctuations. For example, the oceans are a major factor in controlling the behaviour of ice masses. Sea level change has been responsible for driving much of the fluctuation in the Antarctic ice sheets over the past ~14 Myrs (Denton and Hughes, 1986) and the impact of sea level changes upon the present day Greenland and West Antarctic ice sheets is an issue currently attracting a great deal of attention (Dietrich et al., 2007; Pritchard and Vaughan, 2007; Rignot et al., 2004). Changes occur at the marine margin, but the influences may be felt at considerable distances from the ice front (Alley, 1984). Furthermore, changes in large-scale oceanic circulation drive long-term change in the cryosphere. The closing of the Panama seaway for example is thought to have stopped the mixing of Atlantic and Pacific waters, contributing to increased precipitation in the northern hemisphere, thus leading (at least in part) to intensified glaciations (Klocker et al., 2005; Lunt et al., 2008).

Atmospheric circulation changes also dictate the pattern of ice sheet evolution. Antarctic ice expansion over the past 550 kyrs is known to drive northward migration

of the Antarctic Circumpolar Current (by up to 7°) in the Atlantic region (Becquey and Gersonde, 2003). In the southern Andes of Patagonia this northward migration of the Antarctic Polar Front may have caused intensification of westerly winds and may have driven a zone of enhanced precipitation northwards during the LGM (Heusser, 1989). Experiments by Sugden et al. (2002) suggested that precipitation would increase due to advection by stronger winds and at the same time, there would be a tendency for the ice-sheet to migrate towards the precipitation source resulting in more expansive ice sheets to the south.

It is also known that ice-sheet fluctuations may themselves help to drive the global climate system. For example between 47 and 23 ka, Antarctic glaciation leads that in Greenland by 1.5-3 kyrs (Blunier and Brook, 2001; Blunier et al., 1998), potentially driving changes in oceanic and atmospheric circulation that induce glaciation elsewhere. The deuterium excess record from Vostok, Antarctica is known to be determined by its precipitation source regions adjacent to South America (Vimeux et al., 2002), and thus the glacial signals of Patagonia and Antarctica are also linked.

Carbon cycling and its impact on CO_2 and thus on global temperatures is also a critical factor. DeConto and Pollard (2003b) showed that atmospheric CO_2 (PCO_2) is a fundamentally important boundary condition for Cenozoic climate change when they studied the inception of the Antarctic ice-sheet at ca. 34 Ma. Furthermore, McClymont et al., (In Preparation) note increased burial of organic carbon on the ocean floor at ca. 1.15 Ma and hypothesise that this may have caused a lowering of PCO_2 which would contribute, or potentially drive surface cooling in the Pacific and Atlantic oceans. This may have been critical in driving the expansion of the northern hemisphere ice-sheets at ca. 900 ka.

The response of an ice-sheet to a change in mass balance is dependent on the underlying topography (Harbor, 1992; Kerr, 1993). Thus variations in the amount of area located above the snowline can drive change in ice dynamics, causing feedbacks in glacial behaviour (Clapperton, 1990; Hulton and Sugden, 1995). Consideration of mass balances in relation to topographic change show us that the two processes of tectonism and glacial erosion can both operate to drive ice mass fluctuations once ice is established. Singer et al.(2004) for example, suggest that uplift in the Patagonian

Andes after 2 Ma might have increased the ice accumulation area and thus mass balance of the Patagonian Ice Sheet. Subsequent vigorous glacial erosion may then have deepened valleys and thus systematically reduced the ice accumulation area throughout the Quaternary. In addition, topography constrains patterns of ice flow so that fast flowing ice tends to be focussed through large-scale valleys, and slower cold-based ice are found in upland plateau areas where ice is thin (Hall and Glasser, 2003; Hindmarsh, 2003; Sugden and John, 1976; Taylor et al., 2004). Scandinavia, for example, records such ice sheet behaviour, with fast flow focussed through the western fjord regions, and little basal flow occurring in the central upland plateaus (Fabel et al., 2002; Kleman et al., 2007; Stroeven et al., 2002a).

Given that topography may be a key driver of ice sheet behaviour, glacial erosion and the way it alters the landscape may also be linked to changing ice dynamics. The impact of erosion upon ice mass behaviour has long been considered as passive, and thus insignificant when compared to the larger regional- or global-scale drivers of ice sheet behaviour noted above. As this work shows over the following pages, the feedbacks between glacial erosion and ice dynamics are indeed critical in determining the behaviour of ice masses over geological timescales.

1.5 Erosion and Topography

1.5.1 Mechanisms of Glacial Erosion

We have shown that glaciers move via three processes: internal deformation, basal sediment deformation and by basal sliding. This latter mode of flow is what largely determines the pattern of erosion at the base of an ice mass. However, it is important to note that the influence of internal deformation upon the internal thermal dynamics of an ice mass will also influence whether sliding is able to occur at the bed. As indicated above, this study will investigate the feedbacks between the erosion of bedrock (i.e. not including the influence of deformable sediment dynamics) upon ice sheet dynamics. For erosion to occur it is assumed the base of the ice mass must be sliding across its bed. This most often relies upon the ice-bed interface being lubricated by the presence of water by the melting of basal ice under the pressure of

the overlying thickness of ice. Erosion is further dependent upon the balance between the shear stresses imposed by the overlying and sliding ice, and the strength of the bedrock lithology. Thus erosion will occur if the ice is sliding and if the shear stresses overcome the strength of the rock. Rock particles embedded in the base of the ice mass act as the tools with which material is removed from the bedrock surface.

Erosion is thought to happen in two principal ways (Hallet, 1979; Iverson, 1991; Sugden and John, 1976): 1) abrasion, which is the process of fine-grained material being ground over bedrock and 2) quarrying or 'plucking', whereby larger blocks of material fail under the stresses of glaciation. With regard to abrasion, there are a number of theories regarding the particular importance of different controls upon the forces generated at the ice-bed interface. These are: coulomb friction model (Boulton, 1974; Boulton, 1979), where effective normal pressure (ice overburden minus the opposite forces generated by basal water pressures) is the thought to be most important; the sandpaper friction model, which extends the Coulomb model to include the potential impact of the area of the bed occupied by water-filled cavities and; the Hallet friction model (Hallet, 1979), where friction at the bed is thought to be independent of ice thickness and water pressures. With quarrying, the tractive force generated by the moving ice acts to remove fragments of rock where the imposed forces are greater than those holding the rock in place. Essentially, abrasion is simply quarrying that occurs at a small scale whereby the fracturing processes involve large stress differences which occur at the point of contact between the abrading tool and the bedrock surface (Knight, 1999).

1.5.2 Parameterisations of Glacial Erosion

Cuffey et al., (2000) suggest that minimal erosion can occur under cold-based ice but in general the assumption is that for erosion to occur, basal ice must be at pressure melting point. There are many other factors controlling the degree of erosion experienced at the beds of ice masses, but they are not representable at the ice sheet scale. On this scale (i.e. km and larger), the specific processes of abrasion and quarrying are difficult to identify or distinguish between as they work at significantly

smaller scales. This was recognised by those working to formulate 'laws' of large-scale glacial erosion. In predicting patterns and rates of glacial erosion over large areas, the aforementioned processes are therefore often aggregated into a single bulk erosion rate (E). At such scales, it has been possible to generalise erosion into a rule which relate critical factors to E thus allowing the prediction of erosion for a given set of glaciological parameters.

Budd et al., (1979) carried out laboratory experiments and determined that erosion was a function of lithological erodibility (f), basal shear stress (τ_b), effective normal pressure (N) and basal sliding velocity (v_b) thus:

$$E = f\tau_b N v_b \tag{1.1}$$

Oerlemans (1984) used this parameterisation in his numerical experiments of large-scale glacial erosion and noted that the basal shear stress can be eliminated when using a flow law for generating modelled basal sliding velocities. He further noted that calculating E simply as a proportion of v_b made little difference to the resultant pattern of landscape development.

However, Boulton (1974; 1979) suggests that the thickness of overlying ice is also important in controlling the bulk erosion rate so that E might be calculated as a function of lithological erodibility, basal ice velocity and ice thickness (H) thus:

$$E = -f \mid v_b \mid H \tag{1.2}$$

Other laboratory experiments indicate that the concentration of abrading particles at the bed were important (Scholz and Engelder, 1976), leading Hallet (1979) to propose a more complex and 'realistic' model which accounted for concentrations of rock particles (Cr) and their velocities (v_p) and related them to the effective normal pressure thus, where α and n are empirical constants:

$$E = \alpha C_r v_p N^n \quad (1.3)$$

All of the above rules have been shown to predict erosion a realistic manner despite the known importance of additional factors in generating erosion. These include the geothermal heat gradient, lithology, debris concentrations and meltwater production rates (Boulton, 1979; Hallet, 1979; Hallet, 1996; Harbor, 1995; Näslund et al., 2005; Oerlemans, 1984; Paterson, 1994; Schweizer and Iken, 1992; Sugden et al., 2005). However, modelling at the scale of rock particle concentrations is unrealistic at the scale of ice sheets, particularly in regions where lithology is relatively unknown, and the behaviour of internal hydrologic pathways are not well known at present. All of this previous work shows that on a large scale, erosion and glacial landscape evolution can be simply predicted.

1.5.3 Topography and its Relationship with Ice Flow

Glacial landscapes are difficult to interpret because they have often either undergone long periods of continuous glaciation, or they have been subjected to multiple periods of cyclic glacier growth and decay (Kleman et al., 2007). Therefore a sequence of spatially and temporally varying systems can be imagined where each successive erosion pattern is conditioned by previous surface processes. Thus the conditions that have occurred earlier will determine whether later processes of glaciation will lead to protection, modification or removal of deposits and landforms from a region. As a landscape succumbs to erosion by ice the differing styles of ice flow can be classified into 4 broad types that represent differing histories of glacial process (Sugden and John, 1976). These are: *glacial scour* whereby large areas are scoured and smoothed; *linear flow* which is evidenced by focussed selective erosion of valleys into pre-existing plateau surfaces; *deposition* as tills and meltwater deposits accumulate and *protection* where the pre-glacial landscape is essentially retained.

The degree to which this contrast in landscape evolution process occurs is thought to be at least partly driven by the morphology of the pre-existing landscape. Focussed

flow would thus be preferentially located where valleys or channels are already present because the relative thicknesses of an ice sheet is greater here than across surrounding interfluves. Thus in a trough, where ice is thicker, deformation will occur more readily due to the increased driving stresses. Increased ice velocities will be reinforced by heat generated under the thicker ice, and through the increased frictional heating of fast flowing ice (Payne, 1999). Furthermore, strongest erosion, which is associated with the greatest downstream ice discharge, generally occurs around the position of the long-term equilibrium line altitude (ELA) (MacGregor et al., 2000; Montgomery et al., 2001) where ice accumulation equals ablation. The very simple reason for this is that in the accumulation zone ice discharge increases downstream due to the effect of cumulative mass input, but in the ablation zone ice discharge decreases downstream.

The end result of multiple cycles of glaciation is a landform assemblage such as that which characterises for example Scotland or Scandinavia, and which displays features ranging from troughs that enabled highly efficient ice drainage (Evans, 1969; Sugden et al., 2005) through regions of areal scouring (Kleman et al., 2007) to high elevation plateaus that remained protected by cold based ice (e.g. Ballantyne et al., 1998; Kleman and Stroeven, 1997; Li et al., 2005; Phillips et al., 2006; Stroeven et al., 2002b). Figure 1.4 shows examples of such landscapes. The geomorphology of ice sculpted landscapes therefore not only reflects the ice dynamics and more specifically the basal thermal regime of successive ice masses, but is also one of the drivers of ice dynamics. The extent to which this is the case is investigated in the course of this thesis.

Techniques such as thermochronology (e.g. Fitzgerald and Stump, 1997), cosmogenics (e.g. Fabel et al., 2004; Summerfield et al., 1999) and the estimation of offshore sediment volumes (e.g. Bogen, 1996; Jamieson et al., 2005) have been used to determine erosion rates across whole ice drainage basins, and at point locations that have become ice-free. Documented rates (combining bedrock and deformable sediment removal) can range from 0.01 mm yr^{-1} under polar glaciers and ice masses to >100 mm yr^{-1} under temperate glaciers (Bogen, 1996; Hallet et al., 1996). Rates are likely to be towards the lower end of this spectrum when considering bedrock erosion alone. Limited experiments carried out under an Icelandic outlet glacier

suggested that rates of just over 2 mm yr^{-1} were possible on soft bedrock lithologies (Boulton, 1979).

Figure 1.4: Landscapes of large-scale glacial erosion

These photographs illustrate the type of landform expected under conditions of: selective erosion (left) – overdeepened glacial troughs surrounded by zones of less intense erosion or protection; areal scour (middle) – smoothed topography; and cold-based protective ice (right) – where deeply weathered upland plateaus survive under ice. Photographs courtesy of David Sugden.

Erosion rates are variable over space at a number of scales. At the valley scale where glaciers are funnelled through troughs, erosion rates are found to increase away from the lateral margins of the ice covered area (Fabel et al., 2004). Two-dimensional simulations of glacial valley development show that such a pattern is required to produce overdeepened glacial systems from idealised fluvial valley topographies (Harbor, 1992; 1995). On ice sheet scales, rates of erosion vary in line with ice discharge whereby higher rates of erosion might be expected from large ice drainage systems or ice streams, and lower rates will be achieved where the throughput of ice is smaller. Erosion rates will be tempered by harder lithologies (Harbor, 1995). Along the axis of flow, at all scales, maximum erosion rates are generally achieved around the position of the ELA because this is the zone of maximum ice discharge (MacGregor et al., 2000; Montgomery et al., 2001; Sugden and John, 1976). Such a pattern of erosion leads to the development of characteristic valley long-profiles whereby a fluvial valley floor will be lowered more around the ELA and will therefore tend to have a steeper gradient inland and a shallower gradient below the ELA (Fig. 1.5). Overdeepening can occur whereby a central portion of the profile is deepened to such an extent that the gradient below this zone becomes reversed as is typical in fjord topographies (Jamieson et al., 2005).

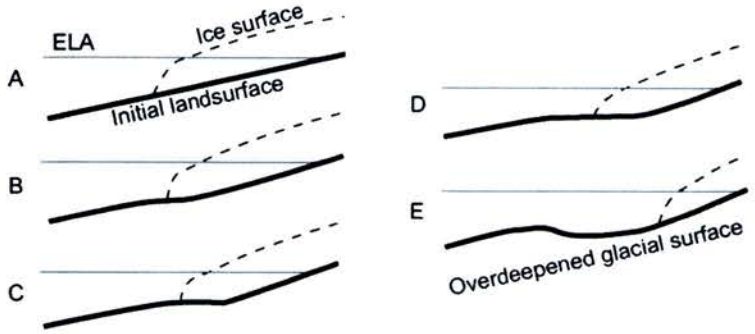

Figure 1.5: Schematic development of glacial long-profiles

Glacial long-profile development under a static climate are illustrated progressing from an initial land surface (A), to an overdeepened glacial trough system (E). Note that the majority of erosion occurs nearer the snout of the glacier due to the long-term position of the ELA. As a result of overdeepening by glacial erosion, the ice is caused to retreat.

1.6 Approach

1.6.1 Ice Sheet Models

Much of our knowledge relating ice sheet dynamics to geomorphology comes from formerly glaciated regions, particularly in the northern hemisphere. We are able to determine glacial limits, the timings of ice mass fluctuations and even make some inferences about the modes of ice flow experienced over time. However, although the geological record is rich, it is limited in its ability to record detailed information about internal ice dynamics. The development of numerical models of ice sheets over the past 30 years has allowed the behaviour of ice to be linked to geological information about past and present ice masses and have been used to make predictions about future and past ice sheet extents. The use of models to simulate future scenarios of ice mass behaviour has recently come to the forefront in estimating impacts of climate change (e.g. Gregory and Huybrechts, 2006; Hagdorn, 2003; Huybrechts et al., 2004; IPCC, 2007). But equally critical to the understanding of future ice sheet behaviour is understanding how ice masses have behaved in the past.

Glaciological modelling has been employed in the reconstruction of ice masses worldwide and at many scales, with their results being calibrated against geological

evidence. Such models have also increased our understanding with regard to ice dynamics, and the influence that external factors such as climate (Hulton et al., 2002; Huybrechts, 1993; Huybrechts et al., 2002; Oerlemans, 1982; Oerlemans et al., 1998), sea level change (Alley, 1984), atmospheric CO_2 (DeConto and Pollard, 2003a; 2003b) and tectonics (Braun et al., 1999; Lunt et al., 2008; Tomkin, 2003) have upon ice masses over a range of temporal and spatial scales (Huybrechts, 1993; Huybrechts and de Wolde, 1999; Huybrechts et al., 2002). However, in many cases the geological record is discontinuous, limiting the ability of the models to be constrained. This is a particular problem when predicting glacial erosion because although we can see the results, establishing which episodes of erosion are responsible for particular landscape components is difficult. As we have indicated, estimations of the kinds of erosion expected under different types of glacial systems have been made. The advantage of using models is that because we know the range of erosion rates that might be likely, models can be repeated to test the impact of this range upon the landscape.

The benefits of using modelling as an approach is that the simulations can be tested for their sensitivity to individual components of the glacial system. This enables calibration and refinement of the physical laws and input parameters to improve predictions. The drawbacks are that there is always some uncertainty involved with the result of a model, and in the case of future predictions this uncertainty is unlikely to be easily quantifiable. Combined with the parameterisations of erosion that have been developed (section 1.5.2) ice sheet models provide the ideal tools with which to investigate the feedbacks between erosion, topography and ice dynamics over long timescales under real, and synthetic scenarios.

1.6.2 GLIMMER

The ice sheet model used in this study is called GLIMMER (General Land Ice Model for Multiply Enabled Regions) and is the latest incarnation of a model that is based upon the models by Huybrechts (1986), Boulton and Payne (1992) and Payne and Dongelmans (1997). Previous versions of this model were used in the EISMINT (European Ice Sheet Modelling INiTiative) benchmark tests which were designed to test and compare ice sheet models and their ability to represent various aspects of

glacial behaviour (Huybrechts and Payne, 1996; Payne et al., 2000). Written in Fortran 95, the current incarnation of GLIMMER is a community model (Hagdorn et al., 2005; Rutt et al., Submitted) enabling the independent development of extensions to be developed and incorporated with the core code in a structured manner. One such extension is that used throughout this thesis to generate glacial erosion. Figure 1.6 shows how the different components of the ice sheet model are related to one another. The model is able to simulate the linkages that are generated in ice masses between temperature and ice flow. This is important, particularly in the context of understanding glacial erosion, because it allows realistic patterns of ice flow (and non-flow) to be generated. The generation of realistic thermal field is critical to the way the landscape develops under ice, because as we have identified above, the landscape is directly related to the degree of sliding being experienced at the base as a consequence of basal melting.

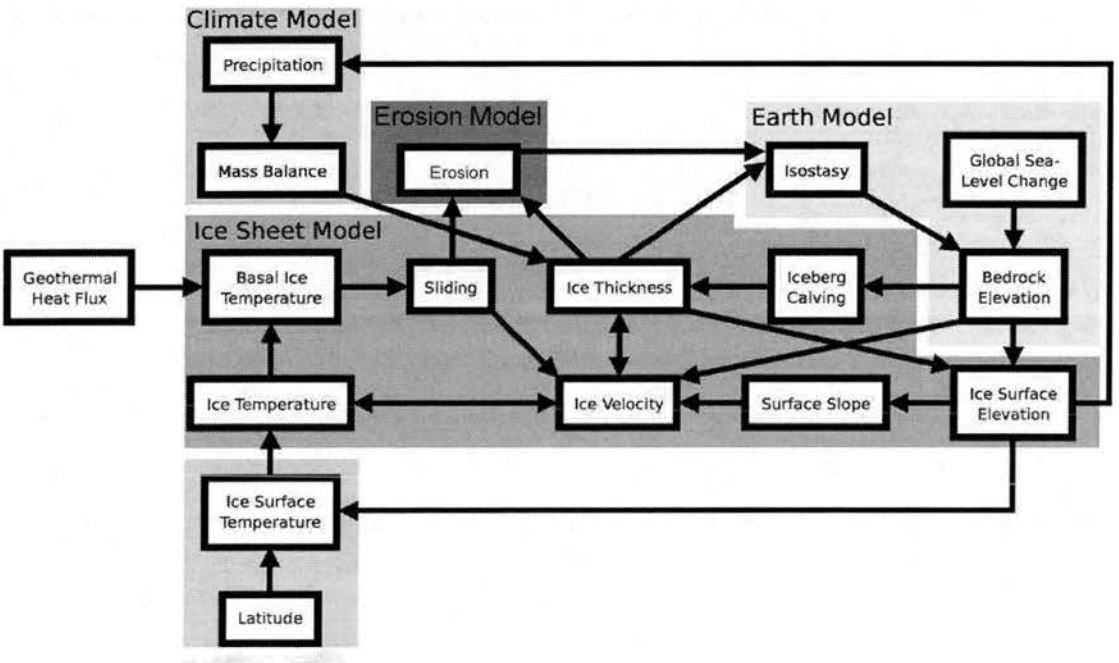

Figure 1.6: Ice sheet model structure

Schematic structure of the ice sheet model showing the connections between climate, ice dynamics, erosion and an Earth model (Modified from Hagdorn, 2003; Siegert, 2001).

The physical equations used in the evolution of ice thicknesses and ice flow are now well established and so are not directly introduced here. Instead I briefly indicate how the model works and then outline in more detail the physics involved with the generation of basal conditions – which are most relevant to the modelling of erosion. We discuss later (section 1.6.3) the numerical feedbacks identified in ice sheet models such as GLIMMER, and show how these can be mitigated in order to ensure we can model erosion-ice feedbacks in a robust manner. A detailed outline of the model physics is given in Payne and Dongelmans (1997) and in Rutt et al., (Submitted).

1.6.3 The Shallow Ice Approximation

The ice sheet uses a continuity equation to evolve ice thicknesses whereby ice thickness is a function of accumulated snow and of the internal velocity vector of the ice. Ice deformation is assumed to be driven by horizontal shear stresses because ice surface slopes are assumed to be small enough that normal stress components can be ignored – the shallow ice approximation (SIA - Hutter, 1983). Therefore, the prediction of patterns of fast-flowing ice in the model is not achieved by modelling the full complement of physics known to be important in the process of ice stream development (Hulton and Mineter, 2000; Payne and Baldwin, 2000). The inclusion of normal stresses are the focus of recent (DePonti et al., 2006; Hindmarsh, 2004) and ongoing (e.g. the Ice Sheet Model Intercomparison Project – Higher Order Models (PMIP-HOM - Pattyn and Payne, 2006)) work but are not yet incorporated into GLIMMER.

It has been shown that the accuracy of the SIA method deteriorates with increasing bedrock slopes (Le Meur et al., 2004). In other words, where bed slopes become pronounced the validity of the SIA method decreases. This has obvious implications with regard to modelling subglacial erosion because as the modelled ice sheet evolves the bed topography will be modified too. It is likely that bedrock slopes over this distance will locally be steeper than ice surface slopes. In order to avoid invalidating the SIA, Hindmarsh (1996; 2006) indicates that relatively high basal

traction conditions should be parameterised because longditudinal stresses become increasingly important when the bed is slippy. For reasons of computational efficiency, comparisons of models which use the SIA vs. higher order physics (such as full-Stokes) have tended to focus upon determining differences across small-scale glaciers rather than ice sheets (e.g. Hindmarsh, 1996; 2005; 2006; Le Meur et al., 2004). Thus it is unclear the degree to which the SIA will introduce error over an ice sheet scale. In the context of this thesis the use of the SIA restricts experiments to the ice sheet scale with resolutions of no less than 5 km which will limit the ice surface slopes that can be generated. The contribution of the SIA to error in ice sheet dymanics is difficult to assess in the absence of a model with higher order physics which can be used to compare results over specific experiments.

The further implications of using the SIA is that modelling small scale glacial dynamics (i.e. at the scale where surface slopes are significant) is not possible, and therefore small-scale interaction with topography cannot be modelled. However, at ice sheet scales, the use of the SIA has been shown to allow the generation of realistic ice sheet geometries. In relation to the prediction of landscape evolution, the use of the SIA is also valid because the physics are valid at a large scale and because at such scales the patterns of evolution are most strongly determined by ice mass fluxes and particularly by the bed geometry.

1.6.4 Basal Ice Velocities

The ability of a modelled ice sheet to grow and interact with its bed and climate is strongly dependent upon basal ice velocities. A nonlinear flow law is used in the calculation of ice velocities in GLIMMER (Glen, 1955). In the context of glacial erosion and basal processes, empirical studies and observations have allowed simplified laws that describe the velocities of the basal ice at any one point to be generated (Kamb and LaChapelle, 1964; Paterson, 1994; Weertman, 1957; Weertman, 1964). These are determined as a function of the basal shear stress (τ_b) and the effective pressure (N - ice overburden pressure minus basal water pressure) thus:

$$v_b = k\tau_b{}^p N^{-q} \tag{1.4}$$

where k is a constant describing the thermomechanical properties of ice and p and q are positive integers (Paterson, 1994). The basal slip coefficient (t_b), also known as the basal traction parameter, determines the dependence of the thermomechanical properties of ice upon N and assume that k and N^q can be integrated as a single parameter. Equation 1 can therefore be simplified (Hagdorn et al., 2005):

$$v_b = t_b \tau_b \tag{1.5}$$

Sliding is assumed to occur when ice temperature at the bed reaches pressure melting point (taking into account both a user defined geothermal heat flux and calculated frictional heat contributions) at which point the ice can detach from the bed and begin sliding due to the presence of water. Its ability to do so is determined by t_b, the calculation of which we outline in section 1.6.3 below.

A key factor in combining the modelling of ice sheets and landscape evolution is the response of the lithosphere to the expansion or contraction of ice, and to the removal of bedrock material. Therefore, in common with the majority of ice sheet models, an elastic lithospheric Earth model is therefore used in GLIMMER (Figure 1.6) to simulate flexural depression and rebound under changes in load (Lambeck and Nakiboglu, 1980).

1.6.5 Numerical Instabilities, Basal Traction and Basal Melt-Rate.

Numerical models of ice sheets have, in the past, been noted to display behaviour attributed to numerical instabilities and feedbacks (Payne and Baldwin, 2000; Payne and Dongelmans, 1997; Payne et al., 2000). In particular, a form of creep instability is known to occur in ice sheet models whereby temperature anomalies generate soft ice which therefore speeds up for a given gravitational driving stress. This generates heat that reinforces this signal, leading to a pattern of warm, fast-flowing ice

interspersed with slow, cold-based ice being generated (Payne and Baldwin, 2000). The results of the second phase of the EISMINT model intercomparison tests, which were designed to identify the effects of thermomechanical coupling in models, show that in circular ice sheets, regularly spaced spokes of warm, fast ice can be generated (Payne et al., 2000). As Payne and Baldwin (2000) indicate, such patterns are generated in the absence of any topographic influence, and are therefore unexpected.

It is thought that such features are related to creep instability resulting from numerical anomalies in the models. Very small changes in ice temperature causes ice to soften, generating a feedback that causes the ice to flow faster and further causing heat generated by dissipation to continue to drive accelerated flow. The increased flow causes local ice thicknesses to become reduced, increasing the volume of ice flowing into the region of the numerical anomaly. The implication of this, in relation to erosion is obvious. Because erosion is critically controlled by ice discharge and thermal regime, it would be possible to excavate glacial valleys in erroneous locations as determined by numerical instabilities. Thus, when investigating modelled ice behaviour and erosion it is important to consider whether the modelled flow and basal sliding will be dominated by such instabilities.

The representation of sliding in GLIMMER is controlled by the parameter of basal slip coefficient (t_b). Basal slip is a term used by the modelling community to describe the degree of slip that can occur at the bed of an ice mass. Increased 'basal slip' describes low traction conditions between the ice and the bed.

We note that the instabilities noted in the EISMINT benchmark tests are prone to occur in models that use a binary representation of sliding where t_b can either be zero or a maximum value. This allows the creation of large contrasts in ice temperature and flow, which can drive the generation of these erroneous features. Therefore, in order not to generate results that are overly biased by such instabilities, we avoid using the on/off method of calculating t_b in our models. Instead, we relate t_b directly to the amount of water being produced at the bed. It is known that the ability of a glacier to slide is related to the presence of water at the bed, and to the overburden pressure (N) which is controlled by basal water pressures (Paterson, 1994). Basal water pressures are not generated in the models due to the numerous complexities

and unknowns relating to subglacial hydrologic dynamics, particularly over extended periods of time. However, on long timescales (thousands of years) basal water pressures are likely to be most consistently related to basal melt-rate (with occasional perturbations due to fluctuations in subglacial and internal drainage).

We therefore use basal melt-rate to control sliding rates at the base. We relate t_b to modelled basal melt-rate (m) through a parabolic expression thus:

$$t_b = am - bm^2 \qquad (1.6)$$

where a and b are coefficients. The maximum basal slip coefficient, $t_{b\max}$, is reached at a maximum melt-rate, $m_{\max}$ (when $dm/dt_b = 0$) thus:

$$t_{b\max} = \frac{a^2}{4b} \qquad (1.7) \quad \text{and} \quad m_{\max} = \frac{a}{2b} \qquad (1.8)$$

and:

$$a = 2\frac{t_{b\max}}{m_{\max}} \qquad (1.9) \quad \text{and} \quad b = \frac{t_{b\max}}{m_{\max}^2} \qquad (1.10)$$

Throughout the course of this thesis, the value of $m_{\max}$ is held constant at 0.05 m yr^{-1}. Such a value is representative of a relatively high basal melt rate under non-temperate ice sheets. Figure 1.7 shows a graphical representation of this relationship, and of a binary relationship, and illustrates our assumption that as melt rates climb towards a maximum, increases in basal water pressure become limited because in reality there will be a tendency for larger water volumes to be evacuated more efficiently by the subglacial hydraulic system. Equation 1.6 is thus employed in the calculation of basal ice velocities as indicated in Equation 1.5.

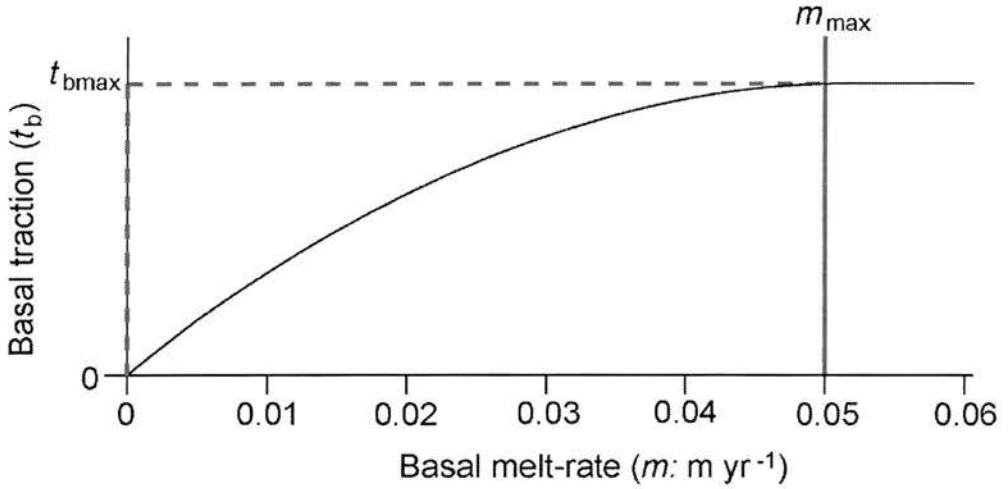

Figure 1.7: Basal slip coefficient (t_b) *and basal melt-rate*

Modelled relationship between basal slip coefficient and basal melt-rate as parameterised by a parabolic curve. Grey dashed line indicates binary relationship between basal traction and basal melt-rate employed by some models. Note that values of t_{bmax} are varied through the thesis and thus are not specifically shown here.

The use of basal melt rate to determine basal ice velocities allows a more graduated transition between zero and maximum ice flow than would be possible when binary (i.e. if $m > 0$, $t_b = t_{bmax}$) representation of sliding is used. Figure 1.8 compares an EISMINT 2h experiment using a binary representation of sliding and basal traction (Huybrechts and Payne, 1996; Payne et al., 2000) against a similar experiment that calculates sliding based on the basal melt-rate method of deriving t_b. The fact that the fingers of hot vs. cold-based ice are not generated in our model (Fig. 1.8) when using a flat bed EISMINT model configuration indicates that the large-scale creep instabilities are not influencing the ice dynamics in our models (Jamieson et al., 2008). Areas of fast vs. cold flow can still be generated when using a topography that is not flat (i.e. when the system is less numerically simple). Thus, once topography is included as an input to the model, we are able to simulate areas of fast flow and thus erosion in a sensible manner without the prospect of generating unexpected streams through numerical instabilities. Any instabilities noted in the following chapters are therefore most likely to be the result of unrealistic topographies or ice sheet/mass balance configurations. In effect they will be real-world phenomena which can only develop in unrealistic situations as opposed to issues of numerical rounding. Because

we can represent basal ice velocity in this sensible way, we will be able to represent a wide range of basal sliding (and thus erosion) rates within a single modelled system – as is likely the case in reality.

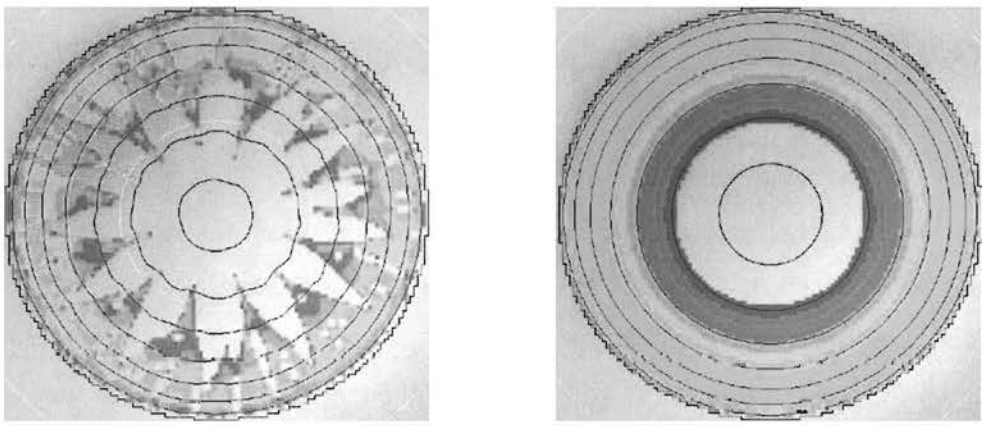

Figure 1.8: Contrasting dynamics by changing basal traction parameterisation

Examples of thermal instability (left) vs. thermal stability (right) in EISMINT style models of ice sheet dynamics – the figures show the pattern of basal melting (and thus basal sliding). The erroneous ice streams in the unstable example are caused by thermal feedbacks (Payne and Baldwin, 2000; Payne et al., 2000), whereas the stable condition is enabled by calculating t_b as a parabolic function of basal melt-rate. This avoids the generation of erroneous zones of fast flow caused by instabilities in GLIMMER and a simple binary sliding switch for melting. After Jamieson et al., (2008).

1.6.6 Modelling Glacial Erosion

Given that erosion is difficult to observe in-situ (Boulton, 1974) numerical simulations provide a way of investigating the impacts of glacial erosion upon topographic development and ice dynamics at a large-scale. A number of numerical experiments have previously been carried out and have variously investigated the relationships between glacial and fluvial erosion of bedrock in tectonic settings (Braun et al., 1999; Tomkin, 2003) and the development of cross and long-valley profiles in 1,2 and 3 dimensions (Anderson et al., 2006; Harbor, 1992; Harbor, 1995; Harbor et al., 1988; MacGregor et al., 2000; Oerlemans, 1984). The impact of

deformable sediment erosion upon ice sheet behaviour has also been a more recent focus of the modelling community (Clark, 1994; Clark et al., 2006; Hildes et al., 2004; Pollard and DeConto, 2003).

However, very little of the work above has focussed on determining the interrelationships between ice dynamics, bedrock erosion and long-term landscape evolution. Instead they focus upon bedrock erosion as a one-way process, and don't consider the response of the ice to erosion in any depth. This is not only because erosion is very often considered to be a passive component of the glaciological system, but because the models are not adequately constructed to consider these feedbacks. This is because much of the work above has concentrated on predicting erosion patterns using models that are not fully thermomechanically coupled. This is a critical flaw because the ability of a glacier to erode is intimately linked to its thermal evolution, not just at the bed, but throughout. Because our work employs a fully thermally coupled model of ice sheet evolution, we are able to predict the pattern of erosion in a way that is more intimately linked to the three-dimensional thermal state of the ice. This both allows more accurate modelling of the pattern of erosion expected under the ice to be carried out and enables the investigation of the feedbacks between the ice and the topography.

We parameterise erosion using a function derived from Boulton's work (Equation 1.2, Boulton, 1974; Boulton, 1979). The rate at which bedrock material is removed is thus assumed to be a function of basal ice velocity and of basal pressures. This is justified because we use medium to high erosion rates in order to test for feedbacks between ice and erosion and so in reality basal debris concentrations would be relatively high. Boulton (1979) and Schweizer and Iken (1992) indicate that this kind of model will be better suited than others under such conditions. Figure 1.6 illustrates the relationship of the erosion model to the overall structure of GLIMMER.

1.6.7 Controlling GLIMMER

In running our experiments, we provide two key inputs for GLIMMER. As a first input, we provide an initial landscape over which we wish to grow an ice sheet. These are provided in the form of a rasterised digital elevation model (DEM), where

each cell over a particular spatial domain contains an elevation value in metres. The majority of the DEMs used as inputs to this work are synthetically generated so that we can control the scale, shape and orientation of topographic features. This is key to this work because we wish to identify the feedbacks between the ice and the changing topography. If we know the initial topographic form, we can more accurately interpret our results as the topography and ice dynamics evolve. Through chapters 2-4, the topographies are all synthetic, and range from simple systems consisting of white noise, to systems with multiple U- or V-shaped valleys, to landscapes generated using a fluvial tectonic landscape evolution model (GOLEM - Tucker and Bras, 1998; Tucker and Slingerland, 1996). In chapter 5, we use a DEM of Antarctica generated from field data (Lythe et al., 2001) to model long-term landscape evolution in a real-world setting. The use of present day DEMs (which reflect past glacial erosion) is a common approach in models of ice sheet reconstruction. As a by-product of this thesis, the use of an erosion model allows the importance of the 'glacial' fingerprint inherent in many real-world DEMs to be discussed in relation to generation of error in models of ice dynamics. In the majority of cases, the synthetic landscapes were created using scripts written in Python (Python Software Foundation, 2008) and Fortran 95.

The second input used to drive our experiments is the climatic forcing. GLIMMER requires that a paramaterisation of mass balance over time is given at run time. There are simple interfaces that allow the user to prescribe the accumulation, ablation, air temperature and lapse-rate to be input, and these are simple to manipulate both spatially and temporally. The evolving surface, a combination of ice surface and topographic surface, will then interact with the climate over time. At its simplest, climate can be uniform, but it can also be formulated so that the vertical position of the ELA is fixed, or so that the pattern of accumulation is circular, as done in the EISMINT benchmark experiments (Huybrechts and Payne, 1996; Payne and Baldwin, 2000). Adding complexity, positive degree day models can be used to predict seasonal melt and refreezing in a more realistic pattern (Reeh, 1991). The pattern of snowfall can also be based upon real-world datasets for particular regions and can then be varied through time using proxy temperature or precipitation data. The majority of the experiments in this work employ simplistic, static climates in

order to build ice sheets that would reach equilibrium if erosion were not also being modelled. Thus the focus is upon the glacial feedbacks in relation to erosion and landscape evolution. The climatic parameterisation used in each set of experiments is described in each individual chapter.

1.7 Thesis Scope

Reiterated, the aim of this project is to investigate feedbacks between glacial erosion, long-term landscape evolution and ice sheet dynamics. This work will show that it is possible to predict patterns of erosion over large spatial and temporal scales by modelling the full thermal field of an ice mass. This thesis thus seeks to revise the view that glacial erosion is a passive component of the glaciological system.

The following 4 chapters of this thesis deal with particular aspects of the nature of interaction between erosion and ice. Each chapter is in the format of a journal paper and each varies significantly in length depending upon the journal/intended journal. Where the chapter has been submitted or published there is detail about authorship and publication status. Where possible, repetition between papers is avoided, but there is a necessary element of duplication of subject matter regarding the model (albeit presented differently) which is used as the basis of the thesis.

Chapter 2 (Jamieson et al., 2008) concerns the implementation and testing of the basal traction parameter/basal slip coefficient parameterisation that is partly outlined above and the coupling of this to the erosion component to the model. It further outlines some of the feedbacks noted within the glaciological system in relation to the prediction of areas of fast vs. slower flow. This paper thus provides the methodological basis upon which the remaining papers are based.

Chapter 3 investigates the feedbacks between particular topographic forms and the distribution of basal sliding and erosion. We thus test which aspects of pre-existing landscape (e.g. relief, topographic wavelength or dominant mode of pre-glacial process) are most important in driving the evolution of basal thermal regime and thus the distribution of erosion.

Chapter 4 (Jamieson and Hulton, Submitted) addresses a problem that has long been puzzling geomorphologists and glaciologists with regard to the evolution of the Patagonian Ice Sheet over the past 1.15 million years. By applying our model to a landscape analogous to the Southern Andes, we are able to show that erosion can drive large-scale changes in ice dynamics and glacial extent.

Chapter 5 focuses on predicting the long-term landscape evolution of Antarctica. Making simple assumptions about the Antarctic climate since the Oligocene, glacial inception and expansion from local to continent scale ice and landscape development is modelled. The results of this model culminate in a continental scale assessment of the degree to which the Antarctic bed has been modified by glacial erosion. A companion to this paper is in press as a book chapter in a volume discussing the current state of knowledge of the evolution of Antarctica (Jamieson and Sugden, 2008). This paper is included in Appendix A. In addition, the generic model that couples climate to GLIMMER was partly written for this thesis (Appendix B) and has been used to test the sensitivity of ice sheet model behaviour to a wide range of parameters and error sources using Greenland as a test bed (Hebeler et al., In Press).

Also appended to this thesis are some of the programs written to generate synthetic topographies and to handle file conversion into the multi-dimensional netCDF data format (Gough et al., 2008) used by GLIMMER. These are included in appendix C.

Chapter 2

Chapter 2 has been published as follows:

Jamieson, S.S.R., Hulton, N.R.J. and Hagdorn, M., 2008. Modelling landscape evolution under ice sheets. Geomorphology, 97(1-2): 91-108.

The erosion module employed here was initially implemented in 2003 by Magnus Hagdorn. Jon Harbor and Jens-Ove Näslund reviewed the manuscript, which was edited as part of a special issue by Arjen Stroeven and Darrel Swift.

The scripts used to generate and convert the input topographies can be found in Appendix C.

Chapter 2 Modelling Landscape Evolution Under Ice Sheets

2.1 Introduction

We aim to investigate the feedbacks between the thermo-mechanical regime of ice sheets and the evolution of subglacial landforms at ice sheet scales. In particular we wish to determine how the shape and scale of a given basal topography influence the pattern of subsequent ice sheet erosion, and thus whether this might act as the essential control on landscape evolution under large-scale glaciation. This is important because it has implications for how we interpret the geomorphological signature of glaciation (especially when considered in tandem with climate), and might give a clearer indication of the timescales over which landscapes react to glacial erosion (e.g. can a glacial trough be cut in a single glacial cycle?). A key question we ask is: when does a fluvial topography become glacial? More specifically, how quickly is a glacial signature superimposed on a fluvial system after glaciation is initiated, and what are the main factors in controlling the speed and pattern of the development of a 'glaciated' landscape? We hypothesise that glacial erosion is maximised in the early stages of glacial superimposition upon a fluvial topography, and that subsequently the topography is adapted such that erosion is minimised, and such that the glacial system can expel ice more efficiently with reduced erosive capacity.

The legacy of Plio-Pleistocene climate variation (e.g. Raymo, 1994) is that large parts of the Earth are characterised by landscapes bearing the fingerprint of multiple continental ice advances. The importance of glaciation as an agent of landscape modification has long been recognised (Forbes, 1843) but the manner in which ice sheets respond to this topographic adjustment remains a topic for debate. Yet for a number of reasons the importance of understanding the influence of erosion and consequent topographic change upon their parent ice masses has never been greater: Firstly, it has been shown that overall ice margin extent has receded throughout the Quaternary in regions such as Patagonia (Mercer, 1983; Rabassa and Clapperton, 1990) and Antarctica (Denton et al., 1993a) while Northern Hemisphere ice volume

is known to have reached a maximum in the mid-late Quaternary (Lisiecki and Raymo, 2005). This might suggest that erosion may contribute to self-limiting behaviour in successive ice sheet extents through the Quaternary (e.g. Hubbard et al., 2005; Singer et al., 2004). Secondly, glacial erosion has been dichotomously hypothesised to either constrain the ultimate height of mountains (Mitchell and Montgomery, 2006) or to increase summit elevations (Molnar and England, 1990; Small and Anderson, 1998) whilst also increasing relief (Brocklehurst and Whipple, 2002; Whipple et al., 1999). Thirdly, there are linkages between erosion and climate, and also with tectonics (e.g. Clark and Pollard, 1998; Molnar and England, 1990; Pollard and DeConto, 2003; Raymo and Ruddiman, 1992), and although the nature of these is still hotly debated, their importance is well established. Thus to understand the role of erosion in long-term climate and landscape evolution in glaciated regions it is important to determine the controls on feedbacks operating within the glacial system.

2.1.1 Glacial Erosion and Topographic Feedbacks

Despite the widespread occurrence of features associated with erosion under ice sheets such as glacial troughs with overdeepened longitudinal profiles and areally scoured bedrock, many questions still remain regarding the long-term evolution of such topographic forms. For example, how quickly does a non-glacial topography become 'glacial', and how does the nature of the preglacial topography affect the nature of glaciation and topographic evolution? The main processes of erosion are abrasion and quarrying which are dependent upon the temperature and velocity of the basal ice, debris concentrations, ice thickness and subglacial water pressure (Hallet, 1979, 1996; Oerlemans, 1984; Paterson, 1994; Sugden et al., 2005). Significant wear to the bed can also be caused by subglacial fluvial action, particularly where sediment can act as a tool for abrasion, but also through chemical dissolution as water comes into contact with soluble minerals in bedrock and sediment. Importantly, for abrasion and quarrying to take place, there must usually be some relative movement between the glacier sole and the bed which therefore requires either water at the bed and/or the basal ice to be at pressure melting point. This

necessitates that either the ice sheet is largely temperate and thus is capable of producing large surface meltwater volumes that can reach the bed, or that the bed can locally reach pressure melting point as a consequence of the thermo-mechanical regime of the glacier even if the temperature of the bulk of the ice sheet is below freezing point. The latter condition requires positive heat balance at the bed which tends to occur if geothermal heat inputs are higher, if there is strong frictional heating caused by fast flowing ice, if heat is advected into a region by a strongly convergent flow of warm ice and if the bed is effectively insulated from the cold ice sheet surface by a large ice thickness. Once the bed reaches pressure melting point, excess heat melts the ice providing water to lubricate the bed and help promote sliding. The effectiveness with which the water promotes sliding depends crucially on the water pressures created (Iken and Bindschadler, 1986), themselves dependent on the bulk permeability of the glacier bed and the nature of subglacial conduits and channels that may act to evacuate water and thus to reduce basal water pressures.

The complexity that arises from the interplay between glacial erosion processes, and both initial and evolving (i.e. preglacial and subglacial) topographic states means that communication between ice and the underlying geomorphology is also critical to the way in which glaciated landscapes evolve. For example, ice might exploit an existing river network (given a large enough accumulation area) such that V-shaped valleys are widened and deepened to enable the more efficient evacuation of ice (Evans, 1969). The valley system therefore tends to become characterised by wide basins and deep troughs, with additional smaller-scale streamlined landforms present depending on local conditions (Sugden and John, 1976). The manifestation of these features affects a topography's ability to support ongoing or further glaciation. For example, selective glacial erosion lowers valley floors relative to peaks and ridges (e.g. Sugden, 1978a) thus altering the mass balance profile of the ice (Kerr, 1993; MacGregor et al., 2000; Oerlemans, 1984).

Within the glacial system, the ice movement which causes erosion at the glacier bed, is not directly coupled to the process of snow accumulation at the surface. Snow provides energy to drive the system but the complexities of the ice sheet's internal physics means that this energy is not available to do work on the bed in a direct and simple way. Predicting the location of melting and non-melting zones and thus of

erosion therefore requires a more complete treatment of ice thermomechanics. A number of authors have used numerical models to explain where erosion occurs and how it feeds back into ice dynamics (Anderson et al., 2006; Oerlemans, 1984; Tomkin and Braun, 2002). One- and two-dimensional experiments by Oerlemans' (1984) indicate that glacier beds are sensitive to erosion rate parameterisation and that temperature (which is the dominant control of basal ice velocity) is the primary control on the pattern of erosion under ice. In addition he finds that alongside the sensitivity of the topography to the ice dynamics, the (pre-) existing topography is critical in focussing erosion.

The U-shaped valley is the result of equilibrium between the landscape and ice and it is predicted that the distribution of glacial erosion is set by the regional pattern of ice discharge (Penck, 1905; Sugden and John, 1976). Näslund et al. (2003) confirm this, finding that basal sliding distance (i.e. basal sliding velocity multiplied by the duration of the sliding) correlates strongly to known areas of glacial erosion under the former Fennoscandian Ice Sheet. Models of U-shaped valley cross section development indicate that under constant ice discharge conditions, it is possible to produce a steady-state U-shaped valley from an initial V-shaped valley in a single glacial cycle (Harbor, 1992; Harbor et al., 1988). However, if discharge is variable, these studies find that ice elevation lowers over-successive glacial cycles for a similar discharge rate, thus predicting that the modification of the valley form impacts upon the glacial dynamics creating a negative feedback between erosion and ice discharge. This negative feedback however, is conditioned by the positive feedback that occurs between pre-existing topography and glacial erosion in that morphology strongly conditions the thermal regime of ice through flow divergence and convergence as the glacier colonises existing valley structures (Glasser, 1995; MacGregor et al., 2000). Further studies conclude that the impact of bedrock erodibility is not as strong a control over valley form as one might think (Harbor, 1995).

The shortcomings of the above models are that they either do not predict basal temperature, or they deal with it in a limited way when modelling erosion. In order to account for such limitations, Hildes et al. (2004) take a non-reductionist approach to the problem of calculating erosion rates by incorporating specific methods for

topographic modification through both abrasion and quarrying with a 3D thermomechanical ice sheet model. Additionally, they add methods for calculating basal water pressure (Flowers and Clarke, 2002) and to account for bedrock lithology. Despite breaking the problem of erosion into its process constituents, the results failed to meet expectations because their integrated erosion estimates were low – most likely, they suggest, as a result of the number of free parameters in the model.

2.1.2 Rates of Glacial Erosion and Recognising Signals of Glaciation

Rates of glacial erosion vary, and arguments continue as to their efficacy when compared with a fluvial regime of a similar magnitude. Indeed, it is not at all clear how quickly a 'non-glacial' topography can become 'glacial', especially when it is considered that glacial erosion rates can vary from ca. 0.01 mm yr^{-1} under polar glaciers on highly resistant crystalline bedrock to 60 mm yr^{-1} for selected temperate valley glaciers in tectonically active regions (Bogen, 1996; Hallet et al., 1996). Patterns of erosion vary, with strongest downstream ice discharge, and thus erosion, being generated around the long-term equilibrium line altitude (ELA) position (MacGregor et al., 2000) where ice accumulation is equalled by ablation. The strongest cross-stream erosion tends to occur in the deepest portions of a valley (Fabel et al., 2004; Harbor, 1992; Li et al., 2005). As indicated above, a U-shaped valley form might be excavated within a single glacial cycle (Harbor, 1992; Harbor et al., 1988), a result supported by morphometric analysis of the Ben Ohau mountain range in New Zealand (Kirkbride and Matthews, 1997).

A number of recent studies have attempted to combine models of ice sheet erosion, fluvial erosion, and surface process development into a single model to test the interplay between fluvial and glacial erosion under orogenic evolution (Braun et al., 1999; Tomkin, 2003; Tomkin and Braun, 2002). They indicate that glacial erosion rates can reach equilibrium with the landscape if the system is undergoing constant uplift (Braun et al., 1999) but that in order to recreate a realistic system, the balance of glacial and fluvial erosion ratios is important. Hallet et al. (1996) show that basins that have been subject to glaciation are able to accumulate equally as much sediment

as an equivalent fluvial system. Studies in the Andes (Montgomery et al., 2001) and in the Himalaya (Brozovic et al., 1997) indicate that in keeping pace with uplift, both rivers and glaciers can erode equally as rapidly.

When considering the output of landscape evolution models it is important to identify that results are suitably realistic. A common approach is to use morphometric analysis techniques as these are often used to determine the dominant processes that influence topographic evolution (e.g. Jamieson et al., 2004; Montgomery et al., 2001). Indicators ranging from simple hypsometric plots (Brocklehurst and Whipple, 2004; Strahler, 1952) to more complex analyses such as sub-ridgeline relief (Brocklehurst and Whipple, 2002) can give an indication of how glaciated a catchment has become. However, working beyond the basin scale is problematic and Wood (1996) indicates that geomorphological characterisation of the landscape requires appreciation of the surface form at a number of scales. Because of the computationally intense nature of landscape evolution models, their output is often of comparably low resolution (i.e. 5 – 20 km) thus obscuring any differential signal between a fluvial and a glacial topography that techniques such as hypsometry or slope-area ratios might otherwise be able to identify. Given that this is the case, in the context of large-scale landscape evolution a key indicator of how glaciated a system has become is the river longitudinal profile because it provides a focussed picture of landscape change along the flow path of either rivers or ice. In addition, the often selective nature of glacial erosion (Phillips et al., 2006; Sugden et al., 2005) means that it will preferentially erode in areas where ice can be deepest – i.e. in valley floors. Therefore, in the context of modelling topographic evolution under ice sheets where complicating factors such as differential tectonics are not considered, longitudinal profiles are ideal for identifying patterns of change and linking them with erosion processes.

2.2 Approach

We use a numerical modelling approach in order to investigate the interactions between ice sheets and topography in a controlled and reproducible manner. Our

overall goal is to build models that produce credibly adequate simulations of landscape evolution under ice sheets. However we assert here that in order to do that we must comprehend some of the basic controls on the large scale patterns of basal thermal regimes under ice sheets and how these interplay with the nature of the underlying topography. We envisage these controls as being both internal to the ice sheet system and deriving as a consequence of the physics of ice flow, and also external, in that for an ice sheet operating under a given climatic regime, the specific detail of ice sheet form and flow patterns is controlled by the existing landscape. Thus for instance, whether or not an ice sheet slides and therefore erodes in a given location may necessitate a high ice mass balance to drive the system but will also be naturally facilitated by having deep valleys that tend to converge fast ice flow. Our primary intention in the first instance is to comprehend better the nature of these controls, and how they develop under evolving landscapes. The topographic inputs to our models are thus all synthetically generated in order that we can control their morphometric character prior to studying the feedbacks between ice and basal boundary conditions. This avoids any complication from real-world topographies where a landscape may have been conditioned by differing (and uncertain) amounts of glacial or other geomorphic processes and where it is thus hard to disassociate the effects of internal and external controls on the erosion patterns.

This study employs the GLIMMER (General Land Ice Model for Multiply Enabled Regions - Hagdorn et al., 2005; Payne, 1999), ice sheet model and combines it with a mechanism for modifying its basal topography in order to ask a number of questions:

- How is the 'work done' at the bed conditioned? Is this influenced to a greater extent by the initial topographic state, or by the distribution of the basal slip coefficient – a parameter that describes the ability of the bed to slide in response to the ice driving stress.
- As an extension of this question we also ask how quickly does a 'fluvial' system become a 'glacial' system? For the purposes of this study, we will consider a system to be glacial when we can observe a significant change in

longitudinal profile geometry such that overdeepening is visible around the location of the long-term ELA.

2.2.1 Objectives

We wish to:

- Investigate how large-scale preglacial U-shaped vs. V-shaped valley topographies affect the spatial distribution of basal traction by initiating an ice sheet on a topography with either sine wave or V-shaped cross sectioned valleys radiating from a central point.
- Use an EISMINT (see below) simplified geometry model configuration, which has simplified, regular boundary conditions (normally used to compare ice sheet models), over a set of random white noise topographies with a known distribution of wavelengths to determine both how and when topographic barriers are affected by glacial erosion and which particular aspects of the glacial or topographic conditions are critical in determining the outcome.
- Initiate an ice sheet model over a topography derived by the GOLEM (Geomorphic/Orogenic Landscape Evolution Model) fluvial/tectonic evolution system (Tucker and Bras, 1998; Tucker and Slingerland, 1996) to determine both the stage at which glacial erosion is maximised between the transition from fluvial to glacial topographic states, and the distribution of any topographic transformation.

2.2.2 The Ice Sheet and Erosion Model

GLIMMER is a three-dimensional coupled thermomechanical community ice sheet model. It is similar to other models of this type, many following Huybrechts (1986), and specifically GLIMMER has led from developments by Boulton and Payne (1992) and Payne (1999). The full physics of the model are outlined elsewhere (Hagdorn et al., 2005) but like many ice sheet models, GLIMMER employs the shallow-ice approximation which assumes that both the topographic and ice surface

slopes are small enough that normal stress components can be ignored (Hutter, 1983; Paterson, 1994). This makes model run times tractable for topographies at ice sheet scales for ~100s kyrs down to about 5 km resolution making it ideal for examining large-scale patterns of erosion under ice. We discuss below the implications of not using an ice model with high-order physics and higher resolution in our initial investigations. Within GLIMMER, isostasy is incorporated by modelling the lithosphere as an elastic plate but also by representing flow within the mantle in response to changing surface loads as an exponentially decaying hydrostatic response function.

In an earlier incarnation, the GLIMMER ice sheet model was one of those used in the EISMINT I and II model intercomparison tests. These tests established benchmarks to aid new ice sheet models to be developed (Huybrechts and Payne, 1996) and further highlighted some issues involved with coupling ice temperature with models of flow (Payne et al., 2000). The tests defined a number of simplified geometry experiments that were then independently reproduced using a number of ice sheet models.

A particularly notable feature of the EISMINT II tests was that in many cases the models showed a steady-state pattern of basal temperatures that included warm zones of ice radiating from a centre in 'streams' separated by colder zones. The ability of ice sheet models to produce such zoning of warmer (fast) and colder (slow) flow has been the subject of some debate within the ice sheet modelling community (Bueler et al., 2005; Hulton and Mineter, 2000; Payne and Baldwin, 2000). The tendency of the models to reproduce areas of warm ice that flows quickly occurs because of the way they represent the positive feedback mechanism of ice creep within their underlying thermodynamic equations. In essence, warm ice is more fluid, flows faster and thus produces more frictional heating which warms the ice further. This effect can be further enhanced if a sliding mechanism is introduced once the basal ice reaches pressure melting point. However, the ice sheet model can only maintain this faster, hotter flow if sufficient snow mass balance is available to supply the fast ice throughput. If not, one of two things occurs: the ice flow regime is temporally variable as the ice reaches a fast flow state, then shuts off through lack of ice, or; the ice sheet supports certain zones of fast flow which are fed by convergent flow over a

wider area. In this case, the more mass throughput on the ice sheet overall, the greater the number of faster streams that can be supported.

A principle question is the extent to which the models can accurately represent the pattern of ice flow caused by this underlying thermomechanical instability. Put simply, what controls whether the model produces many narrow zones of fast flow or a few larger ones? It has been shown that the expression of the instability in the models can be strongly conditioned by the numerical scheme used to solve the ice equations (Bueler et al., 2005; Hindmarsh, 2005). However, once there is even a small amount of variability in the basal topography of the ice sheet, this topography exerts a strong influence on the flow regime produced. The zones of faster flow produced in the models are thus broadly analogous to ice streams found in ice sheets, although the ability of most models to accurately represent the physics of such streams in an adequately accurate manner and at the correct scales is significantly compromised. This is because they often explicitly ignore components of the stress regime which are important in true streaming flow. That said, the physics that predict the basal thermal regime of the ice over larger scales are broadly correct, and the patterns produced are most strongly conditioned by the ice mass flux and basal topography. Hereafter, in recognition of the differences between what we model and what we see in real ice masses, we refer to streams and regions of streaming flow purely in the sense of features predicted by the model.

Of interest in this study is the manner in which the ice interacts mechanically with its underlying bed. If the temperature at the bed is above pressure melting point (adjusted for a geothermal heat flux of -4.2 W m^{-2} and for frictional heat input), the ice can decouple from the bed due to the presence of water. A linear form of linking basal velocity (v_b) to basal shear stress (τ_b) is common in ice sheet models and in the absence of universally applicable physically-derived sliding models the veracity of this relationship is largely derived from observational evidence. For example, Weertman (1957; 1964) hypothesised that ice could slide via regelation and enhanced plastic flow, both of which were confirmed through observation by Kamb and LaChapelle (1964). Refinements to these mechanisms have allowed empirical laws to be determined relating sliding velocity to basal shear stress and effective

pressure (N - ice overburden pressure minus basal water pressure), most of which can be reduced to the form:

$$v_b = k\tau_b{}^p N^{-q} \tag{2.1}$$

k is a constant describing the thermomechanical properties of ice and p and q are positive integers (Paterson, 1994).

In GLIMMER the dependence of the thermomechanical properties of ice upon the effective pressure is parameterised by the basal slip coefficient (t_b) which assumes that k and N^q can be integrated as a single parameter. The slip coefficient (often also referred to as the basal traction parameter), along with basal shear stress allows determination of basal ice velocity (Hagdorn et al., 2005) thus:

$$v_b = t_b\tau_b \tag{2.2}$$

A larger magnitude basal slip coefficient in this case means that ice is able to slide more freely over the bed. The parameterisation in Equation 2 assumes that p=1.

To test the sensitivity of the ice dynamics to basal slip, we will use 2 different parameterisations of t_b in our experiments. The simplest method for calculating the basal slip coefficient is carried out using static values for t_b, whereby if the bed is at pressure melting point, the basal slip parameter will be set at a constant value, otherwise it will be zero. In other words, the velocity, where not zero, is linearly related to τ_b through a basal slip constant that is defined at ice sheet initiation. We have also developed a method that varies t_b with the amount of melt water which the model predicts is produced at the glacier bed. Adjusting this in relation to the melt water production thus approximates the tendency for increased basal water pressure to occur with increased basal melt. It is perhaps a more intuitive way in which to prescribe basal slip, because the relationship of water to basal sliding velocities is critical. As the basal water pressure increases under an ice mass, the effective normal

pressure (N) is decreased as the water acts against the overburden pressure generated by the ice, thus more water means greater potential for basal décollement (Paterson, 1994). Because our model does not yet deal specifically with glacier hydrology, we use basal melt-rate as generated by geothermal and frictional heating as the main influence on sliding rates at the base. In this case, we relate t_b to modelled basal melt-rate (m) through a simple parabolic expression thus:

$$t_b = am - bm^2 \tag{2.3}$$

where a and b are coefficients. The maximum basal slip coefficient, $t_{b\max}$, is reached at a maximum melt-rate, $m_{\max}$ (when $dm/dt_b = 0$) thus:

$$t_{b\max} = \frac{a^2}{4b} \tag{2.4}$$ and $$m_{\max} = \frac{a}{2b} \tag{2.5}$$

and:

$$a = 2\frac{t_{b\max}}{m_{\max}} \tag{2.6}$$ and $$b = \frac{t_{b\max}}{m_{\max}^2} \tag{2.7}$$

In this study, the value of $m_{\max}$ remains constant. We thus assume that, with higher melt rates, further increases in basal water pressure become self-limiting because of the tendency for the greater water volume to be evacuated more efficiently by the subglacial hydraulic system. Thus we choose a value of 0.05 m yr^{-1} for $m_{\max}$ in all experiments which represents a relatively high basal melt rate under non-temperate ice sheets.

Bedrock erosion (E) through time within GLIMMER is dependent upon the mean basal velocities (v_b) and upon the ice thickness (H):

$$E = -f \mid v_b \mid H \tag{2.8}$$

where f is a constant that describes hard bedrock erodibility. This assumes that the rate at which bedrock material is removed is not simply a linear function of basal ice velocity, but also of basal pressures because we assume that where erosion is occurring, basal debris concentrations will be high, and thus, as Boulton (1979) and Schweizer and Iken (1992) indicate, the overburden pressure will be important. The isostatic effect of sediment removal is accounted for but in this case we do not track or deposit any sediment once it has been removed from the bed. Rather we assume it is instantaneously removed from the system. The erosion rate can thus be simply tuned by varying f although here we are less concerned for now with the accurate prediction of absolute rates, and more with the prediction of the overall pattern and feedbacks with the erosion regime. We now outline each problem specifically and introduce results at each stage.

2.3 Problem 1

Our first experiments are aimed at understanding how initial topographies influence the configuration of an ice sheet and the establishment of a basal thermal regime. Additionally, this set of experiments will allow exploration of how sliding works in our model in comparison to how one might expect sliding to operate at large scales in a real glacial system. In this case, we do not incorporate our erosion model because we are interested only in the character of the ice mass in relation to the initial bed condition. The model of basal slip calculation used here is the simple binary prescription of t_b in locations where the bed is melting, and we use 2 different values in different experiments to determine the importance of the general magnitude of t_b to the initial state of the ice sheet.

In addition, the initial topographies (Fig. 2.1) range from 10 m white noise to landscapes that have either 7 or 21 valleys radiating from a central region of 1500 m

elevation with an additional 10 m white noise component where the cross profiles of the valleys are described by either a V-shape (i.e. fluvial cross-profile) or by a sine wave (i.e. a more glacially smoothed cross profile). We use such topographies in order to estimate in a broad fashion, the impact of particular preglacial topographic form upon the establishment of ice streaming, and thus upon the modelled distribution of erosion. The radial topographies are rotated slightly so that none of the valley troughs or ridges aligns with any of the 8 grid cell computation directions and the width of the valleys at any point will be proportional to the circumference of the overlying ice sheet. The white noise acts to model some initial random surface roughness that also stops ice flowing too fast and causing instability in GLIMMER.

The climate used to drive these latter experiments is prescribed by a flat ELA at 1450 m elevation with accumulation/ablation that alters with altitude in a parabolic fashion (Hulton et al., 1994). The mass balance/altitude curve is defined in this way in order that the accumulation and ablation of ice can be related purely to the surface altitude in the model, thus allowing the interplay between topography and air temperature to define how the ice sheet grows. The former experiments are driven by an EISMINT 2h type mass-balance scheme (Payne et al., 2000). We use this EISMINT scheme because we wish to compare the thermal evolution of our ice sheet model with the benchmarks provided by EISMINT and experiment h from this intercomparison determines that basal slip occurs only where basal ice is at melting point.

Thus, a matrix of experiments with differing starting topographies and mass-balances is carried out (Table 2.1). Each experiment is run on a 1280 x 1280 km domain with a resolution of 10 km over a period of 200 kyrs in order to build up a thermodynamically stable ice sheet. The domain has approximately the same dimensions as the EISMINT benchmarks but has twice the resolution. Despite this, we cannot hope to replicate any of the smaller scale features that as geomorphologists we are used to investigating and instead we focus on valley scale interactions between the ice and its topography. We discuss the implications of ice physics and scale in GLIMMER at a later stage .

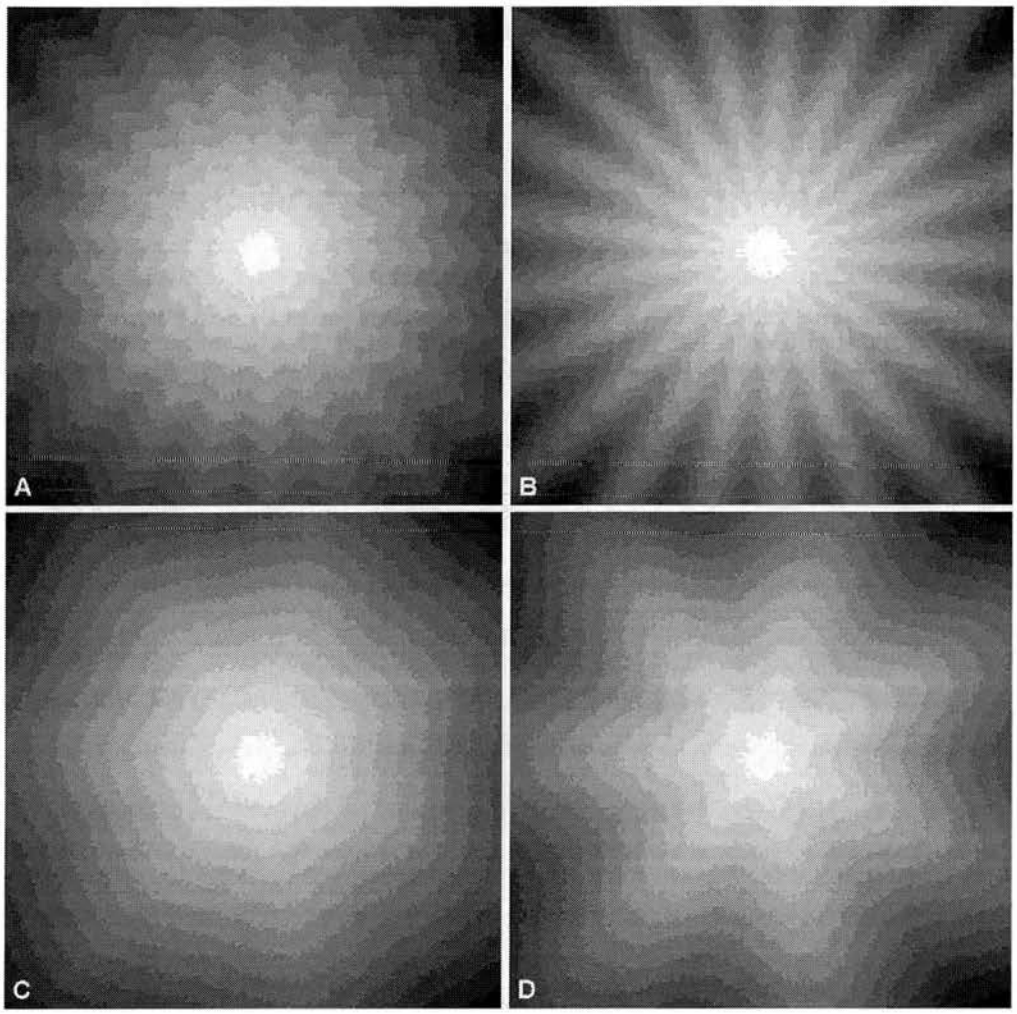

Figure 2.1: Synthetic basal topographies – radial valleys

A - 21 V shaped valleys, B - 21 sine shaped valleys, C - 7 V shaped valleys, D - 7 sine shaped valleys. All topographies range from 0 – 1500 m elevation. Grey shades = 100 m height bands.

Topography	**Mass-balance**	$t_b = 5\ \exp^{-4}$	$t_b = 2\ \exp^{-3}$
White noise	EISMINT 2h	A	B
21 radial (sine)	Altitudinal	C	D
21 radial (V)	Altitudinal	E	F
7 radial (sine)	Altitudinal	G	H
7 radial (V)	Altitudinal	I	J

Table 2.1: Experiment matrix – runs A-J.

We set t_b only where the bed is melting – values are either 5 $\exp^{-4}$ or 2 $\exp^{-3}$ depending upon the experiment.

2.3.1 Results and Discussion

The results of modelling for Problem 1 are shown in Figure 2.2. In the non-topographically constrained experiments (A and B) there is a marked contrast in the glaciological character between the low and high basal slip coefficient systems. Experiment A has a margin that is melting continuously at similar (and low) rates. The ice shows no particular tendency to stream and is stable. However, experiment B shows locally high variability in basal melt rates, and thus rapidly changing basal ice velocities that are manifested in narrow ice streams that display a flickering or switching behaviour. In summary, the fast flowing 'streams' within the models can disappear extremely rapidly (within tens of years), or equally quickly migrate to a new location. This switching behaviour between single model time steps is difficult to illustrate for the models in Problem 1, but we do so for a more extreme case in section 4.1 below. These experiments therefore demonstrate how stream width and the tendency to focus fast flow unstably into limited areas are controlled by basal traction.

The low basal slip parameter model (A) makes the ice quite 'stiff' and for a given surface gradient and thickness it flows less readily via sliding than under the higher basal slip coefficient model (B). Because the ice flows more freely in the latter case, it tends also to produce more frictional heating and also to strengthen convergence of ice (and thus also heat) into areas that start to flow more rapidly. Thus where ice is able to flow more freely in general, the feedback between flow and heating is also enhanced, accelerating the mechanisms that make hot fast flow concentrate spatially. Heat can be easily advected into the streams, and because the high inward velocities mean that it is difficult for the heat to diffuse or advect out of the ice stream, heat is further concentrated within them.

The high slip coefficient parameterisation (B) enables sharper temperature gradients to exist at the stream edges and permits more efficient local ice evacuation and ice surface gradient reduction. This contrasts with the low basal slip coefficient experiment (A) which in order to allow sufficient mass throughput requires a larger portion of the bed to operate at warmer temperatures, but which have lower average velocities. Even though the system operates with a larger area at pressure melting

point, the lower overall mean velocities tend not to permit such strong focusing of heat into streams.

The physical meaning of this experiment is that where the basal slip coefficient is high, for example, in situations which tend to promote high basal water pressures, not only will sliding rates be generally higher for a given ice thickness and surface slope, but also the flow is further concentrated into zones of accelerated flow. This has implications for the distribution for subglacial erosion, as we will show.

Experiments C and D add the sophistication of a radial valley topography with relatively close valley spacing. The results indicate that in C, ice streams are topographically confined towards the margin as they flow within the concave portion of the valley cross profiles. These confined ice streams are stable and do not demonstrate switching behaviour. In model D, which has a higher t_b parameter, the topography also influences the position of streaming with thin regions of fast flow occurring in each radial valley floor. However, unlike C, the ice streams are able to migrate laterally, and although they do not cross the ridgelines, they are not always in the lowest point of the valley. This suggests that although the underlying landscape affects ice sheet dynamics in that it determines the approximate placement of ice streams, it does not influence it sufficiently to turn off the thermal feedbacks which allow switching behaviour to exist. Instead, the t_b parameter is a more important influence on ice dynamics here because it defines the width scale of the ice streams. Where the width of the streams is smaller than the valley width, the streams are able to migrate laterally through time which implies that where ice is effectively more fluid (i.e. in a high basal slip coefficient system) ice dynamics are less affected by topographic variations.

Models E, G and I do not differ significantly from model C and experiments F, H and J show similar behaviour to D, despite the differing topographic form and frequencies. Model H in particular shows ice streams that are strongly related to the position of the valley floors (Fig. 2.2).

The characteristic on/off switching behaviour in some of models A-J is most likely exacerbated by the way in which t_b is prescribed in Problem 1. The basal slip coefficient is either zero or immediately at a maximum value, and due to its

relationship with basal velocities this means that there can be sharp changes in ice conditions – particularly in the high slip coefficient systems. This leads to instability because the ice is highly efficient at responding to temperature gradients, pushing ice through the system, lowering the surface gradients sufficiently to switch a particular stream off while an adjacent stream is generated to respond to steeper gradient ice surfaces beyond margins of the original stream.

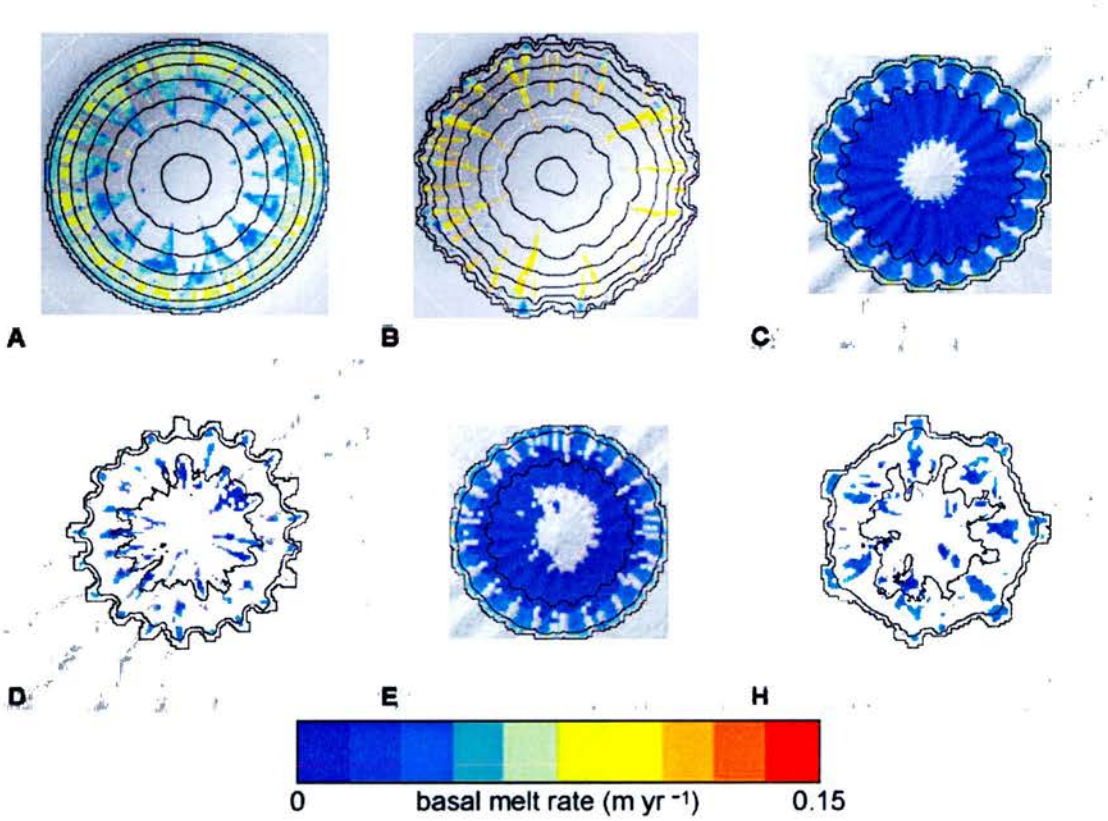

Figure 2.2: Selected ice sheet configurations for Problem 1 after 200 kyrs

Letters correspond to experiment numbers (Table 2.1). Coloured regions show basal melt rates when above pressure melting point. Black lines = 500 m ice thickness contours, white lines = 200 m basal topography contours, greyscale = hillshade of basal topography. It is important to note that all these models are driven by essentially the same climatic conditions and thus variations in the basal melt regime are entirely related to basal topography, and the parameterisation of the basal slip coefficient.

2.4 Problem 2

Our second set of experiments (see Table 2.2) is designed so that we can determine the impact that linking the basal slip coefficient to the basal melt rate might have upon the development of ice sheets. We use the same initial topographies and climates as experiments A-J, and keep the $t_{b\max}$ limited to the same values that were used in the Problem 1 experiments above. The only difference is that t_b is calculated as a function of the melt-rate at the base of the ice as outlined in section 2.2 above. Once again, erosion is not employed.

Topography	Mass-balance	Parabolic t_b up to 5 exp^{-4}	Parabolic t_b up to 2 exp^{-3}
White noise	EISMINT 2h	K	L
21 radial (sine)	Altitudinal	M	N
21 radial (V)	Altitudinal	O	P
7 radial (sine)	Altitudinal	Q	R
7 radial (V)	Altitudinal	S	T

Table 2.2: Experiment matrix – runs K-T.

The basal slip coefficient (t_b) is set as parabolic relationship with basal melt rate and can range up to the value indicated.

2.4.1 Results and Discussion

Figures 2.3 and 2.4 outline selected results from Problem 2. Experiments K and L contrast dramatically with models A and B. Experiment K illustrates a completely stable thermal regime with smoothly variable melting that increases towards the edge of the ice sheet and which is not perturbed by any streaming features. Maximum flow rates are ca. 55 m a^{-1}. Conversely, L shows massive scale switching behaviour (Fig. 2.4) where large portions of the ice mass alternate between being melting or frozen at the bed and large parts of the bed are sliding at up to 200 m a^{-1}.

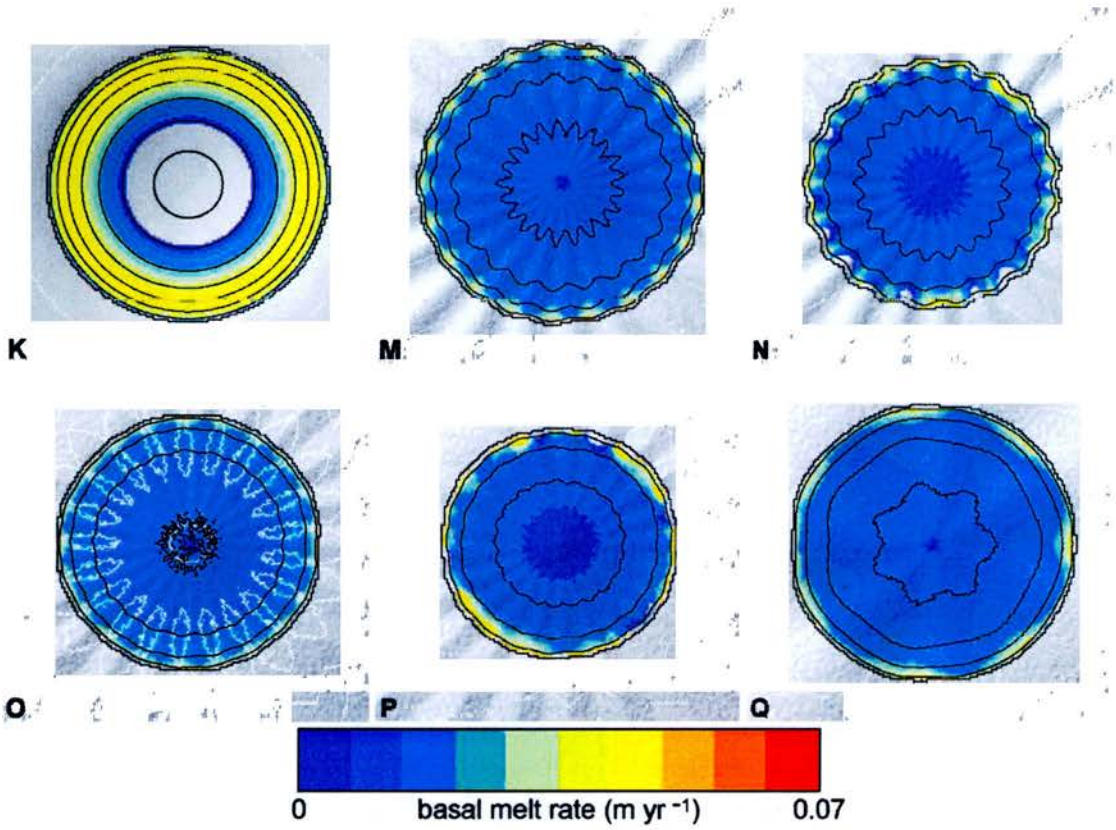

Figure 2.3: Selected ice sheet configurations for Problem 2 after 200 kyrs

Letters correspond to experiment numbers (Table 2.2). Coloured regions show basal melt rates when above pressure melting point. Black lines = 500 m ice thickness contours, white lines = 200 m basal topography contours, greyscale = hillshade of basal topography.

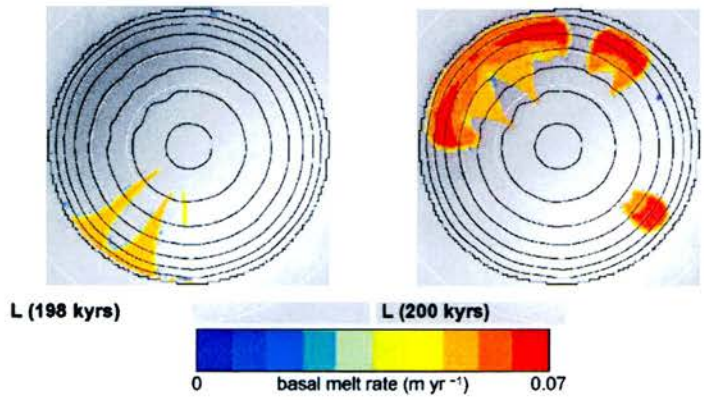

Figure 2.4: Switching behaviour in model L over 2000 years of model time

Coloured regions show basal melt rates when above pressure melting point. Black lines = 500 m ice thickness contours, white lines = 200 m basal topography contours, greyscale = hillshade of basal topography.

These experiments are informative about the role water plays at the bed of an ice sheet and the influence this has on the basal slip coefficient and thus the thermal regime of the glacier. With the higher t_b values capable of being generated in Experiment L, the ice velocities can speed up to a rate at which they can self-adjust to the thermal regime. That is, as frictional heating increases, the greater melting increases the slip coefficient, which allows the ice to slide more readily for a given surface gradient. This then leads to lower overall ice surface gradients for a given mass flux and reduces the relative amount of ice movement produced by internal deformation as against sliding and thus also lowering the internal heating rate within the ice. The steeper vertical temperature gradients that result cause more heat to be drawn into the body of the ice which in turn allows less to be available for melt at the bed. However, when the gradient lowers too much, heat production lowers past a critical threshold and sliding can no longer be maintained, causing large-scale switching. In the case of K, the low t_b values mean that the ice body is too 'stiff' to attain high melt rates and thus switching behaviour cannot occur.

These two experiments can be used as proxies for either rapid evacuation of basal water to a permeable bed (e.g. K) vs. a system where the melt cannot be removed so readily, thus promoting instability (e.g. L). It is also important to note the ease with which a stable non-streaming system can be generated given low enough basal slip parameter values – and that this contrasts with the results of the EISMINT 2 intercomparison tests of thermomechanical coupling in ice sheet models (Payne et al., 2000).

With the inclusion of the radial valley systems (selected results shown in figure 2.3), we see a repeat of the large-scale flickering in the higher t_b systems (N, P, R and T) as multiple ice fronts freeze around the same locality at the same time. However, outside these small frozen areas, all of these models show a bed that is almost entirely at pressure melting point. Models M, O, Q and S (lower t_b) show thermal stability from the outset and have relatively low basal melt rates. Given the contrast between this set of experiments and the equivalent models from Problem 1, this stability might be expected because the t_b is able to be smoothly and continuously

variable as against the binary nature of the t_b parameterisation in Problem 1. This is a clear illustration of the importance of basal hydrology treatment in models of ice sheet evolution – the impact of water on basal sliding rates is critical to the behaviour of ice and the way in which it interacts with its basal topography. However, it is also clear that it becomes much more difficult to generate ice streams in such a system, especially where topography is characterised by large wavelength features as is the case here.

2.5 Problem 3

To better understand the impact of erosion on ice sheet dynamics we now consider how quickly, and at what stage of glaciation a 'non-glacial' topography becomes 'glacial'. In this case we define 'glacial' as having recognisably glacial features such as overdeepened troughs. Here we include the ability to modify the glacier bed by using an erosion parameter linked to basal ice velocity and basal shear stress (as described in section 2.2). Firstly, we re-run experiment P twice using two different hard bedrock erosion parameters (f – see Eq. 8) to obtain different magnitudes of erosion from a similar ice sheet configuration. These models are designated W ('normal' erosion conditions) and X (high erosion conditions). Secondly, we use a variation of the experiments carried out in Problems 1 and 2 whereby we glaciate 2 topographies, each with multiple scale white noise over a central 2000 m peak. The first topography has a radial pattern designed so that valleys are aligned with the direction of ice flow (experiment Y) and the second displays noise stretched in a concentric ring fashion so that the valleys represent a barrier to ice flow (experiment Z). These two experiments will indicate whether significantly different degrees of landscape modification occur given opposite topographic orientations.

We then use GOLEM (Tucker and Bras, 1998; Tucker and Slingerland, 1996) to model a fluvial landscape upon which we can initiate an ice sheet using GLIMMER. GOLEM is run in large-scale detatchment-limited mode for 100 kyrs with a high block uplift rate of 0.005 m/yr that remains constant over this time in order to reach an approximately steady-state fluvial system. The periodic boundary conditions

originally present in GOLEM were switched off in order to generate a ridge-like fluvial topography with an elevation of zero along all boundaries. The resultant topography is a ca. 4000 m ridge that runs for 1850 km at 5km resolution (Fig. 2.5) with an additional 150 km border of zero altitude was added in order to accommodate any lateral isostatic effects. GLIMMER was then used to glaciate and erode this topography for a further 100 kyrs with a similar climate to that used in the radial topography experiments of Problems 1 and 2, but with an ELA of 1800 m. The basal slip coefficient is parameterised using the basal melt-rate method (section 2.2).

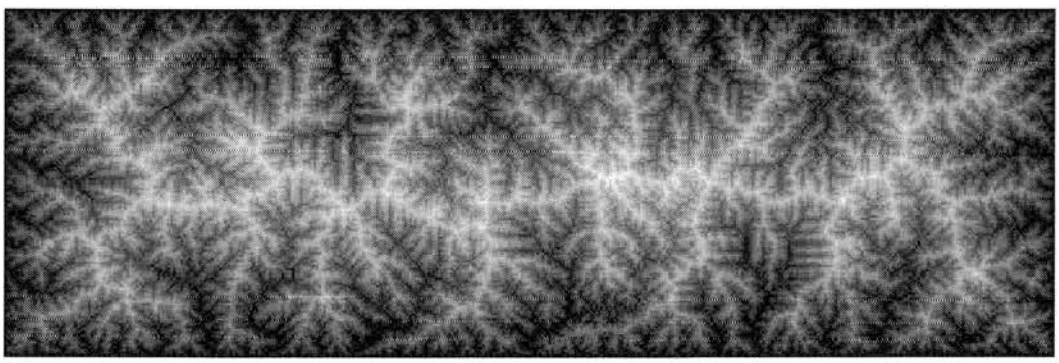

Figure 2.5: Topography generated by GOLEM
Elevations range from 0 m (black) to 4000 m (white).

2.5.1 Results and Discussion

In experiments W and X, bedrock erosion is included. Erosion occurs across the entire bed at rates of up to 0.8 mm yr^{-1} in model W, and 10 mm yr^{-1} in model X, with the greatest sediment excavation occurring in the topographic lows. The subglacial landscape thus heavily influences the distribution of erosion. Additionally, the flickering behaviour seen in experiment P is repeated in both W and X, but starts to die out as time progresses, and in model X the switching does not occur at all once the ice sheet has reached a stable marginal position, by which time up to 200 m of material has been moved from the troughs. We believe that this occurs because in the locations where bedrock erodes the tendency for this to lead to thicker ice causes an associated warming. Thus if the underlying topographic gradient across the edge of a

stream steepens, this tends to sharpen and then preserve the local contrast between areas of warm and cold ice.

Model Y, with its radial bed form, displays thin and focussed ice streams whose positions are largely conditioned by the nature of the bedrock shape (Fig. 2.6). Glacial incision is distributed according to the pattern of the ridges and troughs of the pre-existing topography because t_b is high enough to allow locally high variations in thermal regime and thus ice velocities. Run Z shows rather different results and was designed to show where erosion was focussed if the ice sheet was presented with topographic barriers at the bed. As can be seen in Figure 2.6, the erosion of material has largely ignored the local scale topographic variation, which displays local relief change of ± 600 m in places. Instead the erosive energy of the ice sheet has largely followed the ice surface gradient and has smoothed large fan-like areas of the bed. The width of these eroded regions is controlled by the magnitude and pattern of the basal slip coefficient. Furthermore, despite t_b values that can be as high as in models L, N, P, R and T from Problem 2, the beds here are not fully at melting point. Instead, it would appear that the high frequency topographic variation is bringing about more streaming and further, the pattern of melt is reverting back to a similar distribution as can be seen in experiment A, and in the EISMINT 2h experiments of Payne et al. (2000). Model Z shows that although we think of glaciers as merely modifying the pre-existing fluvial topography, in reality we suggest that the glacial thermal regime will be driven by the direction of ice surface gradient. Experiments Y and Z together indicate that if the topographic lineations are oriented similarly with the ice surface gradient then the flow regime of the ice sheet will reflect these, but will not be the primary control.

Profiles of the topographies before and after glacial incision (Fig. 2.6) illustrate that in places local relief has remained virtually unchanged. However, in other areas where trough excavation has been strong and the intervening ridge has remained protected, local relief has increased significantly, as have summit elevations, supporting the conclusions of a number of previous studies (e.g. Brocklehurst and Whipple, 2002; Molnar and England, 1990; Small and Anderson, 1998; Whipple et al., 1999). As ice streams erode on either side of a ridge, the interplay between erosion and subsequent local isostatic adjustment causes local relief to increase (in

this study by up to 300 m over a 30 kyr period) with the majority of this relief change occurring through glacial erosion rather than isostasy.

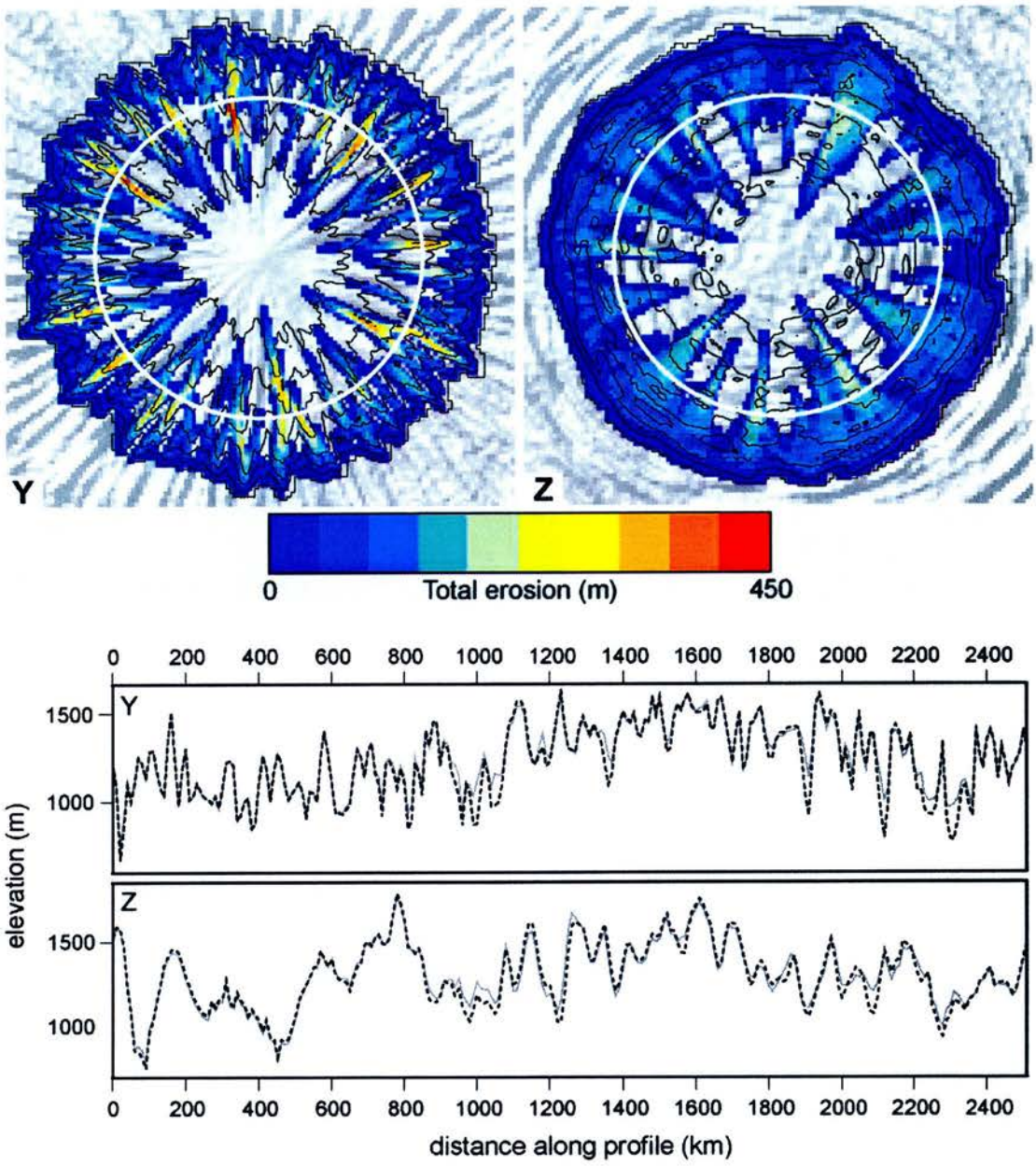

Figure 2.6: Distribution of erosion in experiments Y and Z

Coloured regions show total erosion in metres after 30 kyrs. Black lines = 500 m ice thickness contours, white circle = location of profiles, greyscale = hillshade of basal topography. Profiles of bedrock elevation taken at 400 km radius from centre. Grey line = original topography, dashed black line = topography after 30 kyrs modelled erosion and then 30 kyrs isostatic rebound. Note focussed lines of erosion in Y in contrast to wider fan-like pattern of erosion in Z.

Figure 2.7 shows the pattern of sediment removal over the GOLEM topography during the modelled time period along with ice thickness, vectors of ice flow and a longitudinal profile along the lower portion of one of the major valley systems. Erosion occurs low down in the valleys reflecting the areas where the ice is able to warm up and flow at higher velocity. The use of basal melt rate in the calculation of the basal slip parameter means that the erosion is smoothly variable under the areas of warm based ice. The result is that the valleys are beginning to be opened out as well as overdeepened – exactly what one would expect to see in a glaciated landscape. If basal hydrology were treated more fully, one might expect that local variations in water pressures would lead to more rapidly variable basal slip coefficients. However, this variation is still likely to be relatively smooth when compared to a model that ignores water production in its calculations because beyond certain pressures the basal slip parameter will remain relatively little affected.

We are unable to determine from this experiment whether glacial erosion would be maximised in the early stages of glaciation vs. later glacial cycles. However, with the hard bedrock erosion constant used in this run we achieve ca. 150 metres of erosion at rates of up to 3 mm yr^{-1} in the lower reaches of the topography after 100 kyrs. This is a medium rate (cf Hallet et al., 1996) but already we see the longitudinal profile of some valleys become modified and recognisably glacial. Indeed, Figure 2.7 illustrates that the pattern of erosion is narrowly focussed in the upper reaches of the orogen, and that it becomes broader towards the range front, a result that is supported by topographic analysis of Inugsuin fjord in Baffin Island (Løken and Hodgson, 1971) and the Lambert basin region of East Antarctica (Jamieson et al., 2005) as well as in analytical modelling by Anderson et al. (2006). Additionally, this pattern of erosion vs. preservation is supported by studies that note the survival of relict landscapes in the interior of the region that was covered by the Fennoscandian ice sheet (Fabel et al., 2002; Kleman and Stroeven, 1997; Li et al., 2005; Stroeven et al., 2002a).

Should the ice sheet not have grown, and if fluvial erosion were to have continued for an extra 100 kyrs, the pattern of erosion would have been significantly different. Material would instead have been removed around the central ridge area where

steeper, less stable slopes are denuded, and where high energy bedrock streams are able to incise.

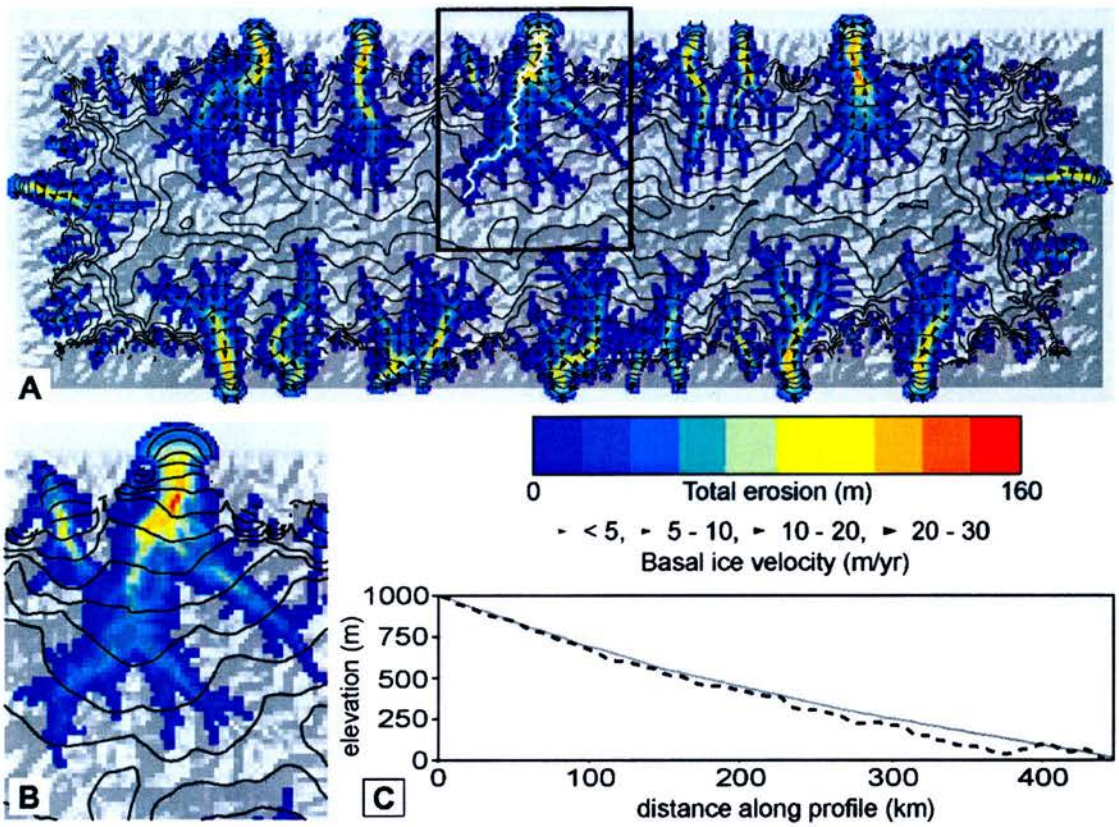

Figure 2.7: Glaciation of a fluvial topography

A - Results from glaciated GOLEM topography. Coloured regions = sediment eroded (up to 160 meters), black arrows indicate direction and magnitude of basal slip velocities drawn at ¼ density. Position of profile marked by white line. B - close up of pattern of erosion across one major basin – position shown by black box in Figure 2.7A. C - Valley longitudinal profile shows pre-glacial fluvial topography (grey) and post-glacial rebounded topography (dashed black). Overall, the pattern of erosion is highly selective, contrasting significantly with the more even erosion rates that would apply in a mature fluvial regime that was eroding in balance with constant tectonic uplift.

2.6 Further Discussion and Future Directions

2.6.1 Landscape Characterisation and GLIMMER

The physics employed in GLIMMER currently do not account for longitudinal stress calculations. Instead, the shallow ice approximation is employed whereby the physical assumptions in the model are only valid if the thickness of an ice sheet is small compared to its lateral extents. This means that the ice cannot respond adequately where basal topography causes ice to flow round bumps that are of a smaller lateral scale than the ice thickness and therefore any topographic interaction with the ice cannot currently be modelled correctly at scales of below 5 km. This has an impact upon how we can determine whether our erosion model is generating good results and our ability to represent topographic forms typically produced in glaciated landscapes.

A comparison with real-world topography often forms the basis of morphometric analysis of model output (e.g. Brardinoni and Hassan, 2006; Brocklehurst and Whipple, 2004), and the recent trends in DEM resolution mean that a glacial terrain is easy to visually identify in high-resolution data. However, because the physics in GLIMMER (as well as many other ice sheet models) limits the resolution, it becomes much more difficult to compare model output to landscapes of known evolution because detail that might discern a fluvial from a glacial landscape is less visible at 5-10 km scales. As previously indicated, one of the most effective indicators that a landscape is evolving from one state to another is the change through time of the river longitudinal profile which is relatively scale insensitive if it covers a sufficient distance. We have already used these to demonstrate that it is possible to generate reasonable patterns of erosion over a range of topographies – some more realistic than others. Topographic profiles may provide us a limited window into the character of topographic evolution that has occurred in GLIMMER, but they do show us that we are generating suitable glacial landscapes when compared with others who have sought to model glacial erosion processes (e.g. Anderson et al., 2006; Brocklehurst and Whipple, 2002; MacGregor et al., 2000). Future developments of our erosion model will include a companion system that seeks to characterise and distinguish

glacial landscapes in a more robust and spatially distributed manner in low resolution digital topographies.

2.6.2 Basal Slip and the Importance of Water

The results of our modelling have shown the importance of the parameterisation of the basal slip coefficient, which describes how slippery the ice sheet can be at its base. This parameter has a strong influence on the behaviour of the ice sheet and in particular, it determines how the ice slides over its bed topography and how easily regions of fast flow can form within the ice and therefore is a critical influence upon patterns of erosion in our model.

Critical to our calculation of basal slip is the rate at which the basal ice is melting. However, under a real glacier, basal melt-rate is not the only influence upon the amount of water reaching the bed. Surface melt water, and its migration to the ice-bed interface is likely to be of critical influence to the sliding behaviour of the ice (Paterson, 1994), and thus will play an important part in determining the pattern and magnitude of erosion. The problem of determining water pathways through ice and subsequent basal water pressures is a difficult one, and thus its inclusion in numerical models of ice sheets is not yet commonplace. However we have demonstrated how important it may be in determining the long-term evolution of landscapes during glacial times. This supports findings by Näslund et al. (2005) who go on to indicate that the correct spatially variable parameterisation of geothermal heat flux is also critical when the amount of sliding at the glacier bed is coupled to the amount of water at the bed.

2.6.3 Modelling Landscape Evolution in Reverse - Backstacking

In this paper, we have modelled landscape and ice sheet evolution forward in time. The combined parameterisation of erosion and the basal slip coefficient has resulted in realistic changes in longitudinal profile evolution, and a predictable spatial distribution of topographic change. Previous work has indicated that it is possible to model landscape evolution under ice sheets in reverse, thus predicting preglacial

topographies (Jamieson et al., 2005). This relies on a technique called backstacking whereby material is not eroded, but is deposited in regions where ice sheet models indicate erosive processes are occurring, thus reconstructing the pre-existing landscape. The approach we have developed in this paper offers the opportunity to refine this backstacking methodology and will enable us to gain a clearer understanding of the feedbacks between real ice sheet systems and their beds over a range of time scales from 10^5 to 10^7 years.

2.7 Conclusions

The numerical modelling approach employed here to investigate various aspects of long-term landscape evolution under ice sheets has given us an important insight into the importance of basal processes and how they feed back into ice dynamics. In particular, we assert that:

- The basal slip coefficient is a key influence upon basal thermal regime pattern. A high parameterisation of the basal slip coefficient (t_b) can cause a thermal feedback due to sharp temperature gradients. Heat is advected into streams, and cannot escape causing rapid ice draw-down until the gradient is insufficient to sustain flow. This is manifested as on/off switching of ice streams. Lower t_b values can stabilise the system because the ice is too stiff to respond quickly to local temperature gradients and so a larger portion of the bed must be at a more constant temperature in order to allow enough ice to be drained through the system.
- The parameterisation of the basal slip coefficient is a critical influence upon the way in which the ice interacts with its bed. A binary type parameterisation may exaggerate any thermal feedbacks, particularly in high t_b systems, because of the steep gradients of temperature that exist under such a system. When production of water at the base is accounted for in the t_b calculation, the system can be either incredibly stable (low t_b values) or can demonstrate large scale tendency to melt or freeze at the bed. This may be a proxy

indicator for how permeable vs. impermeable bed conditions influence the behaviour of ice sheets, or for how well developed the subglacial drainage systems might be.

- The large-scale morphology of the bed shows a greater influence under lower t_b systems because the ice is not fluid enough to respond to thermal instabilities within the ice. Ice streams are more able to migrate within a valley in a high slip coefficient system because of the width-scale of ice streams that can exist under such fluid ice conditions. The thermal feedback allows streams to switch within a single valley in this case. Under lower slip coefficient systems, the width-scale of the ice streams are such that fewer thermal instabilities result, and the system remains largely confined by the preglacial topography.

- Erosion may be influential in stabilising the thermal regime of an ice sheet. As existing valleys are overdeepened they are more likely to become the permanent location of warm-based ice.

- The pattern of erosion that occurs when an ice sheet grows upon a purely fluvial system is somewhat different to what would be expected had the system remained fluvial. Sediment is excavated closer to the ice margins where the ice is warm, with the up ice regions remaining cold based and protective of the bed. In a fluvial system, where slope failure and river incision are the main erosive agents, denudation occurs higher in the catchments where slopes are steeper and rivers have higher energy.

- The degree of topographic alteration required for a landscape to become glacial is difficult to assess. However within a single modelled 100 kyr glacial cycle, and under modest glacial erosion conditions, we are able to show that a preglacial fluvial landscape can display some recognisable elements of a glaciated landscape – particularly in the lower reaches of valley longitudinal profiles.

- The erosion component of GLIMMER will enable us to investigate long-term landscape evolution in regions such as Patagonia and Antarctica where basal modification may have led to a progressive diminution in ice extent with

successive glaciations through the Quaternary (Clark and Pollard, 1998). Furthermore, our approach may help reconcile the apparent discrepancy between maximal ice sheet extents that are asynchronous with maximum Northern Hemisphere ice volume.

Chapter 3 How Does Topography Control Glacial Erosion?

3.1 Introduction

3.1.1 Aim

Our aim is to test the ability of topography to act as the critical control upon the distribution of erosion under an ice sheet. Topography is important in influencing patterns of glacial erosion in much the same way that it determines patterns of fluvial erosion. However, given the inaccessibility of a glacier bed, it is difficult to identify the scales and components of topography that drive these patterns. We use a numerical modelling approach to determine the relationship between glacial erosion and basal topography by growing ice sheets over a number of synthetic landscapes. These topographies have different scales of vertical and horizontal features and thus allow us to test the degree to which various components of landscapes drive glacial erosion patterns.

3.1.2 Justification

Numerous studies have sought to decipher patterns of erosion under former ice sheets but, as Fabel et al. (2004) suggest, determining past landform change in relation to large scale glacial erosion is a particularly challenging aspect of geomorphological enquiry. This study is important because quantitative interrogation of the interactions between ice sheets, topographic scale and form, and glacial erosion will show how significant pre-existing topography is at influencing or driving subsequent landscape evolution under ice sheets. Furthermore, we may discover the stage in the transformation towards a glaciated system at which the greatest degree of change occurs. This work therefore bridges the gap between field investigations of erosion patterns and numerical modelling of past and present ice sheets to help build a more integrated picture of long-term landscape evolution under glacial conditions.

Investigation of the scales at which ice masses are influenced by bed morphology is important because it will aid with the interpretation of past ice mass behaviour, and with the prediction of future dynamic behaviour. Furthermore, clarifying the role of topography in controlling ongoing landscape evolution patterns will aid understanding of glacial landscapes across the globe.

3.2 Background

Much of the present day Earth's surface has been conditioned by erosion under the waxing and waning of ice sheets. This modulation is driven by orbital forcing (Hays et al., 1976) and is perturbed by complex interactions between tectonics (Molnar and England, 1990; Raymo and Ruddiman, 1992), atmospheric CO_2 concentrations (DeConto and Pollard, 2003b), oceanic circulation (Kennett, 1977), atmospheric circulation (Heusser, 1989), and denudation both by ice (Harbor et al., 1988; Oerlemans, 1984; Tomkin, 2003) and hillslope processes (Whipple and Tucker, 2002) as well as by ice sheets themselves (Blunier and Brook, 2001). Thus the evolution of the landscape and of ice sheets are intimately and reciprocally linked; the landscape is partly responsible for determining the pattern of erosion, leading to alteration of the bed topography and thus to perturbations in the relationship between the landscape and the ongoing distribution of glacial erosion.

3.2.1 Topography and the Distribution of Erosion

The feedbacks between topography and erosion are not well studied. Nonetheless, it is clear that topography is one of the central drivers of the spatial distribution of erosion under ice because geometry of the subglacial landscape controls ice mass behaviour (Glasser, 1995; Taylor et al., 2004).

The pattern of glacial erosion of bedrock is most fundamentally controlled by basal thermal regime and in particular by the requirement for basal ice to be at pressure melting point to allow basal water production and sliding (Paterson, 1994; Sugden and John, 1976). Whether or not the bed is at pressure melting point is largely

determined by ice thickness and by basal ice velocity (Boulton, 1979). Patterns of ice flow are thus determined by the presence of ridges and troughs. For example, the presence of a large-scale valley may cause ice flow to converge, focussing flow and generating *selective* erosion. Alternatively, a lack of topographic variability (e.g. a plateau) can mean erosion will be *areal* in nature. Under thin, cold-based ice, the ice mass provides a *protective* cover (Kleman and Stroeven, 1997; Stroeven et al., 2002b). This classification of *selective* erosion (higher erosion rates, focussed flow), *areal* scour (lower erosion rates, unfocussed flow) or cold-based *protection* (little or no erosion of basal flow) was introduced by Sugden and John (1976) and was used to relate ice dynamics to the visible geomorphology.

Additional factors that determine erosion patterns include: the geothermal heat gradient; effective pressure (ice overburden pressure minus basal water pressure), which determines the magnitude of friction operating at the bed; lithology, where softer rock is more susceptible to erosion; debris concentrations, which can either aid with abrasion by acting as 'tools', or, if deep enough, may essentially protect the bedrock landscape; and meltwater production rates which can determine localised increases in velocity, or variations in effective pressure (Boulton, 1979; Hallet, 1979; Hallet, 1996; Harbor, 1995; Näslund et al., 2005; Oerlemans, 1984; Paterson, 1994; Schweizer and Iken, 1992; Sugden et al., 2005). Subglacial topography is critical in influencing many of these factors and as a landscape is modified by ice these relationships change.

3.2.2 Numerical Models of Ice and Glacial Erosion

That topography influences ice dynamics, and therefore the distribution of erosion, is widely recognised. However, quantitative data regarding the magnitude of this influence has rarely been sought. We distil the problem to its simplest form and revisit the perennial question of scales in geomorphology. We suggest that understanding the influence of different scales (horizontal and vertical) of topography upon ice dynamics will aid future interpretation of such landform assemblages. A number of studies relate the present day form of previously glaciated terrain to output from numerical models of ice sheet dynamics (Glasser, 1995;

Näslund et al., 2003). These show that bed geometry is critical to determining ice behaviour, and indicate the importance of being able to model the impacts that topography has upon the thermal field and flow dynamics of an ice mass. Numerical models of ice sheets and of landscape evolution therefore provide ideal tools with which to investigate the feedbacks between ice dynamics and topography.

As glaciation proceeds, landscapes move towards an equilibrium with the overlying ice sheet (Penck, 1905). The overdeepening and transformation of fluvial 'V-shaped' valleys towards 'U-shaped' glacial troughs indicates the increased efficiency with which a topography can evacuate ice (Evans, 1969). Therefore, much glacio-erosional modelling work has focussed upon this transformation (Harbor, 1992; Harbor, 1995; Harbor et al., 1988). However, the V- to U- transformation occurs on a small scale when compared to that of overdeepening along the line of ice flow. This is where we focus our research, a vector of landscape evolution that has previously been modelled in two dimensions on a valley scale (Anderson et al., 2006; MacGregor et al., 2000), albeit without resolving the full thermal regime of the overlying glacier.

Early work by Oerlemans (1984) made the first attempt to bridge the gap between qualitative geomorphology and a quantitative theory of glacial erosion on an ice sheet scale. He modelled erosion as a function of sliding velocity and normal pressure (e.g. Budd et al., 1979) in preference to the model of Boulton (1974) which identifies ice thickness as a control. Although these models all reproduce 'glacial' landscapes, they have never been used to quantify the scale of pre-existing topographic variations required to focus flow, and none operate on a full ice sheet scale. Here we attempt to bridge this gap in understanding using numerical models of glacial erosion under ice sheets as they are superimposed upon pre-glacial landscapes of a schematic nature.

3.3 Method

Although topography is critical to the behaviour of the ice mass, and thus to ongoing patterns of glacial landscape evolution, it is not clear which components of the

landscape are most influential. We test this by breaking landscapes into individual components, such as relief or wavelength and by modelling ice sheet and landscape evolution over synthetic landscapes that characterise these components at different scales.

3.3.1 Objectives

Using this systematic approach we aim to meet the following objectives:

- To use a numerical ice sheet model (GLIMMER - Jamieson et al., 2008; Payne, 1999; Rutt et al., Submitted) to simulate glaciation and erosion over a range of synthetic topographies which display different wavelengths and amplitudes and to observe how these differences in lateral and vertical scale impact upon erosion patterns and rates of landscape evolution under ice.
- To employ a numerical landscape evolution model (GOLEM - Tucker and Bras, 1998; Tucker and Slingerland, 1996) to generate artificial fluvial topographies at a range of amplitudes. These will be glaciated to observe any impact that pre-existing river morphologies may have upon the erosional signal.
- To assess the sensitivity of the model of glacial erosion to identify the importance of basal conditions in perturbing the scales at which landscapes can drive the distribution of glacial erosion.
- To consider whether the pattern of erosion is more strongly controlled during early or during later glacial cycles.

3.3.2 The Ice Sheet Model

Well known physical laws relating to the dynamics of glaciers have long been incorporated into numerical models of ice flow so that predictions might be made about past, present and future ice sheet behaviour (e.g. Hulton et al., 1994; Huybrechts and Le Meur, 1999; Oerlemans et al., 1998). In this work, we use

GLIMMER (General Land Ice Model for Multiply Enabled Regions - Payne, 1999), a community developed ice sheet model that builds upon the foundations laid down by the modelling studies of Huybrechts (1986), Boulton and Payne (1992), Payne and Dongelmans (1997) and Jamieson et al., (2008). The ice dynamics calculations implement the widely-employed shallow ice approximation (Hutter, 1983) which assumes that bedrock and ice surface slopes are small enough that normal stress components can be neglected. The ice flow law parameter is handled by a three-dimensional thermomechanical model. A full outline of the numerics implemented in GLIMMER is provided by Hagdorn et al. (2005) and (Rutt et al., Submitted), and Paterson (1994) provides a useful context to the derivation of these mechanics.

The critical component in the context of modelling landscape evolution under ice is the implementation of an erosion rule and the parameterisation of the basal velocity calculations upon which erosion relies. In this case, as in previous work (Jamieson et al., 2008), we determine a bulk erosion rate E following Boulton (1974) thus:

$$E = -f \mid v_b \mid H \tag{3.1}$$

Where H is ice thickness and (v_b) is basal velocity. f is a parameter describing bedrock erodibility. Where basal ice temperature reaches pressure melting point (taking into account both geothermal and frictional heat contributions), ice decouples from the bed and begins sliding (and thus eroding) due to the presence of water. Its ability to do so in the model is a function of the basal slip coefficient (t_b - also known as the basal traction parameter) which specifies the dependence of the thermomechanical properties of ice upon effective pressure. Higher t_b means that the ice is more *freely able* to slide over the bed (i.e. there is decreased traction) and that the length scales over which ice can accelerate from zero to maximum sliding rate are shortened.

The basal slip coefficient may act to influence glacier behaviour in the same way as we expect deformable sediment availability or basal water saturation to influence ice motion. It is therefore a parameter that effectively combines a number of controls

acting at the bed into a single function. The use of t_b is a standard approach, and we determine it as a parabolic function of basal melt-rate (Jamieson et al., 2008). Once a critical melt-rate is achieved, the basal slip coefficient is no longer able to increase. We have shown that such an approach allows the patterns of basal ice flow that might be associated with ice streaming to be modelled (Jamieson and Hulton, Submitted; Jamieson et al., 2008; Jamieson and Sugden, 2008). Velocities of basal ice are then determined as a function of t_b and of basal shear stress (τ_b) at any one point as follows:

$$v_b = t_b \tau_b \tag{3.2}$$

To ensure results can be compared to real-world systems an Earth model accounts for the elastic behaviour of the lithosphere under variations in load (Lambeck and Nakiboglu, 1980) as generated in this case by both changes in ice thickness and by erosion of bedrock material. This latter inclusion is important as it ensures that as bedrock is removed by glaciation, the landscape is adjusted. Thus modelled ice dynamics can react to ongoing landscape evolution in as realistic manner as possible.

3.3.3 Topographic Boundary Conditions

In glaciating and eroding synthetic landscapes we are controlling the pre-existing geomorphic signal. Thus in contrast to any real-world topography, where complex successions of landscape modification leave their mark on a topography, our results will not be confused by multiple signals of evolution. By controlling the input topographies the character of the feedbacks that exist between glacial erosion and the subglacial landscape can be more readily analysed. Two classes of synthetic topography were generated as inputs to the ice sheet model.

The first class of synthetic topographies consist of a matrix of systems which have variations in wavelength and in relief (Table 3.1). These are generated by superimposing multiple wavelengths (10 km, 30 km, 60 km and 120 km) of white noise upon one another. The amplitude of noise at each wavelength changes so that

the 30 km noise has two times the relief of the 10 km, and the 60 km is two times that of the 30 km noise and so on. Each system is scaled to make multiple versions of each with different overall relief (10 m, 100 m, 500 m, 1000 m). The topographies therefore have hollows and peaks at multiple scales.

Because we are interested in the influence of wavelength in perturbing ice and erosional behaviour, we construct 2 further sets of similar landscapes in which the largest topographic wavelength is 60 km and 30 km respectively. A topography with a particular maximum wavelength also contains noise at all other wavelength below this scale. Figure 3.1 shows examples of these topographies and Table 3.1 shows the details of each topography.

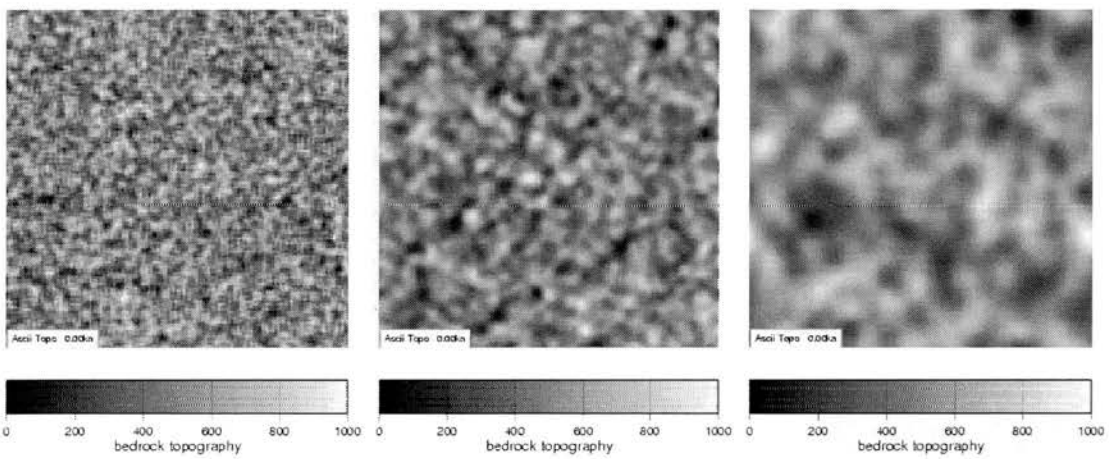

Figure 3.1: Synthetic landscapes generated by multiple wavelength white noise

Left – 30 km maximum wavelength; Middle – 60 km maximum; Right – 120 km maximum. Domains are 1280 x 1280 km in size at 10 km resolution.

The second class of landscapes are generated using GOLEM, a geomorphic and orogenic landscape evolution model (Tucker and Bras, 1998; Tucker and Slingerland, 1996). They have a fluvial fingerprint with no glacial overprint and are effectively 'steady-state' landscapes so that bias from other processes (as might be expected from a real world topography) is not introduced. Multiple versions of this topography are scaled to generate varying relief equivalent to regions of differing tectonic uplift rate. The topographies have a central higher elevation zone, and the fluvial systems drain radially from this area (Figure 3.2) in a similar way that the

present day English Lake District in the UK. Table 3.1 outlines the details of these topographies.

By glaciating these systems, we will identify whether the erosion pattern is dictated by the fluvial geometry of the bed to a greater or lesser extent in comparison to the increasingly glacial system or when compared to the white noise landscapes. In investigating this we test the ideas of Penck (1905) who suggested glacial erosion increases drainage efficiency over that of a fluvial system.

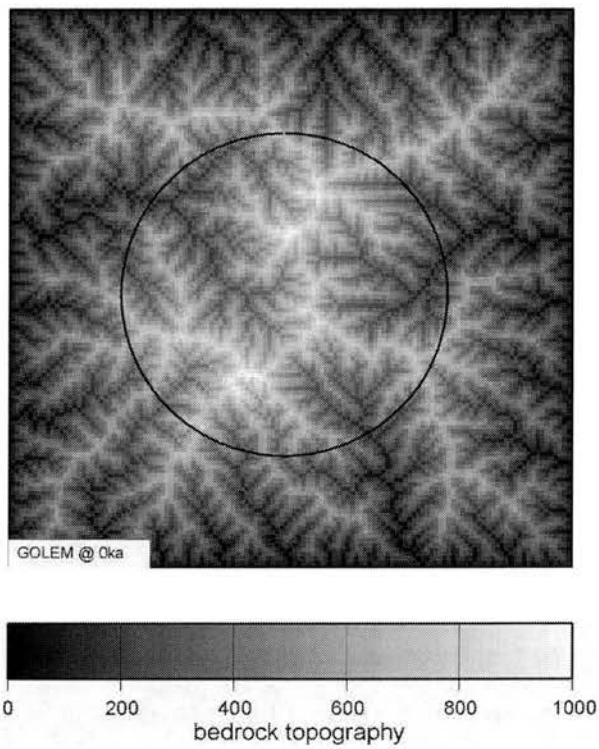

Figure 3.2: The fluvial synthetic topography.

Note that elevation decreases to zero at the edge of the domain. The circle notes the position of profile used in the results section. Topography generated using GOLEM landscape evolution model (Tucker and Bras, 1998; Tucker and Slingerland, 1996).

3.3.4 Climatic Boundary Conditions

The climatic forcing used to drive these experiments describes accumulation and ablation as a parabolic function of distance from the central point of the model domain in a similar manner to the forcing used in the EISMINT benchmark tests for ice sheet models (Huybrechts and Payne, 1996; Payne et al., 2000). Mass balance (M - Equation 3.3) declines from a maximum, M_{max} of 0.5 m yr^{-1} at the centre (x_{centre},

y_{centre}), to zero at a radius R_z of ca. 450 km. M_{slope} describes the rate of accumulation change per unit distance and the radius is weighted such that the rate of change of M becomes steeper with distance from the centre.

$$M(x,y) = \min\left[M_{\max}, M_{slope}\left(R_z - \left(\sqrt{(x - x_{center})^2 + (y - y_{center})^2} \right) \times 1.2 \right) \right] \quad (3.3)$$

This parameterisation of mass balance gives a large central accumulation area within which M is sustained at its maximum and surrounded by a region where ablation ever more rapidly removes mass with distance from the domain centre.

Air temperature at the ice surface is defined by an inverted and rescaled version of Equation 3.3, with a minimum of -20 °C in the centre radiating to a maximum air temperature of 5 °C at the domain corners.

Given a flat bed topography, this style of forcing will generate a circular ice sheet and radially symmetrical ice dynamics (Huybrechts and Payne, 1996; Payne and Baldwin, 2000). The symmetrical nature of these two forcing parameters means that any non-symmetrical behaviour predicted by the model once topography is introduced must be the result of the interaction between ice and bed geometry. Therefore as the topographic boundary condition is varied, we can observe the resultant changes in erosion distribution. Climate remains static throughout the experiments, so any change in accumulation or ablation is driven by topographic (erosional or isostatic) or ice surface geometry changes.

3.3.5 The Experiments

Table 3.1 collates the main characteristics of each of the 32 model runs in our suite of experiments. We vary the topography type (i.e. fluvial vs. noise), topographic relief, maximum topographic wavelength and the maximum allowable t_b value (allowing us to test the impact of changing basal conditions). These specific t_b parameters are chosen to represent end-member states of basal slipperiness that

might be encountered in the real-world (Jamieson et al., 2008). All model domains are 10 x 10 km resolution on a 128 x 128 grid. Experiments are run for 15 kyr using absolute erosion rates which are at least 10 times higher than might expected in reality (Bogen, 1996; Hallet et al., 1996). Time and absolute erosion rates are effectively interchangeable because as Equation 3.1 shows, erosion rate is calculated as a linear function of bedrock erodibility (f). Therefore, if high erodibility is parameterised, erosion will be greater over a given period in comparison to a low erodibility model. In this way, we compress the amount of model time required to glacially erode a landscape over a 150 kyr period into a 15 kyr period.

Experiment Matrix:	**N_{30} 10**	**N_{30} 100**	**N_{30} 500**	**N_{30} 1000**	**N_{60} 10**	**N_{60} 100**	**N_{60} 500**	**N_{60} 1000**
$t_{b\ max}$ **2e-3**	*1*	*2*	*3*	*4*	*5*	*6*	*7*	*8*
$t_{b\ max}$ **5e-3**	*17*	*18*	*19*	*20*	*21*	*22*	*23*	*24*
	N_{120} 10	**N_{120} 100**	**N_{120} 500**	**N_{120} 1000**	**G 10**	**G 100**	**G 500**	**G 1000**
$t_{b\ max}$ **2e-3**	*9*	*10*	*11*	*12*	*13*	*14*	*15*	*16*
$t_{b\ max}$ **5e-3**	*25*	*26*	*27*	*28*	*29*	*30*	*31*	*32*

Table 3.1: Experiment matrix

This table identifies the numbering system used in this paper and the associated details of each model run. The numbers in italics indicate the experiment number which will be referred to in the results and discussion. N = Noise topography – subscript denotes maximum (dominant) wavelength (km); G = GOLEM topography; 10/100/500/1000 = topographic relief in metres; $t_{b\ max}$ = maximum basal slip coefficient value.

3.4 Results

We first present some summary results showing key variables at the end of the simulations. We go on to show how some of these variables change through time and space in each model run. This approach allows us to identify broad trends relating to landscape modification under ice, and to identify critical spatial and temporal patterns related to the feedbacks between ice sheets and glacial erosion. It is important to note that absolute values of erosion are unimportant in the context of this work due to the interchangeable nature of time and erodibility (f). Rather, it is the relative values between experiments that inform us about how patterns of

landscape evolution can change in relation to the types of topography being glaciated.

Figure 3.3 (a-d) shows summary statistics for each model. We first consider average erosion rates from the systems as these are analogous to the information used to monitor rates of landscape change using, for example, offshore sediment volumes (e.g. Bogen, 1996; Taylor et al., 2004). Such measurements essentially indicate the overall susceptibility of an ice drainage system to glacial erosion. Here, we calculate average erosion rate excluding cells where no erosion occurs – i.e. areas where cold-based ice has dominated are not included in the calculation.

As Figure 3.3a shows, average erosion rate is overwhelmingly sensitive to the value chosen for the basal slip coefficient. The relationship between wavelength, relief and average erosion rate is confused in low slip coefficient systems, with no obvious trends visible. However, Figure 3.3a demonstrates that under high t_b conditions, increasing average erosion rate is correlated to increasing topographic wavelength. In longer wave, high slip coefficient systems there is also a positive correlation between average erosion rates and relief. Intriguingly, there appears to be a negative correlation between relief and average erosion rate in the systems that use the 'fluvial' GOLEM topographies under high basal slip coefficient conditions. On the whole however, this change is relatively small scale. With lower values of t_b, the relationship between relief and average erosion rate is unclear.

With changing relief, the range of average erosion rates experienced across different wavelength systems becomes wider as relief increases in high t_b systems. In contrast to this, low t_b conditions cause the range of average erosion rates to become smaller with increasing relief. Basal traction (i.e. basal conditions) thus appears to exert the strongest control on average erosion rates on an ice sheet scale. Relief is also a control, but to a less significant degree.

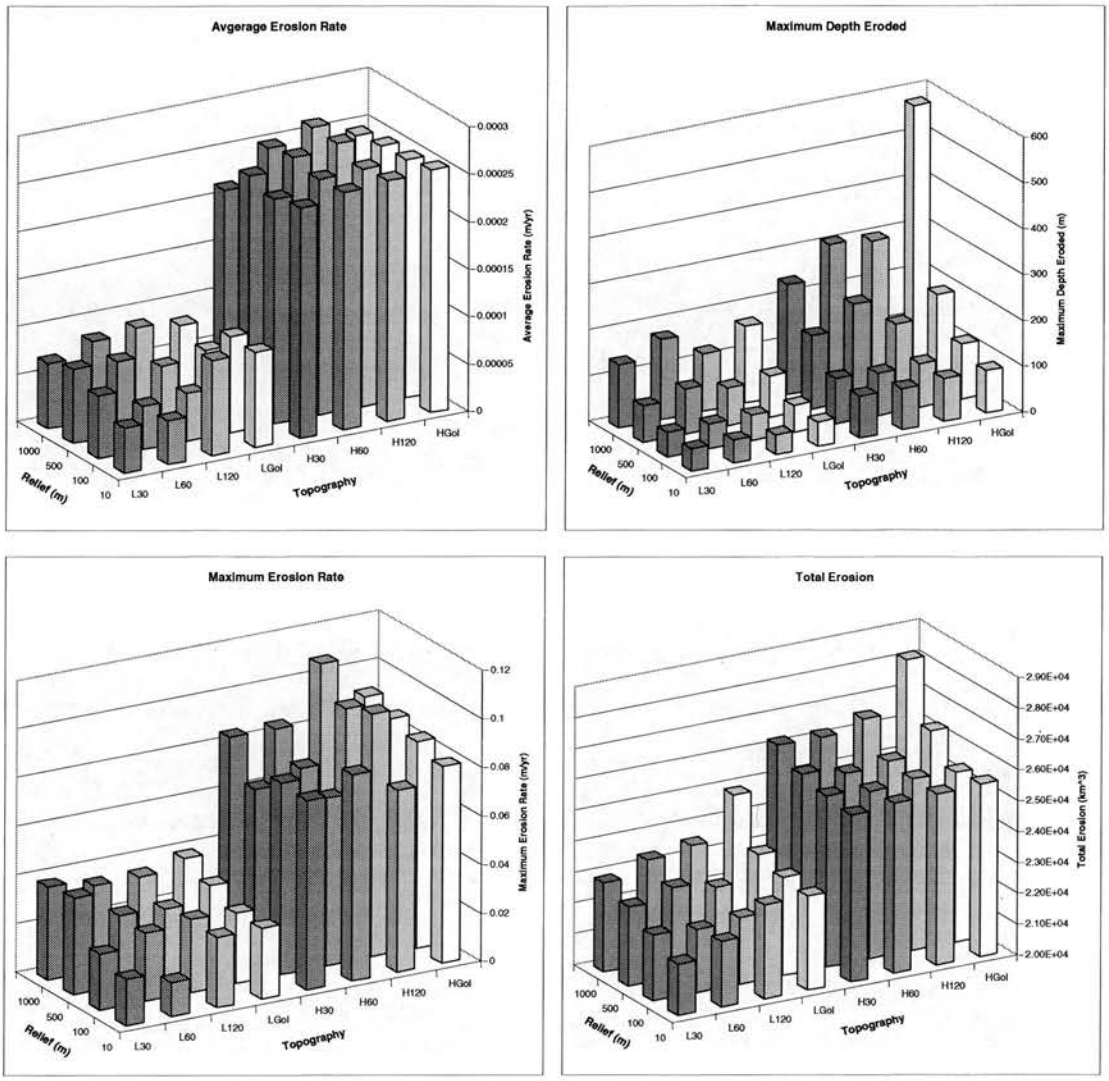

Figure 3.3: Summary model results.

Refer to Table 3.1 for individual experiment numbers and the relief and topography used in each model. A) Average erosion rate (m/yr) for each experiment. B) Maximum depth eroded (m). C) Maximum erosion rate (m/yr). D) Total erosion (km^3). Note that average and maximum erosion rates presented in parts A and C are at least 10 times higher than reality in order to compress model time (see section 3.5). L: Low basal slip coefficient (t_b), H: High basal slip coefficient. Dark grey: 30 km wavelength, Mid grey: 60 km wavelength, Light grey: 120 km wavelength, White: GOLEM topography.

Using average erosion rate may disguise a system with a high erosion range. Therefore, the maximum depth of erosion achieved in each run as plotted against both the relief and wavelength of the associated topographies (Fig. 3.3b). In our experiments, maximum depths of excavation are strongly controlled by the relief of

the underlying landscape (Fig. 3.3b). This trend of increased relief generating increased excavation depths is particularly the case over the 'fluvial' GOLEM landscapes. This implies that the deeper the pre-existing valley, the greater the subsequent incision potential.

Wavelength too, exerts some control over the maximum depths of erosion measured in each model. Figure 3.3b shows that in landscapes with dominant wavelengths of 60 km, the maximum depths of glacial erosion that can be achieved are higher than at either 30 or 120 km. This implies that at topographic wavelengths of ca. 60 km, modelled ice sheets can reach their optimal erosive power. This relationship is clearest in high relief landscapes.

Maximum erosion rates tend to be higher under higher relief systems (Fig. 3.3c). This relationship is most clear in experiments that use lower t_b. Higher t_b systems based upon the white noise landscapes show no discernable trends between wavelength and maximum erosion rate. A trend between relief and maximum erosion rate only becomes visible on long-wavelength (120 km) bed geometries. Where the topography is 'fluvial' the increase in maximum erosion rate very consistently increases with relief regardless of basal conditions. This implies that the fluvial nature of the systems are stabilising the relationships between relief and maximum erosion rate.

Figure 3.3d shows total volumes of bedrock eroded from each experiment. In general (although there are a few minor exceptions), the volume removed from the landscape increases with pre-existing relief. However, in a number of instances – particularly Models 5 and 9 which glaciate on the lowest relief topographies, the volume eroded is higher than that for the next one or two relief steps (i.e. 100 – 500 m). Wavelength also appears to control the total volumes of bedrock removed by ice as volumes eroded increase with wavelength.

These statistics (Fig. 3.3) provide information about ice-sheet wide interactions between topography and the ices masses they support. However, they do not provide data regarding spatial and temporal patterns of glaciological and topographic evolution. For investigating topographic states in a computerised context, morphometric analysis (the quantification of landscape form) is a common approach.

Numerous forms of morphometric information, one of the best known being hypsometry, are useful in characterising terrain (Strahler, 1952; Summerfield, 1991), and for inferring modes of landscape evolution over continuous space (Baroni et al., 2005; Jamieson et al., 2004; Montgomery et al., 2001). Hypsometry however, becomes difficult to monitor in a constantly changing system. Therefore, we present data in a number of simple ways. For example, time-series graphs indicating the area of ice sheet bed undergoing erosion will illustrate the stability of the erosive power under the ice sheet as a whole. We also show more complex time-series' of various variables of model output along circular profiles through which ice flows at the perpendicular. The profiles are taken along the ELA as prescribed in Equation 3.3 to pick out the largest magnitudes of erosional response. These plots inform about both the stability and magnitude of erosion rates, and about how erosion is focussed. Maps of erosion and basal velocities further support such plots. Figure 3.4 shows the position of this profile in relation to patterns of total glacial erosion in two models (1 and 4).

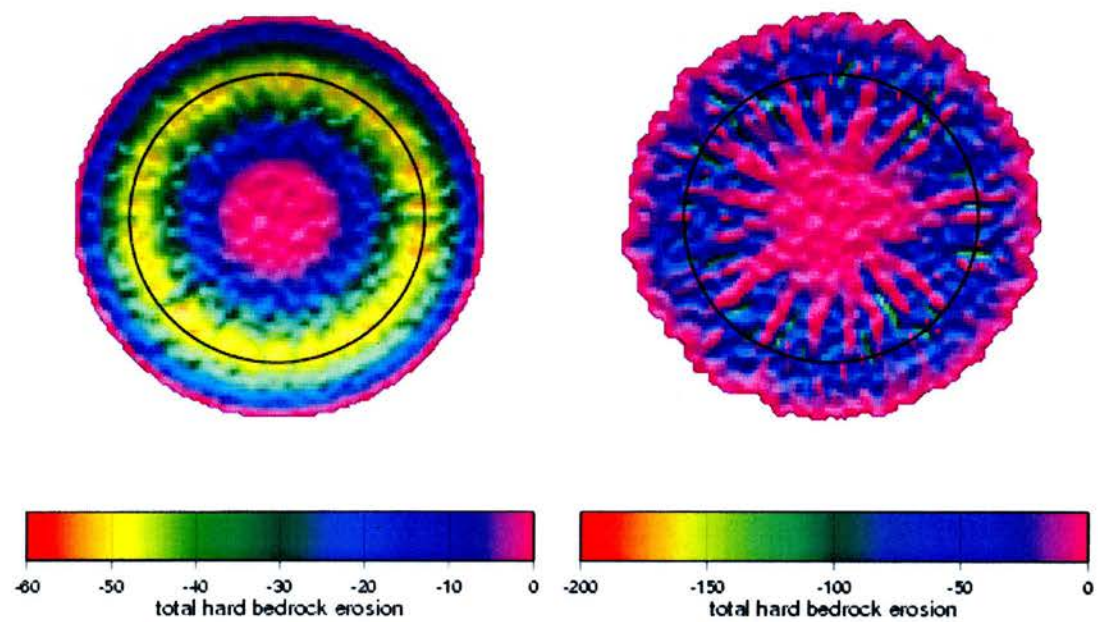

Figure 3.4: Map of erosion distribution

Units are metres and Models 1 (left) and 4 (right) are displayed. Note the scouring in model 1 vs. the focussed erosion that generates radial valleys in Model 4. The black

circle shows the position of the profile (and of the ELA) used in time series profile plots.

3.4.1 30 km Wavelength Results

Figure 3.5 shows time series profiles of erosion rate for Models 1-4 (see Table 3.1). Model 1 (Fig. 3.5a) displays switching (on/off) behaviour whereby large portions of the bed are eroding as ice is purged, followed by a period of erosional inactivity as ice flow decreases as a result of shallower ice surface gradients. Such behaviour has been previously noted in models with radially aligned valley systems (Jamieson et al., 2008). At times where erosion occurs in the low relief model it is evenly distributed around the profile and is analogous to glacial scouring as it is widespread. By increasing relief by an order of magnitude, a wave-like form in the erosion rate plot (Fig. 3.5b) is established alongside the switching behaviour. This represents a large zone of erosion that tends not to remain in the same location, but that propagates around the radius of the ice sheet.

As relief is increased to 500 m, erosion starts to become more linear (the features show up as thin vertical stripes in Figure 3.5c). This corresponds to a short wavelength topographic focussing of erosion as ice flow becomes more constrained by the hollows in the topography. This gives an indication of the scale of relief that is required to generate linear flow (selective erosion) rather than areal flow (glacial scouring). Figure 3.6 illustrates the differences in basal velocity patterns between the 10 m and 1000 m topographies and shows how fast-flowing streams are formed where the relief is more significant.

The wave-like pattern displayed in the erosion rate distribution of the 500 m topography is caused by the spread of a zone of erosion from one side of the ice sheet to the other. This cycle manifests itself at the glacier surface by a laterally pulsating ice dome position caused by the drawdown of ice at one side of the ice sheet and then the other.

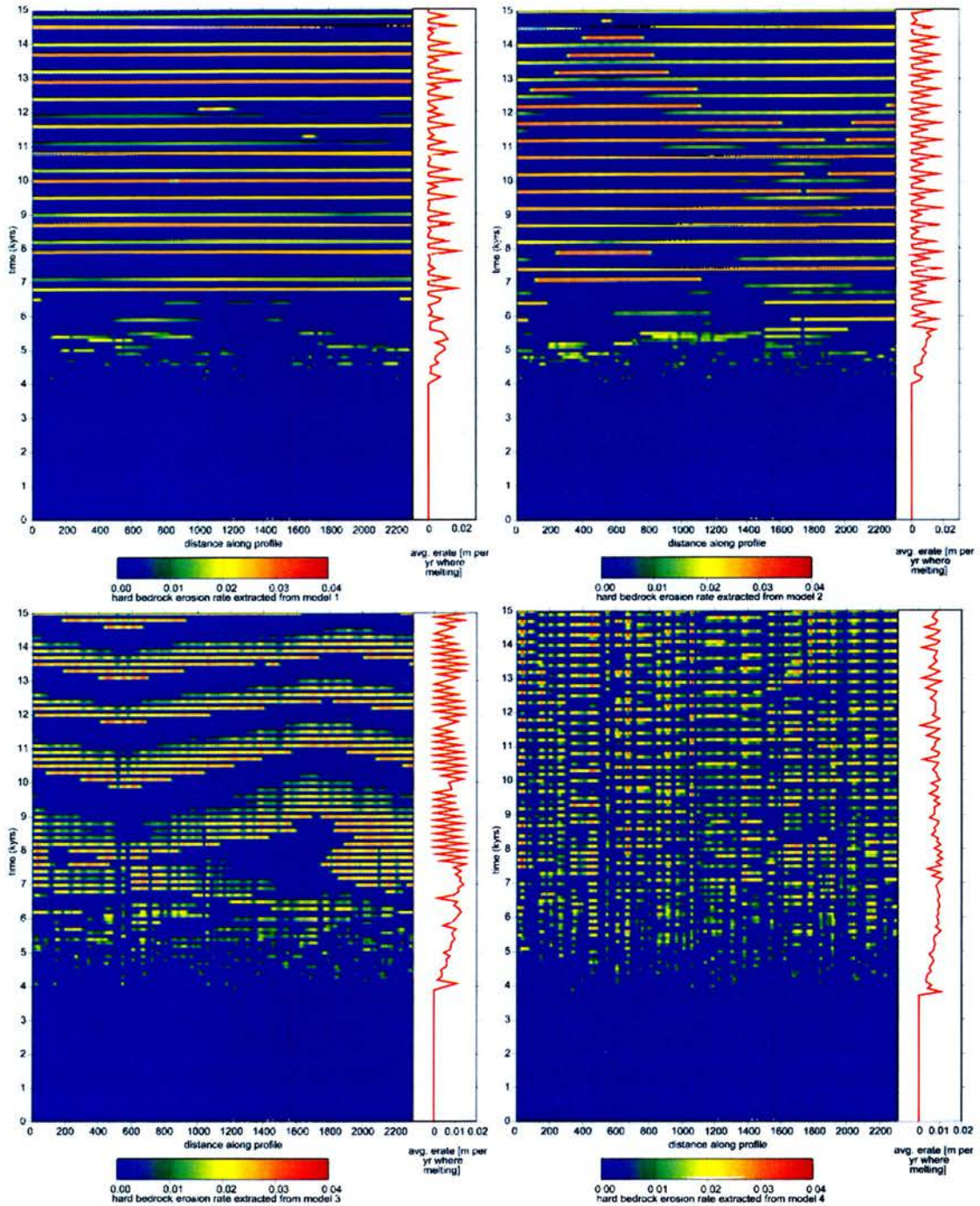

Figure 3.5: Erosion rates in models 1-4

Units are metres yr^{-1} and are recorded along a circular profile (Figure 3.4) for models 1-4 (a-d, left-right, top-bottom). Note the large-scale switching in Model 1, and the lateral migration of erosional activity around the ice margins in Models 2 and 3. Further note the vertical stripes (i.e. constant in space) of focussed erosion that appear in Models 3 and 4. The sub-graphs show ice sheet wide average erosion rates (where erosion is > 0) through time.

This kind of instability does not occur in the 1000 m relief experiment (Fig. 3.5d - model 4) which indicates that at this higher amplitude the topography is acting as a stabiliser for the ice sheet dynamics. For the duration of the model run, the intensity of erosion is focussed into paths that are on the same width-scale as the topographic wavelength (30 km). Erosion occurs in pulses as particular outlets speed up or slow down, but its pattern in space is unchanging. Graphs of ice sheet wide average erosion rates (red plots in Fig. 3.5) illustrate the timescales at which switching behaviour is generated in models 1-4. In all cases there is cyclicity relating to pulses of faster-flowing ice that cover large areas of the bed.

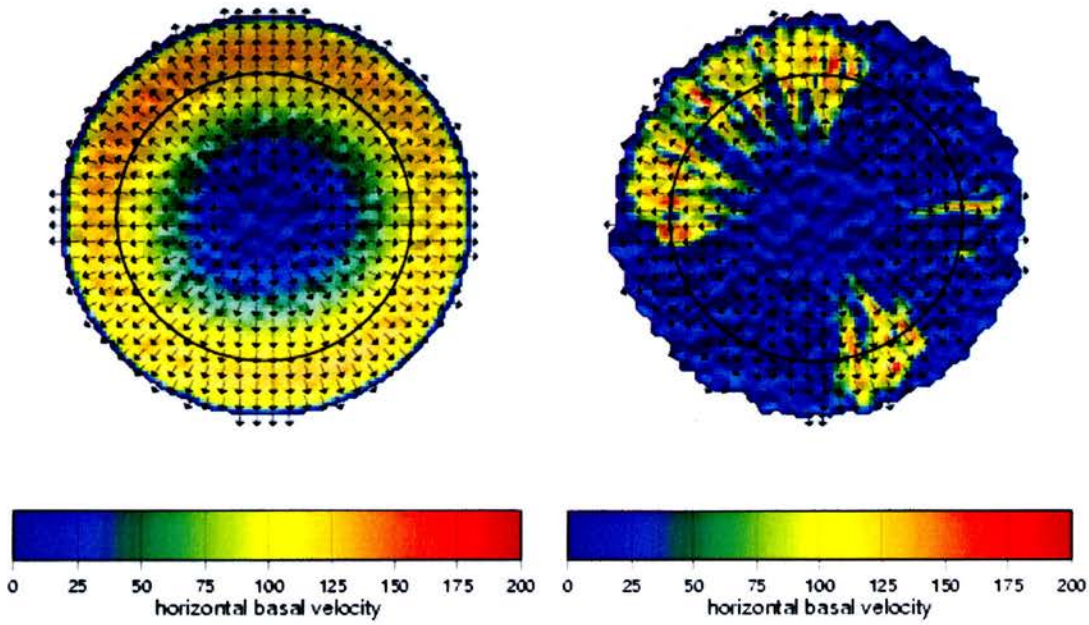

Figure 3.6: Maps of basal ice velocity, models 1 and 4

Units are metres yr^{-1}. Model 1 (left) and 4 (right). Note the pattern of fast flow under the higher relief system begins to replicate that expected in ice streams, with focussed erosion being generated. Arrows indicate direction of basal ice flow where velocity is greater than zero.

The patterns noted above (Fig. 3.5) differ to those under the influence of higher t_b conditions (Fig. 3.7; models 17-20). Higher basal slip coefficients effectively allow the ice to become more fluid. There is no tendency to erode in one topographic hollow over another and instead focussed valley erosion occurs in all hollows. Spatial patterns of erosion remain essentially unchanged regardless of relief (Fig.

3.7) and all of these high basal slip coefficient models are temporally unstable and display switching between individual 'streams' (Fig. 3.8). Erosion in the high relief experiment (Fig. 3.7b) is perhaps more confined to particular valley features as zones of higher erosion rate are revisited more often. In the lower relief system (Fig. 3.7a), although erosion remains focussed into thin 'streams' these streams tend to migrate rapidly to follow the many different paths enabled by the numerous interconnected hollows in the small wavelength topography. Changes in relief do not alter maximum or average erosion rates or the total erosion generated across the system (Figs. 3.3a, 3.3c, 3.3d and 3.7b), but do enable greater depths of valley to be excavated (Fig. 3.3b).

The erosional output of the entire low relief experiment (Model 17) remains relatively steady through time (Fig 3.7a). However, in the 1000 m topography a gradual linear reduction in average erosion rate occurs over time (Fig. 3.7b).

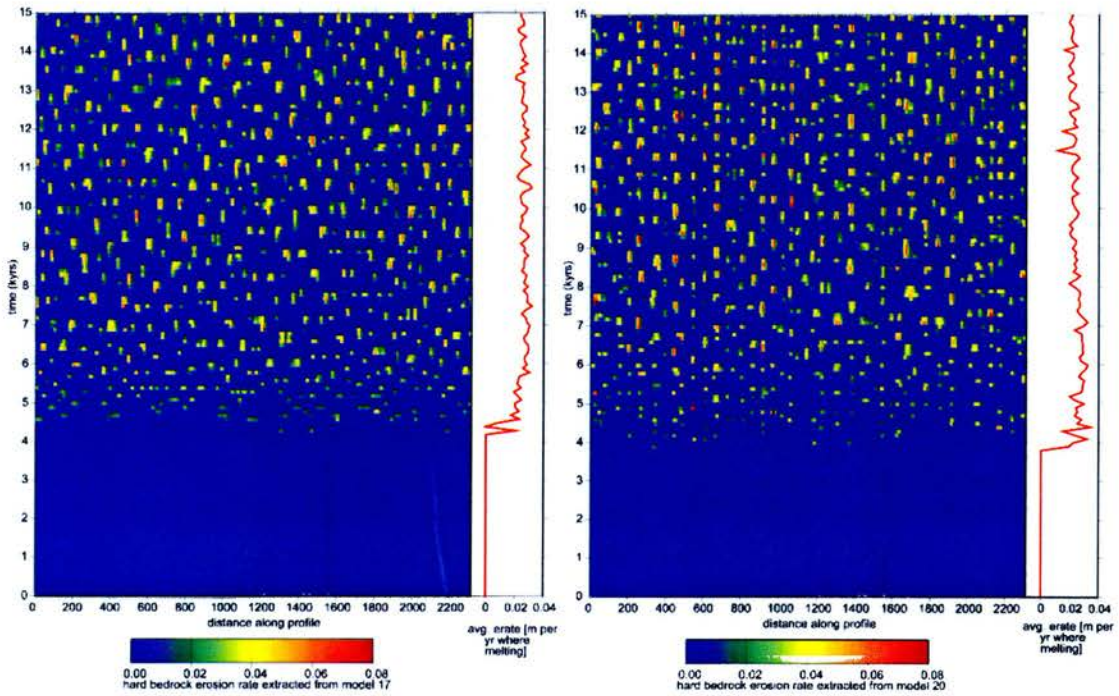

Figure 3.7: Erosion rates for models 17 and 20

Units are metres yr^{-1} along the ELA profile for experiments 17 (left) and 20 (right) demonstrating that with high t_b the spatial distribution of erosion is similar regardless of relief and that in such models the distribution of erosion is strongly controlled by changes in topography at any vertical scale. Graphs show system wide average erosion rate through time.

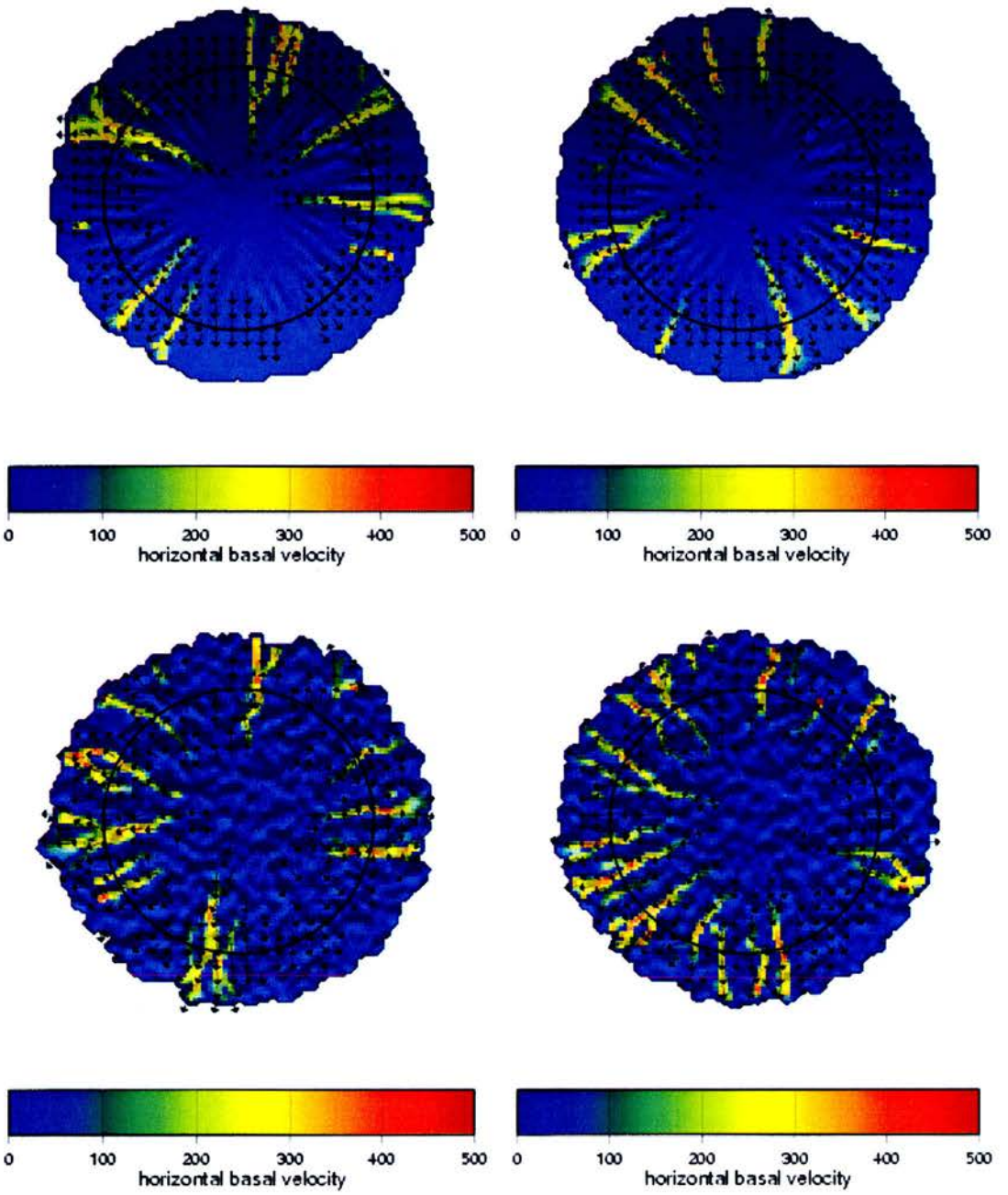

Figure 3.8: Maps of basal ice velocity

Basal ice velocities under high t_b conditions showing that temporally unstable 'stream-like' features are reproduced even under lower relief conditions. Top = model 17 (10 m relief), bottom = model 20 (1000 m relief). The timeslices on the left and the right are 1000 years apart. Units are metres yr^{-1}.

3.4.2 60 km Wavelength Results

Figure 3.9 shows how the patterns of erosion rate change over space and time for Models 5-8 which are initiated over a 60 km wavelength landscape. All of the models, in line with behaviour noted in the short wavelength systems, display spatio-temporal switching illustrated by more intense erosion followed by relative erosional inactivity. Large-scale switching dominates the 10 and 100 m topographies whereby regions of melt, and thus basal sliding and erosion surround the entire circumference of the ice sheets before flow slows for a period following this purge of ice.

The total amount of erosion is greater under over the 60 km systems than over the 30 km simulations. Erosional regimes equivalent to glacial scouring dominate the lower relief models but as relief increases to 500 m and above, erosion preferentially takes advantage of the topographic lows (Figs. 3.9c, 3.9d, 3.10a and 3.10b). Selective erosion predominates despite the continuation of switching behaviour and of glacial scour on the upland areas. The distances over which the erosion rate varies in Models 7 and 8 are larger when compared to Models 3 and 4 (Figs. 3.5c and 3.5d) reflecting the glaciological response to increased topographic wavelength. The overall erosional output of models 5-7 are highly variable as shown by the graphs of average erosion rate (Fig. 3.9a-c). However, once relief reaches 1000 m (model 8), the erosion generated under the entire ice mass becomes more stable, with a gentle downward trend as time goes on (Fig. 3.9d).

Under high t_b conditions (models 21-24), selective erosion is ubiquitous regardless of relief, producing patterns of landscape evolution similar to those in models 16-20 (Fig. 3.7). There is little variation in the spatial or temporal distributions of erosion in Models 21-24. Many locations are repeatedly subjected to erosion indicating, in line with results from shorter wave topographies, that the response of the ice mass to its basal topography is strongly conditioned by factors such as basal sediment saturation at the bed. Increased stability of average ice sheet wide erosion is again a characteristic of these high basal slip coefficient models.

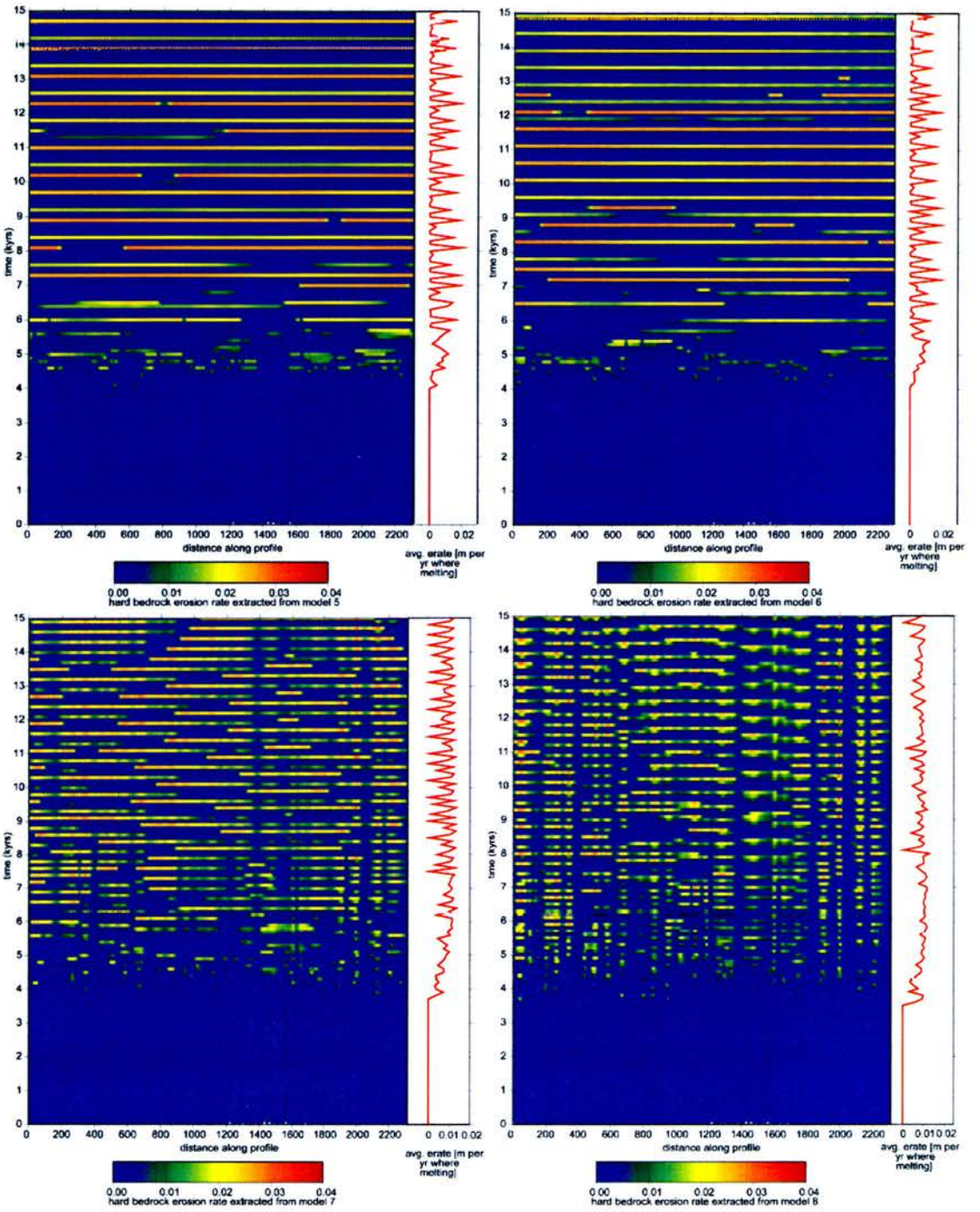

Figure 3.9: Erosion rates for models 5 to 8

Erosion rates in metres yr^{-1} along the ELA profile for Models 5-8 through time. Large-scale switching is evident, and focussing of erosion becomes particularly evident at 500 – 1000 m relief. Average erosion rates produced across the entire ice sheet system becomes more stable with the increased relief (i.e. erosion is occurring all the time under the high relief system, whereas on/off switching is dominant in lower relief models).

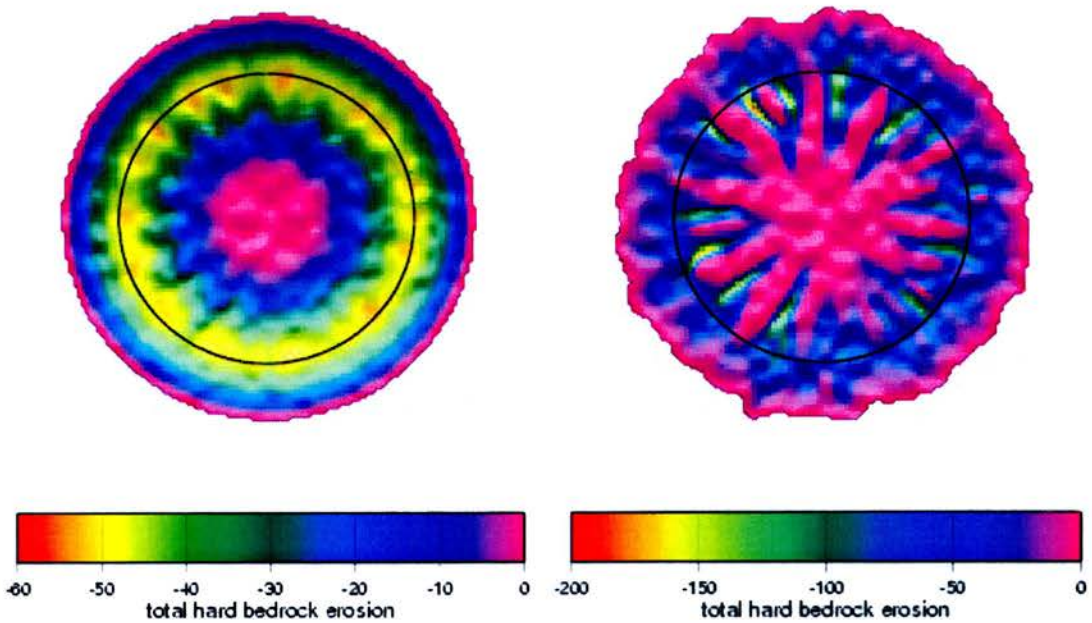

Figure 3.10: Total erosion distributions at the beds of models 6 and 8

Erosion in metres for Models 6 (left) and 8 (right).

3.4.3 120 km Wavelength Results

Figure 3.11 presents the distribution of erosion rates over space and time as the modelled ice sheets evolve over the 120 km wavelength basal topographies (models 9-12). The pattern in Figure 3.11a is the result of a cyclical pattern of basal melting and thus basal velocity that occurs in the low relief topography. This pattern illustrates the development of three very similar zones of erosion that do not remain in one place, but that circulate repeatedly around the ice margin unhindered by effects of any topographic roughness. Switching behaviour in this model therefore displays a rotational momentum, rather than being on/off as noted in the previous systems. Increasing the relief of the basal topography to 100 m is enough to remove this rotational instability and establish a more spatially static system of glacial scour (Fig. 3.11b).

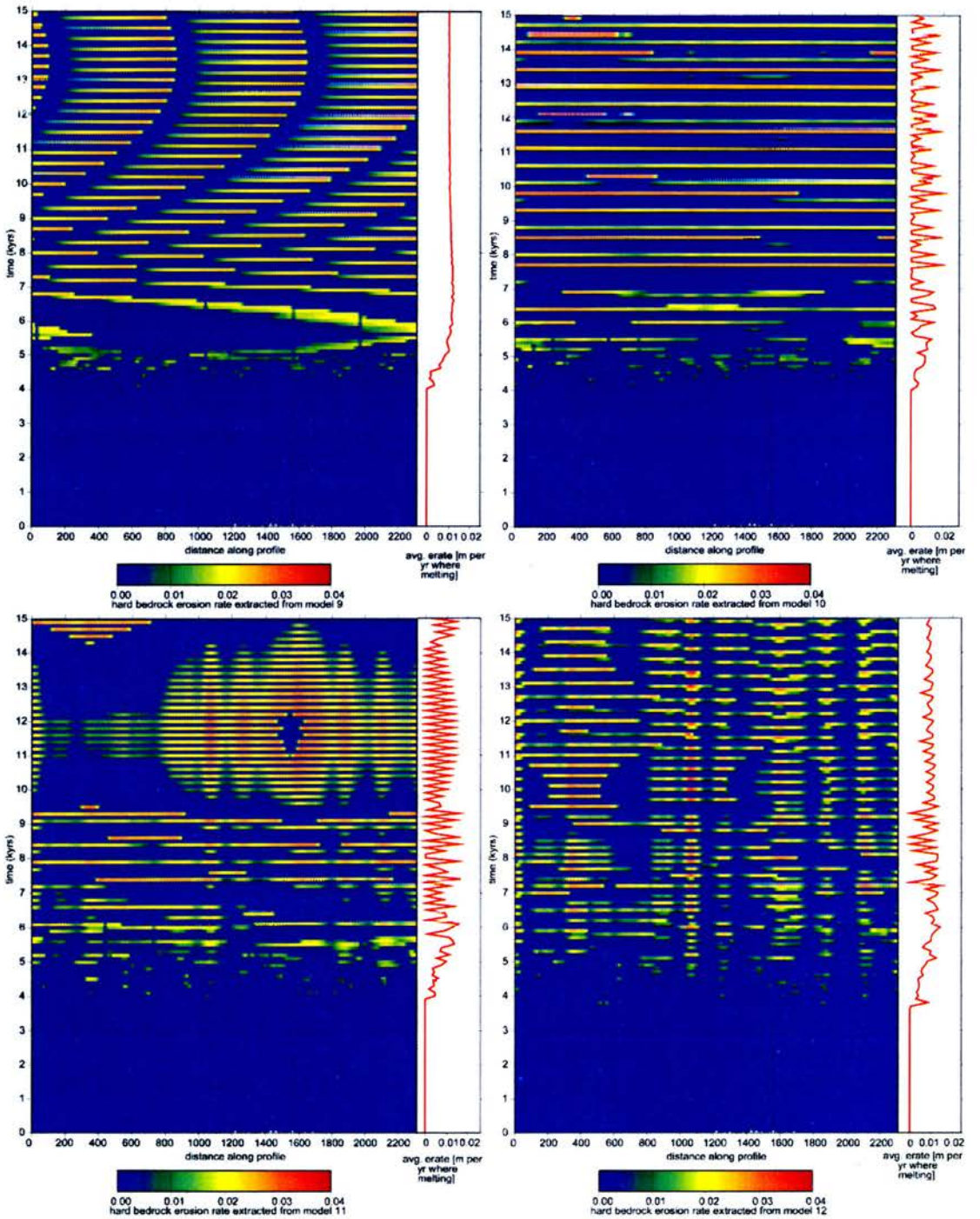

Figure 3.11: Erosion through time in models 9-12

Erosion rates (meters yr^{-1}) for Models 9-12 generated along the ELA profile. Graphs show the average erosion rate being generated across the entirety of the base of the ice sheet.

With relief increased to 500 m (Fig. 3.11c), a zone of increased erosion occurs preferentially over one part of the topography. This contrast may be the result of flow divergence and the associated slowing of ice in this region as upstream ice is diverted into two hollows that are separated by a ridge of higher elevation topography. This perhaps, is the kind of ice dynamics that may be expected in regions of glacial scour and indicates a wavelength/relief combination at which topography is less able to drive focussed flow, but is still able to generate flow divergence or convergence.

A further increase in relief to 1000 m reveals a system that is dominated by focussed flow in the low regions and by cooler protective ice over topographic highs. Glacial incision is thus limited to the lower portions of the topography around the position of the ELA. At this relief, the ice-sheet wide average erosion rate is relatively stable in the short-term with a long-term downward trend, in contrast to the 100 and 500 m models.

Increasing t_b (Fig. 3.12) in the 120 km simulations produces similar outcomes to the previous high t_b models on shorter wavelength landscapes. However, the large amplitude experiment results display higher erosion rates than the low relief models and these high rates are focussed into two broad zones whereby multiple streaming features are located proximal to one another (Fig. 3.12b).

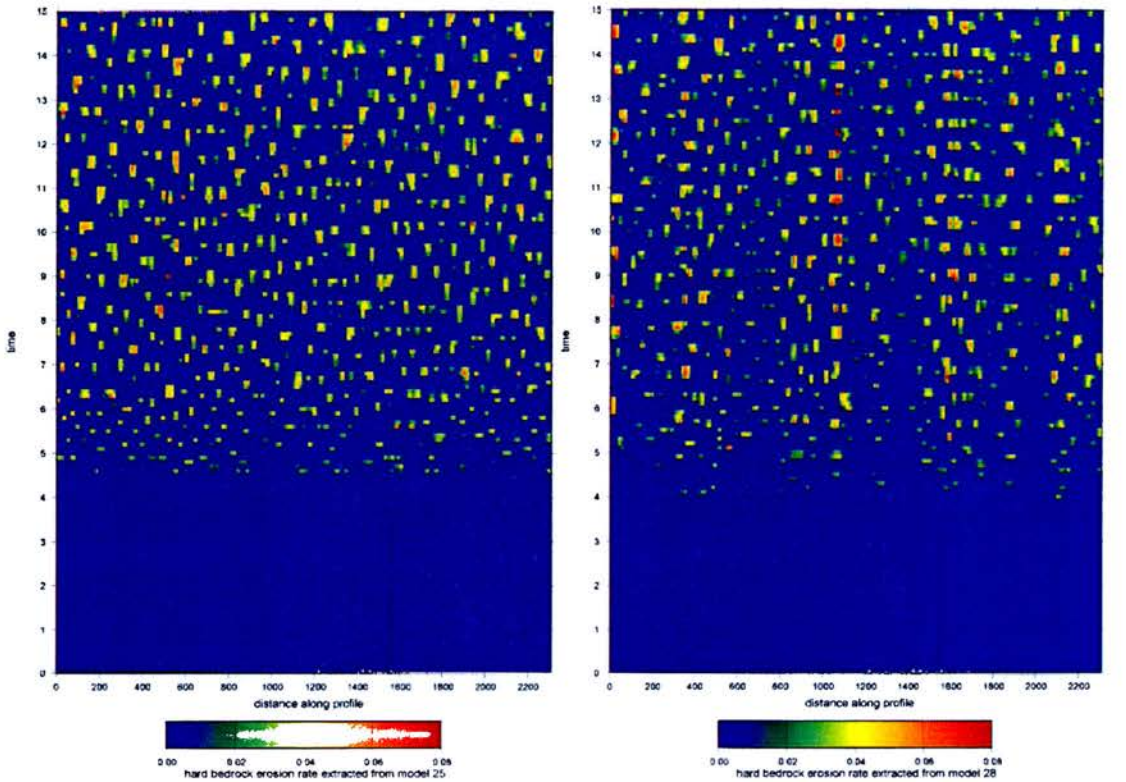

Figure 3.12: Erosion rates in models 25 and 28

Erosion rates (meters yr^{-1}) through time (kyrs) under high t_b conditions over 10 m (left) and 1000 m (right) topographies (Models 25 and 28).

3.4.4 Fluvial Topography Results

Models 13-16 grow ice sheets upon synthetic 'fluvial' topographies generated with the GOLEM geomorphic landscape evolution model (Tucker and Bras, 1998; Tucker and Slingerland, 1996). Figure 3.13 shows the erosion patterns generated. Notable in models 13 (10 m relief) and 14 (100 m relief) is the rotational momentum being sustained over long time periods. However, the direction of this inertia is reversed between models. Both of these experiments have similarly stable total sediment outputs at any given time.

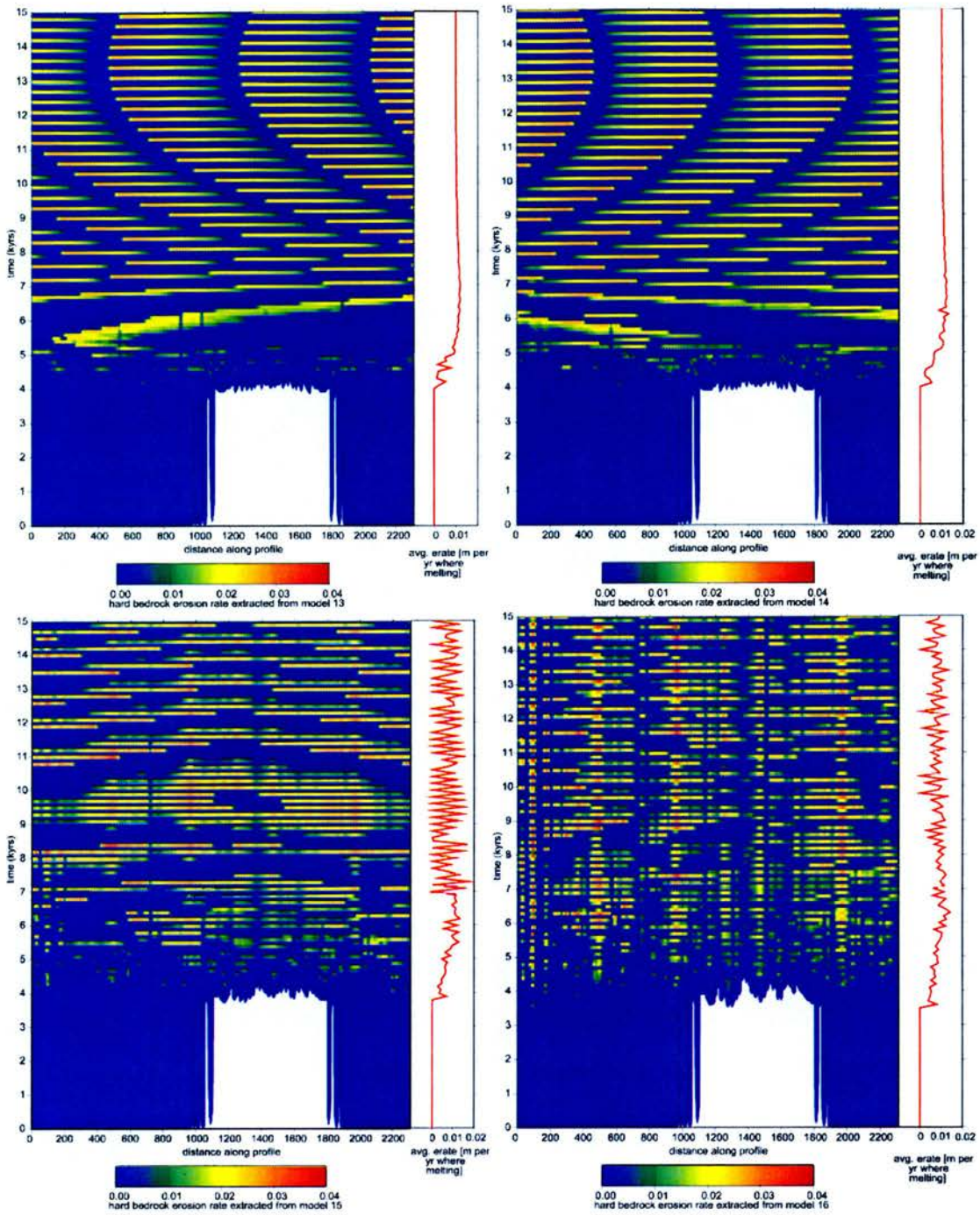

Figure 3.13: Erosion over fluvial topographies

Models 13-16 – spatio-temporal patterns of erosion rates (meters yr^{-1}) at the ELA position. Note the rotational patterns generated in the low relief system. The small graphs show average erosion rates over the whole bed.

Increasing relief to 500 m enhances focussed flow and erosion to a greater extent than in previous experiments of equivalent relief. In addition, a cyclical instability to

the total amount of erosion occurring throughout the ice sheet is also generated (Fig. 3.13c). In increasing relief to 1000 m, focussed flow dominates the model (Fig. 3.13d) with 4 obvious zones of selective erosion being generated. Three of these strong regions of focussed flow correspond to the largest valleys on the 'fluvial' topography that drain the centre of the ice mass. These basins experience gradual overdeepening of their long profiles (Fig. 3.14) as expected from field evidence of glacial erosion of valley floors (e.g. Sugden and John, 1976).

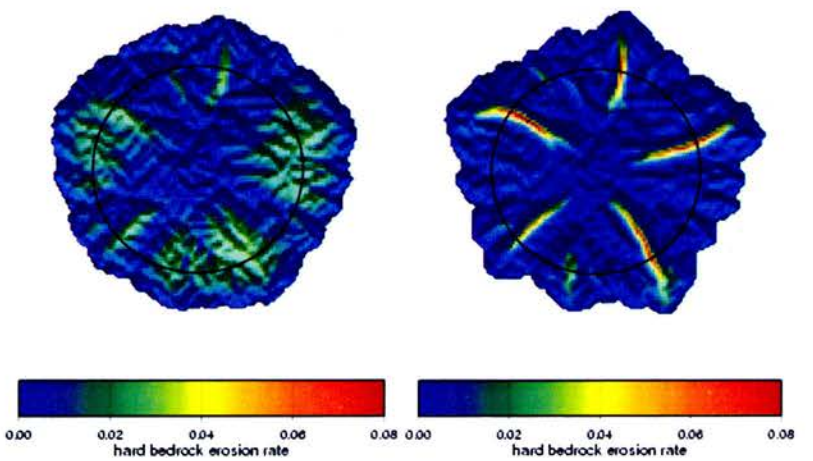

Figure 3.14: Transformation from areal to selective erosion

Maps of erosion rate (meters yr^{-1}) during early and final stages of a long-term glaciation (see section 3.5.3 below) of a fluvial topography (Model 16). Note the increasingly selective nature of the erosion focussing into the overdeepened troughs. Overdeepening occurs to a lesser extent in the 15 kyr version of model 16, but is nonetheless evident.

Experiments 29 – 32 (Fig. 3.15) apply high t_b conditions to ice sheets grown upon the 'fluvial' topographies. As with previous high t_b experiments, the zones of flow and therefore erosion, are focussed into thin 'stream' features regardless of topographic relief and the paths of these flows are determined largely by ice surface slope. As relief increases, the paths become increasingly directed by the topography, and at 1000 m relief (Model 32), the erosion is particularly fast in floors of the largest drainage valleys (Fig. 3.15c and 3.15d). The ice-sheet wide average erosion rate is relatively stable in all 4 of these models, although in the final system, where erosion is being strongly focussed, there is a downward trend to the average erosion rate (Fig. 3.15d). It is clear however, that even small scale variations in topography can

drive erosion in these models, with larger-scale regional landscape variations then enhancing the degree of this erosion.

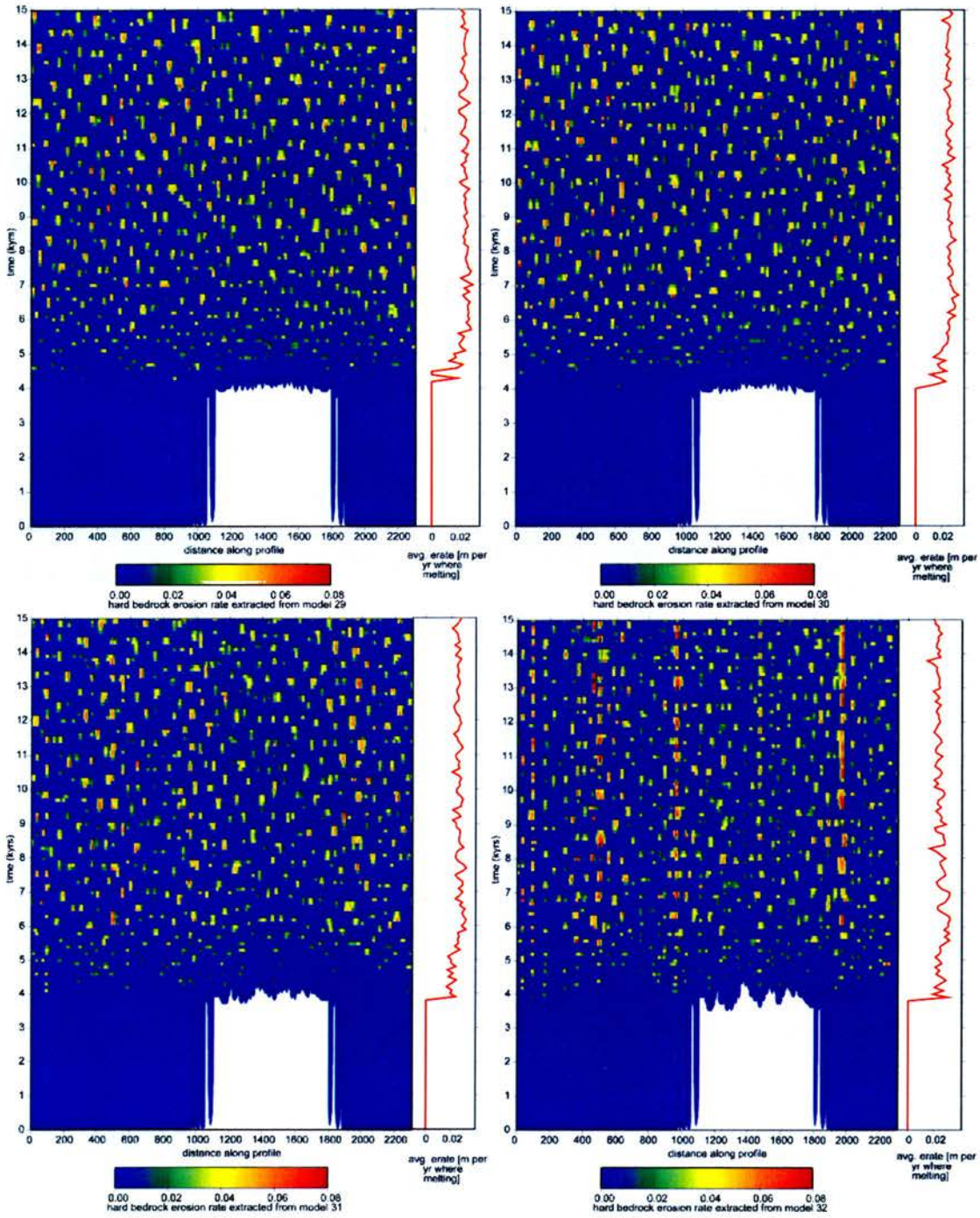

Figure 3.15: Erosion under high t_b conditions on a fluvial topography

Spatio-temporal distribution of erosion rates (meters yr^{-1}) along the ELA as generated under high t_b conditions applied to the GOLEM fluvial bed topography in Models 29-32. Figure 3.2 shows the position of the profile.

3.5 Discussion

3.5.1 Topographic Wavelength

Fisher et al. (2004) indicate that landscape features are 'fuzzy' phenomena in that they can exist at various scales. Our models represent landscape at fixed spatial scales but in reality the fuzzy nature of landscapes are likely to have a fuzzy impact upon the distribution of erosion at the base of an ice sheet. The range of wavelengths tested in our experiments, although limited by model resolution, is enough to suggest a continuum of behaviour in terms of influencing erosional patterns.

Our models indicate that pre-existing valley spacing exerts significant control upon glacial erosion distributions, particularly in regions of significant relief. Shorter wave bed variations lead to the development of thinner 'glacial' valleys whereas longer wave, topographically smoother systems do not focus erosion to such a great extent with more areal scouring occurring instead. The fact that a more selective pattern of landscape modification occurs where the pre-glacial land surface varies over short spatial scales is unsurprising given our knowledge of fluvial systems where stream power increases when water is forced through a narrow gorge.

The degree to which a valley can be overdeepend (i.e. maximum erosion depth – Fig. 3.3b) appears to be critically controlled by the wavelength of the landscape. Maximum depths of erosion occur neither under the short nor the long wave systems, but in the experiments using the 60 km spacing. This may be the result of a balance between the number of pathways along which the ice can be routed and ice discharge which optimally generates accelerated erosion along these pathways. This indicates that at length scales of around 60 km ice is most able to adapt and most efficiently erode the landscape.

The 'basal slipperiness' as controlled by the basal traction parameter (t_b) is used here to test the impact of changing basal conditions (i.e. it combines the degree of saturation of sediment, presence of deformable beds, lithology etc. into a single lumped parameter). Basal slip coefficient parameterisation is the single most important factor in controlling the relationship between topographic wavelength and ice dynamics. Our time-series plots indicate that as t_b increases (i.e. slipperiness

increases), differences between erosion patterns in systems of different wavelengths become small (e.g. Fig. 3.7). Under high t_b conditions, a wavelength of ca. 30 km appears to be the controlling influence on whether erosion is switched on or off in our models. Larger wavelengths then exert only a relatively small extra influence upon the degree of erosion. Depending on the basal conditions of the ice sheet therefore, the influence of the wavelength of the topography will be very differently felt. Higher t_b appears to decouple the influence of the maximum wavelength in the topography from the pattern of erosion. We hypothesise that this is a result of increased sensitivity to minor amplitude topographic changes, and so erosion patterns are being controlled at a much smaller scale than might be expected. If t_b is low, the wavelength of the topography feeds into ice dynamics more evenly at any wavelength – i.e. ongoing erosion will more directly reflect pre-existing topography regardless of wavelength.

3.5.2 Topographic Relief

Our experiments show that relief in pre-existing landscapes is a key factor in focussing glacial erosion, with wavelength then determining the length-scales at which this focussing occurs. Across all of the experiments using between 10 and 100 m relief there are changes in erosion rates indicating that even sub 100 m relief can impact upon erosion and ice flow patterns. When local relief (measured over the dominant topographic wavelength of the system) is this small, flow patterns associated with landscapes of glacial scour are generated, with minor variations in rate over space. As topographic relief increases, so does the total erosion that occurs within the system (Fig. 3.3d). However, because maximum erosion rates (Fig. 3.3c) do not increase at the same rate as maximum erosion depths (Fig. 3.3b), we infer that any overdeepening and increased total erosion is strongly controlled by the increased stream stability afforded by high relief systems. Ice has less 'choice' upon where it can travel due to the confining nature of the ridges which can promote convergence of ice flow. Convergence generates an increasing thermodynamic contribution to ice meaning that streaming behaviour is reinforced. Without significant topographic relief, thin regions of fast flow cannot form unless the t_b is increased.

In a number of experiments (Figs. 3.7b, 3.9d, 3.11d, and 3.13d) we see that as a consequence of selective erosion the average erosion rate being produced across the whole ice sheet can decrease through time. This suggests that the rate of transformation to a glacial landscape becomes slower as time advances. This inference may further be extended to the ability of ice to modify topography over multiple glacial advances where if a topography is not 'reset' by interglacial processes then ice sheet modification may become less effective during successive glaciations.

In low relief systems we find that large areas of the bed display 'switching' behaviour. Although small scale temporal switching between streams does occur in nature, such large scale instabilities are not seen under real world ice sheets. The instabilities occur here because small changes in ice temperature propagate rapidly in the absence of any significant topographic relief. Thus streams cannot form properly without significant relief which, under both past and present day ice sheets, is serving to enable and subsequently sustain erosion. Ongoing erosion will reinforce the relief and drive further selective erosion, not only through overdeepening, but because areas adjacent to ice streams can increase in elevation due to isostatic rebound (Brocklehurst and Whipple, 2002; Jamieson et al., 2008).

3.5.3 Pre-glacial Surface Processes

The fluvial topography is likely to be more efficient than the noisy systems at transporting ice because of the radial valley orientations. This implies that in the noise models, erosion associated with dissecting areas of higher elevation topographic barriers to ice flow may act to stabilise ice dynamics. Furthermore, we note minor reductions in long-term sediment excavation from the fluvial topography as it transforms towards a glaciated terrain. Modelled ice velocities in the fluvial system also decrease gradually as the landscape evolves (Fig. 3.16). This suggests that the fluvial topography is being modified to an extent where ice dynamics are being perturbed and erosion signals begin to change. This indicates that pre-glacial fluvial landscapes become increasingly efficient at removing ice as they become increasingly glaciated.

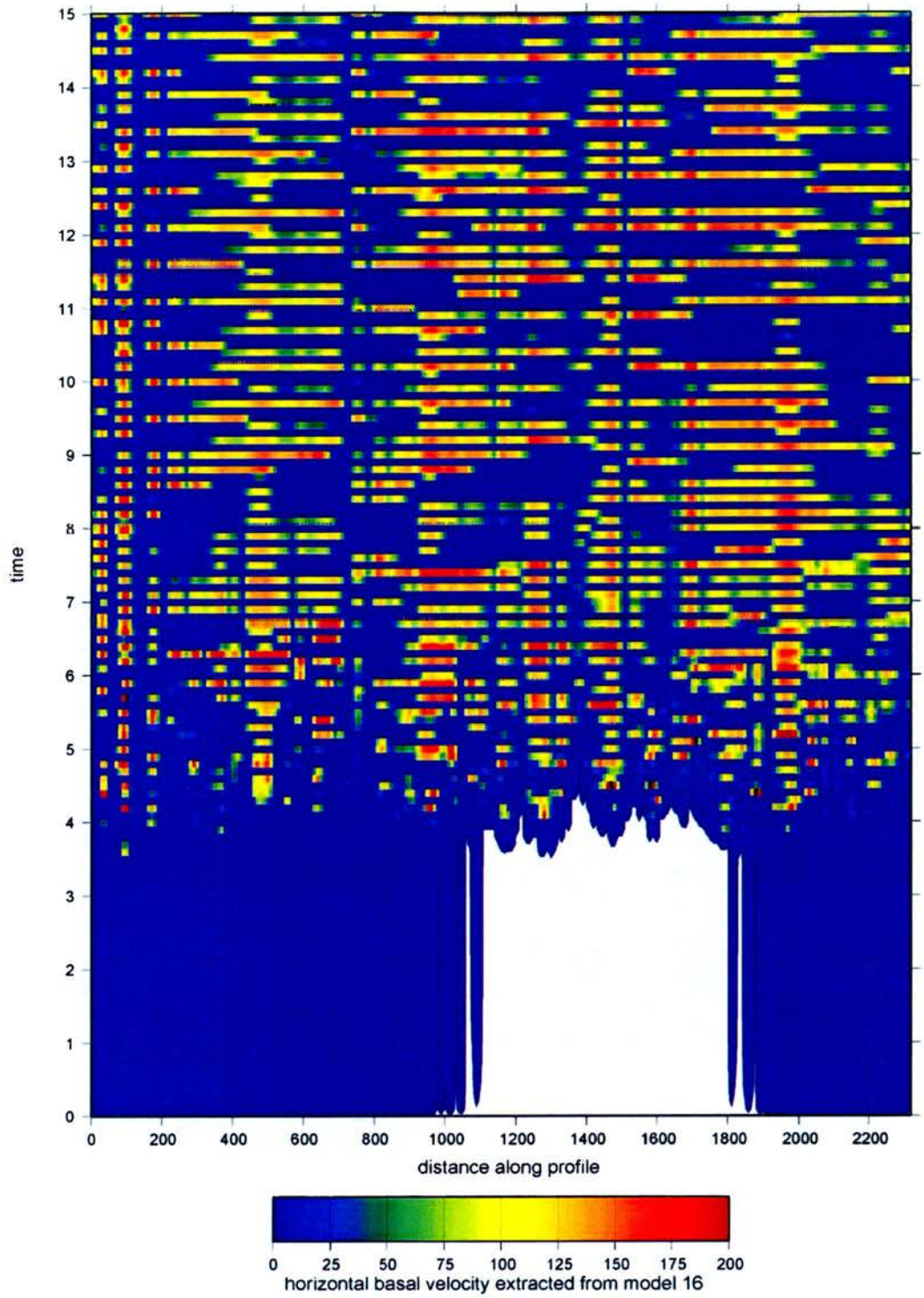

Figure 3.16: Ice velocities over time for fluvial model 16

Modelled basal ice velocity (meters yr^{-1}) through time (kyrs) for Model 16. Note that once the spatial pattern is established, basal ice velocities decrease gradually with time (disregarding the on/off switching). This indicates that the efficiency of the landscape at removing ice changes over this timescale.

In order to test whether this gradual trend of increasingly efficient landscapes can translate to significant change over longer time periods, we run two additional experiments upon both the fluvial and 30 km wavelength 1000 m landscapes. These were run for an extended period of time until significant 2000 m glacial troughs were eroded. As can be seen in Figure 3.17a and 3.17b, basal ice velocities begin to tail off over time along large parts of the profile in both experiments and erosion becomes more selective as time goes on. The development of overdeepening is shown in Figures 3.18a and 3.18a. The mass input does not change and these regions of focussed flow are therefore becoming more efficient at removing ice in comparison to less overdeepened flow paths. At the same time, erosion rates increase in these larger troughs at the expense of the smaller volume pathways (Figs. 3.10e and 3.10f).

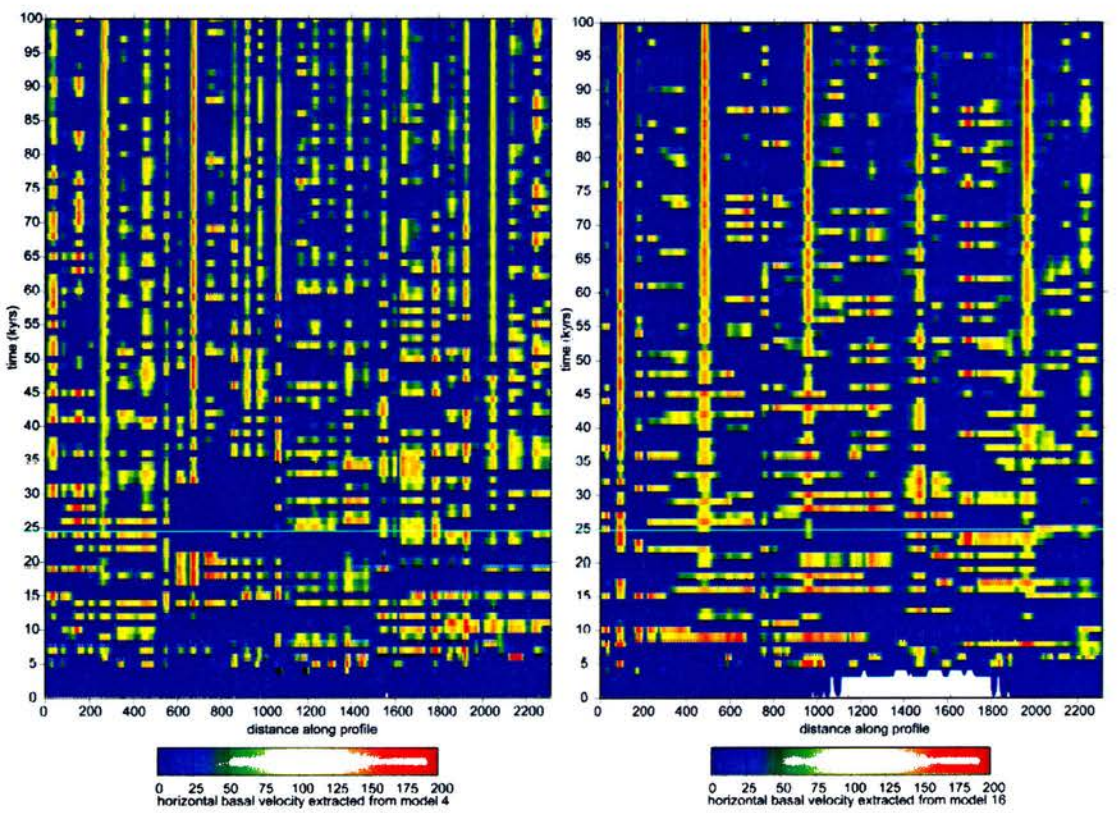

Figure 3.17: Basal ice velocity over time for models 4 and 16

Basal ice velocities (meters yr^{-1}) for longer-term versions of Models 4 (top left) and 16 (top right) Basal velocities gradually decrease along much of the profile at the expense of increased velocities in the streaming regions.

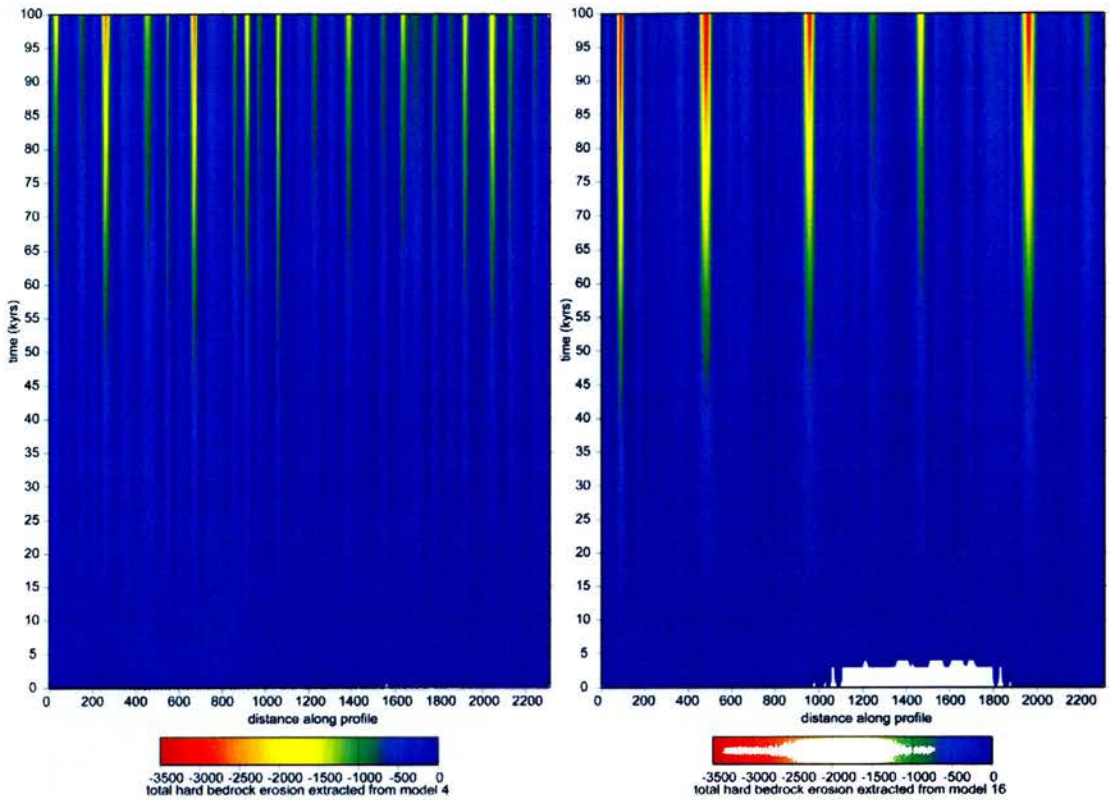

Figure 3.18: Total erosion for models 4 and 16

Total erosion (meters yr^{-1}) for longer-term versions of Models 4 (top left) and 16 (top right). Note how the selective erosion picks out particular channels over others.

It should be noted that any attempt to 'reset' the topography through interglacial surface processes is ignored here. However, across formerly glaciated parts of Sweden particular patterns of selective erosion vs. landscape preservation are repeated through multiple cycles of glaciation despite surface processes that act during interglacial times (Kleman et al., 2007). This suggests that even though we do not model interglacial processes, the patterns of erosion we achieve are not unrealistic.

The increased efficiency noted in our models, is also accompanied by increased erosion along the dominant flow routes (Fig. 3.19a and 3.19b). However, this is being driven to some extent by the static parameterisation of accumulation. Other work has indicated that if accumulation can change dynamically, and erosion excavates the landscape to a significant degree, then ice margins can retreat as a result (Jamieson and Hulton, Submitted). Increased ablation in the efficient

overdeepened areas would therefore reduce the degree of erosion being experienced. Thus the models outlined here show that the glaciological efficiency of a landscape will increase through time. However, it is clear that ongoing erosive potential of the ice mass is critically sensitive to climate.

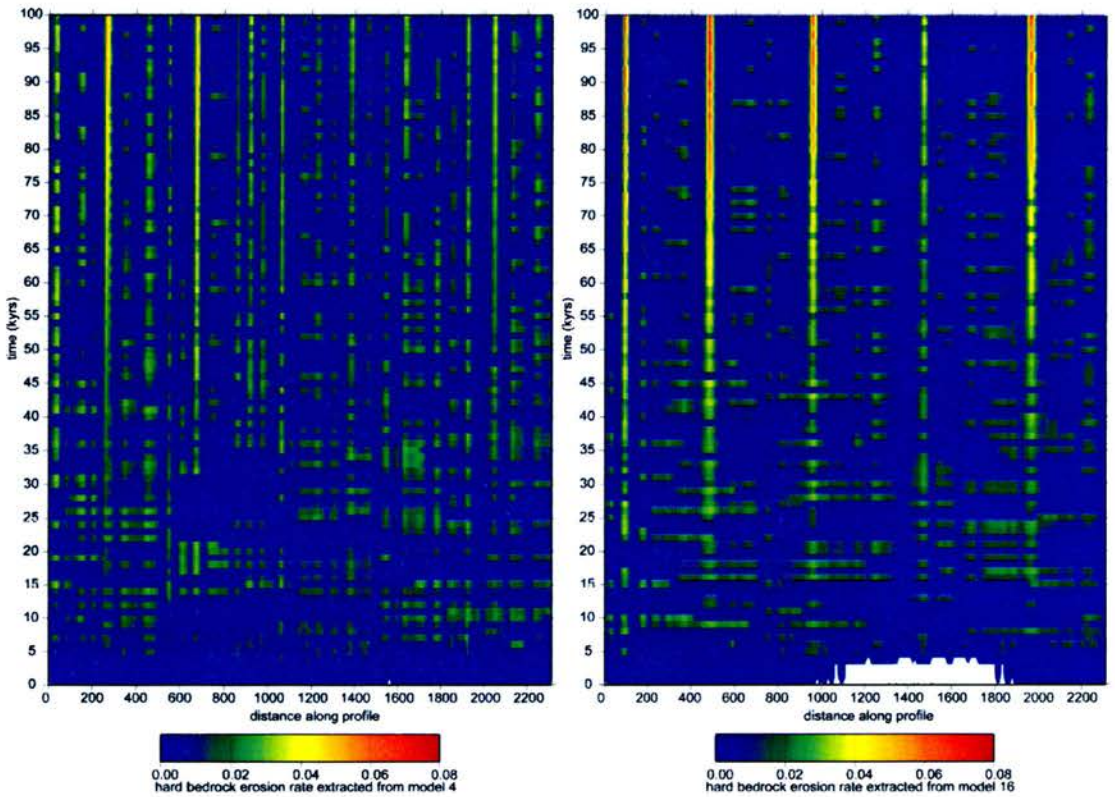

Figure 3.19: Modelled erosion over extended time

Erosion rates for models 4 and 16 (meters yr^{-1}). Note that in these longer term experiments (see also Figs. 3.17 and 3.18), with highly accelerated erosion, the pattern of basal flow becomes more selective with time. Erosion rates increase in the dominant troughs, and decrease in the more minor outlets.

Our results suggest that the dominant pre-glacial process has an impact upon the way the ice dynamics then evolve through time. A more strongly glaciated terrain can drive selective erosion processes to a greater extent than a fluvial system. As indicated in Figures 3.15 and 3.17-3.19, basal velocities and associated erosion patterns are more evenly distributed (i.e. less selective) earlier in the period of transformation from a fluvial to a glacial landscape. This suggests areal scour occurs to a greater degree earlier in an ice sheets existence until selective erosion becomes

increasingly dominant. Modelled ice sheet evolution in Antarctica confirms such a picture where areal scour across large parts of the continent gives way to a more selective erosion regime (Jamieson and Sugden, 2008). Indications from the glaciation of our synthetic topographies suggest that selectivity would become enhanced through time in a region such as Antarctica.

3.5.4 Local Subglacial Factors

The experiments presented here, and other models (Jamieson et al., 2008) indicate the high degree of sensitivity that erosion and ice dynamics have to the parameterisation of the basal slip coefficient. t_b can be considered as a bulk amalgamation, in the absence of specific models and data, of factors including (but not exclusively) lithology, deformable sediment availability and degree of sediment saturation by water (e.g. Jamieson et al., 2008). Our parameterisation of erosion rate dictates that high t_b (i.e. more slippy basal ice) values will generate higher excavation rates (Fig. 3.3). This is to be expected in real-world systems where ice that is more able to slide will generate more sediment. However, because increased t_b alters the length scales over which ice can accelerate to its maximum sliding velocity, the sensitivity of the ice to smaller scale topographic variations is also increased. In our models we test for this sensitivity operating at minimum scales of ca. 10-30 km which is a result of the resolution of our model domain. We note that in both low and high t_b systems, erosion can be focussed into thin streams that are between 10-30 km in width. Therefore, although both high and low t_b systems respond to topographic features that are short wavelength, higher t_b models respond in a stronger manner with a noisier (i.e. binary) regime of flow and erosion. The result is a more selective system of erosion vs. protection where slippery bed conditions prevail.

The reasons for this increased sensitivity are that the higher t_b systems allow sharp temperature gradients to be generated within the ice. This leads to feedbacks in the thermal regime as the ice mass becomes increasingly polarised, with heat being unable to escape from the zones of warm ice. This leads to rapid on/off switching of ice 'streams' through time because as ice is drawn down flow then switch off where the ice gradient becomes too low. This contrasts with lower t_b systems where this

drawdown, and thus switching, is less rapid because the ice is stiffer and less able to respond to changes in thermal gradient and thus to the bed geometry. Thus if a topography varies rapidly, and the system were perfectly fluid, one would expect to see every feature of the subglacial bed manifest itself in the thermal field of the ice mass.

The influence of high t_b on an ice mass in our experiments indicates that although certain ice 'streams' become less temporally stable (i.e. rapid on/off switching occurs), the positions of streams are more established. In addition, the total area of the bed undergoing erosion at any one time becomes more stable.

3.5.5 Model Results vs. Real Erosion Patterns

Our experiments illustrate that an array of erosion patterns can be generated depending upon the form of, and conditions at, the subglacial landscape. For example, the range of erosion patterns are comparable to the variety of patterns that are thought to occur as the East Antarctic Ice Sheet expanded from a series of local ice caps during the early Oligocene towards its present day polar ice sheet configuration (Jamieson and Sugden, 2008). In the Gamburtsev subglacial mountains, corries and hanging valleys were selectively eroded under local glaciation (Perkins, 1984). As the ice sheet expanded, ice in this region became cold-based and protective and a zone of warm-based ice migrated outwards, causing scouring over wide areas where topography is relatively smooth and causing accelerated selective erosion in existing valleys. Similar patterns are also noted in Scandinavia where many fjords were selectively exploited multiple times over a period of 2.6 Million years, but internal areas are subjected to erosion for significantly shorter periods of time (Kleman and Stroeven, 1997; Kleman et al., 2007). Our experiments indicate that selective erosion in overdeepened valleys often occurs in close proximity to zones of minimal modification, a pattern that is repreated in many previously glaciated regions, particularly need ice sheet margins (Hambrey et al., 2007; Li et al., 2005). Thus the pre-existing valley structure is key to the pattern of glacial modification and the large-scale pre-existing fluvial valley structure is preserved. Selective erosion has merely exploited these patterns, as is known to be the case in

Antarctica (Jamieson et al., 2005). Our findings illustrate the importance of topographic influence on erosion rates and are supported by other work in Antarctica (Siegert and Glasser, 1997; Sugden et al., 2005), Scandinavia (Boulton et al., 2003), North America (Sugden, 1978a) and the UK (Glasser, 1995).

Our experiments identify that there are two contrasting temporal and spatial scales upon which erosion patterns are being driven. There is large-scale but short term switching between flow regimes where erosion occurs in pulses over large areas of the bed. This is contrasted by the long-term pattern of landscape evolution that is often highly selective and changes over short spatial scales. Similar dual spatial and temporal scaled oscillations are noted in Antarctica. For example, in West Antarctica, Pine Island Glacier is strongly confined by a topographic trough whereas ice stream B on the Siple Coast is relatively unconfined and has expanded laterally by as much at 4 km between the 1960's and 1990's (Bindschadler and Vornberger, 1998). Furthermore, some of ice streams A-E currently lie asymmetrically within troughs, while other troughs remain unoccupied by streaming ice (Payne, 1999). This may be analogous to the short-term switching noted in our synthetic systems, whereby ice streams linked in to the same source area are cannibalistic in nature, with dominant flow directions constantly changing, but with long-term patterns of flow and erosion being determined by pre-existing subglacial channels.

We suggest that long-term ice dynamics are strongly controlled by topography but that shorter term dynamic behaviour need not be controlled by it. In the long term, topography is a controlling factor on the pattern of erosion, causing excavation in the places we expect, but in the short term the pattern of erosion under an ice sheet can behave in a more dynamic manner. The short term behaviour is related to the shape of topography. As the switching behaviour occurs, drawdown of ice in one drainage system causes erosion. The thermal implications of this are that heat is advected towards the stream at the expense of the neighbouring drainage systems where erosion is therefore less likely to occur.

3.5.6 Topography Stabilises Dynamics

It is likely that the rotational and cyclical behaviour encountered in the low relief models (Figs 3.13a and 3.13b) are the result of modelled instabilities which are emphasised by the presence of a flat bed topography. However, the fact that they occur in our models is informative with regard to the importance of topography. In low relief systems ice is able to behave in a more interconnected way as large parts of the ice sheet are affected by minor thermal perturbations. This can initiate a cyclic intertia probably partly related to the circular nature of the ice mass. In a real system, as in our higher relief experiments, this interconnectedness is perturbed by the basal topography because drainage divides strongly force the thermal regime. Increased t_b can also influence the interconnectedness of the system by effectively enhancing any present topographic effect and desensitising the remaining ice mass from changes across the remainder of the system. Once basal topography, in particular relief, becomes a more significant influence on the ice dynamics, any minor thermal or ice surface gradient changes become negligible in their ability influence the stability of the modelled ice sheet.

3.5.7 Improving Models and the Influence of Error

The sensitivity of the thermodynamic calculations to basal traction is very apparent from our experiments, but it is not possible here to delineate which real-world basal processes are of most importance. The lack of individual data and models for these processes is therefore a key area in which ice sheet models are in deficit. For example, large-scale factors such as internal glacier hydrology and mechanisms of water delivery to the bed are likely to have a critical influence over patterns of long-term landscape evolution. The impact of deformable sediment behaviour and of lithological contrasts upon erosion patterns are also relatively unknown.

On a smaller scale, the parameterisation of erosion in numerical models has much room for improvement. Most models use bulk parameterisations of erosion rate that largely ignore the importance of factors such as the size distribution of 'tools' embedded in the glacier, or bedrock crack densities for example. Although Flowers and Clarke (2002) note that separating the problem of erosion into too many

individual sub-models that rely on unknowns, or that cannot be tied to field evidence is problematic, investigation in these areas may allow refinement of erosion models. This may allow clearer identification of the key interactions between ice sheets and topography.

Understanding the degree to which topography is controlling the pattern of erosion under an ice mass has important consequences for modelling ice mass behaviour of all kinds. Studies of ice sheet and landscape evolution use digital elevation models (DEMs) to represent the topography of the region of interest (e.g. Boulton and Hagdorn, 2006; DeConto et al., 2007; Hulton et al., 2002; Pollard et al., 2005). However, the impact that DEM uncertainty may have upon the outcome of numerical simulations of ice is often neglected (Hebeler et al., In Press). Although DEMs represent the landscape as a continuous structure, the raw data is rarely continuous and their generation often relies upon interpolation (Bamber et al., 2001; Layberry and Bamber, 2001; Lythe et al., 2001). Therefore, error is inherent in all such models. Our experiments show that features on the order of 10's of metres in relief can have an impact upon the distribution of erosion and on the stability of regions of fast flowing ice. Therefore future models of long-term landscape evolution under ice should consider the potential for propagation of error from bed DEMs into model output.

3.6 Conclusions

The importance of a number of different factors as controls upon erosion patterns were tested and include: topographic wavelength, landscape relief, the pre-glacial mode of landscape evolution, and local subglacial conditions. We find that the latter, as controlled in our models through the basal slip coefficient, are most critical in dictating the spatial distribution and rates of glacial erosion. The relief and dominant wavelengths in the landscape are also critical drivers in determining whether the mode of erosion that occurs is selective, areal or protective. It is clear that the interactions between all of these factors will determine how glacial erosion exploits the landscape. We summarise our main findings below:

- Our model of glacial erosion can recreate the range of patterns that relate to the processes which are key to landscape evolution under ice: selective glacial erosion, areal scouring and protection of relict landscapes under cold-based ice. These modelled patterns drive topographic change in patterns analogous to those identified in many previously and currently glaciated terrains.

- Average erosion rates are not significantly changeable in systems with different relief. However, the maximum erosion rates are generally increased in higher relief systems indicating that relief is critical in determining the degree of erosional selectivity that will occur.

- Maximum rates of erosion do not increase to the same degree as maximum erosion depths when relief is varied. This indicates that topographic overdeepenings are likely to be the result of increased temporal stability of ice 'streams' and that this stability is facilitated by the focussing nature of higher relief subglacial landscapes.

- In agreement with earlier work (Jamieson et al., 2008), we find that where ice flow is incising into topographic barriers, the associated focussed erosion may act to stabilise changes in ice dynamics, slowing the drawdown of ice into the ablation zone. This means that ice surface gradients are not subject to the rapid perturbations which can cause instabilities in the ice mass.

- The degree to which relief drives the erosional potential of the ice mass is sensitive to basal traction conditions which effectively determine how 'stiff' ice is. Thus with low t_b ice responds to features on a scale of several 100's of metres but if ice is less stiff, for example due to the presence of saturated basal sediments, then the basal thermal regime can be perturbed by geomorphic features as small as 10's of metres high.

- Thermal feedbacks generated in high t_b systems result in decreased temporal stability for individual streams, but increased erosional stability for the ice sheet as a whole, and increased spatial stability of individual ice streams. The temporal stability of regions experiencing selective erosion under conditions

of focussed flow is increased by larger relief in basal topographies and is particularly enhanced under shorter wavelength systems where relief is high.

- Ongoing glacial erosion and the transformation from a fluvial to a glacial terrain leads to increasingly efficient ice drainage and is accompanied by a transformation towards more selective erosion. Whether this is accompanied by increased or decreased ice sheet wide average erosion is very dependent upon climatic patterns.

- Temporal and spatial instabilities generated in a number of our models may be analogous to the kinds of behaviour occurring in West Antarctica. Here some ice streams have low velocities and other high, and others are migrating within their subglacial valley system. Our models also show that the 'interconnectedness' or ease of communication between ice streams is critically controlled by the processes encompassed in the basal traction parameter and by topography.

- It is clear that the use of t_b as a lumped variable that encompasses numerous potential processes operating at the ice-bed interface is restrictive. Methods for modelling deformable sediment conditions and its behaviour under changing basal water saturation are required, as are methods for simulating changes in lithology and at a smaller scale of factors such as bedrock crack density.

- Numerical feedbacks are common in models of ice sheet evolution. Our model is able to minimise localised creep instability, the most commonly identified of these. However, inherent error in the bed DEMs used in glaciological studies and the potential propagation of this error into modelled glacial dynamics and erosion may be a substantial issue for the modelling community to address.

Chapter 4

Chapter 4 has been submitted for publication as follows:

Jamieson, S.S.R. and Hulton, N.R.J., Submitted. The role of glacial erosion in limiting ice sheet extents. Nature Geosciences.

Nick Hulton (supervisor) developed the original ideas for this chapter which were used as initial justification for this PhD project.

David Sugden and Erin McClymont provided insightful comments on this manuscript.

Chapter 4 Does Glacial Erosion Control Ice Sheet Stability?

4.1 Summary

Ice sheet dynamics depend upon the links between glacier flow, climate, the oceans and topography. However, of these, topography is the only component traditionally viewed as playing a passive role in controlling ice sheet stability. We use an ice sheet model that links the thermal regime an ice mass to patterns of glacial erosion and show the first time that the modification of topography by ice sheets generates feedbacks on scales sufficient to control long-term ice sheet stability. Glacial erosion can induce ice margin retreat over periods of 10^5 - 10^6 years independently of climate change. By modelling erosion over a synthetic 'fluvial' topography we simulate a system that progressively increases ice discharge efficiency and that as a result reduces ice sheet extents by ca. 20% over 1.15 million years. Such feedbacks may drive the pattern of successively smaller Pleistocene ice sheets that occurred in Patagonia despite the opposite global trend towards increasingly intensive glaciation over the last 640 kyrs.

4.2 Background

External influences on glacier dynamics include tectonic subsidence (Clapperton, 1990; Singer et al., 2004), CO_2 forcing (DeConto and Pollard, 2003b), sea-level change (Denton and Hughes, 1986), migration of circulation currents (Heusser, 1989) and the build up of sea ice (Clapperton, 1990). Variations in the total surface area located above and below the snowline drive changes in ice dynamics by changing mass balance profiles and modifying pathways of ice drainage (Hulton and Sugden, 1995; Kerr, 1993). The potential influence of topography has been appreciated in the context of transforming fluvial landscapes to glacial systems (Clapperton, 1990; Kerr, 1993; Oerlemans, 1984; Penck, 1905) but few systematic attempts have been made to assess it. Harbor (1992) indicates that palaeoglacier reconstructions must consider the degree to which the palaeotopography has been

modified because palaeo ice discharge will change as a result. Modelling and field investigations of ice sheet dynamics and associated erosion and sediment production shows that rapid and irregular ice margin movement can be generated independently of climate because such systems are inherently unstable (Clark, 1994; Clark et al., 1999; Pollard and DeConto, 2003). However, in a more regular and predictable manner, over 10^5 - 10^6 years, glacial erosion of bedrock has also been hypothesised to cause large-scale ice margin retreat in ice sheets (Clapperton, 1990). Initial experiments demonstrated that this could lead to retreat where eroding ice streams were smaller in width than the wavelength of lithospheric flexure (Oerlemans, 1984).

Glacial-interglacial fluctuations documented by benthic $\delta^{18}O$ records show that intense Pleistocene glaciations achieved their greatest extent and volume after ca. 640 ka (Fig. 4.1) (Lisiecki and Raymo, 2005). However, geomorphological evidence in a number of regions shows the opposite tendency, with maximum ice extents occurring at earlier times (Singer et al., 2004; Sugden and Denton, 2004). This is a long-standing puzzle in Patagonia where the maximum Pleistocene ice sheet (the Greatest Patagonian Glaciation, GPG) (Caldenius, 1932) is dated to ca. 1.15 Ma (Singer et al., 2004), 550 kyrs prior to the most globally intensive Pleistocene glaciations (Fig. 4.1). Dating of well-preserved moraine systems indicate that ice sheets since the GPG have been successively less extensive (Fig. 4.1) (Kaplan et al., 2004; Singer et al., 2004). Indeed, at the last glacial maximum (LGM) the Patagonian Ice Sheet covered one third the area of the GPG. Another example occurs in Antarctica where the maximum glaciation occurred during the Mid-Miocene (~14 Ma) and where subsequent glaciations have been more limited even during the Pleistocene Ice Age cycles (Sugden and Denton, 2004). One suggestion is that bed erosion may be responsible for altering the behaviour of these ice sheets over long timescales.

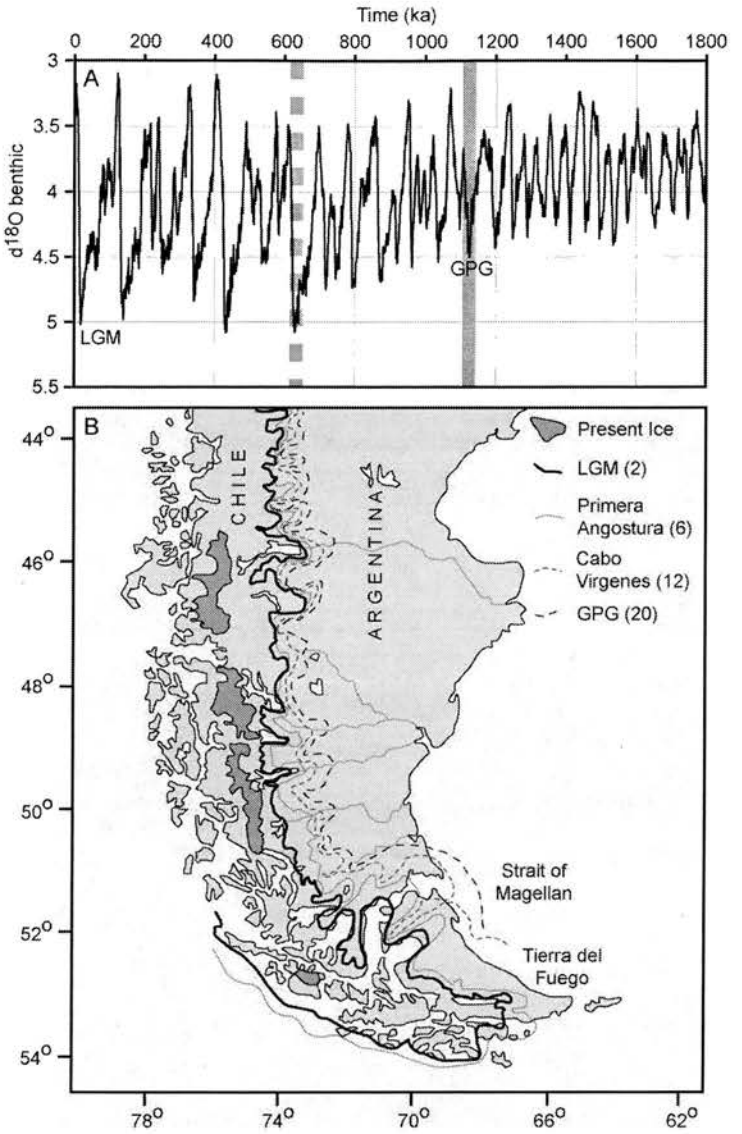

Figure 4.1: Glacial-Interglacial variability and the Patagonian Ice Sheet

A) Benthic $\delta^{18}O$ stack (Lisiecki and Raymo, 2005), a record of glacial-interglacial variability since 1.8 Ma. Downwards shifts in $\delta^{18}O$ reflect increased ice volume combined with cooling deep sea temperatures. The dashed vertical line thus marks the onset of the more intense glaciations that characterise the Late Pleistocene. The solid grey line marks the timing of the GPG (the Greatest Patagonian Glaciation, the most extensive ice limit recorded in the Patagonian geomorphological record (Caldenius, 1932)). LGM - Last Glacial Maximum. Note that the GPG occurs at ca. 1.15 Ma and although global ice volumes steadily increase during each of the next 7 glacial cycles, the Patagonian record displays the opposite trend with maximum ice sheet extents becoming successively smaller. B) Former ice sheet extents in Patagonia determined by geomorphological mapping of moraine limits. Note that the ice sheet becomes smaller during each successively recorded glacial cycle. The numbers in parentheses identify oxygen isotope stage after (Rabassa et al., 2000; Singer et al., 2004). Note that the retreats of the ice margins are greatest around the valley floors of the large-scale drainage systems.

4.3 Approach

To solve the problem presented by the evidence above we use a numerical ice sheet and erosion model (Jamieson et al., 2008; Payne, 1999) to simulate the growth of ice sheets and the resultant landscape evolution over a 1.15 Myr period. The model physics reproduce the feedbacks that occur between fast flow and ice temperature, allowing realistic prediction of ice convergence and its associated glaciological feedbacks. These feedbacks form the primary control on the basal thermal regime, enabling accelerated mass throughput and the generation of areas of streaming flow to be modelled – critical when investigating glacial landscape evolution.

Ice masses slide (and therefore erode) at the bed only where the basal ice temperature reaches pressure melting point and water is produced (Paterson, 1994). Patterns of basal ice flow that are equivalent to streaming ice can be modelled (Jamieson et al., 2008), which is key to modelling patterns of erosion.

Glacial erosion is parameterised as a function of basal ice velocity (υ_b) and ice thickness (H) (Boulton, 1979) thus:

$$E = -f \mid \upsilon_b \mid H \tag{4.1}$$

Erosion is made more or less effective using a scaling factor (f) that describes the susceptibility of rock to erosion and is kept constant here. To drive our model, accumulation and ablation are prescribed as a function of elevation and at 1800 m both air temperature and accumulation are zero (Hulton et al., 1994). Accumulation rises to a plateau of 0.4 ma^{-1} at an elevation of 2300 m and air temperature is parameterised using a vertical lapse rate of -5 °C km^{-1}. Thus the model embodies a simple, well known, feedback whereby ice sheets partially sustain themselves by virtue of having large areas at high elevation which are in positive mass balance.

The input topography is a continental-scale 4 km high mountain range generated at a resolution of 5 km using a fluvial-tectonic landscape evolution model (Tucker and Bras, 1998). The use of such a synthetic topography allows us to identify the timeline

of evolution from a 'fluvial' towards a 'glacial' landscape and its impact upon ice sheet behaviour. This is crucial given that glacial erosion is thought to push a topography towards equilibrium with the overlying ice (Penck, 1905). The principal process being modelled is therefore the modification of a fluvial system by glacial erosion, with the scaling of the valley spacing both before and after glaciation being controlled by the pre-glacial topography.

In order to test the sensitivity of our model to repeated glaciation, the retention of the erosional signal through multiple glacial cycles is simulated by imposing repetitive pseudo-100 kyr cycles on the climate. Each cycle is characterised by a gradual global temperature drop of 10 °C over 90 kyrs, a 10 kyrs long period at -10 °C to allow ice sheet stabilisation, and then a rapid 10 °C rise in temperature. We carry out a further sensitivity test to ensure that the impact of the flexural response of the lithosphere upon the behaviour of the ice can be distinguished from that of the glacial erosion.

4.4 Results

In our experiments ice expands to cover an area of 9.7×10^5 km^2 with ice thicknesses of up to 2700 m and a surface profile perturbed by subglacial ridges and valleys (Fig. 4.2). Ice grows to the mountain front within ca. 150 kyrs, and a mature thermal regime and associated erosion pattern are established (Fig. 4.3). The modelled erosion is highly selective (Fig. 4.2) and generates overdeepening of pre-existing valley long-profiles (Fig. 4.4). This selectivity is driven by initial spatial variation in basal melt rates determined by the form of the evolving valley systems through a combination of two factors: 1) ice confluence, leading to frictional heating and convergent heat advection; and 2) the presence of insulating thicker ice in the deep valleys. This is consistent with studies indicating that the progression from flow convergence in an ice sheet interior towards focussed valley constrained flow at the margins promotes glacial fjord development (Glasser, 1995; MacGregor et al., 2000). The mean elevation of the bedrock topography is eroded by only ca. 12 m and this modification is skewed towards the lower ablation zone (Fig. 4.5). Topographic relief increases by ca. 400 m, ca. 80 % of which is a direct result of glacial

excavation, with the remainder resulting from localised isostatic effects where zones adjacent to intense erosion are protected by cold-based ice and are uplifted (Fig. 4.2).

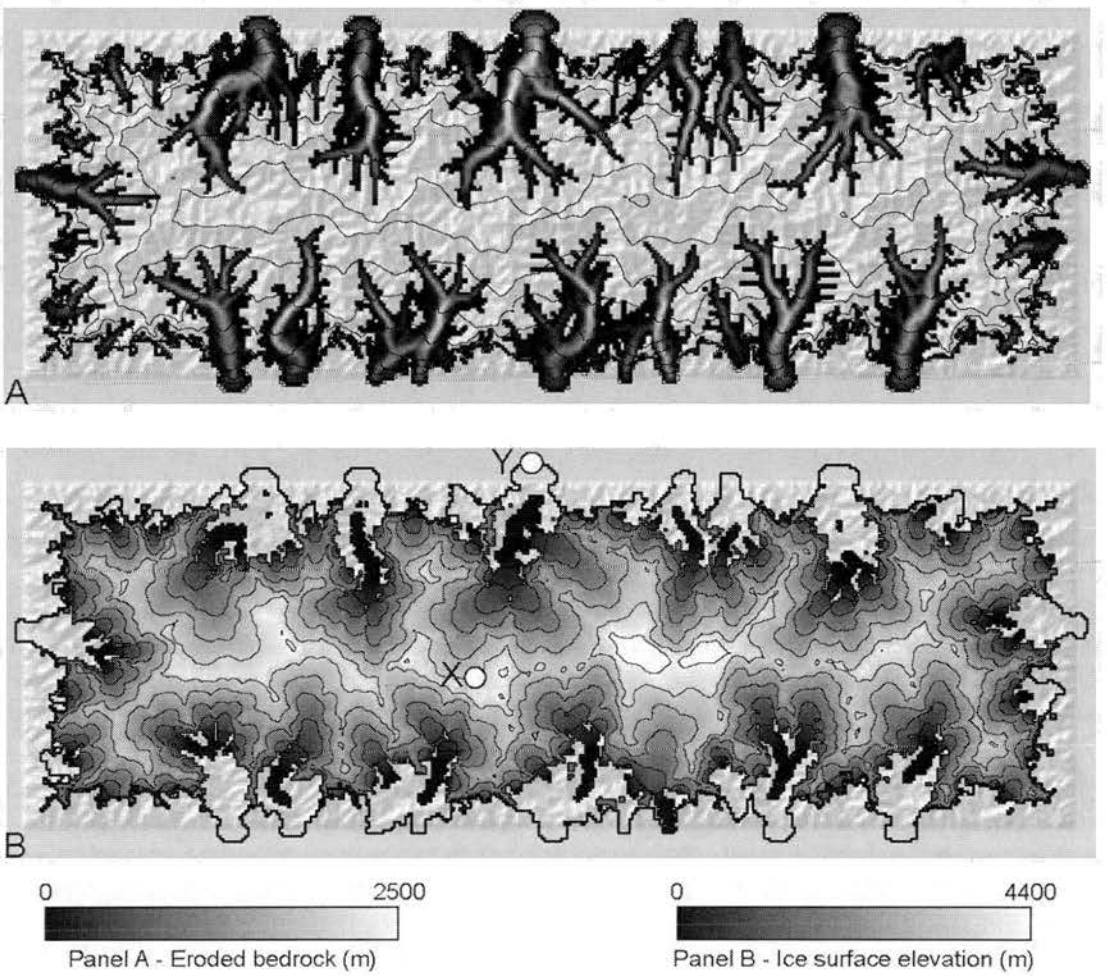

Figure 4.2: Maps of erosion and self-limiting behaviour.

A) Total erosion distribution at the end of the simulation after 1.15 Myrs. The contours show 500 m ice surface at maximum extent and erosion is shown by the greyscale shading. Note the selective nature of the erosion in overdeepening large-scale pre-existing drainage systems. B) Map showing ice retreat over 1.15 Myrs. Heavy black line shows ice sheet maximum which occurs early in the model run. Greyscale shading and 500 m contours show ice surface after 1.15 Million years. Significant ice sheet retreat occurs in the main ice drainage systems and is a result of erosionally driven mass balance changes. X and Y indicate the location of the profile in Figures 4.3 and 4.4.

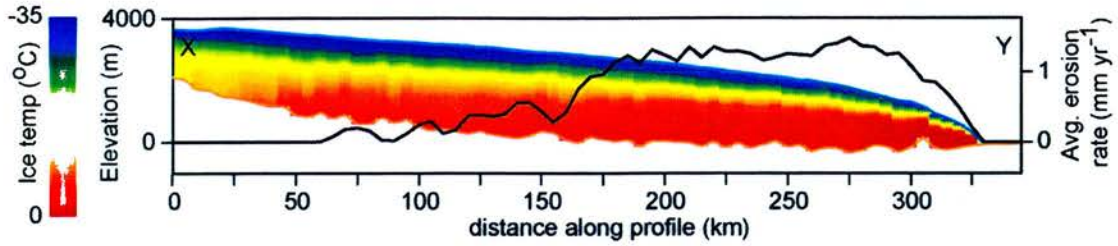

Figure 4.3: Ice temperature profile through outlet glacier at maximum ice sheet extent.

The associated profile of average erosion rate over a 1.15 million year time period is superimposed. Profile X-Y is identified on Figure 4.2B and follows the path of ice flow between each point.

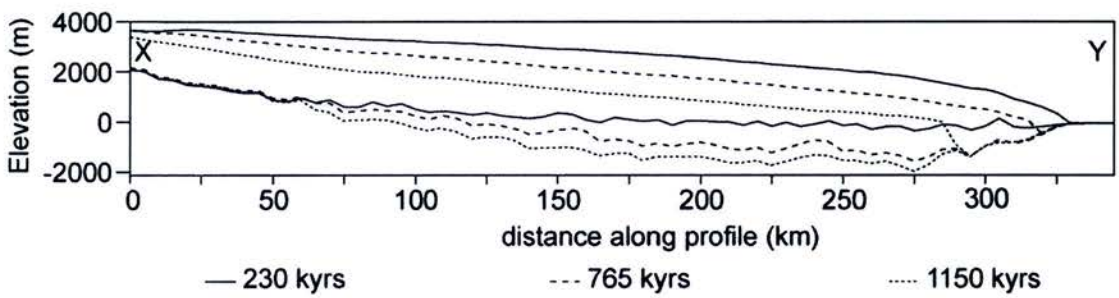

Figure 4.4: Profile of outlet glacier retreat

Profiles of ice surface and bedrock elevation at three time intervals showing the retreat of an ice stream from its maximum extent. Note that as bedrock erosion continues, a progressively larger area of ice surface sinks below the ELA (1800 m) forcing the ice mass into an increasingly negative state of mass balance finally resulting in retreat of the ice margin. Profile X-Y is marked on Figure 4.2B and follows the path of ice flow between each point.

The result of long-term erosion under a constant climate is to induce ice margin retreat in the modelled ice sheet (Fig. 4.2). Smaller drainage systems retreat earliest due to short residency times for ice and increased sensitivity to mass balance changes, and the larger systems begin retreat by ca. 400 kyrs. Retreat occurs at different times and rates depending upon the characteristics of the drainage system. After 1.15 Myrs, ice margin retreat is significant (Figs. 4.2 and 4.4) and the ice sheet loses ca. 20% of its area compared to maximum extent, corresponding to a ca. 50 % ice volume reduction (Fig. 4.5). Rates of landscape evolution are greater in the earlier stages of transformation from the fluvial to the glacial system. Our models

yield average erosion rates ranging from ca. 1.1 mm yr^{-1} under maximum ice conditions, to ca. 0.8 mm yr^{-1} after 1.15 Myrs and are in line with estimates of higher rates estimated in a number of regions (Bogen, 1996).

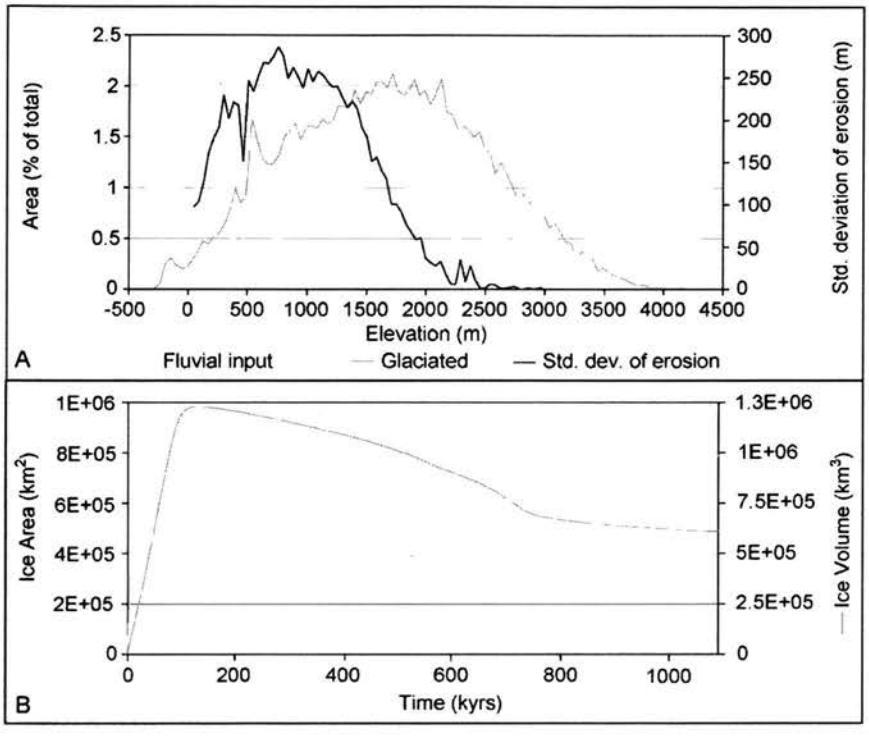

Figure 4.5: Modelled ice sheet and subglacial topographic change through time.

A) Hypsometric plots of the pre-glacial fluvial and resulting glaciated topographies showing the changing distribution of land area over elevation as glacial erosion proceeds. The standard deviation of total erosion is superimposed to identify where the bulk of topographic change has occurred, and to relate this to resultant post-glacial topographic state. Note that the majority of topographic change occurs below the ELA (1800 m) as indicated by the crossing of the hypsometric plots at this point. *B*) Graph of evolving ice sheet volume and ice sheet area over 1.15 Myrs. Note that the ice sheet tends towards an equilibrium state as predicted by Penck (1905).

4.5 Mechanism

The process of margin retreat is driven by erosion as it increases discharge across and below the ELA. This pushes the glacial system into a more negative state of mass balance as ice surface area below the ELA subsequently increases. The ice sheet therefore becomes increasingly efficient at losing mass because ice is drawn through the system at a growing rate. The process is reinforced by feedback effects

as cold areas of ice get cooler, and warm, faster flowing regions become warmer. This latter thermal feedback increases the ability of the ice sheet to transport mass, making it even more responsive to variations in snowfall, thus further focussing erosion (Jamieson et al., 2008). As erosion proceeds, the outlet tongues are lowered and are increasingly subject to ablation, thus causing onset of retreat for the ice stream (Fig. 4.4). The process we identify is therefore consistent with previous studies that model bedrock erosion on valley glacier scales which also note erosion induced retreat (MacGregor et al., 2000; Oerlemans, 1984). The retreat mechanism is strongly dependent upon vertical and spatial climatic gradients. The implication is that glacial sensitivity to erosional feedback is greater in maritime areas than in continental ones due to the steeper vertical mass balance gradients encountered in coastal areas.

4.6 Discussion

Using a repeated cyclical climate to force expansion and contraction of ice we find that the impact of erosion upon ice dynamics in earlier glacial cycles is retained during following glaciations. This is the case regardless of the inclusion of isostatic adjustment, confirming that the retreat mechanism recorded in our experiments is purely the result of long-term glacial landscape evolution rather than the product of transient isostatic states. Therefore, assuming interglacial denudation processes do not fully reset a glaciated topography, the mechanism identified here can generate systematic (as opposed to irregular) reductions in maximum ice extents through successive glacial cycles without changing climatic intensity. This can therefore explain the survival of older moraine complexes beyond LGM moraines in many glaciated landscapes (Clapperton, 1990; Rabassa et al., 2000; Singer et al., 2004).

The mechanism identified here could potentially be countered by tectonic uplift whereby the landscape would increase in elevation and thus maintain positive mass balance due to cooling. The selective nature of glacial erosion means that the mechanism inherently produces differential uplift. Uplift is generated across the ridges where there is no erosion because the wavelength of lithospheric response is

larger than that of the glacial trough. This process has been identified in a number of previously glaciated regions (Montgomery, 1994; Small and Anderson, 1998). The erosion-induced reduction in the size of the ice sheet, however, restricts the continuation of this ridgeline uplift because the area available to potential isostatic uplift by this mechanism also decreases accordingly. Therefore, although changing climate can drive mountain uplift (Molnar and England, 1990), such a mechanism could not be sustained over long timescales unless ice mass input was to continually increase through another mechanism.

4.7 Conclusions

Our results show that glacial erosion of bedrock is critical in determining the dynamics of large-scale ice sheets (MacGregor et al., 2000; Oerlemans, 1984). Erosion can reduce ice sheet extent over multiple glacial cycles. The implication is that understanding patterns and rates of glacial erosion, both past and present, are critical to predicting future ice mass behaviour over timescales greater than 10^5 years. There are implications for interpreting field observations of regional ice limits in relation to the spatial synchronicity of the onset of margin retreat. Glacial erosion therefore helps explain the puzzle of how ice sheet growth can follow a pattern that counters the record of glaciation intensity. We show that landscapes in the early stages of being transformed from fluvial to glacial support the largest ice sheets. Furthermore, our model indicates that the most rapid rates of long-term landscape evolution occur under these earlier, larger glacial conditions, with later incarnations of ice masses becoming less erosionally effective.

Chapter 5

Early components of Chapter 5 have been published as part of a paper that discusses the landscape evolution of Antarctica as follows:

Jamieson, S.S.R. and Sugden, D.E., 2008. Landscape evolution of Antarctica. In: A.K. Cooper et al. (Editors), Antarctica: A Keystone in a Changing World - Proceedings of the 10th International Symposium on Antarctic Earth Sciences. The National Academies Press, Washington D.C., pp. 39-54.

This paper can be found in Appendix A.

The great majority of work in Chapter 5 was carried out by me based on initial ideas by David Sugden and Nick Hulton (supervisor).

The model used to generate the input climates for this chapter can be found in Appendix B.

Chapter 5 Modelling the Glacial Landscape Evolution of Antarctica.

5.1 Aim

We aim to model the patterns of glacial erosion that have existed across Antarctica since the Oligocene. Over ca. 34 million years Antarctica has been subject to erosion associated with local, regional and continental scale glacial conditions. The degree and nature of this evolution is difficult to determine for the Antarctic due to the inaccessibility of the bed. The behaviour and interactions between ice and topography inferred from limited geological evidence around the margins of Antarctica has been useful for interpreting the subglacial conditions and dynamics of the Antarctic Ice Sheet as it evolved. However, the development of numerical models of ice sheet dynamics and glacial erosion offer the potential to investigate the nature of this evolution at a large scale, over long time periods and under different glaciological regimes.

Predicting the modes of long-term landscape evolution in Antarctica over such a timescale is a significant challenge. It is an important one however, because it will give new insights regarding the degree to which Antarctica has been sculpted by ice, and the extent to which the pre-glacial landscape has driven the pattern of glacial evolution. Such an assessment has never been made on a continental scale for Antarctica, and by linking this to evidence from on and off shore we take a unique approach towards achieving our goal. Understanding how the landscape has been modified by the ice will be useful for relating ice sheet fluctuations to geomorphological evidence. This will aid in the interpretation of past and the prediction of future ice sheet behaviour.

5.2 Background

5.2.1 Geological Setting

Antarctica is a former fragment of the Gondwanan supercontinent (Figure 5.1) and was separated from its parent over a ca. 100 million year period between 160 and 55 Ma. This led to the eventual creation of the Tasmanian Passage at between ~35.5 and 30.2 Ma (Stickley et al., 2004). Around 31 Ma, the opening of the Drake Passage occurred (Lawver and Gahagan, 2003), and with this the Antarctic Circumpolar Current (ACC) was likely initiated.

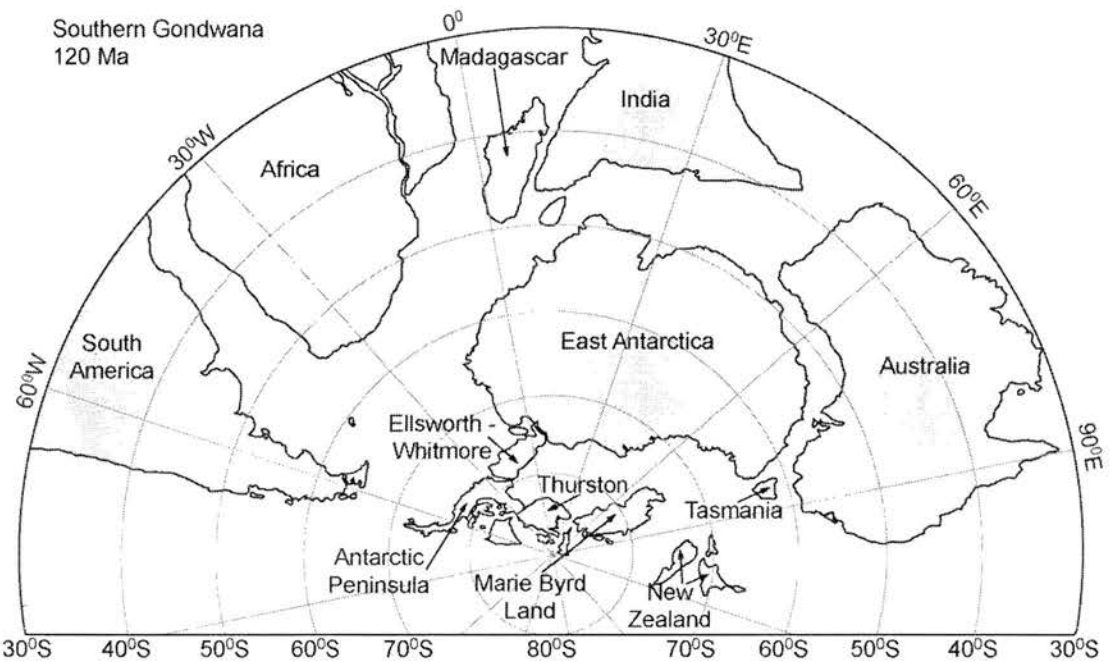

Figure 5.1: Breakup of Gondwana at 120 Ma.

Note that at this time only India and Africa were separated to the extent that significant seaways had opened up.

This long-term creation of seaways around Antarctica is favoured by some as the central cause of initiation of ice growth through the associated changes to oceanic circulation and productivity patterns (Lawver et al., 1991; Livermore et al., 2007). However, there is debate about whether Antarctic ice or changes in oceanic structure came first (Hay et al., 2005). However, modelling studies indicate a reduction in atmospheric CO_2 concentrations may have been the main cause of ice sheet initiation

(DeConto and Pollard, 2003b; Huber and Nof, 2006), with the effects of the ACC being felt subsequently (Barker and Thomas, 2004). Climatic cooling as a result of lowered CO_2 concentrations and increased moisture availability due to the proximity of the ocean (Kennett, 1977) gave rise to conditions suitable for ice growth by ca. 34 Ma.

The ice free regions of Antarctica have been subjected to modification by fluvial processes over at least the past 118 Myrs and the first rivers likely began to discharge from the Lambert basin region of East Antarctica. It is therefore possible to predict that river systems similar in scale to the Orange River in South Africa or the Murray-Darling Rivers in Australia would have been generated in Antarctica (Jamieson et al., 2005). On a smaller scale, dendritic river patterns have been identified in the Transantarctic Mountains (TAM) of Victoria Land (Baroni et al., 2005; Sugden et al., 1999) indicating that fluvial incision enhanced the denudation of the mountains between 55 and 34 Ma. This enhanced denudation along the TAM is thought to be on the order of 4-6 km since the early rifting in the Cretaceous (Fitzgerald and Stump, 1997). Figure 5.2 shows the pattern of river networks that would be expected after removing the present day ice sheet and compensating for the flexural isostatic rebound. Such dendritic patterns indicate that a fluvial signature is retained on a large scale under the ice sheet despite 34 Million years of glaciation at different scales. We hypothesise that the existence of a multi-scaled fluvial signal in the subglacial topography likely influenced the pattern of glacial erosion vs. landscape preservation as the ice sheet grew.

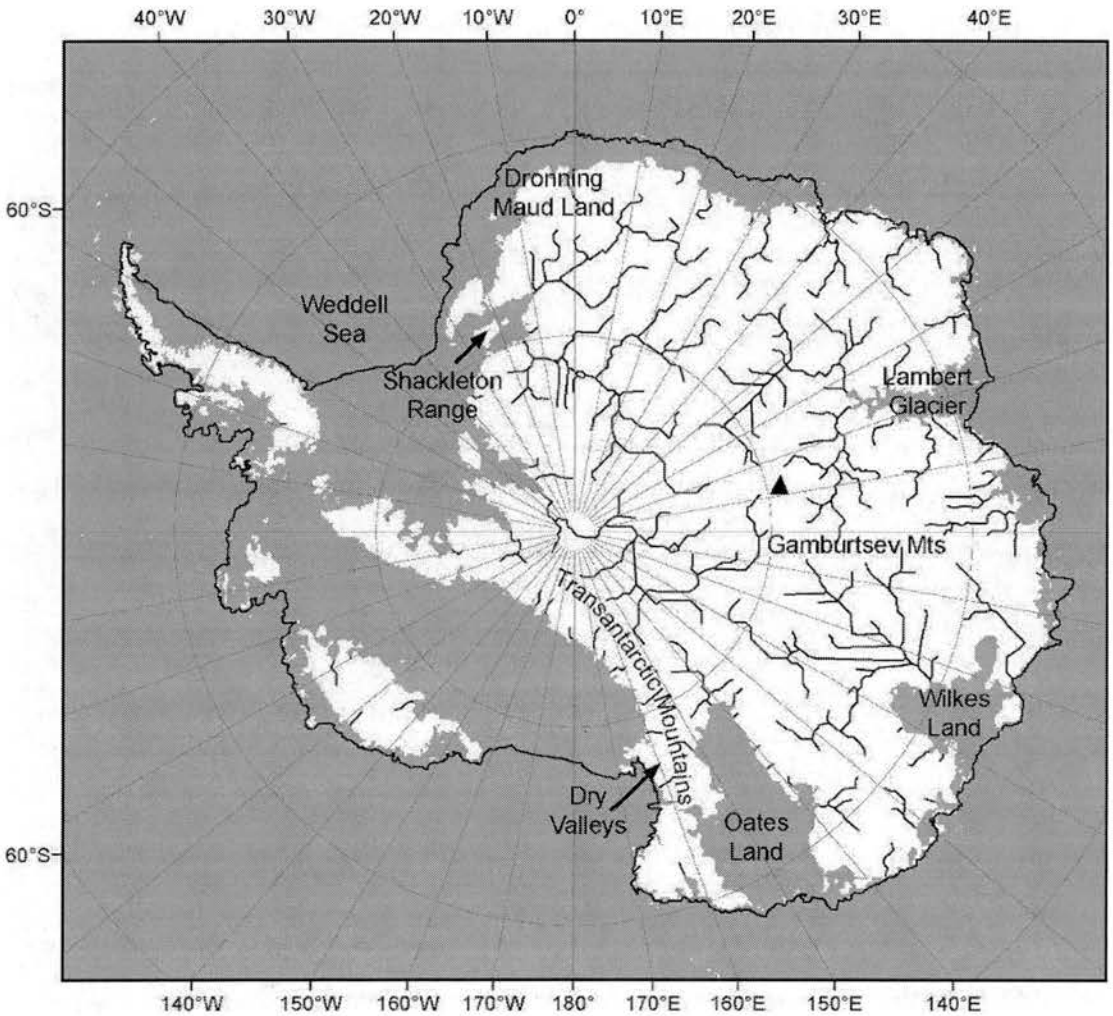

Figure 5.2: The fluvial structure of the Antarctic topography

Reconstruction of river patterns on the rebounded subglacial topography of present day Antarctica. The sea level is 100 m lower than today to represent subsidence associated with crustal cooling and flexure of mature passive continental margins. The topography is based on the BEDMAP subglacial topography and ice thickness datasets at a nominal cellular scale of 5 km (Lythe et al., 2001).

5.2.2 Antarctic Climate/Glacial History

Antarctica was primed for glacial conditions in the Early Oligocene (ca. 34 Ma) due to decreased CO_2 concentrations in the atmosphere, the proximity of moisture from the ocean, and the sensitivity of climate to relief which was generated at the coast through rift-related tectonism and associated erosion induced uplift (Huybrechts, 1993; Kerr and Huybrechts, 1999). Initial ice growth is documented in the benthic oxygen isotope record by a sharp increase in global $\delta^{18}O$ concentrations, marking a rapid ca. 4 $^{\circ}C$ drop in temperature (Figure 5.3 - Zachos et al., 2001). Evidence from

the CIROS-1 core drilled in the McMurdo Sound adjacent to the TAM suggests that in the Early Oligocene the climatic conditions were sufficiently warm that beech forest could be supported (Mildenhall, 1989). The inference is that climate was similar to present day Patagonia (McCulloch et al., 2000). Under decreasing temperatures the vegetation survived as sparse scrub forest or as moss tundra in favoured locations (Raine and Askin, 2001). This land cover change was recorded by 24.2-18 Ma as a transition from clay minerals like smectite, typical of forest soils, towards strong illite formation which is characteristic of soils developing in polar environments (Ehrmann et al., 2005).

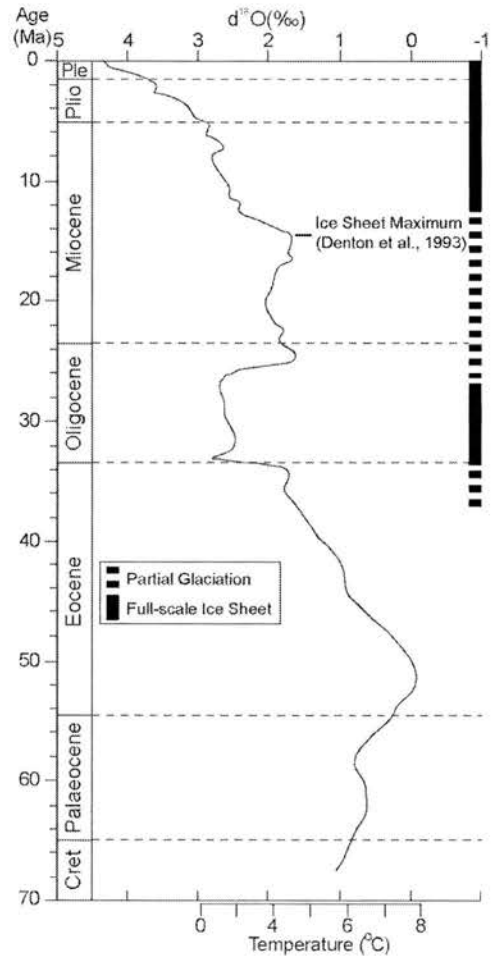

Figure 5.3: Global deep-sea oxygen isotope curve

This curve indicates glacial intensity over the various stages of Antarctic glaciation and is a 5 point running mean. Temperature is applicable only to pre-Antarctic glaciation (ca. 34 Ma) because $\delta^{18}O$ is calibrated for an ice free ocean system. After Zachos et al., (2001) and Jamieson et al., (2005).

The global ice volume record of Zachos et al., (2001) indicates that there may have been a period of warming in the late Oligocene and Early Miocene, but it is unclear whether this warming was significant or if it even occurred at all (Jamieson et al., 2005). However, for the ca. 20 Myrs following glacial inception, the ice sheet volume fluctuated on a similar scale to the Pleistocene ice sheets of the Northern Hemisphere (Naish et al., 2001; Pekar and DeConto, 2006). The first step in cooling of the climate in the Early Oligocene was followed between ca. 14.2-12.7 Ma (mid-Miocene) by a significant cooling within Pacific surface waters (Holbourn et al., 2005; Shevenell et al., 2004). At this time, a switch from warm- to cold-based local glaciation is inferred from changes in till facies in the McMurdo sector of the TAM, representing a decline in atmospheric temperatures. The ice sheet is thought to have reached its maximum size at ca. 14 Ma, and in East Antarctica is thought to have retreated back to a size similar to present by ca. 13.5 Ma (Anderson, 1999). Since the mid-Miocene maximum hyper-arid polar conditions have prevailed (Denton et al., 1993b; Marchant et al., 1996).

A full polar ice sheet is likely to have existed for the past ca. 14 Myrs, and has fluctuated in size to a relatively minor degree, with changes in size largely controlled by sea level change (Denton and Hughes, 1986). This is exemplified by the case of the ice sheets size at the Last Glacial Maximum (LGM). This period was marked by thickening of ice at the coast in response to global sea level lowering (Denton et al., 1991) and an ice sheet that expanded slightly to reach the continental shelf edge around the majority of Antarctica (Anderson et al., 2002). Furthermore, the ice sheet in Mac Robertson Land has displayed a similar profile for the last ca. 7 kyrs, coincident with sea level stabilisation after the decay of the northern hemisphere ice sheets (Mackintosh et al., 2007).

The present day ice sheet is shown in Figure 5.4 and its bed geometry in Figure 5.5. It has ice thicknesses of up to 4400 m and is currently subject to snowfall of up to 0.5 m in coastal regions (Vaughan et al., 1999). The mean annual temperature at sea level is presently ca. -15 $^{\circ}$C but varies between ca. 0 $^{\circ}$C in summer and -30 $^{\circ}$C in winter (Anderson, 1999). The West Antarctic Ice Sheet (WAIS) is less stable than its East Antarctic counterpart because of its maritime regime whereby a large percentage of its bed is significantly (over 1 km) below sea level. This makes it

highly responsive to sea level change in comparison to the East Antarctic Ice Sheet (EAIS) (Anderson et al., 2002). This dynamic behaviour is typified by the presence of ice streams with high discharge rates (100's to 1000's of metres per year) that are showing evidence of response to global climate change over short timescales (e.g. Pine Island Glacier - Payne et al., 2004; Rignot, 2002; Shepherd et al., 2004). The EAIS has average ice thicknesses of ca. 2500 m (Lythe et al., 2001) is much more stable, and is currently gaining mass in the interior (Davis et al., 2005).

We can see therefore, that the knowledge of climate and ice sheet response in Antarctica since the Miocene is limited in resolution. However, the key regime changes are recorded in the geomorphic record of Antarctica.

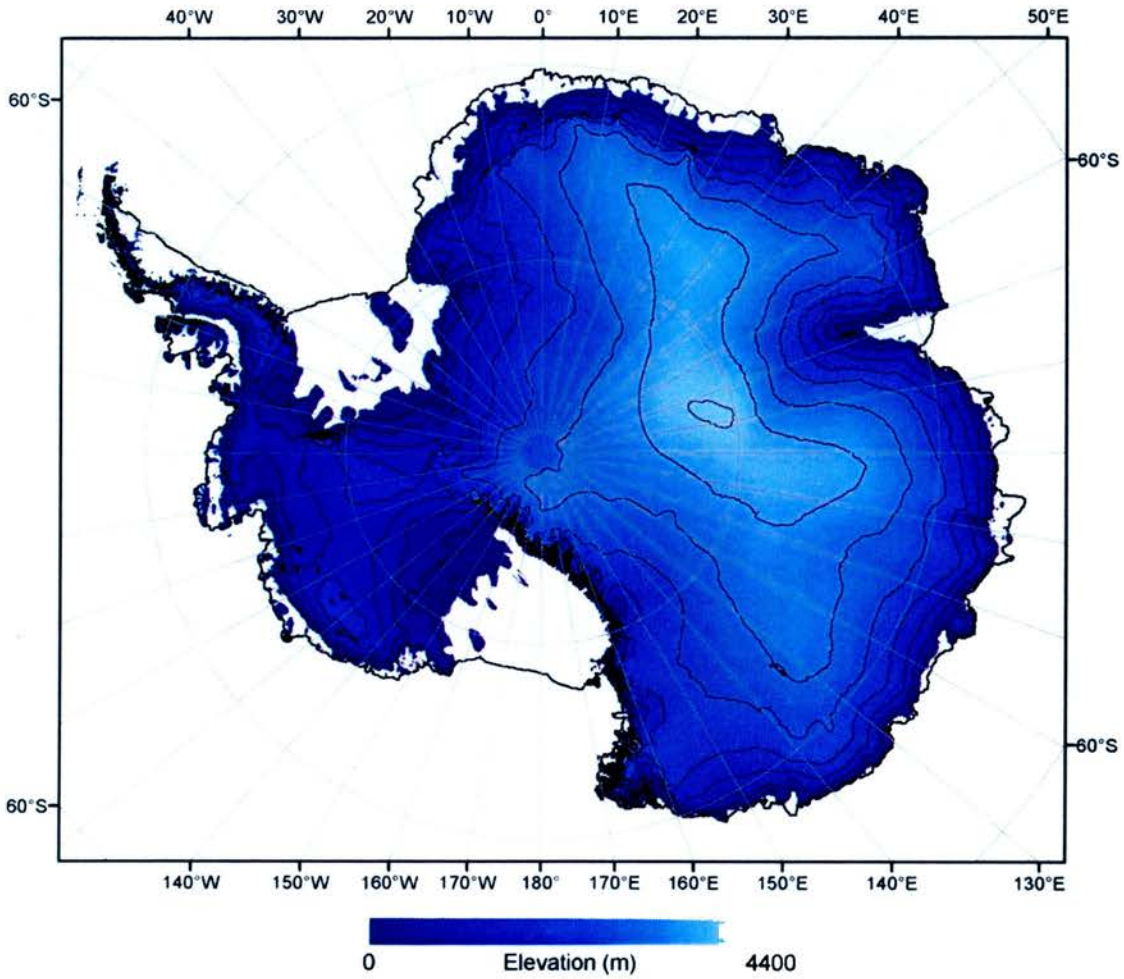

Figure 5.4: The present day Antarctic Ice Sheet

Data from the BEDMAP dataset (Lythe et al., 2001). Contours = 500 m ice surface, thick black line shows outline of present day ice shelves.

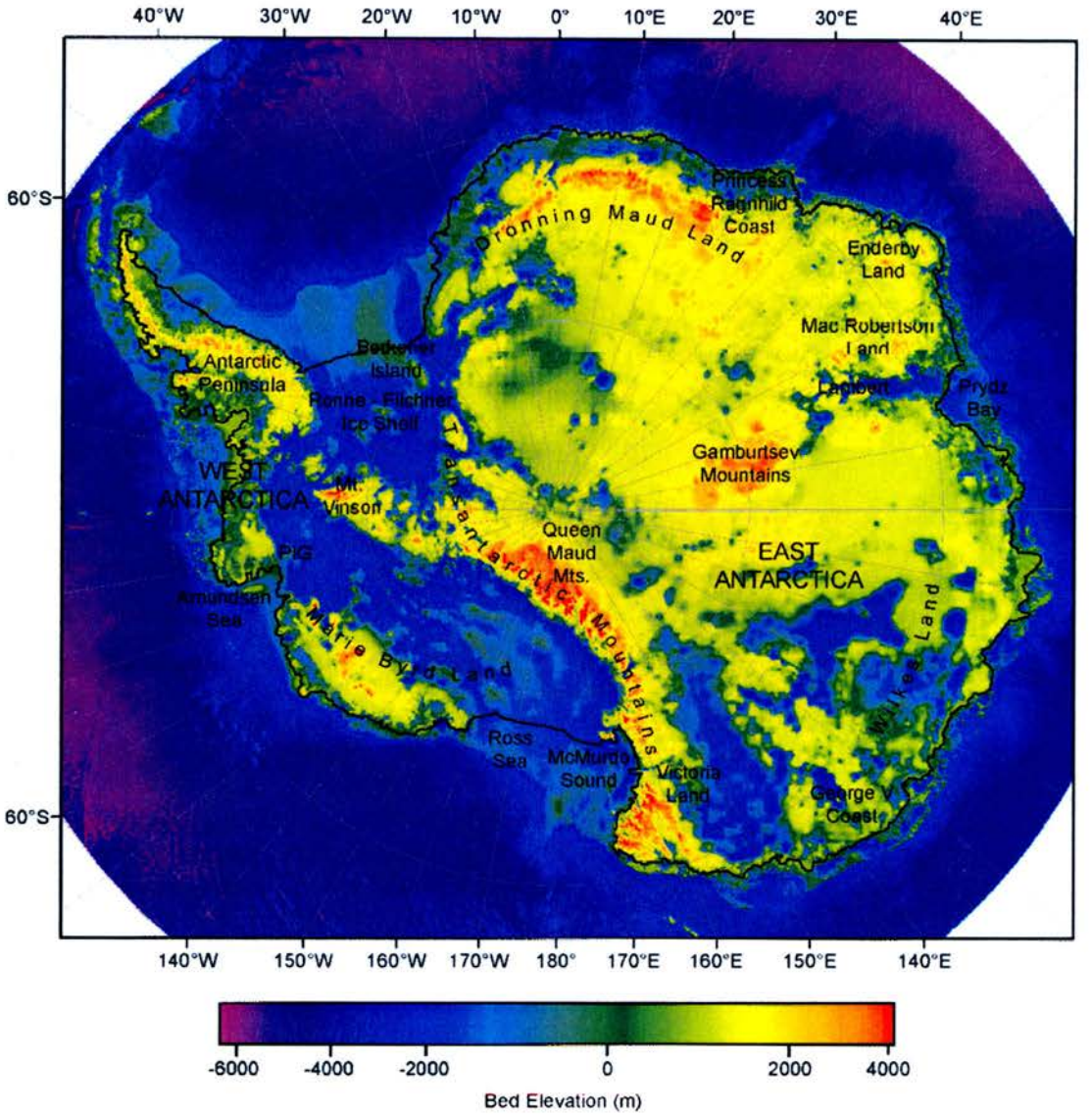

Figure 5.5: Present day subglacial landscape of Antarctica

The present day subglacial bed geometry of Antarctica and key locations mentioned in the text. Data from BEDMAP (Lythe et al., 2001).

5.2.3 Landscapes of Glaciation

The evidence above points to multiple scales of glaciation throughout the last 34 million years as localised and regional glaciation gives way to continent-wide glaciation. Therefore we might expect that the bed geometry of Antarctica displays features related to various glacier flow regimes under these different scales of ice mass. Much of our knowledge of landscape modification under ice is gained from investigations of formerly ice-covered areas in the northern hemisphere.

Geomorphological studies have enabled the landform assemblages associated with small and large-scale glaciations to be related to ice dynamics (Stumpf et al., 2000). The spatial variation of sliding leads to the generation of differing styles of glacial landscape which can be classified (Sugden, 1978a; Sugden and John, 1976). The most spectacular glacial features, such as troughs incised into plateaus, are formed under conditions of selective linear erosion whereby ice flow becomes focussed – often by topography. When ice subjects wide areas to glacial scour where the ice sliding at the bed is inferred to be slower and less focussed it creates regional landscapes of smoothed bedrock. Where ice is cold-based, water production and thus sliding, does not occur and so the landscape is largely protected from modification. Geomorphology thus reflects the behaviour of former ice masses and has been widely used in reconstructing ice sheet dynamics (e.g. Briner et al., 2006; Davis et al., 2006; Hall and Glasser, 2003; Kite and Hindmarsh, 2007; Phillips et al., 2006; Stroeven et al., 2002a; Sugden, 1978a).

5.2.4 Antarctic Geomorphology

Figure 5.6 shows an early analysis of the distribution of landscapes and a prediction of the modes of erosion that have occurred in Antarctica (Sugden and John, 1976). This prediction has stood the test of time remarkably well. On a continental scale for example, the Lambert basin of East Antarctica was one of the first sites to discharge ice upon the development a continental-scale ice sheet (Barrett, 1996; Jamieson et al., 2005). Selective erosion has dominated here causing the overdeepening of the Lambert Graben (Hambrey et al., 2007). On the other side of Antarctica numerous troughs cut across the TAM indicate the long-term importance of selective glacial erosion under local and continental scale focussed flow conditions.

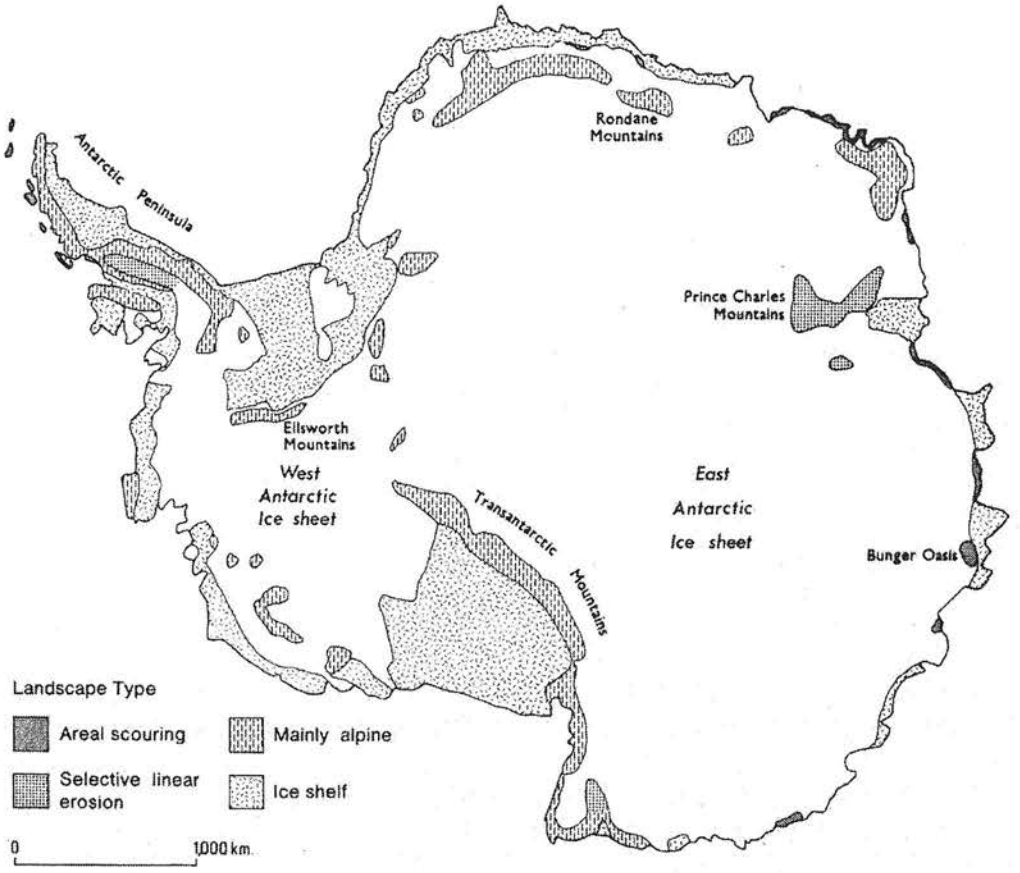

Figure 5.6: Reconstruction of erosion regimes in Antarctica

A compilation map of the landscapes of glacial erosion in Antarctica predicting the modes of glacial erosion effective since the establishment of the Antarctic ice sheet (from Sugden and John, 1976).

On a local scale, there is evidence to suggest that the Gamburtsev subglacial mountains were subject to relatively small scale modification under early glacial conditions (Perkins, 1984). Evidence of localised ice conditions has been found in the subglacial topography of Dronning-Maud Land where cirques and U-shaped valleys have been preserved for at least 2.5 Myrs (Holmlund and Naslund, 1994). Furthermore, Baroni et al., (2008) have identified that during the Oligocene, localised warm-based (and thus eroding) ice deposited the Ricker Hills Tillite in the Victoria Land sector of the TAM. This region is characterised by alpine (i.e. localised) glacial features with trimlines defining the upper limit of warm-based ice, and thus indicating the protection of the high-level areas since the Oligocene. It is also possible to identify evidence of multiple scales of glacial modification in some

parts of Antarctica. For example, geomorphological investigations in Marie Byrd Land have indicated that as ice retreated from the coastal mountains since the LGM, regional ice flow which overtopped the massifs was subsequently replaced by localised radial flow (Sugden et al., 2005).

It is evident that geomorphological studies tend to rely on detailed data from either focussed subglacial regions, or from relatively localised ice free areas. The opportunity offered by numerical modelling is such that reproducible simulations predicting geomorphic evolution can be constructed despite a lack of direct access to the majority of the Antarctic bed.

5.2.5 Objectives

The objectives of this research are:

- To link the modern day Patagonian climate to a numerical ice sheet model and predict the growth of ice on Antarctica during Oligocene times, and its development from localised ice caps to continental scale ice sheet.
- To employ a model of glacial erosion coupled to the ice sheet model to predict the spatial distribution of landscape development under the varying scales of ice sheet.
- To construct a generalised classification of modes of landscape modification in Antarctica. In particular we will predict and map the distribution and temporal stability of selective focussed erosion, areal scour, or protection under cold-based ice over the last 34 Myrs. We will further predict the degree to which ice flow has changed direction over different parts of the Antarctic bed.

5.3 Approach

The model of glacial inception and development by DeConto and Pollard (2003a; 2003b) was successful in identifying key sensitivities affecting Antarctic Ice Sheet-

climate interactions in relation to changing forcing factors (e.g. greenhouse gas concentrations, orbital forcing or oceanic circulation). However, it relies upon output from global circulation models (GCMs) which are computationally hungry, and are rarely fully coupled to models of ice sheet development. CGMs also make numerous assumptions with regard to the climate system, and generally only operate over scales of 100's of kilometres. The alternative to using such an approach is to employ a parameterisation based upon modern climate as the foundation for driving the pattern of surface mass balance in a model (Huybrechts, 1993; Huybrechts et al., 2000; Oerlemans and Van Der Veen, 1984). Such an approach will be employed here and is suited to testing ice sheet response to changes in bedrock geometry and to simulating past and future glacial response to changes in temperature and precipitation (DeConto and Pollard, 2003a).

We have argued that parts of the Antarctic continent at 34 Ma had similar climate to present day Patagonia (Mildenhall, 1989; Raine and Askin, 2001). This presents us with a starting point in terms of climatic parameterisation that will allow us to test whether a modelled pattern of glaciation fits with the idea of localised glaciation at this time. We can then model the progression from localised, through regional towards full-scale ice sheet dynamics. Carrying out this experiment using an ice sheet model that contains an erosion algorithm allows us to simultaneously predict the degree and distribution of bedrock excavation that might have occurred under such stages of ice sheet growth.

5.3.1 Ice Sheet Model

We use an ice sheet model (GLIMMER - Payne, 1999; Rutt et al., Submitted) that follows Huybrechts (1986) and that has benefited from developments by, amongst others, Boulton and Payne (1992), Payne (1999) and Jamieson et al. (2008). The model was one of those used in the EISMINT model intercomparisons (Huybrechts and Payne, 1996; Payne et al., 2000), a set of experiments designed to set benchmarks for model development. Calculations of ice dynamics are handled using the shallow ice approximation (Hutter, 1983), a scheme which assumes the slopes of the bedrock and of the ice surface are shallow and thus that normal stress components are negligible. The model calculates the thermodynamics associated

with ice flow in a three-dimensional grid. The calculations of these ice temperatures are used to predict ice rheology and to determine the basal ice conditions. The degree of ice advection and diffusion, the surface air temperatures, and the degree of frictional and geothermal heating are important factors in determining ice temperature.

The geometric evolution of an ice mass is influenced by patterns of ice flow, accumulation, ablation and basal melting, the latter being critical for predicting distributions of glacial erosion. The model does not specifically incorporate ice shelves but for this Antarctic experiment it instead calves a percentage of its mass at the coastal ice boundary until such a stage that the East and West Antarctic Ice Sheets converge, whereupon 100% of floating ice is calved. An Earth model (Lambeck and Nakiboglu, 1980) accounts for elastic lithospheric behaviour under changes in load caused by the evolution of ice thickness and by the removal of bedrock material.

5.3.2 Erosion Parameterisation

A pre-requisite to the occurrence of erosion at the bed of an ice mass is the presence of water (Hallet, 1979, 1996; Oerlemans, 1984; Paterson, 1994) which provides the lubrication and allows sliding to occur. Although minor erosion can occur without it (Cuffey et al., 2000), the distribution of the basal ice at pressure melting point is the largest factor in driving patterns of erosion (Sugden, 1978a). Basal melting in GLIMMER is a function of ice thickness (and therefore topography), ice temperature, ice velocity and thus frictional and geothermal heating. Where pressure melting point is reached, ice detaches from the bed and begins sliding. The pattern of this process can therefore be used to infer the occurrence of selective erosion, areal scour and, if the ice remains cold-based and cannot slide readily, the protection of the landscape.

The incorporation of bedrock erosion is outlined in more detail in previous work (Jamieson et al., 2008). We calculate a bulk erosion rate as a function of basal ice velocity, ice thickness and bedrock erodibility (Boulton, 1974). Critically, erosion is modelled not only as a function of ice discharge, but of basal thermal regime, making

this model unique in comparison to other models used in predicting glacial erosion (Anderson et al., 2006; MacGregor et al., 2000; Tomkin, 2003; Tomkin and Braun, 2002). Basal ice velocities are determined by the shear stresses generated at the base of the ice sheet, and is scaled by a parameter called basal traction (or basal slip coefficient: t_b) which controls how easily the sliding can occur. As in other experiments (Jamieson and Hulton, Submitted; Jamieson et al., 2008), the influence of basal water in the pattern of sliding is incorporated into the calculation of basal traction whereby traction is a parabolic function of melt-rate. This allows the transition from cold to warm-based ice to be accompanied by a smooth transition in basal traction, and thus ice velocity which generates realistic patterns of ice flow akin to the patterns associated with ice streams (Jamieson et al., 2008). It also minimises the impact of erroneous creep instability that can be generated in ice sheet models (Payne and Baldwin, 2000; Payne et al., 2000).

5.3.3 Bedrock Geometry

The bed topography employed in our experiments is the BEDMAP dataset of Antarctica (Figure 5.5; Lythe et al., 2001) interpolated to 20 km resolution. The topography is isostatically rebounded to model the removal of the present day ice load (Figure 5.4; Lythe et al., 2001) and thus provides an ice-free region upon which to initiate glaciation. Figure 5.7 shows the amplitude of the isostatic rebound signal over Antarctica.

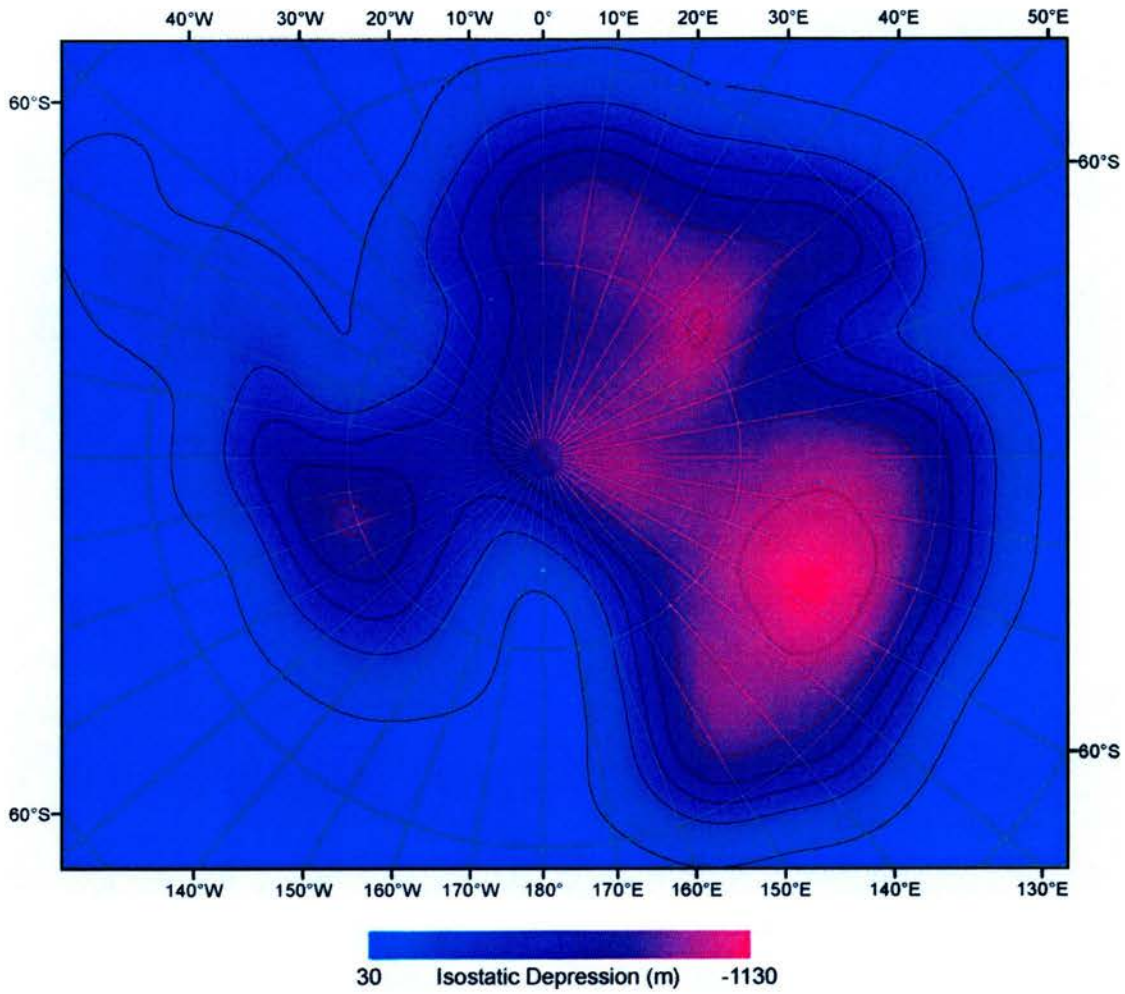

Figure 5.7: Present day ice load

The present day lithospheric depression caused by the current ice load calculated for the Antarctic Ice Sheets. The depression is flexural, and thus there is a lateral fore-bulge area which is currently raised by up to 30 m.

5.3.4 Climate Parameterisation

An estimation of the present day surface mass balance of Antarctica is shown in Figure 5.8 (Vaughan et al., 1999) and indicates that up to 0.5 m yr^{-1} of accumulation is occurring, most of which is felt in the coastal regions. The accumulation rate in the interior is minimal and very little ablation occurs because of the low mean annual air temperature at sea level of -15 °C (Anderson, 1999). As already noted, the climate at the Eocene-Oligocene boundary is similar to present day conditions in southern Patagonia and supported *Nothofagus* trees (Mildenhall, 1989; Raine and Askin, 2001). Such southern beech trees currently grow in Tierra del Fuego at the southern

tip of South America. Therefore, because the warmest mean annual air temperature (MAAT) that occurs in this lowest latitude region of Patagonia is 7 °C (Figure 5.9; McCulloch et al., 2000), we use that value to generate the pattern of ice at the time of glacial inception in Antarctica.

The pattern of mass balance in Antarctica today (Vaughan et al., 1999) shows the effect of continentality upon precipitation, whereby interior regions are much drier than at the coast. A similar pattern is likely to have existed over Antarctica ever since it broke away fully from Gondwana. Therefore, we use this present day pattern of snowfall to dictate the pattern of accumulation throughout our experiment (Figure 5.9; McCulloch et al., 2000). The assumption we make is that the continental gradient of precipitation remains constant since the Oligocene. In reality, this is likely to change because cooler areas will become subject to drying more readily than the warmer areas. However, given that the interior is subject to very low magnitude precipitation, we suggest that the impact of applying this assumption is relatively minor. Mean annual precipitation (MAP) near the margins of the present day southern Patagonian ice fields is ca. 2 m per year (Figure 5.9; McCulloch et al., 2000). We use this value as the basis for uniformly scaling the present day Antarctic accumulation pattern by four times, from a maximum of 0.5 m per year, to a maximum of 2 m per year to infer precipitation rates at 34 Ma. The precipitation is then linearly reduced over the course of our experiment until the present maximum Antarctic 0.5 m value is reached.

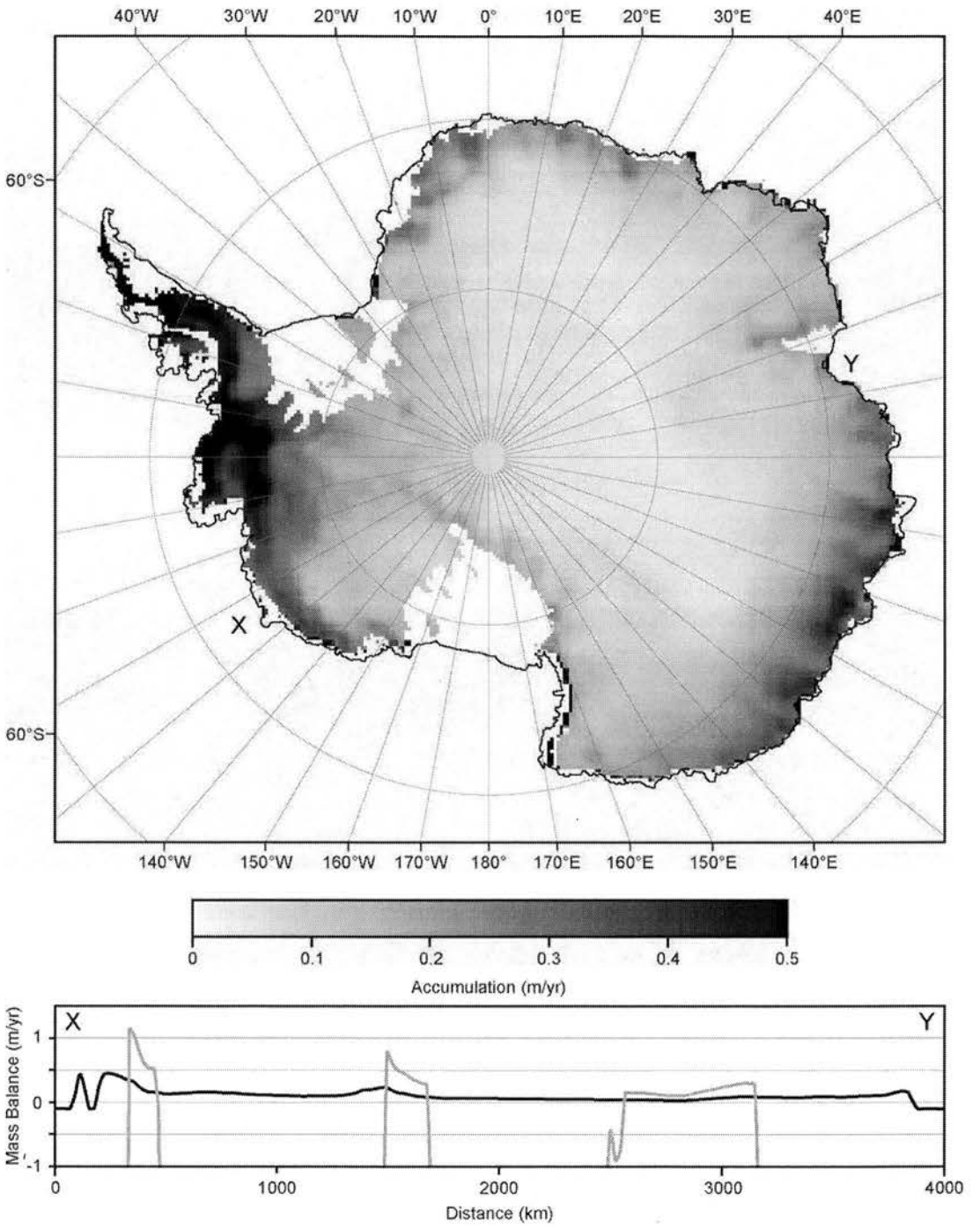

Figure 5.8: Present day accumulation in Antarctica

Data from Vaughan (1999). Profile X-Y shows mass balance for present day (black line) and under a warmer Patagonian style climate (grey line). Note that there under a Patagonian regime, there are zones of increased accumulation at high altitudes and that accumulation is discontinuous because of high ablation across the continental lowlands.

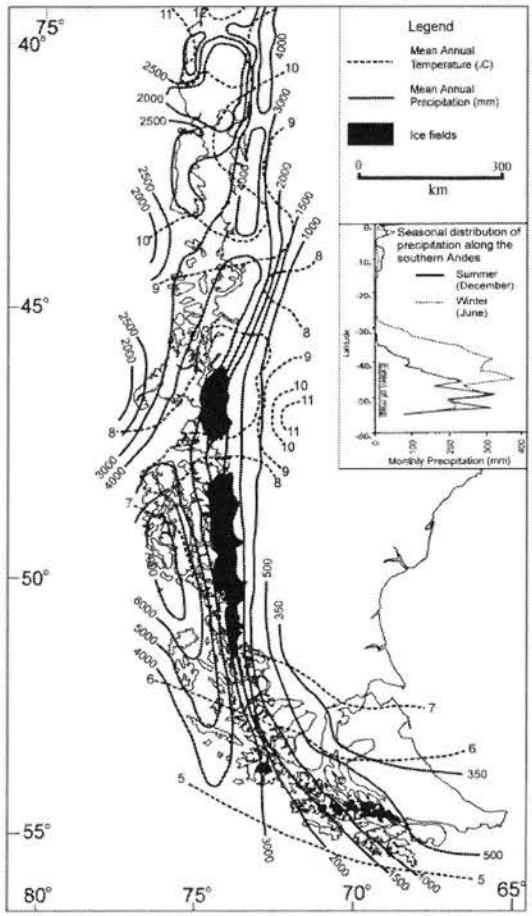

Figure 5.9: Climate in South America

Main climatic features of Southern South America after (McCulloch et al., 2000) and Romero (1985). Inset shows the seasonal migration of the Westerlies (Lawford, 1993).

In order to model the transition from glacial inception towards a full-scale ice sheet similar in size to the present day, we start ice growth using a Patagonian-style MAAT at sea level of 7 °C and a MAP of 2 m per year. We apply a vertical lapse rate of -9 °C km^{-1} to account for changing temperature over the land and ice surfaces. During the experiment we gradually reduce the MAAT and MAP in a linear fashion until they reach the present day values of -15 °C and 0.5 m per year respectively. We then let the final continental scale ice sheet reach full equilibrium with its climate for 50 kyrs.

Under warmer climatic conditions, the pattern of mass balance for Antarctica becomes unrealistic because little melt occurs at the present day. We therefore model ablation using a positive degree day (PDD) scheme (Reeh, 1991). This assumes melt

at the ice or land surface is proportional to the number of days (integrated through time) that air temperature (T) is above freezing. The number of positive degree days is therefore proportional to the energy available for melting. Melt (w) is calculated by:

$$w = \alpha \int_{year} \max(T,0)dt \tag{5.1}$$

where α is the degree day factor (ddf) describing the density and albedo of snow or ice. The melt calculation applies an annual sinusoidal cyclicity (i.e. seasonality) to air temperature, which is generated using a mean annual temperature and an associated half-range. Further diurnal departures from the sinusoidally shifted mean annual temperature are accounted for by assuming that this variability has a normal distribution with a standard deviation of 5 °C. The model incorporates a firn model to account for the fraction of melted snow that refreezes to become superimposed ice. Figure 5.8 shows a profile (X-Y) through the accumulation generated by this scheme.

5.4 Results

5.4.1 Present Day Control Model

To test the capability of our model to generate realistic ice sheet geometries we use the present day climatic data (Anderson, 1999; Vaughan et al., 1999) to model the current Antarctic Ice Sheet. Figure 5.10 shows the result and although this slightly over-estimates the maximum ice sheet thicknesses, it does not do so significantly. In East Antarctica, the modelled system shows slightly steeper surface gradients towards the coast and then a flatter interior region when compared to reality. A lack of proper ice shelf representation results in ice grounding further into the Ross Sea than is actually the case. In West Antarctica, the model predicts ice thicknesses well. Moreover, the patterns of basal sliding generate streaming features that on a large scale replicate those indicated by the balance velocity map of Antarctica (Bamber et

al., 2000; Huybrechts et al., 2000). This gives us confidence that we can predict the zones of erosion as they evolve under the expanding ice sheet.

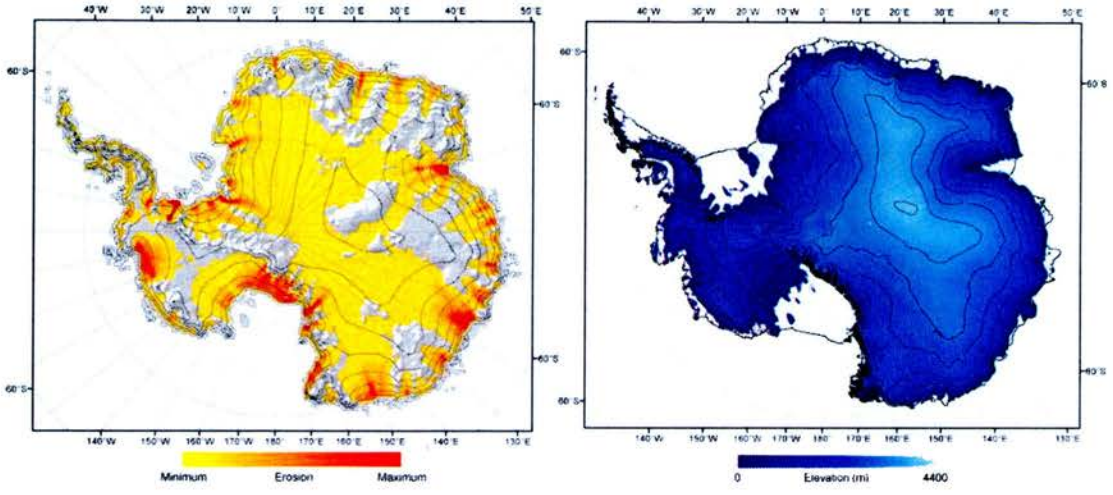

Figure 5.10: Comparison between modelled and present day ice sheets

Modelled present day ice surface and subglacial basal sliding conditions showing predicted zones of erosion (left) and present day ice surface for comparison (right). Black contours show 500 m ice surface contours and the maximum elevation in the modelled system (left) just exceeds 4400 m. Areas of no colour indicate cold-based ice is predicted by the model.

5.4.2 Modelled Ice Expansion in Antarctica

Using our slowly cooling and drying climate model we model ice expansion across Antarctica. The different stages of growth are shown in Figure 5.11. Initially (Fig. 5.11a), ice growth is restricted to localised glaciation in Dronning Maud Land, the Gamburtsev Mountains and in the Ross sector of the Transantarctic Mountains. Numerous smaller glaciers also grow across the remainder of MacRobertson Land adjacent to the Lambert Graben region. Ice growth in West Antarctica is limited to local mountain glaciers and across the continent, ice thicknesses are limited to below ca. 2000 m.

As cooling continues (along with drying), ice grows from the mountain centres in East Antarctica (Fig. 5.11b) generating 2 regional scale ice sheets that dominate the Gamburtsev and Dronning Maud areas. This gradual drop in temperature of ca. 4 $^{\circ}$C allows the ice masses reach ca. 3000 m in thickness, with rapid expansion being caused by the merging of numerous localised accumulation centres. At this stage, the ice margin on the eastern margin of the Gamburtsev region lies at the shore of

present day Lake Vostok. Ice expansion around the TAM is relatively limited at this time, as it is in West Antarctica.

A further drop in temperature of 1.6 °C brings MAATs at sea level close to zero and the glacial system is characterised by large-scale coalescence of local and regional ice masses to form a single East Antarctic Ice Sheet (Fig. 5.11c). The EAIS is topographically pinned around the Lambert region although the Lambert, Fischer and Mellor glaciers are all now established at the head of the Lambert Graben. The TAM ice centres and the EAIS are not linked and it is likely that significant amounts of melt water might be directed through the small ice-free area separating the two. This ice-free topographic hollow is above sea level and is therefore likely to have been a significant ice marginal lake.

Figure 5.11d illustrates that as the mean annual temperature at sea level drops to ca. -4 °C, the EAIS amalgamates with localised ice in the TAM creating a continental-scale ice sheet and establishing large-scale ice discharge through the TAM. For the first time, the majority of the EAIS margin discharges directly into the ocean. A secondary ice sheet in central Wilkes Land also expands to become water terminating and West Antarctic ice also largely terminates in water. This stage of glaciation represents the regime under which ice extents are likely to have become more strongly controlled by sea level.

Figure 5.11e shows an almost full EAIS aside from the regions that terminate into the large embayments around the George V coast and Wilkes Land. The expansion here is slowed in the model due to the lack of representation of ice shelves. Ice shelves would likely cover these intermediary areas and therefore ice mass loss would be reduced, allowing more rapid ice sheet growth than shown in the model. This stage is also marked by the WAIS beginning to coalesce, and with MAATs at sea level being only ca. 8 °C warmer than the present day this indicates the sensitivity of the WAIS to changes in air temperature due to its marine setting.

The establishment of a WAIS similar to present day heralds the final stage of full polar ice sheet growth. The joining of the EAIS and WAIS is shown in figure 5.11f and largely occurs by ca. -12 °C and is relatively stable as temperature drops to -15 °C. An independent ice mass is shown on Berkener Island between the Ronne and

Filchner Ice Shelves showing that the presence of ice in this area is very sensitive to air temperature.

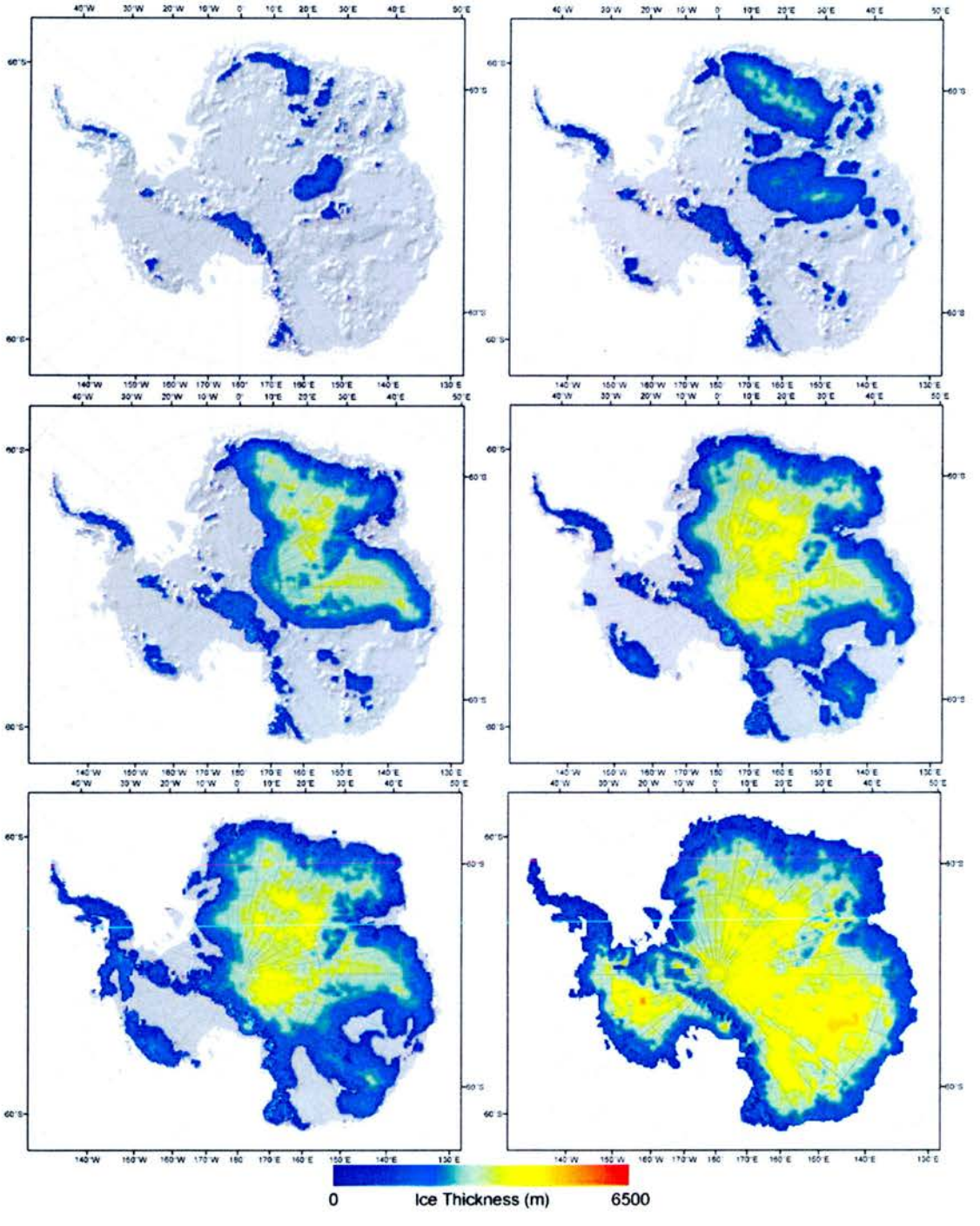

Figure 5.11: Selected modelled stages of ice growth since Oligocene times

Parts a-f numbered from left to right, top to bottom. MAATs at sea level for each stage are, from left to right, top to bottom: 6.5 °C, 2.4 °C, 0.8 °C, -3.9 °C, -6.6 °C and -15 °C.

5.4.3 Sensitivity to Precipitation

It was important to test how critical precipitation rates are in determining the pattern of ice sheet growth. As McCulloch et al. (2000) indicate, precipitation in some parts of Patagonia reaches 3 m yr^{-1} (Figure 5.9). Therefore we initiated a sensitivity experiment using this higher figure of 3 m of precipitation at the first stage of ice sheet growth and, as before, linearly reduced this amount to the present day Antarctic maximum of 0.5 m yr^{-1} (Vaughan et al., 1999).

Under this increased precipitation regime, the patterns of glaciation are similar to our first model although growth occurs more rapidly and earlier. Given the focus of this paper is to establish predicted modes of glacial landscape evolution, the impact of increased precipitation upon our model results is therefore minimal. Furthermore, given that the Antarctic ice expansion since the Miocene is characterised by 2 large step changes in climate, the differences in accumulation and the associated rate of expansion are unlikely to have a significant impact upon the patterns of landscape evolution experienced over the past 34 Myrs.

5.4.4 Patterns of Erosion Under Expanding Ice

Figure 5.12 shows the modelled erosion patterns associated with selected stages of ice growth in Antarctica at snapshots identical to those in Figure 5.11. At the initial stage of ice growth (Fig. 5.12a), erosion occurs around the fringes of the ice masses. Apart from in the TAM, East Antarctica displays limited spatial variation in modelled erosion rates. In West Antarctica, large erosion rates on Mt. Vinson are likely erroneous and are generated by instantaneous avalanching that generate large ice thicknesses that lead to rapid ice flow in a focussed area. At this stage of ice expansion we note that amongst other areas, the central core of the Gamburtsev Mountains lies under cold-based ice and thus does not undergo erosion.

Figure 5.12b shows that as the ice sheets grow in size, zones of warm-based ice extend down from the relatively smooth higher elevation plateaus. Indeed, in East Antarctica, 'streams' extend into Enderby Land and generate zones of focussed erosion. In addition, under the two larger ice masses, significant portions of the bed

are undergoing widespread but low rates of erosion. Given that the spatial variation of erosion rate in these areas is limited, it is likely that this represents areal scour, with the ice sheets gradually smoothing the topography over time. The expanse of cold-based protective ice is increased, with significant areas of upland Dronning Maud Land undergoing no erosion. The Gamburtsev Mountains too remain protected. In West Antarctica, the relatively small ice sheet on the peninsula is supporting locally high erosion at the ice sheet margins, probably due to the presence of pre-existing valley topographies.

As the ice sheet in East Antarctica coalesces into a single larger ice mass (Fig. 5.12c and 5.12d) the levels of erosion being experienced around the ice sheet margins increase in magnitude and in variability with individual troughs supporting streaming flow and focussed erosion. In particular, the Mellor, Fischer and Lambert Glaciers which flow into the Lambert Graben illustrate the importance of topography in causing flow convergence and accelerated erosion. Figure 5.12c indicates that the landscape surrounding the Gamburtsevs is subjected to areal scour but the mountain core remains protected. As the EAIS reaches a more mature state (Fig. 5.12d) the zone of protection around the mountain cores expands significantly. The along-flow transition (i.e. from the centre towards the edge of an ice mass) from protected land to areal scour and then to selective erosion is more clear at this stage. This pattern of erosion changes little in Figure 5.12e, although the ice along the Antarctic Peninsula begins causing selective erosion along the entire coastal regions. This is coincident with ice expansion to cover all of the land area above sea level in West Antarctica.

Figure 5.12f illustrates the distribution of erosion under present day conditions. As the ice thicknesses in East Antarctica increase during the final stage of expansion, the zone of areal scour between the TAM and the Lambert region is re-established after being under cold-based ice. Very large parts of the bed in East Antarctica are subject to uniformly low rates of erosion in comparison the ice margin. The WAIS is fully established and ice grounded below sea level generates high rates of erosion. The gradient of the continuum between zero and high erosion rates is much steeper in this area, and indicates that although the WAIS is thinner, smaller and shorter-lived than the EAIS, once established it is a significant agent of landscape modification.

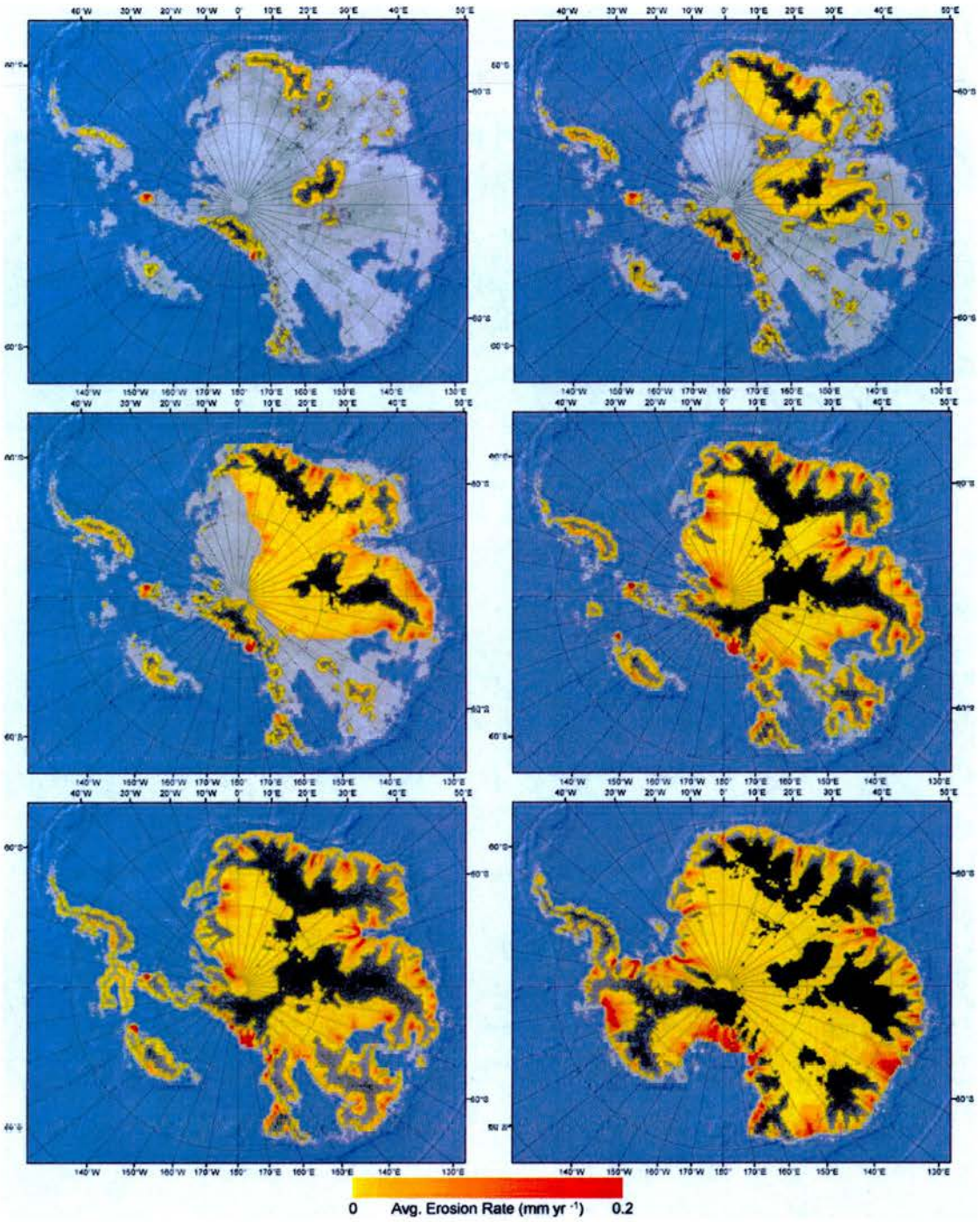

Figure 5.12: Modelled erosion rates through stages of ice growth in Antarctica

Parts a-f numbered from left to right, top to bottom. MAATs at sea level for each stage are, from left to right, top to bottom: 6.5 °C, 2.4 °C, 0.8 °C, -3.9 °C, -6.6 °C and -15 °C. The greyscale shading illustrates the upper land/ice surface (darker = higher) and the blue represents sea level. Note that although absolute erosion rates are presented here, the maximum rate is somewhat arbitrarily set in the model. Instead, the critical factor for identifying modes of landscape evolution is the relative rates of erosion over space and time.

At all stages, erosion rates are most significant closer to the ice margins, coinciding with the position of the ELA where ice discharge is highest. What is clear from Figure 5.12 is that during initial stages of growth, the relative erosion rates in East Antarctica are outpaced by those in the deep valleys of the TAM and in pre-existing troughs in West Antarctica. This indicates that highly focussed flow and selective erosion are more likely to occur where pre-existing topography enables flow convergence and rapid variations in ice thicknesses (i.e. valleys vs. ridges). Critically, these maps of model output indicate how ice flow patterns change from locally radial towards continentally radial as the ice masses expand and coalesce. Therefore the present day Antarctic bed landscape must record a complex history relating to local, regional and continental scale stages of ice growth.

5.4.5 Modes of Landscape Evolution

In order to predict the patterns of landscape evolution experienced under 34 Myrs of glacial conditions we link the pattern of changing climate (Fig 5.3; Zachos et al., 2001) and the scales of modelled ice sheet state associated with these changes (Fig. 5.13). By doing this, we can predict the total amount of erosion that has occurred through time, as well as the lengths of time over which focussed flow, areal flow, and cold-based ice have been present.

The record of global ice volume provided by Zachos et al., (2001) cannot be directly used to identify exact temperature changes since ca. 34 Ma. This is because the temperature calculations carried out on this $\delta^{18}O$ record were derived using a Standard Mean Ocean Water (SMOW) value of 1.2 ‰ which wrongly assumes an ice free ocean existed throughout. However, we can identify the timings of fluctuations in ice sheet size over this time to carry out a simple classification. Using the evidence for the timings of transitions between particular scales of glaciation we identify the lengths of time (in Myrs) over which each of the 6 stages of modelled ice sheet growth (Figs. 5.11 and 5.12) have existed (Fig. 5.13). This enables us to generate end-member indications of the absolute amount of material removed from the Antarctic bedrock surface since glacial inception. It also enables us to predict the lengths of time over which different types of glacial flow, and therefore erosion, have been active.

We use measurements of excavation rates under glaciers in the northern hemisphere to constrain our classification. Rates of between 0.1 and 100 mm yr^{-1} have been measured or inferred for a range of glacial systems although this upper limit relates to erosion of deformable sediment (Hallet et al., 1996). Alley et al., (2003) suggest rates as high as 10 mm yr^{-1} are possible. In the southern hemisphere, Rocchi et al., (2006) infer an average erosion rate of 0.5 mm yr^{-1} across the surface of the Dorrel Rock complex in Marie Byrd Land, Antarctica but indicate that this was not sustained for more than 6 Myrs. We therefore treat this latter value as an absolute maximum potential erosion rate for our erosion reconstruction.

In order to test the degree to which the landscape may have been modified, we use the timings assigned to each glacial scale (Table 5.1, Figure 5.13) and integrate erosion rates over the last 34 Myrs. A selection of three maximum erosion rates are tested (0.1 mm yr^{-1}, 0.2 mm yr^{-1} and 0.5 mm yr^{-1}), each in a separate integration. We assume selective erosion occurs where erosion rates are in the top 60% of the range of rates modelled. Areal scour is therefore represented by the lowest 40% of erosion rates, and protection is defined where erosion rate is zero at any time step.

Time	Details	Ice Sheet Scale
34-14 Ma	Ice sheets oscillate on similar scales to northern hemisphere Pleistocene ice sheets (Naish et al., 2001; Pekar and DeConto, 2006). This is analogous to fluctuations between growth scales 1-3 in our model and we classify this by assigning 6.66 Myrs of time to each of these three states (a total of 20 Myrs).	(Fig. 5.12a-c)
14-13.6 Ma	Step cooling drives ice expansion to its maximum size creating a continental polar ice sheet (Anderson, 1999; Denton et al., 1993b; Holbourn et al., 2005; Marchant et al., 1996). We assign 0.2 Myrs to each model step.	(Fig. 5.12d-e)
13.6-0 Ma	EAIS and WAIS are confined to the continent, operating on a scale similar to present day Antarctic Ice Sheets with minor fluctuations (Denton and Hughes, 1986; Denton et al., 1993b; Marchant et al., 1996). This 12 Myrs of Antarctic glacial history is captured in our model by the final step.	(Fig. 5.12f)

Table 5.1: Time assigned to each stage of Antarctic ice growth

Division of time applied to each scale of modelled ice sheet in order to predict the nature of erosion across Antarctica since the Oligocene.

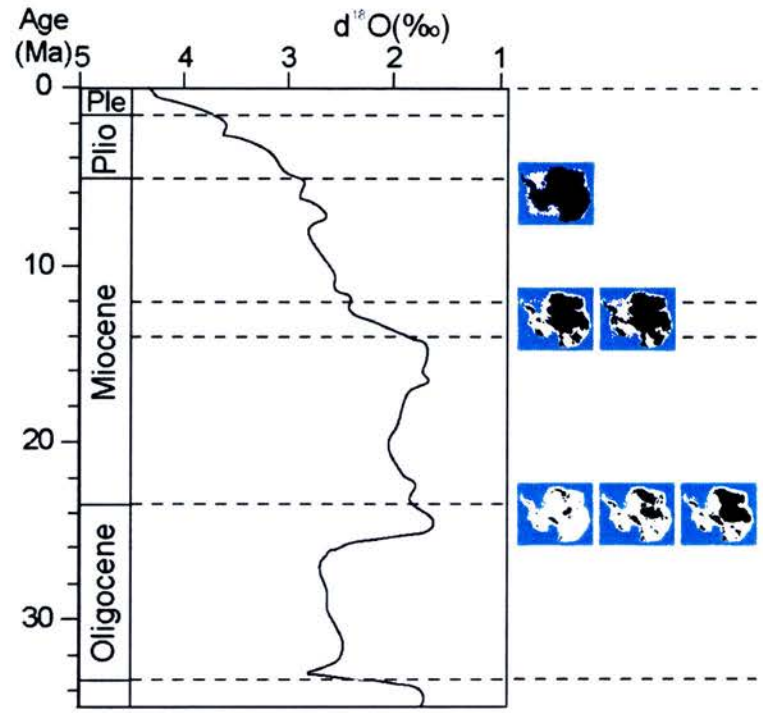

Figure 5.13: Scales and timings of the Antarctic Ice Sheet

Schematic illustrating the scales of modelled ice sheet associated with each time period in comparison to the benthic $\delta^{18}O$ record (Zachos et al., 2001). Black areas indicate scale of ice growth used. Refer also to Table 5.1 for timings.

The results of our temporal integration of modelled erosion rates are shown in Figure 5.14. The spatial pattern of erosion (Fig 5.14a) is the same for each erosion rate integration, but maximum depths of excavation differ. Using the intermediate value for maximum erosion rate (0.2 mm yr^{-1}), we find that up to ca. 2800 m of excavation can be achieved if topographic focussing of erosion is particularly strong. Throughout the interior, the land surface is subject to less than 200 m of erosion indicating that the Antarctic Ice Sheets have been relatively ineffectual at modifying the large parts of the topography. The degree of excavation at the margins of the continent increases as expected given a) the long-term existence (12-14 Myrs) of the continental scale ice mass and the long-term position of the ELA, and b) the larger volumes of ice that are discharged under continental ice conditions.

By increasing (0.5 mm yr^{-1}) or decreasing (0.1 mm yr^{-1}) the erosion rates used in the integrations, maximum depths of excavation change to ca. 7000 m or ca. 1400 m respectively. This 7000 m upper limit represents a depth of excavation that is highly

unlikely because there are no present day troughs that approach this depth in terms of their topographic relief so such a depth of material could not have been removed. Additionally, the volumes of material sequestered offshore do not support it. We estimate that for each of the three maximum erosion rates tested, the overall volumes of sediment lost would be: 0.1 mm – 5.02 x 10^5 km^3; 0.2 mm – 1.004 x 10^6 km^3; 0.5 mm – 2.51 x 10^6 km^3. Over 34 Myrs, these convert to spatially averaged erosion rates (including areas of cold-based ice) of 0.0011, 0.0022 and 0.0055 mm yr^{-1} consecutively.

The lower two of these measurements compare remarkably well to estimates of glacigenic sediment volume from Prydz Bay where the largest ice drainage system in the world discharges. Here, it is estimated that over the past 12-14 Myrs, average erosion rates would be only 0.001-0.002 mm yr^{-1} (Cooper et al., 2001; Cooper et al., 1991; Jamieson et al., 2005; O'Brien et al., 2001; Stagg, 1985). Given that the Lambert trough exploits a Permian age graben that extends into India (Federov et al., 1982; Mishra et al., 1999), it is likely that the relief in such an area would have been significant prior to glaciation. In the Lambert region, we predict ca. 2000 m of incision in the trough, and less than 200 m of scouring on the flanks of the graben. Given that the total relief in this region at the present day is ca. 2500 - 3000 m (Mishra et al., 1999), this indicates that the minimum pre-glacial trough relief would be significant at ca. 700 - 1200 m if our prediction is correct. A feature of such a scale would be large enough to generate significant selective erosion from the outset as ice expanded to cover Antarctica. Therefore, we estimate that a modelled maximum erosion rate of 0.2 mm yr^{-1} (equivalent to ca. 2000 m of excavation in the Lambert trough) is at the upper level of what the Antarctic bed may have experienced.

Figures 5.14b-d show our predictions of erosion regimes scaled over time and Figure 5.15 shows which areas experience different combinations of erosion regime over time. It should be noted that because we use only a simple set of 6 ice sheet scales, certain features that one might expect to be picked out (e.g. erosion along the trough now occupied by Lake Vostok) may not be highlighted at this temporal resolution.

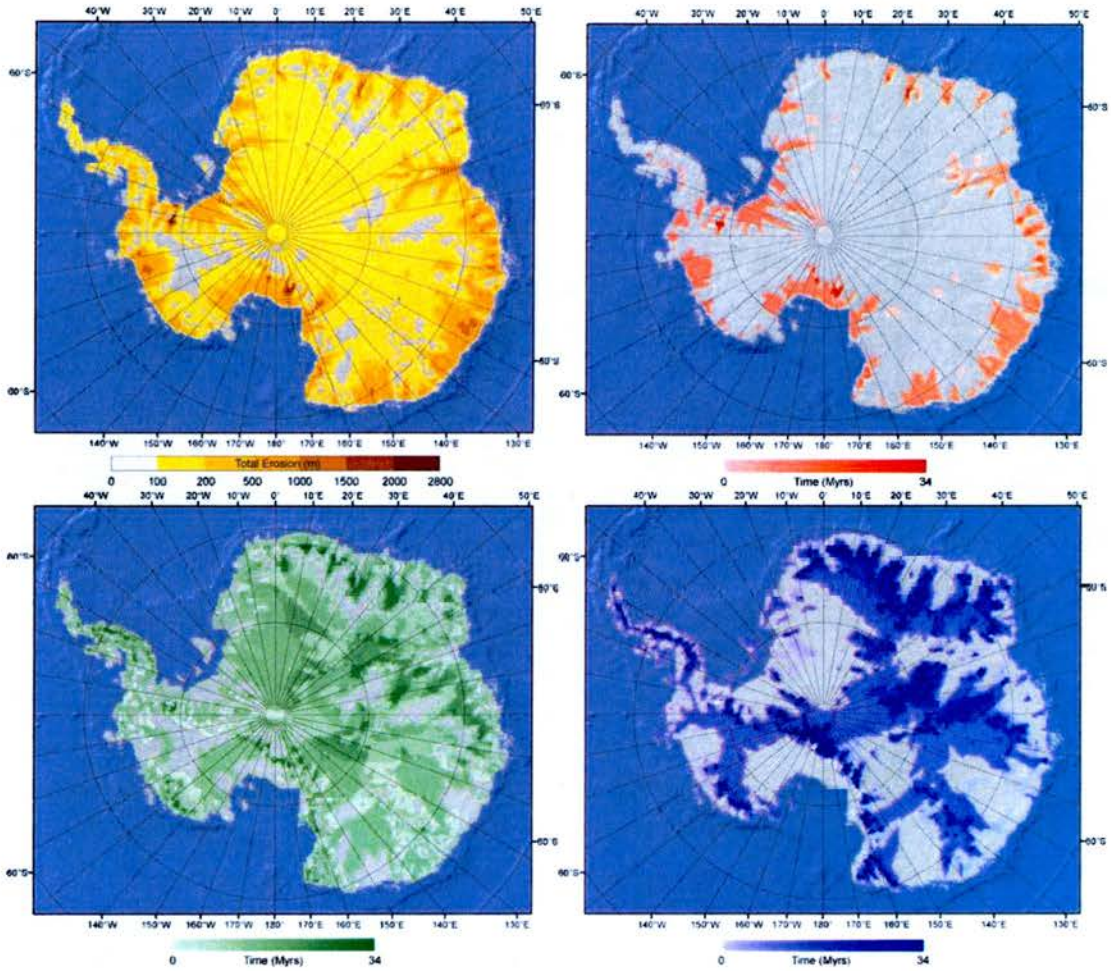

Figure 5.14: Modelled erosion patterns for Antarctica

Time-integrated analysis of predicted total erosion and of the longevity of particular erosion regimes. A) Total depths of erosion across Antarctica based on integration of erosion rates through time. Erosion is calculated assuming each ice sheet state (Fig. 5.12) exists for a particular period of time, as described above. Note that the maximum value of ca. 2800 m displayed here relates to a maximum erosion rate of 0.2 mm yr^{-1}. This would increase to ca. 7000 m if maximum erosion rates were to be 0.5 mm yr^{-1}, and would decrease to ca. 1400 m under maximum erosion rates of 0.1 mm yr^{-1}. B) Time over which selective erosion has been dominant at incising the topography. C) Time over which areal scour has been dominant in smoothing the Antarctic bedrock. D) Time over which cold-based ice has been protecting the landscape.

Figure 5.14b shows that where selective erosion occurs it is commonly stable for the last ca. 12 Myrs, with only a few localities (Queen Maud Mts., Lambert Graben feeder glaciers and Princess Ragnhild Coast) showing that selective erosion has been entrenched for 20-34 Myrs. Figure 5.14c shows that areal scour has been widespread, and is often established for over 20 Myrs. In particular, our model suggests that parts

of Queen Maud Land have been under areally flowing ice since the Oligocene. Figure 5.14d is interesting because it suggests that a number of areas of the East Antarctic bed may have been subject to little or no erosion since the Oligocene. In particular, the Gamburtsev Mountains, large parts of Dronning Maud Land and parts of the inner TAM may have survived unchanged.

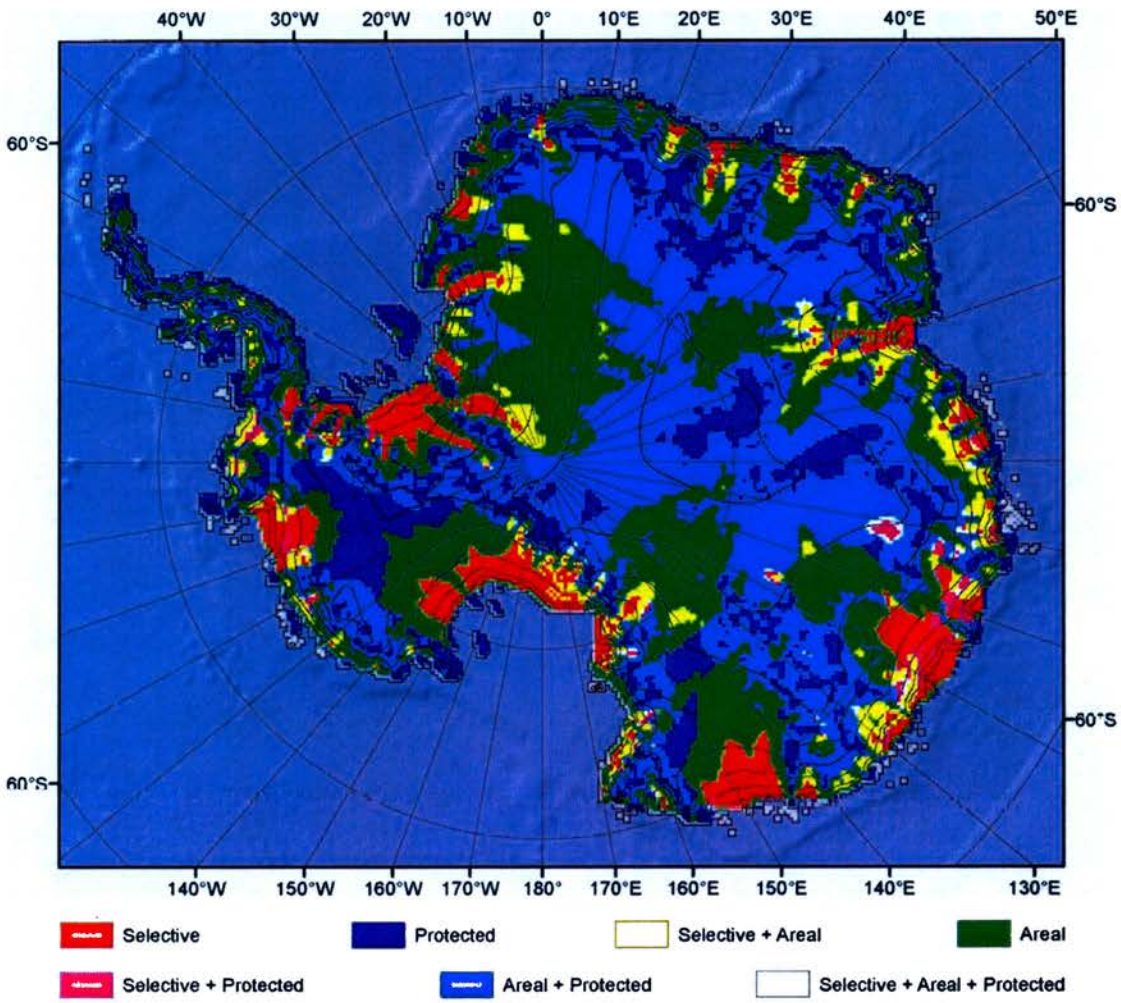

Figure 5.15: Areas of the Antarctic bed that experience differing erosion regimes

Combined prediction showing unique combinations of erosion regime. See text for details of determining each mode of landscape evolution.

5.4.6 Stability of Ice Flow

When considering modes of long-term landscape evolution on Antarctica, we can make further inferences about the degree of streamlining to which the landscape is likely to have been subjected. Over 34 million years, the probability of streamlined

features being produced will increase if the direction of basal ice motion remains consistent throughout. In contrast, areas experiencing multiple changes in ice flow direction may be characterised by an irregular pattern of bed features and less extensive erosion. Figure 5.16 indicates, using the same 6 snapshots of ice sheet development as our temporal analysis, the *maximum* degree to which ice flow direction at the bed has changed between glacial inception and the establishment of a full-scale polar ice sheet.

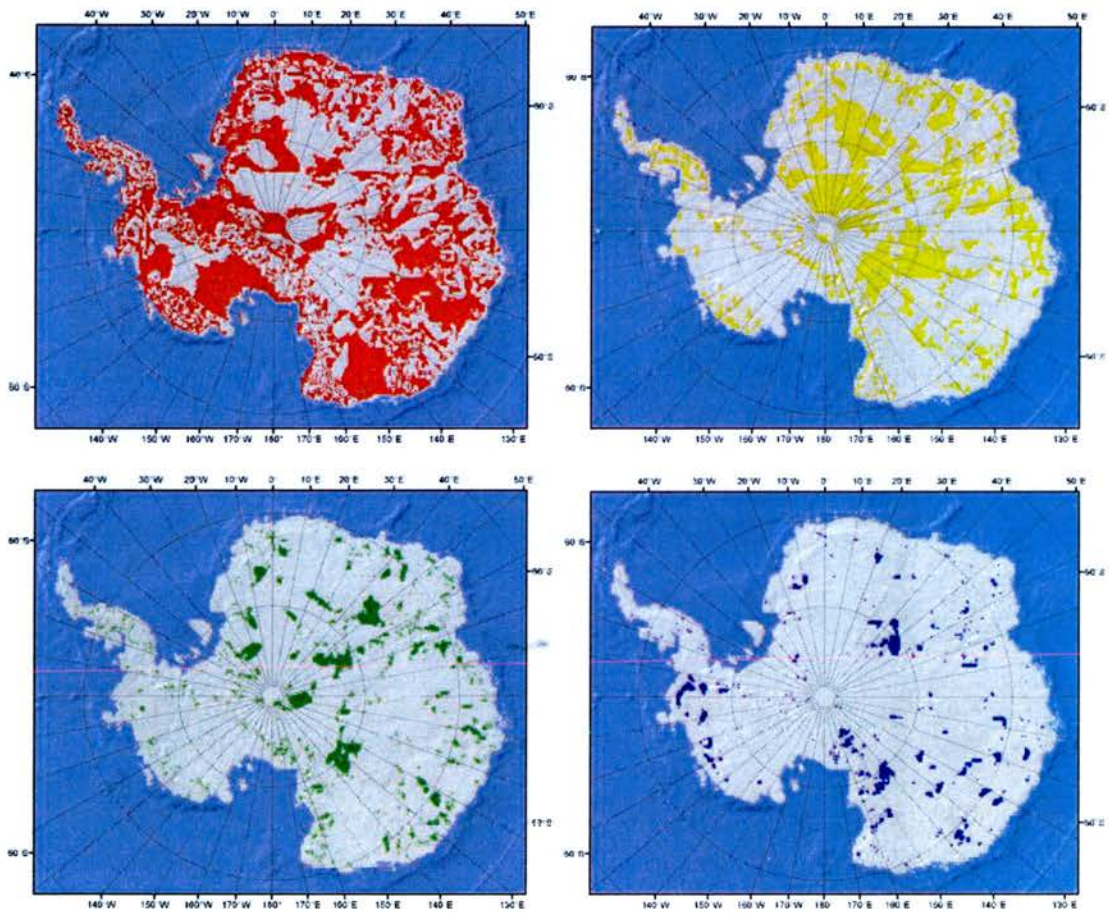

Figure 5.16: Maximum changes in ice flow direction

Maximum changes in basal flow direction through time across 6 representative snapshots of glacial evolution. As the ice expands, the basal flow direction changes by: A) less than 10 degrees; B) 10-45 degrees; C) 45-90 degrees and D) 90-180 degrees.

What we determine from Figure 5.16 is that much of the Antarctic bed has been subjected to only minor changes in direction of basal flow. This is particularly the case in areas where the basal topography is significantly below sea level, and therefore are glaciated last in our model configuration. Notable from this analysis is that a large proportion of the East Antarctic bed has seen between 10° and 45° change in basal flow direction. The majority of the contrast occurs between local and continental scaled ice, indicating that more local and regional fingerprints of glacial erosion may become overprinted by the later establishment of a full ice sheet.

In West Antarctica, bordering the Amundsen Sea and nearby Pine Island Glacier (PIG) our model indicates that ice flow has fully reversed over time. PIG itself shows no change in direction but is adjacent to this reversal feature and is located between two localised ice caps that flow towards it prior to WAIS establishment (Fig. 5.12e). The implication is that PIG may have acted as a discharge route for these ice caps prior to becoming established as a conduit for ice under full WAIS conditions.

5.5 Discussion

5.5.1 Ice Sheet Growth

The pattern of initial ice growth in our model compares favourably to previous models by both DeConto and Pollard (2003a; 2003b) and by Huybrechts (1993). Both of these models were generated in order to test different hypotheses relating to glacial conditions in Antarctica and each used different approaches to model climate (i.e. GCM predictions vs. parameterised accumulation and temperatures). However, on a large scale these models produce very similar initial and ongoing stages of ice growth to the approach employed here, with local ice centres giving way to regional and then continental ice coverage.

Geomorphological evidence from the northern hemisphere along with output from our models suggest glacial erosion is likely to have stripped hundreds of metres of material from the land surface. This is enough to generate characteristically glacial features across the bed whilst at the same time retaining the large-scale pre-glacial fluvial landscape signal. Therefore, on a continental scale the drainage pathways do

not change significantly as a result of long-term glacial erosion, a point supported by previous work (Jamieson et al., 2005).

5.5.2 Areal Scour

Our model indicates that areal scouring occurs extensively under different stages of Antarctic ice growth (Figs. 5.14 and 5.15). Evidence that landscapes of areal scouring are indeed likely to be widespread across the Antarctic bed is provided in regions that were formerly covered by ice during an expanded phase of glaciation. Warm-based ice is known to have existed across the continental shelf where regional erosion surfaces dip towards the land (Anderson, 1991; Anderson and Bartek, 1992) and in the inner shelf of the Antarctic Peninsula there are zones where sediment cover has been removed (Anderson, 1999). Denton and Sugden (2005) indicate channels extending from sea level to 2100 m in elevation at the front of the TAM in the Ross Sea sector are also associated with areal scouring under larger ice conditions. Many such zones of erosion found in the geomorphological record are not predicted in our model because they are associated with a more expansive Antarctic Ice Sheet. However, because our model over-predicts ice thicknesses around the TAM range front (Figure 5.11f), fortuitously we see that it predicts various degrees of areal scour at the edge of the McMurdo Sound region (Figure 5.14c).

5.5.3 Selective Erosion and Protection

We show that selective erosion occurs consistently around the margins of East Antarctica once the ice sheet reaches its full extent and also indicate that areas of relatively un-modified landscape are often found nearby (Figs. 5.14 and 5.15). This is expected given that evidence from formerly glaciated parts of the northern hemisphere also correspond to this pattern, particularly under full-scale ice sheet conditions (Goodfellow et al., 2007; Kleman et al., 2007; Sugden, 1978a). The pattern modelled in Antarctica can be tied to geomorphic evidence around the margins of the EAIS where glacial troughs are incised into a relict landscape protected under cold-based ice. Such adjacency of ancient weathered surfaces and

glacial troughs is seen for example, in the Prince Charles Mountains that bound the western margin of the Lambert glacier (Hambrey et al., 2007). Here sediments that make up the Late Miocene Pagodroma Group have survived relatively untouched by glaciation at the same time as ongoing selective erosion occurred in the neighbouring Lambert trough and its tributaries.

Similar proximities of landform survival vs. erosion are seen in the TAM (Sugden and Denton, 2004) which may account for significant uplift in the region (Stern et al., 2005). They are also seen around the rim of Dronning Maud Land where an early Permian planation surface is incised by 1.2 km deep glacial troughs (Naslund, 2001), in individual massifs in Marie Byrd Land (Sugden et al., 2005) and along the Antarctic Peninsula. The survival of pre-glacial topography can also be seen in the Victoria Land sector of the TAM, where the valley system is fluvial in origin (Baroni et al., 2005). Thus the essential large-scale spatial pattern of the landscape remains preserved, although in areas of selective flow the amplitude of this landscape may be increased through both erosion and adjacent uplift (Jamieson et al., 2008; Stern et al., 2005). All of these regions of selective erosion and protection are predicted by our model.

The implication of this is that although glacial erosion has modified the topography of Antarctica, the pattern of modelled ice growth here is likely to be robust because the main inception points in the landscape have survived. Furthermore, evidence for the survival of the pre-glacial topography, along with our model results which suggest widespread areas are relatively unmodified, indicates that the use of a present day (rather than pre-glacial) topography as the initial input for our model has not introduced significant errors in the patterns of erosion.

5.5.4 Erosion Regime - Stability and Controls

Figures 5.14 and 5.15 show that areas that have been subjected to areal scour during the experiment often coincide with areas that have also seen a degree of protection at some stage through the evolution of the ice sheet. Furthermore, we can see (Fig. 5.16) that areas that are subjected to greater than 10 degrees of directional change are largely coincident with areas that undergo areal scour, and not selective erosion. This

indicates that the smoother nature of the bed in regions subject to areal scouring enables the basal sliding regime to change more readily. Thus in relatively smooth areas of the landscape, upstream of the ELA, the topography is unable to drive ice flow convergence, and so the temperature of the ice is relatively homogenous. This results in either areal scour, or in cold-based ice depending on the climate and scale of the ice sheet.

Modelled selective erosion, in contrast to areal erosion, is characterised by being relatively spatially and temporally stable. Figure 5.14 shows that in the TAM, selective flow has operated over long timescales in close proximity to areas of cold-based ice. Our results agree with the geomorphic record (Naslund, 2001; Sugden and Denton, 2004). In areas that experience selective erosion the direction of basal ice flow shows little tendency to change direction (Figure 5.16). Directional and temporal stability is promoted in the trough areas because the ice experiences a thermal feedback driven by the convergence of ice through narrow topographic features. This causes heat to be drawn in to the troughs, and the steep, confining topography means that the thermal gradient is also steep and that heat cannot escape from the fast-flowing ice. Thus areas laterally adjacent to regions of selective flow can remain relatively cold, enabling landscapes to be protected and in turn reinforcing the contrast between warm and cold ice. The inference of this is that because ice is flowing and eroding selectively, it is likely to have done so under every episode of glaciation. Pre-existing fluvial bedrock geometry is therefore the strongest control upon the spatial variability of the basal thermal regime and upon the pattern of glacial landscape evolution.

Climate is a weaker control on the generation of focussed vs. areal erosion regimes. This is because climate generally varies on a regional scale. Local scale (e.g. valley to sub-valley scale) factors are therefore the most important factors in determining the pattern of landscape evolution under ice. Climate acts on a regional wavelength to further drive the magnitude of this pattern, for example through the position of the ELA or through increased snowfall in coastal regions (Figure 5.8; Vaughan et al., 1999).

5.5.5 Pre-Oligocene Drivers of Erosion Pattern?

We have shown that the Oligocene fluvial topography of Antarctica is critical in determining patterns of glacial erosion and ice sheet development, and that it survives on a large scale under the present ice sheet. However, the drivers of landscape evolution may extend further back in time than the Oligocene.

The most strongly selective erosion is modelled in Dronning Maud Land (Figs. 5.14 and 5.15) across the region that is coincident with the portion of the Antarctic Plate that was first rifted by ca. 118 Ma from India (Fig. 5.1). Interactions between processes of passive margin development and fluvial denudation and mass wasting in response to ongoing coastal uplift generate large amplitude topographies. We suggest that the mature nature of the passive margin development in Dronning Maud Land has enabled such significant fluvial features to form that focussed glacial flow occurs on a larger scale than around other parts of the Antarctic margin. The Permian age tectonic feature of the Lambert graben is also thought to be a strong influence upon the development of fluvial and subsequently, glacial patterns (Jamieson et al., 2005; Mishra et al., 1999). Thus both tectonic and fluvial processes are driving the pattern of subsequent glacial erosion.

In the case of the Gamburtsev subglacial mountains, there has been some question as to how such a feature could form in the centre of the continent and survive under extended periods of glacial and fluvial erosion. Theoretical work suggests that such a mountain range could form through erosional unloading (Monnereau et al., 1993). Such a mechanism would suggest that the Gamburtsevs could grow through isostatic adjustment as a result of erosional unloading by ice, generating a hotspot which causes the land surface to become elevated. This would imply that the mountain range has grown subsequent to the Antarctic Ice Sheet becoming established. An alternative viewpoint is that the mountains are an ancient remnant of an earlier mountain range that existed when Antarctica was still part of Gondwana and that drained in a similar radial pattern as the mountains of today (Veevers, 1994). This latter mechanism would require the Gamburtsevs to have survived under 34 Myrs of glaciation. Our work supports the latter of these theories (Figure 5.14d), indicating

that ice has prevented any significant denudation of the mountains and excluding the possibility that a hotspot could generate such a feature beneath the ice.

5.6 Conclusions

We predict for the first time, evolving patterns of glacial erosion across Antarctica. By comparing modelled erosion patterns to geological data from Antarctica and the northern hemisphere we assert that the pre-glacial landscape is the critical driver of glacial landscape evolution. The important outcomes of this work are as follows:

- Our deliberately simple approach of using present day Patagonian climate statistics in tandem with a map of present day Antarctic accumulation provides an insight into the manner of ice sheet growth across the continent, the changing basal regimes, and the associated pattern of long-term landscape evolution. Our results show that local scale Oligocene ice caps expand under progressively cooler conditions to become regional scale ice sheets before amalgamating to develop the continental scale Antarctic Ice Sheet by around 12-14 Ma.
- We show that a wave of erosion (largely areal scour) is pushed across the continent as ice sheet expansion occurs. As ice reaches the uplifted and fluvially incised passive margin topography near the coast, focussed flow and therefore selective erosion to develops. Overdeepening of the radial pre-existing fluvial valley systems follows.
- Upland areas in central Antarctica and in Dronning Maud Land, where glacial inception occurred, survive under cold-based ice. We infer that the Gamburtsev Subglacial Mountains have remained largely unchanged for 34 Myrs.
- We make large-scale estimates of the total amount of material that has been removed from Antarctica since the Oligocene. Average bedrock erosion rates are calculated to be between 0.0011 and 0.0022 mm yr^{-1}, agreeing closely

with estimates from the Lambert/Prydz Bay region of East Antarctica (Jamieson et al., 2005). Rates are not uniform, with much of the interior experiencing less than 200 m of erosion in contrast to the coastal troughs where selective erosion has excavated up to a maximum of 2800 m of material.

- Once selective bedrock erosion becomes established in the troughs that dominate the coastal regions of Antarctica, it is persistent. In these areas, the direction of ice flow is also unlikely to change, thus leading us to predict that streamlined bed features will predominate.

- Our model predicts that areas of strong selective flow persist in close proximity to areas that are protected under cold-based ice. Therefore, we show that the strongest modification of the bed geometry occurs adjacent to the weakest - a regime that is bourne out by field evidence in a number of areas (Hambrey et al., 2007; Naslund, 2001).

- Subglacial bed geometry is crucial in determining ongoing patterns and rates of bedrock excavation. The stability of regimes of selective erosion, along with the relatively low rates of excavation generated by our model suggests that the pre-Oligocene fluvial and tectonic character of Antarctica has been retained over 34 Myrs and has driven the evolution of glacial dynamics and of landscape evolution.

- Large parts of Dronning Maud Land, the first part of Antarctica to be rifted from Gondwana, are protected by the ice. Here, contrasts between selective erosion and protection are particularly strong and may be the result of glacial incision occurring on a mature passive margin. This illustrates the importance of large-scale tectonic processes in driving patterns of ice sheet development.

Chapter 6 Conclusions

6.1 Introduction

This thesis has investigated the occurrence of, and feedbacks between, glacial erosion, long-term landscape evolution and ice dynamics on an ice sheet scale. Despite over 160 years of investigation of glacial landscapes, an understanding of the nature of their evolution and of the evolution of their overlying ice masses remains incomplete. In particular, the long-held view that erosion is a passive component of the glaciological system has rarely been questioned. Given the spatial and temporal scales at which ice sheets operate, and of the inaccessibility of glacier/bedrock interfaces, we used a numerical modelling approach to query this viewpoint by achieving the following research objectives:

- An ice sheet model able to predict patterns of basal sliding in a manner that appears plausible was coupled to a model of glacial erosion (Chapter 2).
- The ice sheet/erosion model was used to determine how landscape geometry controls glacial dynamics and how this drives patterns of glacial erosion over time (Chapter 3).
- The effects of erosion on ice dynamics and ice margin behaviour over 10^5 - 10^6 year timescales were linked to conditions thought to have been experienced in Patagonia over the last 1.15 Myrs (Chapter 4).
- The model was employed in predicting, for the first time, the pattern of long-term landscape evolution of Antarctica as ice expanded from local to continental coverage over the past 34 Myrs (Chapter 5).

This chapter summarises the principal conclusions and outlines the implications of this work. It further indicates directions of future research aimed at developing the ideas presented here in order to build a more detailed picture of interactions between glacial erosion, ice mass dynamics and evolving landscapes.

6.2 Summary of Principal Conclusions

6.2.1 Modelling Erosion Under Ice Sheets

In order to provide a modelling platform with which to investigate interactions between ice sheets, erosion and topography we coupled an erosion model to the GLIMMER ice sheet model (Payne, 1999; Rutt et al., Submitted). This enabled predictions to be made regarding patterns of landscape evolution in relation to basal thermal regime. The eroding glacial landscape system was modelled for long-term persistent glaciation using a selection of synthetic landscapes and a range of basal slip regimes. In the experiments that calculate sliding velocities as a function of basal melt-rates, ice sheets were generated that were not subject to numerical instabilities of the kind identified in the EISMINT intercomparison tests (Payne and Baldwin, 2000; Payne et al., 2000). Thus we provided a stable platform for the remainder of our experiments, which relied upon being able to predict erosion in a glaciologically sensible pattern. We note that an important caveat regarding the use of the shallow ice approximation which assumes that ice surface and bedrock slopes are negligible. On an ice sheet scale (i.e. the scales employed throughout this thesis) it is not thought that the SIA will introduce significant error but future work will attempt to assess the validity of this assumption (see section 6.4.4).

We found that erosion appears to stabilise the thermal regimes of the modelled ice sheets. The generation of glacial signals upon initially fluvial systems can occur within 100 kyrs of initial glaciation when conservative erosion rates are modelled. The selective erosion of pre-glacial fluvial systems increases relief locally as valley long-profiles are overdeepened and the erosional unloading generates uplift along the flanks of glacial valleys.

6.2.2 How Topography Controls Erosion

By isolating various elements of landscapes such as relief and wavelength we tested the response of modelled circular ice sheets and erosion to the scaling of these components. Further, by glaciating fluvial systems with different relief, we tested

how erosion patterns and ice dynamics changed as landscapes become increasingly glaciated. We found that the sensitivity of an ice sheet to the landscape is critically determined by basal boundary conditions as parameterised using the basal slip coefficient (t_b) of the model. This indicates that where basal slip is increased, focussed erosion patterns can readily be driven by relief on the order of hundreds of meters. Such basal conditions (analogous to zones of water-saturated sediment, or perhaps to deformable sediment availability) decrease the temporal stability of erosion under individual ice streams, but increase average erosional stability over an ice sheet as a whole. Focussed flow is generally enhanced in short wavelength landscapes and where relief is greatest, and the occurrence of glacial overdeepenings are strongly related to the temporal stability of fast flowing ice.

The transformation from a fluvial to a glacial landscape is concurrent with progressively efficient ice drainage. Widespread areal scour and minor selectivity is replaced over time by minimal areal scour, or by cold-based ice, and increased selective erosion. Topography drives patterns of erosion so that pre-existing valleys are exploited and overdeepened whereas adjacent regions are subject to minor areal scour or remain protected under cold-based ice. These patterns are strongly dependent upon climate being cold or wet enough to drive continued incision.

Oscillations in the flow regime of modelled ice sheets are present where topographic amplitude is low (but not flat). This may be related to the fact that some of the topographies are radial in nature but do not pose any significant barrier to ice movement. Thus the minor topographic variations cause slight perturbations in the ice surface geometry which then drives cyclical instabilities in the model. Thus this is not a numerical instability in the sense experienced in the EISMINT II experiments (Payne and Baldwin, 2000; Payne et al., 2000) but is a real phenomena introduced by an unrealistic topography. In nature, where topography on an ice sheet scale is more significant in magnitude, such instabilities do not occur. In any case, short-term instabilities leave the underlying landscape largely unaffected.

6.2.3 Glacial Erosion and Ice Sheet Stability

The assumption that climate is the sole driver of the pattern of ice margin extents (and continued incision) is questioned in Patagonia. Although global glacial intensities reached a maximum at ca. 640 ka, the maximum Patagonian Ice Sheet occurred at ca. 1.15 Ma and maximum ice sheet extents have decreased successively during each subsequent glacial expansion. We tested the hypothesis that erosion is not a passive component of the glacial system, and that it may have contributed significantly to the generation of this pattern of long-term ice sheet instability in Patagonia.

By eroding a synthetic fluvial landscape under a static climate we found that the extents of an ice sheet analogous to that of Patagonia were reduced by ca. 20% over a 1.15 Myr period. The mechanism of retreat is driven by the overdeepening of topography downstream of the ELA, making the topography more efficient at losing ice mass. The reduction in glacier tongue extents cannot be countered unless climate becomes cooler and/or wetter through climate change or through tectonism. Thermal feedbacks re-enforce this mechanism as fast flow in overdeepened areas draws in more heat and, where climate can keep pace, increases selective erosion. Retreats are greatest during early glaciations, and slow with time as an equilibrium is reached between climate, ice sheet and topography. Rates of retreat differ depending upon the topographic characteristics of the drainage basins, allowing adjacent systems to begin retreating at different times.

Relief production through localised isostatic rebound after bedrock removal slows with time indicating that although glacial erosion can drive mountain uplift, it cannot be sustained unless the mass balance of ice sheets continually increases. Erosion is therefore likely to have played an important part in driving successive reduction in maximum ice sheet extents in Patagonia over the last 1.15 Myrs.

It is possible that deformable sediment will enhance the dynamic impact of erosion upon ice sheet behaviour. Deformable sediment can more easily be eroded, but is hypothesised to introduce irregularities in ice margin fluctuations (Clark, 1994; Clark and Pollard, 1998). We suggest that the combination of erosion of both deformable sediment and bedrock may result in increased amplitudes of margin fluctuation

whilst also retaining the regularity of retreating margin position enabled by bedrock erosion. Ongoing landscape evolution under ice sheets can therefore drive changes in ice dynamics at a significant scale.

6.2.4 Modelling the Long-term Landscape Evolution of Antarctica

Using the ice sheet and erosion model, the link was made between climate change and prediction of landscape evolution across Antarctica over the past 34 Myrs. This study is the first of its kind to do so on a continental scale with previous studies being confined to the ice free coastal regions of Antarctica. Using a combination of present day Antarctic and Patagonian climates as a template, and by inducing gradual cooling and drying, 34 Myrs of ice sheet growth were modelled. Associated patterns of glacial erosion related to the local, regional and continental scale ice masses were thus predicted.

By linking records of global glacial intensity to different scales of ice sheet (local, regional, continental), we calculate the length of time each ice sheet configuration has existed, and identify total erosion accordingly. A wave of areal scour removed up to 200 m of bedrock as ice expanded from local to regional ice centres. Upon reaching a continental scale, the bed of the Antarctic Ice Sheet experienced a significant degree of selective erosion around the coast, overdeepening existing troughs. The already deeply incised passive margin topography of coastal Antarctica drives this selectivity, particularly in Dronning Maud Land. The pre-glacial topography, which is fluvial in nature, survives on a large scale under the ice and has been an important driver of glacial erosion. A number of regions, including the Gamburtsev subglacial mountains, are likely to have remained relatively untouched by glacial erosion for ca. 34 Myrs. This lack of modification is evidence that our method of growing an ice sheet on the present day topography (i.e. not a pre-glacial topography) is robust, and that the modelled Oligocene sites of inception are likely to be a good fit to reality.

6.2.5 Synthesis

In summary, there is a clear link between glacial erosion and patterns of evolving glacial dynamics. Furthermore, pre-glacial landscape geometry drives the distribution of this erosion. As erosion modifies the bedrock geometry, the relationships between the ice and climate are also changed. Erosion increases the efficiency with which landscapes can expel ice and, where climate allows, can cause large-scale changes in ice dynamics. The transformation towards most efficient ice drainage tends to occur more rapidly during the earlier periods of modification from fluvial to glacial landscapes.

Relationships between landscape, glacial erosion and ice dynamics are controlled to a great degree by basal traction. Topographic relief and wavelength are also critical in forcing the pattern of ice dynamics and thus erosion generated at the base of an ice sheet. These components of the landscape and of the ice/bed interface, along with climate, control the thermal regime of the ice sheet. Thus whether a topography is incised through selective erosion, smoothed by glacial scour, or protected under cold-based ice, the relief, wavelength and most critically traction conditions will determine the ability with which climate can communicate with the bed via the ice sheet. This highlights the potential importance of the role of deformable sediment in relation to both filling topographic hollows, allowing enhanced erosion in some regions, and particularly the impact that it may have upon the basal traction being experienced.

6.3 Implications

The critical outcome of this research is that glacial erosion should not be considered a passive component of any glacial system. This has a number of implications for research in glaciology and geomorphology.

6.3.1 Interpreting Geomorphology in Relation to Ice Dynamics

We have shown that glacial erosion can alter the stability of ice sheets. The implication of this is that ice sheets will reduce in extent through successive glaciations unless climate or tectonism can adjust to account for this.

Geomorphological and numerical reconstructions of ice sheet behaviour largely ignore the fact that erosion is important in controlling the behaviour of ice. For example, there is often an assumption that terminal moraines in adjacent drainage systems are contemporaneous. However, in regions that have been subject to multiple stages of glaciation, where erosion has been significant but spatially variable, we indicate that this will have an impact upon the synchronicity of retreat between ice lobes. The onset of margin retreat could occur over a range of timescales depending upon the shape and hypsometry of ice drainage systems. Thus although a moraine system that is traced over a regional area may represent a maximum LGM ice sheet extent for example, it is difficult to be confident that ice would have retreated from this position at the same time across the entire region. Furthermore, whereas earlier glacial retreats would be linked to large-scale changes in climate, later retreats after overdeepening over multiple glacial cycles occurs may be more readily triggered by relatively minor climatic warming or drying. In addition, the speed of an ice masses response to climate change may be accelerated where overdeepening has occurred. Glaciologists who study ice mass behaviour on timescales on the order of 10^5 years or greater therefore need to account for the fact that erosion can significantly alter mass balance profiles.

6.3.2 Rates of Glacial Erosion

Glacial erosion is not always rapid. There is a general assumption that average glacial erosion rates are larger (particularly under ice sheets) than those under interglacial fluvial erosion conditions. There is very little evidence to support this. This work showed how low erosion rates can be when averaged over a given area. Although high erosion rates can be generated, their focussed nature, coupled with the strong thermal feedbacks that are associated with drawdown of heat into ice streams, means that large regions can remain relatively unmodified over significant time periods. As a consequence of this, the large-scale pre-glacial topographic structure of a landscape can easily survive under an ice sheet and will be exploited to become overdeepened. It is likely that if deformable sediment were included in the model of glacial erosion then erosion rates would likely increase. However, at the same time, sediment deposition may slow or effectively reverse erosion rates in some areas.

6.3.3 Basal Traction Parameterisation

The experiments conducted during the course of this thesis suggest that the treatment of t_b, a common feature of most glacial models, is too simplistic. The method of calculating the basal slip coefficient is critical to predicting the stability and spatial patterns of basal sliding and landscape evolution. The parameterisation of t_b employed here helps resolve issues of numerical instability and enables realistic patterns of basal flow to be modelled. However, the experiments conducted in this thesis illustrate how important it may be to model the hydrological system of an ice sheet when simulating ice sheet behaviour over any timescale. Any perturbations in the basal hydrology will likely cause significant changes to the behaviour of the ice, and to the pattern of bedrock erosion. Further to this, the potential importance of deformable sediment in relation to basal traction, both in terms of enhancing basal sliding and in terms of increasing the permeability of the bed to allow enhanced meltwater evacuation, is clear (see 6.4.3).

6.3.4 Erosion and Uplift

The results of experiments that erode fluvial landscapes (Chapters 2 and 4) have implications for the argument surrounding the generation of uplift through erosion, and the modification of climate through this uplift. Molnar and England (1990) suggested that erosion can generate uplift, which therefore causes change in climate. Studies confirm that uplift can be generated as a result of erosion on a valley scale (Montgomery, 1994; Small and Anderson, 1998). However, the experiments carried out here indicate that if erosion is glacial in nature (rather than fluvial) and is occurring under an ice sheet (as opposed to under alpine glaciers) then the potential for uplift is limited in scale. Although uplift can be generated in regions adjacent to zones of selective erosion, it cannot be maintained over significant periods of time unless climate cools or becomes wetter. Given that large regions of the Earth have been covered repeatedly by ice sheet scale glaciations throughout the Pleistocene, erosion induced uplift and consequent climate change is likely to occur only in

mountain chains where alpine glaciation is dominant (e.g. Himalaya, Andes and Rockies). In such regions, because a landscape's ability to evacuate ice becomes greater through time due to glacial erosion, the mass balance of the alpine glaciers will be lowered as a result. Thus, glaciers would become less extensive and the ability to drive uplift will become retarded in comparison to that under fluvial conditions unless climate cools or becomes wetter. Uplift could be driven by glaciers over a more prolonged series of glacial cycles if fluvial erosion during interglacial periods was able to 'reset' the topography to a significant degree.

6.3.5 Cold-based vs. Warm-based Erosion

Using the assumption that glacial erosion is controlled by the presence of water at the bed, 'glacial' landscapes that reproduce features identified in reality can be generated. Implicit in this assumption is that erosion under cold-based ice does not occur. However, there is limited evidence indicating that erosion can occur under ice masses that are cold-based (Cuffey et al., 2000). The contrast between lack of erosion under cold ice in the model and the observational evidence indicates that where glacial erosion is generated under cold-based ice the processes must be distinct from those in warm-based settings. In fluvial modelling, detachment and transport limited erosion are treated separately due to their differring controlling factors. Likewise, when modelling glacial erosion this work suggests the processes of warm- vs. cold-based erosion should be treated separately.

6.3.6 Digital Elevation Models and Error Propagation

The work presented here indicates that depending upon basal conditions, ice dynamics can be perturbed by relatively small-scale features in the landscape if traction at the bed is low (i.e. high basal slip coefficients). The implication of this is that error in digital elevation models (DEMs), which are used as inputs to models of ice sheets and glaciers, will likely propagate into calculations of ice mass behaviour. This is supported by Hebeler et al. (In Press) who introduced error to bed DEMs in a suite of 150 experiments modelling the growth of the Scandinavian Ice Sheet. They

show that depending on the selection of model parameters, 1-6.6 % variation in ice sheet extent is generated as a result of introduced DEM error. This is important when it is considered that BEDMAP, a bed DEM conceived specifically for use in modelling Antarctic Ice Sheet evolution, contains spatially variable error of between 50 and 500 m in the vertical, and of between 200 and 10,000 m in space (Lythe et al., 2001). Furthermore, the creation of DEMs necessarily simplifies topography to a given resolution, thus introducing further error. In the case of ice sheet modelling, this latter form of error is balanced by the fact that most ice sheet models also work at reduced resolutions.

6.3.7 Digital Elevation Models – Present vs. Past Topographies

The use of DEMs as inputs to models which seek to reconstruct past ice mass behaviour is widespread, but it should be noted that there is a critical issue that is often overlooked in relation to this. Namely, if topography controls ice mass behaviour then modelling ice expansion over a DEM of the present day topography makes the assumption that the topography has not changed between the time period of interest and the present day. This is clearly not the case because glacial erosion modifies the topography over time. There are two potential ways of dealing with this issue, one of which, backstacking, is outlined in section 6.4.1 below. The other approach, as employed to date in this thesis, is to try and assess the degree to which model results might have changed given a (non-existent) DEM from a different time period.

Using Antarctica as an example (Chapter 5), our model of landscape evolution indicates that although erosion has been significant in a number of regions it is driven by pre-existing topography. Thus it follows that because there are features of selective erosion in present day Antarctica, their generation is likely to have been driven by pre-existing structures. In addition, our model indicates the importance of cold-based ice in preserving the landscape meaning that in many regions the present day bedrock topography may be largely similar to the pre-glacial landscape. Geomorphological evidence from the northern hemisphere along with output from our models suggest glacial erosion is likely to have stripped hundreds of metres of

material from the land surface. This is enough to generate characteristically glacial features across the bed whilst at the same time retaining the large-scale pre-glacial fluvial landscape signal. Therefore, on a continental scale the drainage pathways do not change significantly as a result of long-term glacial erosion, a point supported by previous work (Jamieson et al., 2005).

The implication is that using present day topographies to model patterns of large-scale ice sheet expansion is not likely to be subject to significant error. Large-scale patterns of erosion too, ares likely to be robust although the exact rates of erosion may be overestimated in certain regions using our model. However, modelling glacial and landscape evolution at a small scale will necessarily be subject to a greater degree of error.

The potential risk associated with modelling at a particular scale should be considered in relation to the importance it may have upon model results. For example, modelling landscape evolution from 1 Ma to present using 100 m DEMs will clearly be subject to large degrees of error, thus making the experimental design unfit for purpose. However, a similar experiment over only 20 kyrs (where one would expect much less erosion to have occurred) may be perfectly feasible. It is also critically important to minimise the risk of this error by comparing modelled erosion rates against other sources of information about past rates of landscape evolution (e.g. cosmogenics). Thus, landscape evolution models can be tuned to data in a number of focussed zones and more widespread patterns of modelled landscape change analysed.

6.4 Future Research

Although this thesis answers a number of questions regarding the interactions between landscape and ice sheets, it is clear that many questions remain. The questions driven by issues identified during the course of this thesis provide ample scope for future work:

6.4.1 Backstacking

When simulating ice sheet development and dynamics in a region like Antarctica, modellers are forced to use the present day topography and assume that it has not been changed by glacial erosion. We know from our work (Chapter 5), and from common sense that this is not the case. Thus there is an implicit assumption by all modellers that glacial erosion is unimportant in changing the behaviour of ice masses. Again, we know that this cannot be the case (Chapters 3 and 4). However, the model developed here offers the potential to solve this problem through the technique of *backstacking*. This involves running erosion in reverse, placing material back into the place from which it would have been excavated, and controlling the pattern and rates at which this is done using the basal thermal regime of an ice sheet model. This methodology was tested previously in a simple, non-coupled manner for the Lambert basin of East Antarctica (Jamieson et al., 2005). Reconstructing pre-glacial landscapes will allow ice sheet and landscape evolution to be modelled and will provide better understanding of long-term ice sheet dynamics. This may be critical when considering the future stability of ice masses. For example, in the context of the stability of the Greenland and West Antarctic Ice Sheets under changing climate (Hansen, 2005; Huybrechts and de Wolde, 1999; Lenton et al., 2008) their behaviour will have been conditioned by previous glacial and landscape evolution patterns.

6.4.2 Fluvial vs. Glacial Landscape Evolution

There has been long-standing debate regarding the efficacy of fluvial erosion vs. glacial erosion. It is apparent from our work that the pre-glacial influence of fluvial erosion is critical to the behaviour of ice masses. If an understanding of ice mass behaviour or glacial landscape evolution over multiple glacial cycles is to be gained, the simultaneous consideration of fluvial erosion will offer the greatest potential to do so. The coupling of GLIMMER to a model of fluvial/tectonic landscape evolution such as GOLEM (Tucker and Bras, 1998; Tucker and Slingerland, 1996) or CHILD (Tucker et al., 2001) would provide the ideal model with which to investigate the interactions between fluvial and glacial landscapes. As well as being able to model

the evolution of a coupled landscape, the impact of fluvial 'resetting' of topography upon glacial dynamics could be investigated. Conversely, the impact upon fluvial dynamics of the perturbation of the landscape by glacial erosion could also be identified.

Landscape response through glacial interglacial cycles could be modelled, as could the response of the landscape, rivers and ice masses to variations in periodicity and amplitude of climate. Although previous attempts have been made to couple fluvial and glacial erosion (e.g. Anderson et al., 2006; Braun et al., 1999; MacGregor et al., 2000; Tomkin, 2003), these determine glacial erosion as a function of ice discharge and ignore the thermal regime of the ice mass. The unique dimension that the use of GLIMMER offers is that glacial erosion is modelled as a function of the basal thermal regime. This is critical to determining the distribution of erosion.

6.4.3 Deformable Sediment

Although this thesis has made progress in understanding interactions between bedrock landscape evolution and ice sheets, it ignores the potential influence of deformable sediment at the bed. Figure 1.1c shows how deformable sediment influences ice flow. Our experiments have shown that basal traction is a critical control over the behaviour of ice sheets. The presence of deformable sediment may alter the sensitivity of our models to basal traction because:

- Deformable sediment will facilitate greater degrees of basal sliding for any given basal shear stress. Therefore the dynamic fluctuations experienced by the ice sheets may be exaggerated over and above that experienced in the simulations carried out in this thesis. A degree of stochastic variability in ice margin fluctuations may also be introduced (e.g. Clark, 1994; Clark et al., 2006; Clark and Pollard, 1998).
- A sediment column would change basal water pressures because water drains through a potentially broad column between the ice and bedrock (rather than along a single thin interface). In terms of our current model however, this

behaviour would not change as we have no way to accurately simulate the delivery of water to the bed from upstream or from above (via. Moulins etc.).

- Deformable sediment is more readily erodible than hard bedrock. Therefore the magnitude of modelled landscape evolution is likely to increase where deformable sediment is included. This may enhance the reaction of ice to changing topography. Conversely, sediment deposition in localised regions may retard the response of the ice mass to basal processes.

Therefore an important future direction for research into glacial landscape evolution will focus upon how to model how deformable sediment production (i.e. by erosion of bedrock) and the deformation and erosion of the sediment influences ice sheet behaviour. Such a model would also enable prediction of the spatial distribution of depositional features such as terminal moraines through time and would be beneficial to the geomorphological and glaciological communities.

The model could be extended further to include lithological tracking allowing the provenance of glacial sediment to be determined. This is an approach that has been tested in a simple way using GLIMMER in the context of diamond exploration and glacial erosion of kimberlites (Agnew, 2005). Further, the composition of glacial sediments could be predicted and compared to data gathered in the field. The inclusion of deformable sediment may also reduce the sensitivity of modelled ice sheets to the parameterisation of t_b. If the volume and composition of basal sediments can be predicted, the rules for bedrock erosion might be better parameterised via the inclusion of 'tools' of various lithologies, sizes and spatial densities (Hallet, 1979; Scholz and Engelder, 1976).

6.4.4 Erosion and the Shallow Ice Approximation

As indicated in Chapter 1, the use of the shallow ice approximation (SIA) as a computationally efficient method of calculating glacier flow has potential consequences for model accuracy (Hindmarsh, 2006; Le Meur et al., 2004). Over low resolution domains, surface and bedrock slopes may be low enough that longitudinal stresses can be ignored (Hutter, 1983; Paterson, 1994). However, this is

not certain and in order to test the impact of the SIA on patterns of landscape evolution future work will focus upon comparisons between simulations using the SIA and those using higher order physics to calculate long-stresses.

Furthermore, the implementation of such higher order models will, computer power permitting, allow more detailed simulations of coupled ice mass and topographic evolution to be carried out. The interrelationships between smaller topographic features and evolving ice masses will therefore be possible to determine and will be more readily comparable with field observations which tend to be taken on a local scale.

6.4.5 An Integrated Approach?

Having provided a framework for modelling landscape evolution under ice sheets over the course of this thesis, it is clear that a more integrated approach to understanding long-term landscape evolution is required. The linkages between glacial erosion, glacial dynamics, fluvial erosion, climate and tectonics all play a critical role in modifying the landscape over long time periods. Approaching the puzzle of how landscapes and ice interact therefore requires a multi-disciplinary approach encompassing all of these large-scale processes. The integration of model (e.g. global climate models, ice sheet models, tectonic/fluvial models), remotely-sensed, field-based (e.g. mapping, point measurements, cosmogenics, fission-tracking) and historical approaches would provide the framework within which to do so. The issue that faces those who seek to understand the dynamic behaviour of the landscape is that model predictions and field and remote data collection are applicable over a variety of spatial and temporal scales that do not necessarily compliment one another (Figure 6.1).

If coupled together, the capacity of these approaches to provide insight into the earth system at multiple scales would be significantly advanced. Addressing the issue of differing scales of both process and of techniques is a significant challenge. Despite this, achieving an integrated approach to understanding landscape evolution is a worthwhile and important goal. Using modelling as the core approach will promote

the generation and testing of hypotheses which can be verified using observational records.

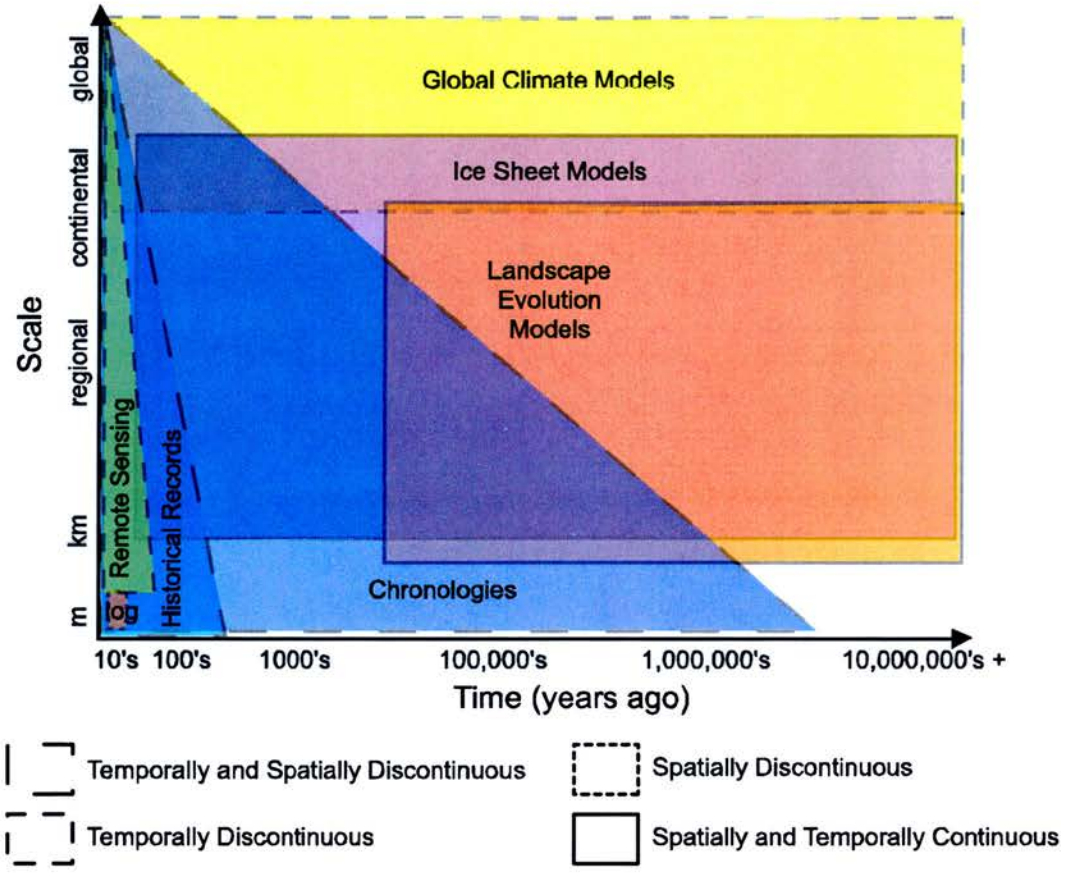

Figure 6.1: Scales of approach to investigating earth systems

Shaded areas show different approaches to investigating components of the earth system and how these work over various temporal and spatial scales (log = data logging at point locations). The challenge is to integrate complimentary approaches to address key issues in earth systems science over particular spatial or temporal scales. The outlines of the shaded areas indicate whether these approaches are able to operate continuously over space and time. For example, global climate models can simulate spatially continuous climate for any given time period but, due to their complexity, can only do so for a limited lengths of time. Integrating approaches that operate on these scales will be a challenge but will present significant opportunity for understanding interactions between different components of the Earth system.

Appendix A: Landscape Evolution of Antarctica

This appendix contains the companion paper to Chapter 5. It has been published as follows:

Jamieson, S.S.R. and Sugden, D.E., 2008. Landscape evolution of Antarctica. In: A.K. Cooper et al. (Editors), Antarctica: A Keystone in a Changing World - Proceedings of the 10th International Symposium on Antarctic Earth Sciences. The National Academies Press, Washington D.C., pp. 39-54.

Antarctica: A Keystone in a Changing World

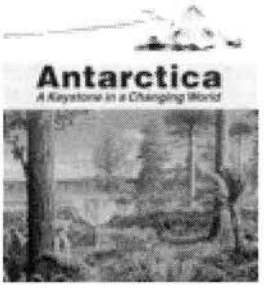

Proceedings of the 10th International Symposium on Antarctic Earth Sciences, Santa Barbara, California, August 26 to September 1, 2007, Alan K. Cooper, Peter Barrett, Howard Stagg, Bryan Storey, Edmund Stump, Woody Wise, and the 10th ISAES editorial team, Polar Research Board, National Research Council, U.S. Geological Survey

ISBN: 0-309-11855-7, 164 pages, 8 1/2 x 11, (2008)

Cooper, A. K., P. J. Barrett, H. Stagg, B. Storey, E. Stump, W. Wise, and the 10th ISAES editorial team, eds. (2008). *Antarctica: A Keystone in a Changing World.* Proceedings of the 10th International Symposium on Antarctic Earth Sciences. Washington, DC: The National Academies Press.

Landscape Evolution of Antarctica

S. S. R. Jamieson and D. E. Sugden[1]

ABSTRACT

The relative roles of fluvial versus glacial processes in shaping the landscape of Antarctica have been debated since the expeditions of Robert Scott and Ernest Shackleton in the early years of the 20th century. Here we build a synthesis of Antarctic landscape evolution based on the geomorphology of passive continental margins and former northern mid-latitude Pleistocene ice sheets. What makes Antarctica so interesting is that the terrestrial landscape retains elements of a record of change that extends back to the Oligocene. Thus there is the potential to link conditions on land with those in the oceans and atmosphere as the world switched from a greenhouse to a glacial world and the Antarctic ice sheet evolved to its present state. In common with other continental fragments of Gondwana there is a fluvial signature to the landscape in the form of the coastal erosion surfaces and escarpments, incised river valleys, and a continent-wide network of river basins. A selective superimposed glacial signature reflects the presence or absence of ice at the pressure melting point. Earliest continental-scale ice sheets formed around 34 Ma, growing from local ice caps centered on mountain massifs, and featured phases of ice-sheet expansion and contraction. These ice masses were most likely cold-based over uplands and warm-based across lowlands and near their margins. For 20 million years ice sheets fluctuated on Croll-Milankovitch frequencies. At ~14 Ma the ice sheet expanded to its maximum and deepened a preexisting radial array of troughs selectively through the coastal mountains and eroded the continental shelf before retreating to its present dimensions at ~13.5 Ma. Subsequent changes in ice extent have been forced mainly by sea-level change. Weathering rates of exposed bedrock have been remarkably slow at high elevations around the margin of East Antarctica under the hyperarid polar climate of the last ~13.5 Ma, offering potential for a long quantitative record of ice-sheet evolution with techniques such as cosmogenic isotope analysis.

INTRODUCTION

Our aim is to synthesize ideas about the evolution of the terrestrial landscapes of Antarctica. There are advantages to such a study. First, the landscape evidence appears to extend back beyond earliest Oligocene times when the first ice sheets formed. Thus events on land may potentially be linked with atmospheric and oceanic change as the world switched from a greenhouse to a glacial world and saw the development of the Antarctic ice sheet. This helps in establishing correlations or leads and lags between different components of the Earth system as a way of establishing cause and effect in global environmental change. Second, the evidence of landscape evolution can be used to refine models of Earth surface processes and their interaction with the wider global system (e.g., by linking conditions in the terrestrial source areas with the marine record of deposition). Third, there are analogies in the Northern Hemisphere of similar-size former Pleistocene ice sheets where the bed is exposed for study. The glaciological body of evidence and theory built on such a base over 150 years is helpful in assessing the nature of the inaccessible topography beneath the Antarctic ice sheet. As such it can illuminate interpretations of subglacial conditions and the dynamics of the present ice sheet.

The crux of any reconstruction of landscape evolution

[1]School of GeoSciences, University of Edinburgh, Edinburgh, EH8 9XP, Scotland, UK (Stewart.Jamieson@ed.ac.uk, David.Sugden@ed.ac.uk).

in a glaciated area is the extent to which ice sheets have transformed a preexisting fluvial topography. For 150 years there has been debate between those highlighting the erosive power of ice and those indicating its preservative capacity. In 1848 Charles Lyell, on his way over the formerly glaciated eastern Grampians of Scotland to receive a knighthood from Queen Victoria, wrote in his diary, "Here as on Mt Washington and in the White Mountains the decomposing granite boulders and the bare surfaces of disintegrating granite are not scored with glacial furrows or polished." Such observations subsequently led to the idea of unglaciated enclaves that escaped glaciation completely (e.g., in Britain: Linton, 1949; and in North America: Ives, 1966). In Antarctica, scientists on the early 20th-century expeditions of Scott and Shackleton debated the issue, with Taylor (1922) arguing that the landscape was essentially glacial in origin but cut under earlier warmer glacial conditions, and Priestley (1909) arguing that glaciers had modified an existing fluvial landscape. The debate has continued; some argue for dissection of the Transantarctic Mountains by glaciers since the Pliocene (van der Wateren et al., 1999) while others point to the important role of fluvial erosion at an earlier time (Sugden and Denton, 2004).

This paper contributes to this debate by outlining the main variables influencing landscape evolution in Antarctica and then developing hypotheses about what might be expected from both a fluvial and a glacial perspective and the interaction of the two.

WIDER CONTEXT

East Antarctica consists of a central fragment of Gondwana and is surrounded by rifted margins (Figure 1). The initial breakup of Gondwana around most of East Antarctica took place between 160 Ma and 118 Ma. The separation of India and Antarctica took place first, while the separation of Australia from Antarctica took place in earnest after 55 Ma. Tasmania and New Zealand separated from the Ross Sea margins at around 70 Ma. West Antarctica comprises four separate mini-continental blocks: Antarctic Peninsula, Thurston, Marie Byrd Land, and Ellsworth-Whitmore, thought to be associated with extensional rifting. The drift of the continents opened up seaways around Antarctica and changed ocean circulation and productivity. A long-held view is that this permitted the development of the Antarctic Circumpolar Current, which introduced conditions favorable for glaciation (i.e., cooler temperatures and increased precipitation) (Kennett, 1977). In addition, recent climate modeling studies have suggested that a reduction in atmospheric greenhouse gases may have played an important role in the triggering of Antarctic glaciation (DeConto and Pollard, 2003; Huber and Nof, 2006). Critical dates for the development of ocean gateways are ~33 Ma, when a significant seaway opened up between Antarctica and Australia (Stickley et al., 2004), and ~31 Ma, when Drake Strait between the Antarctic Peninsula and South America became a significant seaway (Lawver and Gahagan, 2003).

The stepwise glacial history of Antarctica has been pieced together from marine records. Ice sheets first built up at ~34 Ma and their growth was marked by a sudden rise in benthic $\delta^{18}O$ values (Zachos et al., 1992). On land on the Ross Sea margin of Antarctica, beech forest similar to that in Patagonia today gave way to scrub forest and this change was accompanied by a progressive shift in clay minerals from smectite, typical of forest soils, to chlorite and illite characteristic of polar environments (Raine and Askin, 2001; Ehrmann et al., 2005; Barrett, 2007). Glaciation for the next ~20 million years was marked by ice volume fluctuations similar in scale to those of the Pleistocene ice sheets of the Northern Hemisphere. These fluctuations are demonstrated

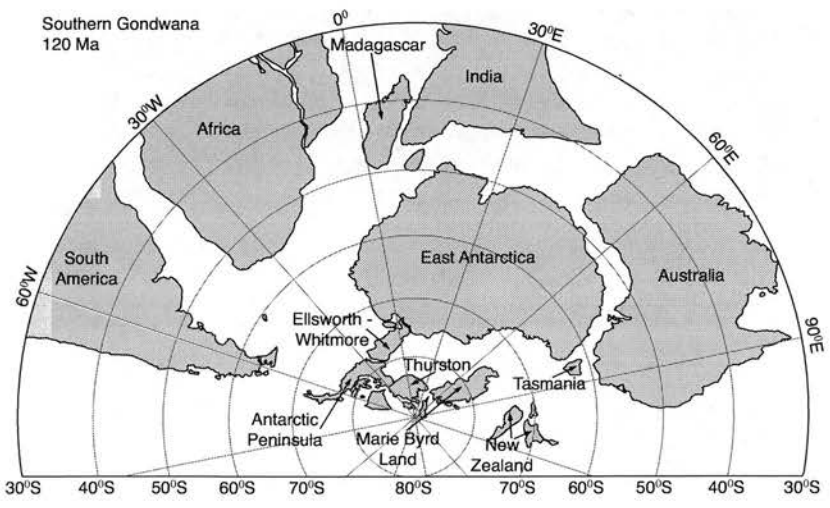

FIGURE 1 The location of Antarctica within Gondwana. The reconstruction shows the fragmentation of the supercontinent at 120 Ma (modified from Lawver et al., 1992).

by strata from 34 Ma to 17 Ma cored off the Victoria Land coast near Cape Roberts (Naish et al., 2001; Dunbar et al., forthcoming), high-resolution isotopic records from near Antarctica (Pekar and DeConto, 2006), and by ice-sheet modeling forced by reduced atmospheric CO_2 levels and contemporary orbital insolation changes (DeConto and Pollard, 2003). During the same period, the Cape Roberts record shows a progressive decline in meltwater sediments accumulating offshore and a vegetation decline to moss tundra, both indicating progressive cooling. A second stepwise cooling of Pacific surface waters of 6-7°C accompanied by a glacial expansion occurred in the mid-Miocene at ~14 Ma and is indicated in the marine isotope record (Shevenell et al., 2004; Holbourn et al., 2005). This event is also recorded in the transition from ash-bearing temperate proglacial deposits to diamict from cold ice in the Olympus Range of South Victoria Land at the edge of the South Polar Plateau (Lewis et al., 2007). Geomorphic evidence indicates that the present hyperarid polar climate of interior Antarctica was established at this time, along with the present structure of polar ocean circulation. Subsequent increases in ice-sheet volume, such as occurred in the Quaternary, involved ice thickening at the coast in response to a lowering of global sea level (Denton et al., 1989).

LANDSCAPE EVOLUTION: THE FLUVIAL SIGNAL

Hypothesis

One can predict in qualitative terms the landscape that would accompany the separation of a long-lived continent such as Gondwana. There would be integrated continental-scale river networks similar in scale to that of the Orange River in South Africa and the Murray River in Australia. Presumably these Antarctic rivers would have developed in a semiarid, seasonally wet climate, especially those in the interior of the supercontinent far from the sea. The rifted margins would have been subjected to fluvial processes related to the evolution of passive continental margins. This has been the focus of much research in recent years and is well summarized by Summerfield (2000). Beaumont et al. (2000) developed a coupled surface process-tectonic model of passive continental margin evolution at a classic diverging rift margin (Figure 2A). The main feature is the uplift of the rifted margin inland of a bounding fault running parallel to the coast. The uplift is a result of thermal buoyancy and crustal flexure in response to denudation near the coast and deposition offshore. Erosion is stimulated by the steep surface gradients created by the lower base level as the rift opens up. Mass wasting and rivers with steep gradients carve a coastal lowland and valleys into the upland rim. A seaward-facing escarpment forms at the drainage divide. Preexisting rivers may keep pace with the uplift and traverse the escarpment and allow dissection to spread behind the escarpment. Subsidiary erosion surfaces may form in response to lithological contrasts in rock type and in response to secondary faults that develop parallel to the coast. Observations on other Gondwanan margins suggest that most erosion occurs within 10-20 million years of the rift opening up (Persano et al., 2002). Subsequently, cooling and crustal flexure may cause subsidence and the seaward ends of the valleys are flooded by the sea.

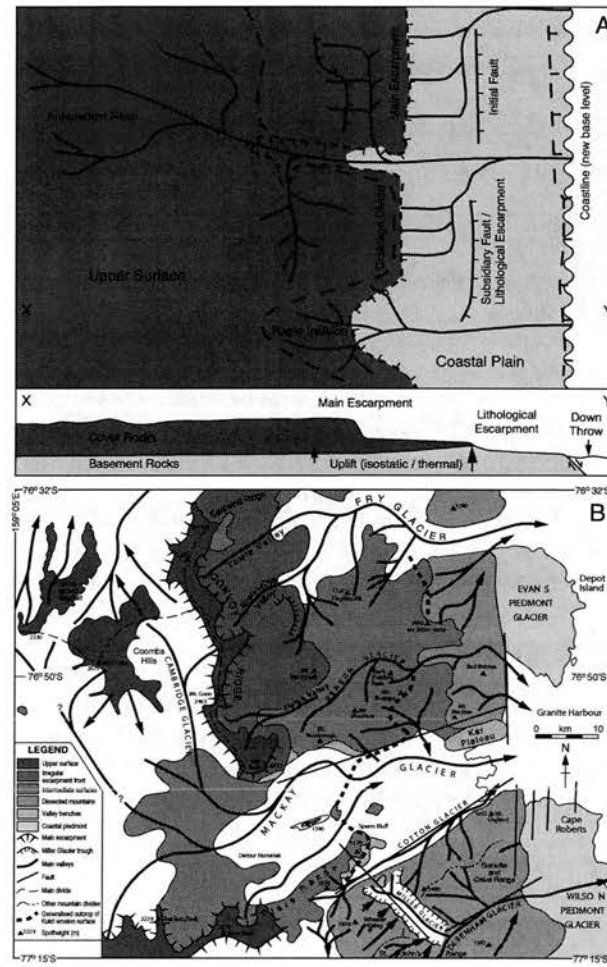

FIGURE 2 (A) Typical landscapes of a passive continental margin as modeled by Beaumont et al. (2000), using a numerical coupled tectonic-earth surface process model of landscape evolution. The new base level creates a pulse of erosion and associated rock uplift that leads to a staircase of coastal erosion surfaces separated by escarpments and incised river valleys, some of which may maintain their valleys across the escarpment crest. (B) Geomorphic map of the Convoy Range and Mackay Glacier area, showing the staircase of seaward-facing escarpments, erosion surfaces, dissected mountain landscapes near the coast, and the dendritic valley patterns radiating from a high point in the Coombs Hills. Principal faults parallel to and at right angles to the mountain front are taken from Fitzgerald (1992).
SOURCE: Sugden and Denton (2004). The model in (A) simulates the field evidence in remarkable detail.

The model applies to idealized young rift margins, and there are often more complex relationships affecting other continental margins of Gondwana (Bishop and Goldrick, 2000). Factors such as time elapsed since rifting, proximity to the rift, inherited altitude of the margin, tectonic downwarping, and crustal flexure can all affect the amplitude of the topography and the evolution of any escarpment.

Antarctic Evidence

Figure 3 shows a reconstruction of the continental river patterns inferred to exist if the Antarctic ice sheet is removed and the land compensated for isostatic depression by full flexural rebound. The map is based on the BEDMAP reconstruction of subglacial topography with a nominal resolution of 5 km (Figure 4) (Lythe et al., 2001). Sea level is assumed to lie at −100 m to represent the subsidence associated with the crustal cooling and flexure of mature passive continental margins. The reconstruction is based on hydrological modeling methods for cell-based digital elevation models whereby water is deemed to flow to the lowest adjacent cell. There are many uncertainties, not the least of which is that large areas have little data, but a sensitivity analysis suggests that models forced by a range of different assumptions yield a network that is essentially similar from run to run (Jamieson et al., 2005). The reconstruction shows that there are integrated networks leading radially to major depressions at the coast, such as the western Weddell Sea, Lambert, Wilkes Land, and Oates Land basins. The dendritic pattern of the network, the centripetal pattern of flow from the subglacial Gamburtsev Mountains, and the topological coherence of the tributaries are demonstrated by bifurcation ratios that are representative of other river basins, such as the Orange River in South Africa (Jamieson et al., 2005). These observations imply a fluvial signature in the subglacial landscape on a continental scale.

Such a conclusion is reinforced by investigation of the valley patterns on mountain areas rising above the present ice-sheet surface. Good examples of former fluvial valley systems now occupied by local glaciers exist in the Transantarctic Mountains. The valley networks of several basins in northern Victoria Land have been ordered according to fluvially based Horton-Strahler rules (Horton, 1945; Strahler, 1958) and the dendritic pattern and hierarchical relationships between valley segments, and variables such as cumulative mean length are typical of river networks (Baroni et al., 2005). The Royal Society Range shows a similarly dendritic network radiating from one of the highest summits in Antarctica at over 4000 m (Sugden et al., 1999).

The landforms near the coast of the Antarctic passive continental margin are well displayed in the relatively glacier-free area of the Dry Valleys and adjacent Convoy Range (Figure 2B). Many features expected of a fluvial landscape are present. These include erosion surfaces rising inland from

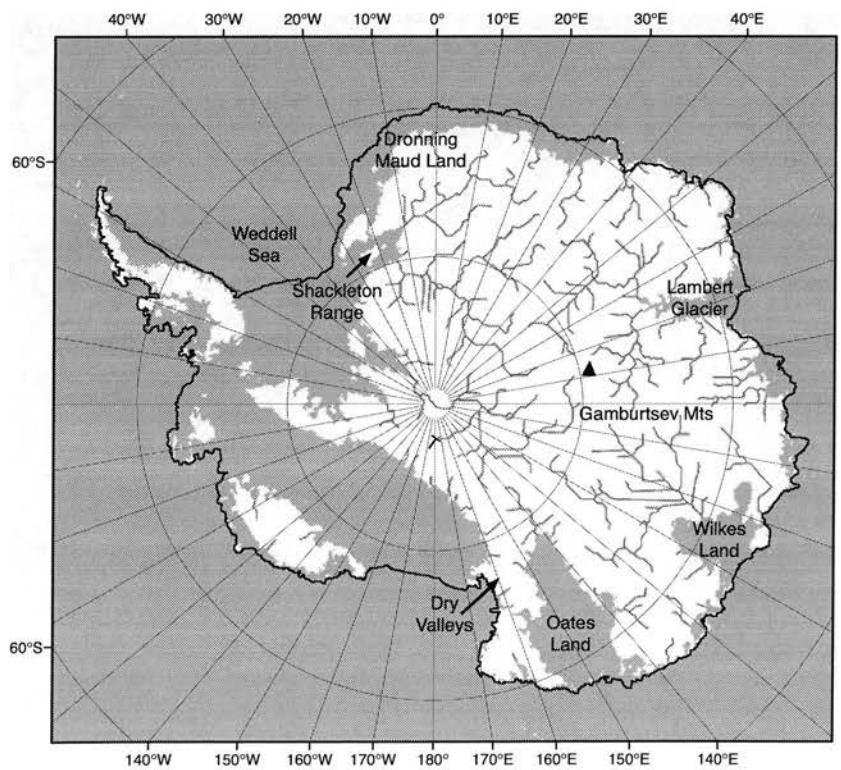

FIGURE 3 Reconstruction of the continental-scale river patterns beneath the present ice sheet. We assume that the land is isostatically compensated and that sea level is 100 m lower than today. The model uses the BEDMAP subglacial topography at a nominal cellular scale of 5 km (Figure 4). BEDMAP data are from Lythe et al. (2001).

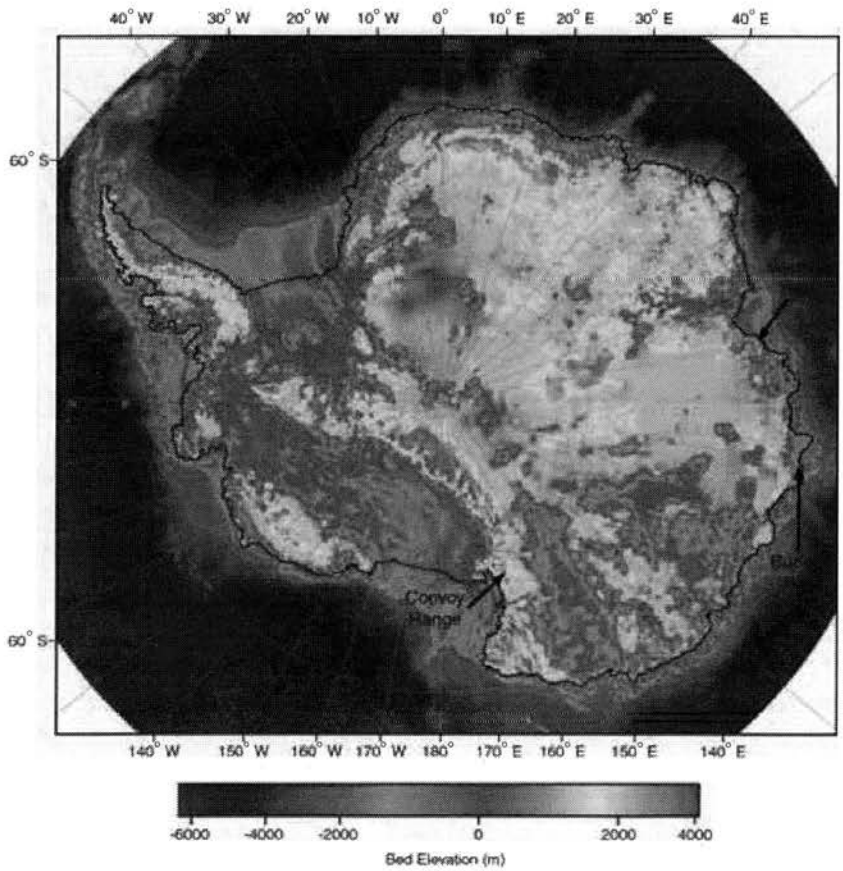

FIGURE 4 The present-day subglacial topography of Antarctica. BEDMAP data are from Lythe et al. (2001).

the coast and separated by escarpments, a coastal piedmont, an undulating upper erosion surface dotted with 100-450 m inselbergs, a seaward-facing escarpment 1000-1500 m in height, and intermediate erosion surfaces delimited by lithological variations, notably near horizontal dolerite sills. Sinuous valleys with a dendritic pattern can also be found. Most run from the escarpment to the sea, but others, such as that occupied by Mackay Glacier, breach the escarpment and drain the interior through tributaries bounded by additional escarpments. In detail the valleys have a sinuous planform, rectilinear valley sides with angles of 26-36°, and often lower-angle pediment slopes in the valley floors (Figure 5). The floor of the southernmost Dry Valley, Taylor Valley, is below sea level toward the coast, where it is filled with over 300 m of sediments of late-Miocene to recent age (Webb and Wrenn, 1982).

The erosion of the coastal margin has been accompanied by the denudation of a wedge of rock thickest at the coast and declining inland. This is displayed in the coastal upwarping of basement rocks and in the denudation history indicated by apatite fission track analysis. Both lines of evidence agree and point to the denudation since rifting of 4.5-5 km of rock at the coast falling to ~1 km of rock at locations 100 km inland (Fitzgerald, 1992; Sugden and Denton, 2004). The fission track analyses suggest that most denudation occurred shortly after 55 Ma.

The evidence presented above is powerful affirmation that the normal fluvial processes of the erosion of a passive continental margin explain the main landscape features of three mountain blocks of the Transantarctic Mountains extending over a distance of 260 km. In these cases it is the fault pattern and the position of the drainage divide that are the main controls on topography and determine the differences in the landscapes of each block. It is not possible to apply the model of passive continental margin evolution to other sectors of East Antarctica without more detailed evidence, but similar landscapes occur in the Shackleton Range (Kerr and Hermichen, 1999) and in Dronning Maud Land (Näslund, 2001). One exception is the Bunger Hills and Vestfold Hills sector of East Antarctica east of the Lambert Glacier, where there is no escarpment. The matching piece of Gondwana is India, which separated early, and a longer and more complex evolution of the rift margin may explain the lack of an escarpment today.

It seems reasonable to argue that the framework of passive continental margin evolution applies to Antarctica and that in many areas a major pulse of fluvial erosion and accompanying uplift was a response to new lower base levels

FIGURE 5 George Denton and David Marchant in Victoria Valley, Dry Valleys, a typically fluvial landscape with rectilinear slopes and a shallow pediment slope leading to the valley axis. The slopes have escaped modification by overriding ice.

following continental breakup. Since breakup took place at different times, the stage of landscape evolution will vary from place to place in Antarctica. Furthermore, where large-scale tectonic features such as the Lambert graben disrupt the continental margin, they are likely to focus the fluvial system in a distinctive way (Jamieson et al., 2005).

LANDSCAPE EVOLUTION: THE GLACIAL SIGNAL

Hypothesis

The beds of former Northern Hemisphere mid-latitude ice sheets form the basis of understanding how glaciers transform preexisting landscapes. There are differences in that the Antarctic ice sheet has existed for tens of millions of years rather than a few million, but there are important similarities in that the North American ice sheet was of similar size and volume as the Antarctic ice sheet, and in that both have fluctuated in size in response to orbital forcing during their evolution, albeit to varying extents.

At the outset it is helpful to distinguish two scales of feature: Those that reflect the integrated radial flow of the ice sheet at a continental scale when it is close to or at its maximum and those that reflect the local and regional flow patterns as ice flows radially from topographic highs.

The key to landscape change by large ice sheets is the superposition of a continental-scale radial flow pattern on the underlying topography. Such patterns are easily obscured by local signals but one can identify the following:

- Erosion in the center and wedges of deposition beneath and around the peripheries (Sugden, 1977; Boulton, 1996);
- Continental shelves that are deeper near the continent and shallower offshore as a result of erosion near the coast, often at the junction between basement and sedimentary rocks (Holtedahl, 1958);
- Radial pattern of large 10-km-scale troughs that breach and dissect the drainage divides near the coast and may continue offshore (e.g., in Norway, Greenland, and Baffin Island) (Løken and Hodgson, 1971; Holtedahl, 1967);
- Radial pattern of ice streams with beds tens of km wide, streamlined bedforms in bedrock and drift, and sharply defined boundaries (Stokes and Clark, 1999); and
- Radial pattern of meltwater flow crossing regional interfluves, as revealed, for example, by the pattern of eskers in North America (Prest, 1970).

Local and regional patterns also display radial configurations and reflect multiple episodes of reduced glaciation. Distinguishing features of marginal glaciation are corries or cirques, the dominant orientation of which, northeast facing,

is determined in the Northern Hemisphere by slopes shaded from the sun and subject to wind drift by prevailing westerly winds (Evans, 1969). Stronger local glaciation typically builds ice caps on mountain massifs with ice flow carving a radial pattern of troughs, so well displayed in the English Lake District and Scotland, for example.

Clearly there will be a complex interaction between local, regional, and continental modes of flow depending on such factors as climate, ice extent, and topographic geometry. We attempt to model this complexity in Figure 6 by showing various stages of evolution of the Antarctic ice sheet using GLIMMER, a three-dimensional thermomechanical ice-sheet model as described by Payne (1999) and Jamieson et al. (forthcoming). The intention is to illustrate the range of different ice-sheet geometries that would be expected at various stages of Croll-Milankovitch glacial-deglacial cycles. The model is run for an arbitrary 1 million years with stepped temperature changes every 50 kyr falling from present-day Patagonian values to present-day Antarctic values. This timescale is designed to allow the ice to achieve approximate equilibrium at all times and to allow the isostatic response of the bedrock to reach a balance with these fluctuations in ice thickness. Patagonian climate statistics are used to simulate the climate inferred from vegetation associated with the initial glaciation of Antarctica (Cape Roberts Science Team, 2000; Raine and Askin, 2001). Modeled precipitation follows the pattern of net surface mass balance derived by Vaughan et al. (1999). At the beginning of the model run, maximum coastal precipitation at sea level is scaled up to 2 m per year, four times that of the present day. The maximum then falls linearly to 0.5 m per year by the end of the model run. Mean annual temperatures fall from 7°C at sea level to present values of −12°C through the model run. Melt rates under warmer climatic conditions are calculated using a positive degree-day model (Reeh, 1991) whereby ablation is proportional to the number of days where temperature is above the freezing point. Diurnal variability is accounted for by using a normal distribution of temperature with a 5°C standard deviation. The pattern of mass balance used to drive ice growth is shown in Figure 7.

The bed topography is derived from BEDMAP (Figure 4) (Lythe et al., 2001) and is flexurally rebounded to compensate for the lack of an ice sheet. The use of an isostatically compensated present-day topography ignores tectonic movements and means that the results of the modeling become more uncertain as one goes further back in time. However, there is less risk in East Antarctica, where the main topographic features were established by Oligocene times. For example, geological evidence in the form of basement clasts in Oligocene strata cored off the Victoria Land coast (CIROS-1 drillcore) (Barrett et al., 1989) and Cape Roberts (Cape Roberts Science Team, 2000) suggests that the Transantarctic Mountains had been eroded deep enough to form a significant feature by Oligocene times. Furthermore, the Gamburtsev Mountains are considered to be a Pan-African feature with an age of 500 Ma (van de Flierdt et al., 2007).

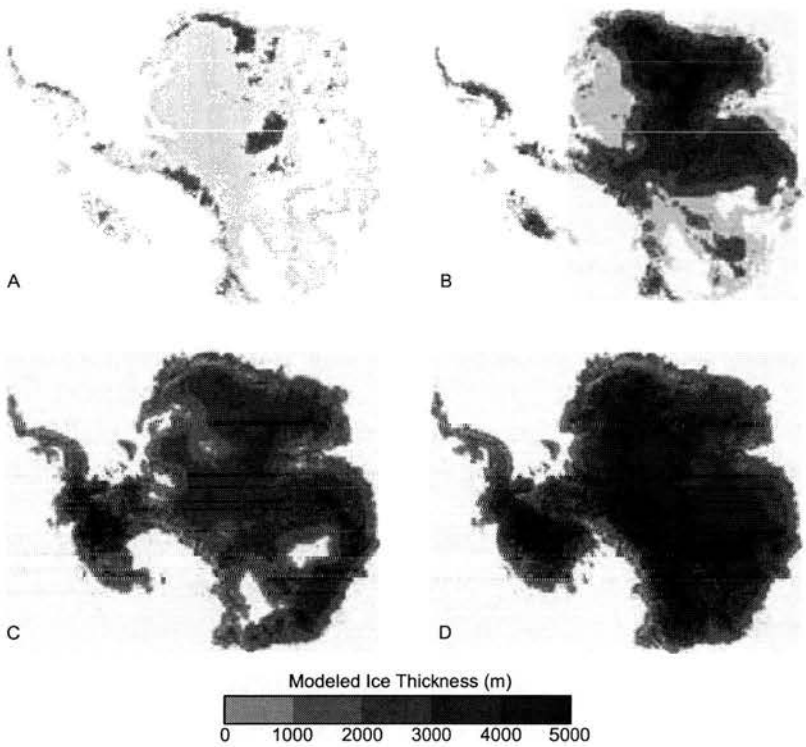

FIGURE 6 Model of the Antarctic ice sheet, generated using the GLIMMER 3-D thermomechanical model and the stepped transition from a Patagonian-style climate to the present polar climate. The four stages (A-D) illustrate the range of variability to be expected as the Antarctic ice sheet experienced many Croll-Milankovitch glacial cycles during its early evolution.

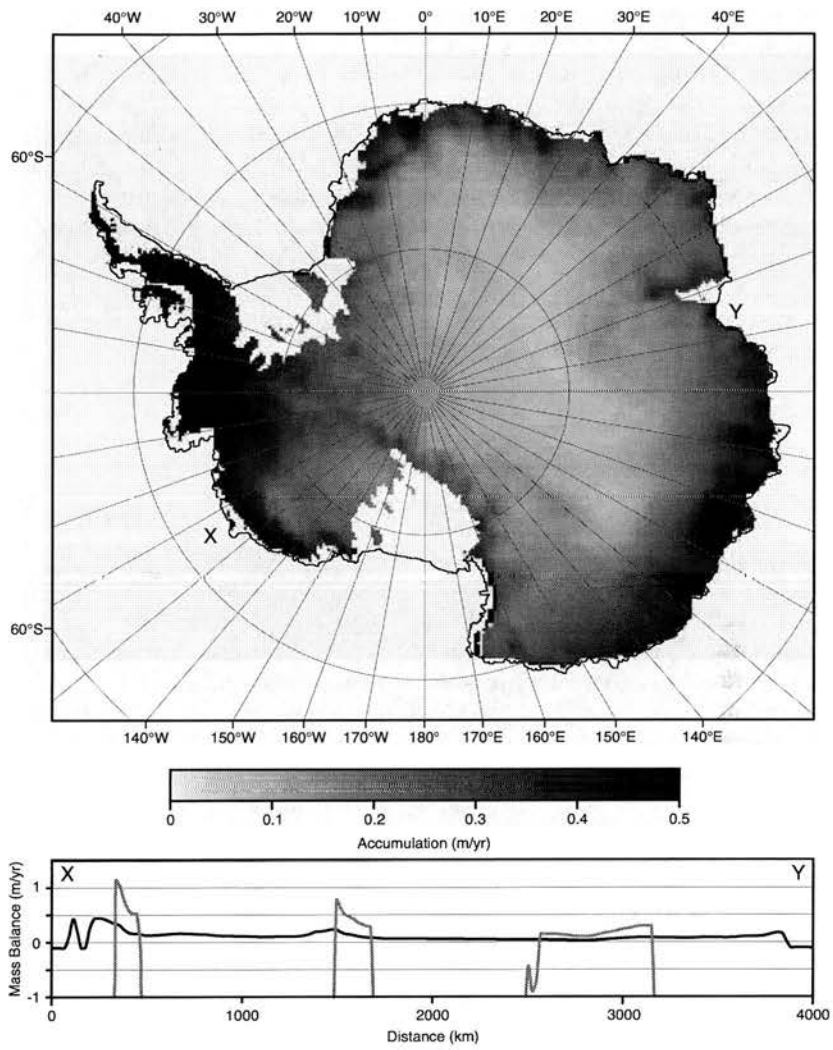

FIGURE 7 Present-day accumulation is used to drive a simulated Antarctic ice sheet (Vaughan et al., 1999). Profile X-Y shows that under a Patagonian-style regime (grey line) there are zones of increased accumulation at high altitudes. Accumulation is discontinuous because of high levels of ablation across much of the continental lowlands. The present-day accumulation is shown by the black line.

The different stages of growth illustrate the principal pattern of glaciation of Antarctica. Initial growth is in coastal mountains, such as in Dronning Maud Land, along the Transantarctic Mountains, in the West Antarctic archipelago, and in the high Gamburtsev Mountains in the interior. The ice spreads out from these mountain centers, first linking the main East Antarctic centers and then the West Antarctic centers. The model is deliberately simple but it suffices to show that glaciation starts preferentially in maritime mountains and in interior mountains if they are high enough. It also serves to illustrate the complexity of the changing pattern of flow as different ice centers merge and ice flow evolves from locally radial to continentally radial. The subglacial landscape of Antarctica can be expected to consist of a palimpsest of landforms related to these local, regional, and continental stages, while eroded material will experience a complex history of temporary deposition and changing flow paths before being delivered to the coastal margin by the continental ice sheet.

Antarctic Evidence

The evidence of continental radial patterns of erosion is spectacular. The Lambert trough, which is 40-50 km across and 1 km deep, drains 10 percent of the East Antarctic ice sheet. It is coincident with a graben and is comparable to, but deeper and longer than, the North American equivalents, such as Frobisher Bay in Baffin Island. And then there is the spectacular series of troughs cutting through the Transantarctic Mountain rim. Webb (1994) has previously suggested that the Beardmore trough, 200 km long, 15-45 km wide, and over 1200 m deep, exploited a preexisting river valley. Unloading due to glacial erosion may have contributed to isostatic uplift of the adjacent mountains (Stern et al., 2005). Offshore there are continuations of such troughs incised

into the continental shelf of both East and West Antarctica (Wellner et al., 2001). Other troughs, such as that running parallel to Adelaide Island on the Antarctic Peninsula, have exploited the junction between basement and sedimentary rocks (Anderson, 1999). A series of ice streams flow into the Ross Sea and Weddell Sea embayments. They are underlain by deformable till and, in the case of the Rutford ice stream, by streamlined bedforms (Smith et al., 2007). There is also growing evidence of radial outflow of basal meltwater (Evatt et al., 2006). Hundred-meter-deep rock channels and massive staircases of giant potholes represent large-scale outbursts of subglacial meltwater across the Transantarctic Mountains rim in the McMurdo area (Denton and Sugden, 2005; Lewis et al., 2006).

There is also evidence of local and regional glacial landforms. Early studies of the subglacial Gamburtsev Mountains revealed characteristic trough overdeepening and the presence of hanging valleys, pointing to a local glaciation (Figure 8). The glacial landscapes of Dronning Maud Land too were created by local mountain glaciation and not the present ice sheet (Holmlund and Näslund, 1994). Recent geophysical surveying has demonstrated the presence of lakes in overdeepened troughs radiating from the Ellsworth Mountain core (Siegert, pers. comm., 2007). Overdeepening in the topographically constrained part of a fjord, and the rock threshold at the point when the trough opens out, are well-known characteristics of fjords in the Northern Hemisphere (Løken and Hodgson, 1971; Holtedahl, 1967). Similar features are found to radiate from uplands now below sea level in the Ross Sea embayment (De Santis et al., 1995; Sorlien et al., 2007). In these latter cases the troughs are revealed by seismic survey. In the McMurdo Dry Valleys area of the Transantarctic Mountains a phase of local glaciation is represented by troughs identified on the inland flank of the mountains (Drewry, 1982) and troughs exploiting sinuous river valleys, such as the Mackay Glacier. Finally, the compact wet-based glacial deposits (the Sirius Group deposits) distributed at high elevations along 1000 km of the Transantarctic Mountains in the Ross Sea sector represent glaciation centered on the mountains (Denton et al., 1991, 1993). The deposits are characterized by local lithologies and the till components contain striated stones and a matrix typical of glacial erosion under warm-based ice. Some of these deposits incorporate remains of *Nothofagus* (southern beech) forest representative of a cool temperate environment.

LANDSCAPE EVOLUTION: THE COMBINED SIGNAL

Hypotheses

It is possible to relate subglacial landscapes to the processes by which glaciers modify preexisting topography. A simple classification scheme recognizes landscapes of areal scouring with abundant evidence of glacial scour; those of selective linear erosion where troughs dissect plateaus; those with no sign of glacial erosion and devoid of glacial landforms; and depositional landscapes composed of till and meltwater deposits (Sugden, 1978). The differences are related to whether the basal ice is at the pressure melting point. A key assumption is that ice erodes effectively when the base

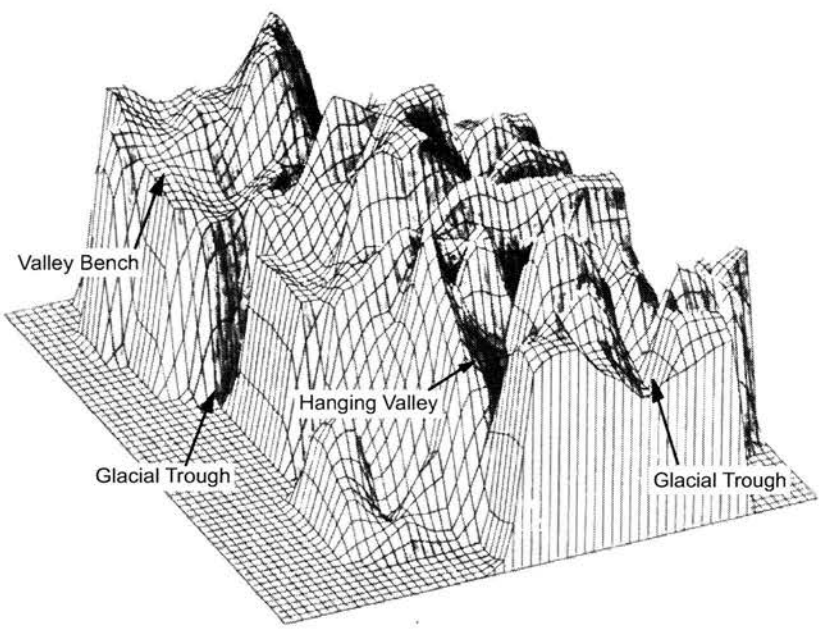

FIGURE 8 An early reconstruction of the landscape of the subglacial Gamburtsev Mountains based on the analysis of radio-echo sounding data. The arrows pick out diagnostic glacial features such as overdeepening and hanging valleys presumed to have been formed by local mountain glaciation (modified from Perkins, 1984).

is at the pressure melting point because sliding takes place between the ice and bedrock, permitting several processes to entrain bedrock and to deposit material. Such a situation explains landscapes of areal scouring, the linear erosion of troughs, and zones of deposition. The converse is that when the basal temperature is below the pressure melting point there is no sliding at the ice and rock interface. In such situations ice can be essentially protective and leave little sign of erosion. There is debate as to how protective the ice may be (Cuffey et al., 2000), but recent work on cosmogenic isotope analysis demonstrating the age of exposure and the time buried beneath ice has shown that the hypothesis holds in many areas of the Northern Hemisphere (Briner et al., 2006; Stroeven et al. 2002).

Armed with these observations it is possible to hypothesize about the landscape beneath the Antarctic ice sheet and suggest local, regional, and continental patterns. The numerical model of ice-sheet growth can be used to predict the changing pattern of glacial erosion during glacial cycles. Figure 9 shows the distribution of basal ice at the pressure melting point during stages of regional and continental glaciation. The regional pattern shows how the peripheries of the regional ice sheets are warm-based near their margins and inland to the vicinity of the equilibrium line where the ice discharge is highest and generating most internal heat. These will be the areas of glacial erosion. The influence of topography is clear in that warm-based ice is focused on the depressions and major valleys where ice is thicker and flows faster. These low-lying areas at the pressure melting point are also those in which subglacial lakes might accumulate. What is striking is the way this zone of peripheral warm-based ice and erosion is a wave that sweeps across the landscape as the ice sheet grows to its continental maximum. At the macroscale the zone of warm-based ice is more extensive around the continental margins, especially in the vicinity of the main preexisting drainage basin outlets. Under both scenarios the ice over the main uplands remains below the pressure melting point.

From the above we can predict that the landscape in lowland areas of the Antarctic ice sheet will be underlain by a landscape of areal scouring. This relates both to the presence of ice at the pressure melting point and to the progressive erosion of rock debris by radial outflow of ice at different scales. Interaction between local and ice-sheet maximum flow directions and rock structure will determine the roughness and degree of streamlining of landforms. Flow in the same direction under both local and continental modes will favor elongated streamlined bedforms, perhaps with plucked

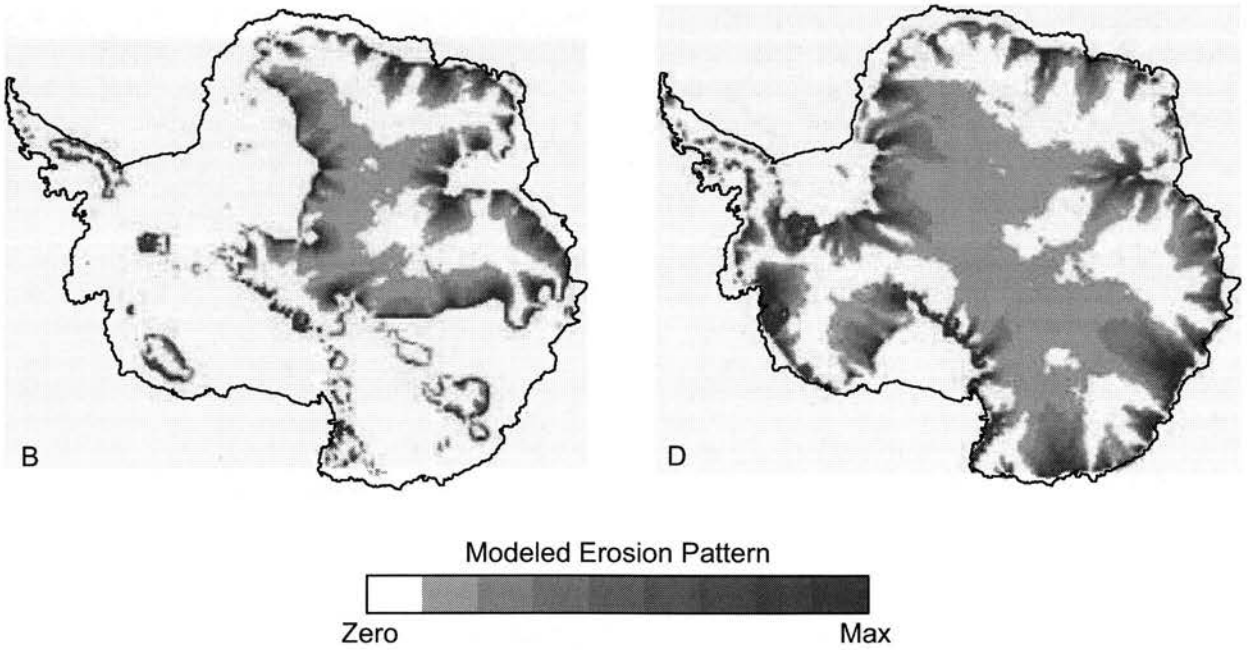

FIGURE 9 Modeled distribution of basal ice at the pressure melting point during intermediate and full stages of Antarctic glaciation (letters correspond to snapshots in Figure 6). Erosion, thought to be associated with sliding under such basal conditions, is concentrated toward the ice-sheet margins and at the beds of major outlet glaciers. A wave of erosion accompanies the expansion of local and regional ice to a full continental ice sheet.

lee slopes, while complex flow changes will leave an irregular pattern. Areal scouring will be clearest on the lowlands and diminish upslope on upstanding massifs where summits may show no sign of glacial modification. This latter pattern reflects the effects of topography on the basal thermal regime and implies that the ice remained cold-based during local, regional, and continental stages of glaciation. Judging by the geomorphology of glaciated shields of the Northern Hemisphere, erosion will have removed some tens of meters of material, much of it initially as weathered regolith. This is sufficient to modify but not erase the preexisting river landscape, as argued for northern Europe (Lidmar-Bergstrom, 1982). However, given the longer duration of glaciation in Antarctica one would expect a greater depth to have been removed. The products of this erosion will be deposited offshore.

Antarctic Evidence

There is no direct evidence of areally scoured landscapes beneath the ice sheet. However, there are many observations from around the margins of Antarctica to indicate that such landscapes are likely to be widespread. Areas formerly covered by an earlier expanded ice sheet display extensive landscapes of areal scouring. This includes oases in East Antarctica, such as the Amery Oasis bordering the Lambert Glacier (Hambrey et al., 2007); the Ross Sea area where the scouring is most prominent near sea level and can be traced to elevations of 1000-2100 m along the Transantarctic Mountains front (Denton and Sugden, 2005); the inner parts of the offshore shelf in many parts of West Antarctica; and the offshore shelves surrounding islands off the Antarctic Peninsula and sub-Antarctic islands (Anderson, 1999). In all these situations meltwater channels testify to the activity of basal meltwater. Whereas all these observations are consistent with the view that warm-based ice occurred beneath thicker parts of the ice sheet when it was more extended and in maritime environments, what is surprising is that striated, scoured rock surfaces also define trimlines around mountains protruding above the ice sheet, even in the interior, such as the Ellsworth Mountains (Denton et al., 1992). The implication of shallow surface ice at the pressure melting point is that surface climatic conditions must have been within a few degrees of freezing point and thus several tens of degrees warmer than at present.

Landscapes of selective linear erosion are common in the mountainous rim of East Antarctica. In many areas glacial troughs are clearly delimited and excavated into a landscape-preserving fluvial valley form, often bearing diagnostic subaerial weathering forms such as regolith and tors. Such a description would apply to the landscapes bordering the Lambert Glacier (Hambrey et al., 2007), the Shackleton Mountains (Kerr and Hermichen, 1999), exposed escarpments in Dronning Maud Land (Näslund, 2001), the mountain blocks of the Transantarctic Mountains in Victoria Land (Sugden and Denton, 2004), and the plateaus of the Antarctic Peninsula area (Linton, 1963). As in the Northern Hemisphere such a description also applies on the scale of individual massifs. For example, upstanding nunataks in the Sarnoff Mountains of Marie Byrd Land are bounded by lower slopes with clear evidence of glacial scouring and yet their summits have retained an upper surface with tors, weathering pits, and block fields. In this case cosmogenic isotope analysis demonstrates that the mountains have been covered by ice of several glacial maxima and that weathering has continued sporadically in interglacials for ~1 million years (Sugden et al., 2005). The selectivity reflects the difference between the thicker, converging ice that scours as it flows round the massif and the thin diverging ice covering the summit that remains cold-based during each episode of overriding.

The implication of the above is that the hypothesis relating glacial modification of a preexisting landscape to the presence or absence of warm-based ice may be helpful in describing and understanding the landscape evolution of Antarctica. When the basal thermal regime remains the same beneath both local and full ice-sheet conditions, then the glacial transformation, or lack of it, will be clearest. What is exciting about the present time is that cosmogenic isotope analysis offers the opportunity to quantify such relationships.

CHRONOLOGY OF LANDSCAPE EVOLUTION

A number of dates help firm up the relative chronology of landscape evolution. Early studies of offshore sediments in Prydz Bay established the presence of fluvial sediments below the earliest glacial sediments, the latter dated to ~34 Ma (Cooper et al., 1991; O'Brien et al., 2001). The location, structure, and nature of the sediments suggest that the deposits have been derived from rivers flowing along the Lambert graben. Probably the deposits began to accumulate when rift separation began around 118 Ma (Jamieson et al., 2005).

Some large glacial troughs were cut by late Miocene times. In the Lambert Glacier area the offshore sedimentary evidence points to an ice sheet that discharged from a broad front on the offshore shelf until the late Miocene but experienced a switch to deposition within the overdeepened Lambert glacial trough subsequently. Ice-sheet modeling suggests that the deepening of the trough changed the dynamics of glacier flow and ablation to such an extent that calving velocity could match ice velocity and that the glacier was no longer able to advance through the deep water of the trough (Taylor et al., 2004). The implication is that the trough was excavated deeply by the late Miocene. Similar relationships occur in the glacially deepened mouths of the Dry Valleys in the McMurdo Sound area. Microfossils at the bottom of the Dry Valleys Drilling Project (DVDP-11) drillcore at the mouth of Taylor Valley are late Miocene in age (Webb and Wrenn, 1982). Marine shells deposited in a fjord in the glacial trough of Wright Valley are Pliocene in

age and overlie a till of >13.6 Ma (Hall et al., 1993). These age relationships in glacial troughs related to ice flow from the interior of Antarctica demonstrate that they were cut by the late Miocene.

There is evidence from the McMurdo Sound area that the Antarctic ice sheet overrode marginal mountains and extended to the outer shelf at its maximum in the mid-Miocene. The case is argued out in a series of detailed papers in the Dry Valleys area, the key chronological fixes of which are:

- There is clear evidence that ice overrode all except perhaps the highest mountains in the Royal Society Range in the form of ice scouring on cols and subglacial meltwater channels that cross the mountains. The direction of flow is conformable with models of ice expansion to the outer edge of the offshore shelf (Sugden and Denton, 2004).
- $^{40}Ar/^{39}Ar$ dating of in situ volcanic ash deposits overrun by such ice and those ashes deposited on till sheets associated with such overriding ice constrains the event to between 14.8 Ma and 13.6 Ma (Marchant et al., 1993).
- Landscapes of areal scouring molded by the maximum ice sheet in front of the Royal Society are older than 12.4 3 ± 0.22 Ma, the age of the oldest undisturbed volcanic cone known to have erupted onto the land surface (Sugden et al., 1999).
- $^{40}Ar/^{39}Ar$ analyses of tephra show that the major meltwater feature represented by the Labyrinth in Wright Valley predates 12.4 Ma and that the last major outburst occurred some time between 14.4 Ma and 12.4 Ma (Lewis et al., 2006).
- ^{3}He ages of individual dolerite clasts in meltwater deposits from the overriding ice sheet reveal exposure ages between 8.63 ± 0.09 and 10.40 ± 0.04 Ma. Allowing for erosion, they are calculated to have been exposed for ~13 Ma (Margerison et al., 2005).

As yet there are few comparable terrestrial dates elsewhere in Antarctica, but it is worth drawing attention to work on the flanks of the Lambert Glacier in which there is biostratigraphical evidence of a pre-late Miocene phase of glacial erosion and deepening, followed by a 10-million-year period of exposure (Hambrey et al., 2007). It is tempting to equate the deepening to the same ice-sheet maximum.

In the McMurdo Sound area it is possible to establish that a phase of warm-based glaciation occurred before the mid-Miocene overriding ice. The critical evidence is that warm-based tills in the high mountains bounding the Dry Valleys, and indeed the Sirius Group deposits, have been modified by overriding ice. Typically there are erosional patches excavated into a preexisting till with material dragged out down-ice (Marchant et al., 1993) and ripple corrugations with a spacing of 25-50 m that are a coherent part of the overriding meltwater system (Denton and Sugden, 2005). One important fix on the switch from warm-based to cold-based local glaciation has been reported from the Olympus Range in the McMurdo Sound area of the Transantarctic Mountains (Lewis et al., 2007). Here a classic warm-based till with meltout facies is overlain by weathered colluvium that is itself overlain by tills deposited by cold-based glaciers. The minimum date of transition is fixed by volcanic ashes interbedded between the two sets of tills and has an age of 13.94 Ma. Such a transition beneath small local glaciers is argued to represent an atmospheric cooling of 20-25°C. Moreover, the transition occurs before one or more major ice-sheet overriding events in the same area.

DISCUSSION

Here we attempt a synthesis of landscape evolution of Antarctica, based mainly on terrestrial evidence (Table 1). Inevitably the hypothesis is based on partial information and is biased toward the data-rich McMurdo Sound area of the Transantarctic Mountains. Nevertheless it seems helpful to try and generalize more broadly.

An early pulse of fluvial erosion was associated with the breakup of Gondwana and the creation of new lower base levels around the separating continental fragments. The timing of the pulse varied with the time of base level change around each segment. Erosion removed a wedge of material from around the margins of East Antarctica and the smaller continental fragments of West Antarctica. Escarpments

TABLE 1 The Chronology of Landscape Evolution in Antarctica Based Mainly on Terrestrial Evidence

>55-34 Ma	Passive continental margin erosion of coastal surfaces, escarpments, and river valleys, removing 4-7 km of rock at the coast and 1 km inland since rifting. Cool temperate forest and smectite-rich soils, at least at coast.
34 Ma	Initial glaciation of regional uplands with widespread warm-based ice, local radial troughs, and tills. Climate cooling.
34-14 Ma	Local, regional, and continental orbital ice-sheet fluctuations associated with progressive cooling, declining meltwater, and change to tundra vegetation. Local warm-based glaciers in mountains.
~14 Ma	Expansion of maximum Antarctic ice sheet to edge of continental shelf linked to sharp temperature decline of 20-25°C. Change from warm-based to cold-based local mountain glaciers. Selective erosion of continental-scale radial and offshore glacial troughs and meltwater routes.
13.6 Ma to Present	Ice sheet maintains hyperarid polar climate. Slight thickening of ice-sheet margins during Pliocene warming in East Antarctica. Outlet glaciers respond to sea-level change, especially in West Antarctica. Extremely low rates of subaerial weathering. Glacial erosion restricted to outlet glaciers and beneath thick ice.

and erosion surfaces formed and were dissected to varying degrees by fluvial erosion. The degree of dissection increased with the complex geometry and small size of each fragment and was more pronounced near the coast. The interior of East Antarctica was characterized by large river basins, presumably more arid in the interior than at the coast. The climate was sufficiently warm to support beech forests around the coast. Soils contained the clay mineral smectite, derived from the chemical weathering associated with forests.

Around 34 Ma declining atmospheric carbon dioxide and the opening of significant seaways between Antarctica and the southern continents were factors in bringing the two conditions necessary for glaciers: cooling and increased precipitation from circumpolar storms. Glaciation began in a Patagonian-type climate, at least in the Transantarctic Mountains, and was centered on maritime mountains of East and West Antarctica and high continental mountains in East Antarctica. The record from the Cape Roberts cores of fluctuating ice-sheet extent, which is supported by marine oxygen isotope records, points to a dynamic ice sheet responding to orbital fluctuations in the same way as the Pleistocene ice sheets of the Northern Hemisphere. The preexisting regolith was progressively removed from the continent to create a subglacial landscape of areal scouring, probably in a complex series of flows as glacier extent and flow directions oscillated between an interglacial and ice-maximum state. Modeling suggests a wave of erosion was associated with each expansion of ice from the mountain centers. The presence of warm-based local glaciers in the Transantarctic Mountains suggests relatively warm interglacial periods.

The terrestrial record agrees with the marine record in pinpointing a sharp temperature decline associated with the expansion of the Antarctic ice sheet over its continental shelf at ~14 Ma. Perhaps the expansion was triggered by a change in ocean circulation or declining atmospheric carbon dioxide. Perhaps it too could have been related to the internal dynamics of the ice sheet in that earlier glaciations had deposited shoals on the offshore shelf, reduced calving, and allowed the ice to advance to the outer edge, behavior well known in the case of fjord glaciers (Mercer, 1961).

The mid-Miocene maximum ice sheet eroded troughs on a continental-scale, cutting selectively through the mountain rim, deepening the interior parts of the offshore shelf (and subsea basins?) in West Antarctica. Land surfaces covered by thin diverging ice remained essentially unchanged. Perhaps the offshore deepening was such that in cycles of growth and decay the ice could no longer advance to the shelf edge, as demonstrated by the behavior of the Lambert Glacier. Alternatively the change in ocean and atmospheric conditions after the mid-Miocene maximum to a hyperarid polar climate may have deprived the ice sheet of moisture. But after ~13.6 Ma the ice retreated to its present continental lair, at least in East Antarctica, and remained essentially intact. Coastal fjords were filled with shallow marine Miocene sediments. The retreat and subsequent stability of the full ice sheet and its associated polar climate is demonstrated on land by the remarkably low erosion rates in the Transantarctic Mountains as revealed by $^{39}Ar/^{40}Ar$ dating of volcanic ashes and cones, by cosmogenic isotope analysis, and by the preservation of fragile deposits and buried ice (Brook et al., 1995; Ivy-Ochs et al., 1995; Summerfield et al., 1999; Marchant et al., 2002). Offshore the growth and decay of the maximum ice sheet is demonstrated by a widespread unconformity and dating evidence of a retreat of the ice in the Ross Sea area after 13.5 Ma (Anderson, 1999).

The implication of the above is that fluctuations of the Antarctic ice sheet in the Pleistocene are forced by changes in sea level. In East Antarctica the fluctuations are relatively minor. Outlet glaciers thicken and advance seaward in response to a lowering of sea level in the Northern Hemisphere, as demonstrated in the case of the outlets flowing through the Transantarctic Mountains (Denton et al., 1989). Slight thickening occurs in Mac Robertson Land (Mackintosh et al., 2007), but the ice does not extend far offshore (O'Brien et al., 2001; Leventer et al., 2006). In agreement with such a limited expansion, the coastal oases of the Bunger Hills and the Larsemann Hills appear to have remained ice-free during the last glacial cycle (Gore et al., 2001; Hodgson et al., 2001). In West Antarctica the Pleistocene behavior is markedly different. Here ice appears to have extended to the edge of the continental shelf and occupied deep troughs extending ~100 km from the present coast (Bentley and Anderson, 1998; Ó Cofaigh et al., 2005). In this case and following Mercer (1978), one can surmise that the grounded ice streams occupying the topography below sea level between the individual massifs are especially susceptible to sea-level changes.

It is interesting that the ice sheet achieved its present profile in Mac Robertson Land 6000 years ago (Mackintosh et al., 2007). This is the time when global sea level had largely completed its recovery following the final disappearance of the North American ice sheet. The coincidence supports the view that Antarctic ice fluctuations in the Pleistocene are a response to sea-level changes driven primarily by the Northern Hemisphere ice sheets.

WIDER IMPLICATIONS

The thrust of this overview is that information about the evolution of passive continental margins and the processes and forms associated with mid-latitude Northern Hemisphere ice sheets is a useful guide for reconstructing the evolution of the landscape in Antarctica. At present there are insufficient constraints to do more than outline possibilities in a qualitative way. Nonetheless even a preliminary view provides some insights into the debate about the relative importance of fluvial and glacial agents of erosion. Further, there seems ample scope for a focused modeling exercise increasingly founded on quantitative field data.

What is also encouraging about the emerging terrestrial

record of landscape evolution is that the main stages match the records obtained from deep-sea and inshore cores. At present, given the uncertainties associated with each dating technique, it is not possible to be sufficiently precise to establish cause and effect and thus understand better the links between the ocean, atmosphere, and ice sheet in influencing or responding to environmental change.

One important implication arising from this overview is the realization that fragile features in the landscape can be very old, whether they have been protected beneath ice or subject to a hyperarid climate with minimal erosion. It is possible for striations and moraines to survive for millions of years. Thus, it is possible that features such as trimlines with striations and associated moraines may date from glaciation prior to the mid-Miocene. Pleistocene changes in ice elevation may be indicated only by a sparse scatter of boulders. If so, then reconstructions of former Pleistocene ice thicknesses based solely on trimline and striation evidence can be misleading.

It is worth reflecting on the richness of the record of landscape evolution in Victoria Land. At least in part this must be due to ease of access and proximity to the permanent base of McMurdo Sound. If so, there is the prospect of equally rich archives in other parts of Antarctica. The challenge is to develop and explore these further to improve our understanding of landscape evolution and its contribution to the wider sciences.

ACKNOWLEDGMENTS

The authors are indebted to the U.K. Natural Environment Research Council for support. Author D.E.S. is grateful for support from the Division of Polar Programs of the U.S. National Science Foundation, the British Antarctic Survey, the Carnegie Trust for the Universities of Scotland and ACE (Antarctic Climate Evolution) Program. We are most grateful to Peter Barrett, David Elliot, Adrian Hall, and Andrew Mackintosh for their thoughtful and helpful comments on the manuscript.

REFERENCES

Anderson, J. B. 1999. *Antarctic Marine Geology.* Cambridge: Cambridge University Press.

Baroni, C., V. Noti, S. Ciccacci, G. Righini, and M. C. Salvatore. 2005. Fluvial origin of the valley system in northern Victoria Land (Antarctica) from quantitative geomorphic analysis. *Geological Society of America Bulletin* 117:212-228.

Barrett, P. J. 2007. Cenozoic climate and sea level history from glacimarine strata off the Victoria Land coast, Cape Roberts Project, Antarctica. In *Glacial Processes and Products*, eds. M. J. Hambrey, P. Christoffersen, N. F. Glasser, and B. Hubbard. *International Association of Sedimentologists Special Publication* 39:259-287.

Barrett, P. J., M. J. Hambrey, D. M. Harwood, A. R. Pyne, and P.-N. Webb. 1989. Synthesis. In *Antarctic Cenozoic History from CIROS-1 Drillhole, McMurdo Sound,* ed. P. J. Barrett. *DSIR Bulletin* 245:241-251. Wellington: DSIR Publishing.

Beaumont, C., H. Kooi, and S. Willett. 2000. Coupled tectonic-surface process models with applications to rifted margins and collisional orogens. In *Geomorphology and Global Tectonics,* ed. M. A. Summerfield, pp. 29-55. Chichester: Wiley.

Bentley, M. J., and J. B. Anderson. 1998. Glacial and marine evidence for the ice sheet configuration in the Weddell Sea-Antarctic Peninsula region during the Last Glacial Maximum. *Antarctic Science* 10:307-323.

Bishop, P., and G. Goldrick, 2000. Geomorphological evolution of the East Australian continental margin. In *Geomorphology and Global Tectonics,* ed. M. A. Summerfield, pp. 225-254. Chichester: Wiley.

Boulton, G. S. 1996. Theory of glacier erosion, transport and deposition as a consequence of subglacial sediment deformation. *Journal of Glaciology* 42:43-62.

Briner, J. P., G. H. Miller, P. Davis, and R. C. Finkel. 2006. Cosmogenic radionuclides from fjord landscapes support differential erosion by overriding ice sheets *GSA Bulletin* 118:406-420.

Brook, E. J., E. T. Brown, M. D. Kurz, R. P. Ackert, G. M. Raisbeck, and F. Yiou. 1995. Constraints on age, erosion and uplift of Neogene glacial deposits in the Transantarctic Mountains determined from in situ cosmogenic ^{10}Be and ^{26}Al. *Geology* 23:1057-1152.

Cape Roberts Science Team. 2000. Summary of results. In *Studies from Cape Roberts Project: Initial Report on CRP-3, Ross Sea, Antarctica,* eds. P. J. Barrett, M. Sarti, and S. Wise. *Terra Antartica* 7185-203. Siena: *Terra Antarctica* Publication.

Cooper, A., H. Stagg, and E. Geist. 1991. Seismic stratigraphy and structure of Prydz Bay, Antarctica: Implications from ODP Leg 119 drilling. In *Ocean Drilling Program Leg 119 Scientific Results*, eds. J. B. Barron and B. Larsen, pp. 5-25. College Station, TX: Ocean Drilling Program.

Cuffey, K. M., H. Conway, A. M. Gades et al. 2000. Entrainment at cold glacier beds. *Geology* 28:351-354.

De Santis, L., J. B. Anderson, G. Brancolini, and I. Zayatz. 1995. Seismic record of late Oligocene through Miocene glaciation on the central and eastern continental shelf of the Ross Sea. In *Geology and Seismic Stratigraphy of the Antarctic Margin,* eds. A. K. Cooper, P. F. Barker, and G. Brancolini, *Antarctic Research Series* 68:235-260. Washington, D.C.: American Geophysical Union.

DeConto, R. M., and D. Pollard. 2003. Rapid Cenozoic glaciation of Antarctica induced by declining atmospheric CO_2. *Nature* 421:245-249.

Denton, G. H., and D. E. Sugden. 2005. Meltwater features that suggest Miocene ice-sheet overriding of the Transantarctic Mountains in Victoria Land, Antarctica. *Geografiska Annaler* 87A:67-85.

Denton, G. H., J. G. Bockheim, S. C. Wilson, and M. Stuiver. 1989. Late Wisconsin and early Holocene glacial history, inner Ross Embayment, Antarctica. *Quaternary Research* 31:151-182.

Denton, G. H., M. L. Prentice, and L. H. Burckle. 1991. Cainozoic history of the Antarctic Ice Sheet. In *The Geology of Antarctica,* ed. R. J. Tingey, pp. 365-433. Oxford: Clarendon Press.

Denton, G. H., J. G. Bockheim, R. H. Rutford, and B. G. Andersen. 1992. Glacial history of the Ellsworth Mountains, West Antarctica. In *Geology and Palaeontology of the Ellsworth Mountains, West Antarctica,* eds. G. F. Webers, C. Craddock, and J. F. Splettstoesser. *Geological Society of America Memoir* 170:403-442.

Denton, G. H., D. E. Sugden, D. R. Marchant, B. L. Hall, and T. I. Wilch. 1993. East Antarctic Ice Sheet Sensitivity to Pliocene Climatic Change from a Dry Valleys Perspective. *Geografiska Annaler* 75A:155-204.

Drewry, D. J. 1982. Ice flow, bedrock and geothermal studies from radio-echo sounding inland of McMurdo Sound, Antarctica. In *Antarctic Geoscience*, ed. C. Craddock, pp. 977-983. Madison: University of Wisconsin Press.

Dunbar, G. B., T. R. Naish, P. J. Barrett, C. R. Fielding, and R. D. Powell. Forthcoming. Constraining the amplitude of late Oligocene bathymetric changes in western Ross Sea during orbitally-induced oscillations in the East Antarctic Ice Sheet. 1. Implications for glacimarine sequence stratigraphic models. *Palaeogeography, Palaeoclimatology, Palaeoecology*, doi:10.1016/j.palaeo.2007.08.018.

Ehrmann, W. U., M. Setti, and L. Marinoni. 2005. Clay minerals in Cenozoic sediments off Cape Roberts (McMurdo Sound, Antarctica) reveal the palaeoclimatic history, *Palaeogeography, Palaeoclimatology, Palaeoecology* 229:187-211.

Evans, I. S. 1969. The geomorphology and morphometry of glacial and nival areas. In *Water, Earth and* Man, ed. R. J. Chorley, pp. 369-380. London: Methuen.

Evatt, G. W., A. C. Fowler, C. D. Clark, and N. R. J. Hulton. 2006. Subglacial floods beneath ice sheets. *Philosophical Transactions of the Royal Society of London* 364:1769-1794.

Fitzgerald, P. G. 1992. The Transantarctic Mountains of southern Victoria Land: The application of fission track analysis to a rift shoulder uplift. *Tectonics* 11:634-662.

Gore, D. B., E. J. Rhodes, P. C. Augustinius, M. R. Leishman, E. A. Colhoun, and J. Rees-Jones. 2001. Bunger Hills, East Antarctica: Ice free at the Last Glacial Maximum. *Geology* 29:1103-1106.

Hall, B. L., G. H. Denton, D. R. Lux, and J. G. Bockheim. 1993. Late Tertiary Antarctic paleoclimate and ice-sheet dynamics inferred from surficial deposits in Wright Valley. *Geografiska Annaler* 75A:239-267.

Hambrey, M. J., N. F. Glasser, B. C. McKelvey, D. E. Sugden, and D. Fink. 2007. Cenozoic landscape evolution of an East Antarctic oasis (Radok Lake area, northern Prince Charles Mountains), and its implications for the glacial and climatic history of Antarctica. *Quaternary Science Reviews* 26:598-626.

Hodgson, D. A., P. E. Noon, W. Vyverman, C. L. Bryant, D. B. Gore, P. Appleby, M. Gilmour, E. Verleyen, A. Sabbe, V. J. Jones, J. C. Ellis-Evans, and P. B. Wood. 2001. Were the Larsemann Hills ice free through the Last Glacial Maximum? *Antarctic Science* 13:440-454.

Holbourn, A., W. Kuhn, M. Schulz, and H. Erlenkeuser. 2005. Impacts of orbital forcing and atmospheric carbon dioxide on Miocene ice-sheet expansion. *Nature* 438:483-487.

Holmlund, P., and J. O. Näslund. 1994. The glacially sculptured landscape in Dronning Maud Land, Antarctica, formed by wet-based mountain glaciation and not by the present ice sheet. *Boreas* 23:139-148.

Holtedahl, H. 1958. Some remarks on the geomorphology of continental shelves off Norway, Labrador and southeast Alaska. *The Journal of Geology* 66:461-471.

Holtedahl, H. 1967. Notes on the formation of fjords and fjord valleys. *Geografiska Annaler* 49A:188-203.

Horton, R. E. 1945. Erosional development of streams and their drainage basins: Hydrophysical approach to quantitative morphology. *Geological Society of America Bulletin* 56:275-370.

Huber, M., and D. Nof. 2006. The ocean circulation in the Southern Hemisphere and its climatic impacts in the Eocene. *Palaeogeography, Palaeoclimatology, Palaeoecology* 231:9-28.

Ives, J. D. 1966. Block fields, associated weathering forms on mountain tops and the nunatak hypothesis. *Geografiska Annaler* 48A:220-223.

Ivy-Ochs, S., C. Schlüchter, P. W. Kubik, B. Dittrich-Hannen, and J. Beer. 1995. Minimum ^{10}Be exposure ages of early Pliocene for the Table Mountain Plateau and the Sirius Group at Mount Fleming, Dry Valleys, Antarctica. *Geology* 23:1007-1010.

Jamieson, S. S. R., N. R. J. Hulton, D. E. Sugden, A. J. Payne, and J. Taylor. 2005. Cenozoic landscape evolution of the Lambert basin, East Antarctica: The relative role of rivers and ice sheets. *Global and Planetary Change* 45:35-49.

Jamieson, S. S. R., N. R. J. Hulton, and M. Hagdorn. Forthcoming. Modelling landscape evolution under ice sheets. *Geomorphology*, doi:10.1016/j.geomorph.2007.02.047.

Kennett, J. P. 1977. Cenozoic evolution of Antarctic glaciation, the circum-Antarctic Ocean and their impact on global oceanography. *Journal of Geophysical Research* 82:3843-3860.

Kerr, A., and W. D. Hermichen. 1999. Glacial modification of the Shackleton Range, Antarctica. *Terra Antartica* 6:353-360.

Lawver, L. A., and L. M. Gahagan. 2003. Evolution of Cenozoic seaways in the circum-Antarctic region. *Palaeogeography, Palaeoclimatology, Palaeoecology* 198(1-2):11-37.

Lawver, L. A., L. M. Gahagan, and M. F. Coffin. 1992. The development of seaways around Antarctica. *Antarctic Research Series* 56:7-30.

Leventer, A., E. Domack, R. Dunbar, J. Pike, C. Stickley, E. Maddison, S. Brachfeld, P. Manley, and C. McLennen. 2006. Marine sediment record from the East Antarctic margin reveals dynamics of ice sheet recession. *GSA Today* 16(12):4-10.

Lewis, A. R., D. R. Marchant, D. E. Kowalewski, S. L. Baldwin, and L. E. Webb. 2006. The age and origin of the Labyrinth, western Dry valleys, Antarctica: Evidence for extensive middle Miocene subglacial floods and freshwater discharge to the Southern Ocean. *Geology* 34:513-516.

Lewis, A. R., D. R. Marchant, A. C. Ashworth, S. R. Hemming, and M. L. Machlus. 2007. Major middle Miocene global climate change: Evidence from East Antarctica and the Transantarctic Mountains. *Geological Society of America Bulletin* 119(11):1449-1461, doi:10.1130/B26134.

Lidmar-Bergstrom, K. 1982. Pre-Quaternary geomorphological evolution in southern Fennoscandia. *Sveriges, geologiska undersökning C* 785:1-202.

Linton, D. L. 1949. Unglaciated areas in Scandinavia and Great Britain. *Irish Geography* 2:77-79.

Linton, D. L. 1963. The forms of glacial erosion. *Transactions of the Institute of British Geographers* 33:1-28.

Løken, O. H., and D. A. Hodgson. 1971. On the submarine geology along the east coast of Baffin Island. *Canadian Journal of Earth Sciences* 8:185-195.

Lythe, M., D. G. Vaughan, and BEDMAP Consortium. 2001. BEDMAP: A new thickness and subglacial topographic model of Antarctica. *Canadian Journal of Earth Sciences* 106:11335-11352.

Mackintosh, A., D. White, D. Fink, D. B. Gore, J. Pickard, and P. C. Fanning. 2007. Exposure ages from mountain dipsticks in Mac Robertson Land, East Antarctica, indicate little change in ice-sheet thickness since the Last Glacial Maximum. *Geology* 35:551-554.

Marchant, D. R., G. H. Denton, D. E. Sugden, and C. C. Swisher III. 1993. Miocene glacial stratigraphy and landscape evolution of the western Asgard Range, Antarctica. *Geografiska Annaler* 75A:303-330.

Marchant, D. R., A. R. Lewis, W. M. Phillips, E. Moore, R. Souchez, G. H. Denton, and D. E. Sugden. 2002. Formation of patterned ground and sublimation till over Miocene glacier ice, southern Victoria Land, Antarctica. *GSA Bulletin* 114:718-730.

Margerison, H. R., W. M. Phillips, F. M. Stuart, and D. E. Sugden. 2005. Cosmogenic ^{3}He concentrations in ancient flood deposits from the Coombs Hills, northern Dry Valleys, East Antarctica: Interpreting exposure ages and erosion rates. *Earth and Planetary Science Letters* 230:163-175.

Mercer, J. H. 1961. The response of fiord glaciers to changes in the firn limit. *Journal of Glaciology* 3:850-858.

Mercer, J. H. 1978. West Antarctic Ice Sheet and CO_2 greenhouse effect: A threat of disaster. *Nature* 271:321-325.

Naish, T. R. et al. 2001. Orbitally induced oscillations in the East Antarctic ice sheet at the Oligocene/Miocene boundary. *Nature* 413:719-723.

Näslund, J.-O. 2001. Landscape development in western and central Dronning Maud Land, East Antarctica. *Antarctic Science* 13:302-311.

Ó Cofaigh, C., R. D. Larter, J. A. Dowdeswell, C.-D. Hillenbrand, C. J. Pudsey, J. Evans, and P. Morris. 2005. Flow of the West Antarctic Ice Sheet on the continental margin of the Bellingshausen Sea at the Last Glacial Maximum. *Journal of Geophysical Research* 110(B11):103, doi:10.1029/2005JB003619.

O'Brien, P. E., A. K. Cooper, C. Richter et al. 2001. Leg 188 summary: Prydz Bay-Cooperation Sea, Antarctica. *Proceedings of the Ocean Drilling Program, Initial Reports* 188:1-65. College Station, TX: Ocean Drilling Program.

Payne, A. J. 1999. A thermomechanical model of ice flow in West Antarctica. *Climate Dynamics* 15:115-125.

Pekar, S. F., and R. M. DeConto. 2006. High-resolution ice-volume estimates for the early Miocene: Evidence for a dynamic ice sheet in Antarctica. *Palaeogeography, Palaeoclimatology, Palaeoecology* 231:101-109.

Perkins, D. 1984. Subglacial landscape in Antarctica. Unpublished Ph.D. thesis. University of Aberdeen.

Persano, C., F. M. Stuart, P. Bishop, and D. N. Barfod. 2002. Apatite (U-Th)/He age constraints on the development of the Great Escarpment on the southeastern Australian passive margin. *Earth and Planetary Science Letters* 200:79-90.

Prest, V. K. 1970. Quaternary geology of Canada. *Economic Geology Report* 1:676-764.

Priestley, R. E. 1909. Scientific results of the western journey. In *The Heart of the Antarctic*, vol. 2, ed. E. H. Shackleton, pp. 315-333. London: Heinemann.

Raine, J. I., and R. A. Askin. 2001. Terrestrial palynology of Cape Roberts drillhole CRP-3, Victoria Land Basin, Antarctica. *Terra Antartica* 8:389-400.

Reeh, N. 1991. Parameterization of melt rate and surface temperature on the Greenland ice sheet. *Polarforschung* 59(3):113-128.

Shevenell, A. E., J. P. Kennett, and D. W. Lea. 2004. Middle Miocene Southern Ocean cooling and Antarctic cryosphere expansion. *Science* 305:1766-1770.

Smith, A. M., T. Murray, K. W. Nicholls, K. Makinson, G. Aoalgeirsdottir, A. E. Behar, and D. G. Vaughan. 2007. Rapid erosion, drumlin formation, and changing hydrology beneath an Antarctic ice stream. *Geology* 35:127-130.

Sorlien, C. C., B. P. Luyendyk, D. S. Wilson, R. C. Decesari, L. R. Bartel, and J. B. Diebold. 2007. Oligocene development of the West Antarctic Ice Sheet recorded in eastern Ross Sea strata. *Geology* 35:467-470.

Stern, T. A., A. K. Baxter, and P. J. Barrett. 2005. Isostatic rebound due to glacial erosion within the Transantarctic Mountains. *Geology* 33:221-224.

Stickley, C. E., H. Brinkhuis, S. A. Schellenberg, A. Sluijs, U. Rohl, M. Fuller, M. Grauert, M. Huber, J. Warnaar, and G. L. Williams. 2004. Timing and nature of the deepening of the Tasmanian Gateway. *Paleoceanography* PA4027, doi:10.1029/2004PA001022.

Stokes, C. R., and C. D. Clark. 1999. Geomorphological criteria for identifying Pleistocene ice streams. *Annals of Glaciology* 28:67-74.

Strahler, A. N. 1958. Dimensional analysis applied to fluvially eroded landforms. *Bulletin of the Geological Society America* 69:279-300.

Stroeven, A. P., D. Fabel, C. Hättestrand, and J. Harbor. 2002. A relict landscape in the centre of Fennoscandian glaciation: Cosmogenic radionuclide evidence of tors preserved through multiple glacial cycles. *Geomorphology* 44:145-154.

Sugden, D. E. 1977. Reconstruction of the morphology, dynamics and thermal characteristics of the Laurentide ice sheet at its maximum. *Arctic and Alpine Research* 9:21-47.

Sugden, D. E. 1978. Glacial erosion by the Laurentide ice sheet. *Journal of Glaciology* 20:367-392.

Sugden, D. E., and G. H. Denton. 2004. Cenozoic landscape evolution of the Convoy Range to Mackay Glacier area, Transantarctic Mountains: Onshore to offshore synthesis. *GSA Bulletin* 116:840-857.

Sugden, D. E., M. A. Summerfield, G. H. Denton, T. I. Wilch, W. C. McIntosh, D. R. Marchant, and R. H. Rutford. 1999. Landscape development in the Royal Society Range, southern Victoria Land, Antarctica: Stability since the middle Miocene. *Geomorphology* 28:181-200.

Sugden, D. E., G. Balco, S. G. Cowdery, J. O. Stone, and L. C. Sass III. 2005. Selective glacial erosion and weathering zones in the coastal mountains of Marie Byrd Land, Antarctica. *Geomorphology* 67:317-334.

Summerfield, M. A. 2000. Geomorphology and global tectonics: Introduction. In *Geomorphology and Global Tectonics,* ed. M. A. Summerfield, pp. 3-12. Chichester: Wiley.

Summerfield, M. A., D. E. Sugden, G. H. Denton, D. R. Marchant, H. A. P. Cockburn, and F. M. Stuart. 1999. Cosmogenic isotope data support previous evidence of extremely low rates of denudation in the Dry Valleys region, southern Victoria Land. *Geological Society of London Special Publication* 162:255-267.

Taylor, G. 1922. *The Physiography of McMurdo Sound and Granite Harbour Region.* British Antarctic (Terra Nova) Expedition, pp. 1910-1913. London: Harrison.

Taylor, J., M. J. Siegert, A. J. Payne, M. J. Hambrey, P. E. O'Brien, A. K. Cooper, and G. Leitchenkov. 2004. Topographic controls on post-Oligocene changes in ice-sheet dynamics, Prydz Bay region, East Antarctica. *Geology* 32:197-200.

van de Flierdt, T., G. E. Gehrels, S. L. Goldstein, and S. R. Hemming. 2007. Pan-African Age of the Gamburtsev Mountains? In *Antarctica: A Keystone in a Changing World—Online Proceedings for the Tenth International Symposium on Antarctic Earth Sciences,* eds. Cooper, A. K., C. R. Raymond et al., USGS Open-File Report 2007-1047, Extended Abstract 176, http://pubs.usgs.gov/of/2007/1047/.

van der Wateren, F. M., T. J. Dunai, R. T. Van Balen, W. Klas, A. L. L. M. Verbers, S. Passchier, and U. Herpers. 1999. Contrasting Neogene denudation histories of different structural regions in the Transantarctic Mountains rift flank constrained by cosmogenic isotope measurements. *Global and Planetary Change* 23:145-172.

Vaughan, D. G., J. L. Bamber, M. Giovinetto, J. Russell, and A. P. R. Cooper. 1999. Reassessment of net surface mass balance in Antarctica. *Journal of Climate* 12:933-946.

Webb, P.-N. 1994. Paleo-drainage systems of East Antarctica and sediment supply to West Antarctic Rift System basins. *Terra Antartica* 1:457-461.

Webb, P.-N., and J. Wrenn. 1982. Upper Cenozoic biostratigraphy and micropaleontology of Taylor Valley, Antarctica. In *Antarctic Geoscience*, ed. C. Craddock, pp. 117-1122. Madison: University of Wisconsin Press.

Wellner, J. S., A. L. Lowe, S. S. Shipp, and J. B. Anderson. 2001. Distribution of glacial geomorphic features on the Antarctic continental shelf and correlation with substrate: Implications for ice behavior. *Journal of Glaciology* 47:397-411.

Zachos, J. C., J. Breza, and S. W. Wise. 1992. Early Oligocene ice sheet expansion on Antarctica, sedimentological and isotopic evidence from the Kergulen Plateau. *Geology* 20:569-573.

Appendix B: Generic PDD Model

This appendix contains details and Fortran code regarding the implementation of the PDD scheme used in Chapter 5 and in 2 papers (Hebeler et al., In Press; Jamieson and Sugden, 2008).

Introduction to the Generic PDD Scheme

The Generic PDD Scheme is a climate driver module for the GLIMMER ice sheet model. It provides a method of driving GLIMMER by generating accumulation in a time-variable way and ablation of snow using the positive degree day method (PDD). It extends the PPD scheme that is already part of GLIMMER in a number of important respects:

1. Whereas the original PDD scheme enables simple PDD parameter input by way of a section in the configuration file, this new scheme extends this to allow PDD parameters to be input as fields in the initial input netCDF file. Parameters can be mixed and matched to use any combination of spatial or non-spatial input.
2. This scheme reads text files describing shifts in PDD parameters and shifts these parameters through time accordingly. At present only mean air temperature at sea level (sstm) and mean precipitation at sea level (pptm) can be shifted over the course of time.

This documentation outlines the method of installation, describes the interface to the model, and outlines how the calculations are made.

Using the Generic PDD Scheme

Installation

1. Firstly, follow the GLIMMER documentation (Hagdorn et al., 2005) to ensure that GLIMMER is fully installed in a directory that we will refer to as

$GLIMMER_PREFIX. Further, you must ensure that the NetCDF library (Gough et al., 2008) is also installed in a known directory on your system.

2. Download the Gen PDD tar-ball from the GLIMMER site and unpack it to the $GLIMMER PREFIX/src directory thus:

```
tar -xvzf Gen PDD.tar.gz
```

3. The module is then complied using the following set of commands:

```
./configure --prefix=$GLIMMER PREFIX --with-
netcdf=path/to/netcdf/ --with-glimmer-
prefix=path/to/GLIMMER/if/in/non/standard/place

make && make install
```

Note: the with-glimmer-prefix option is only required if GLIMMER is installed to a non-standard place.

2.2 Configuration

In order to use the generic pdd mass-balance scheme, a section headed [Gen pdd climate] (Table 1) must be added to your GLIMMER configuration file. Additionally, a [GLIMMER annual pdd] section can also be specified in order to alter the parameters of the annual PDD scheme interface (Hagdorn et al., 2005). This is used in turn by the Generic PDD mass-balance scheme described in this document. Any of the specified parameters can then be optionally given within that section. If no parameter is specified, then the default values will be used. The sstm and pptm files need only contain shift values for particular times. Shifts for intervening times will be automatically calculated using a linear interpolation. In order to then run the climate driver the config file is passed - in the normal fashion - to the gen pdd glide executable that comes as part of the Generic PDD scheme. For example:

```
echo configuration file.config | path/to/gen pdd
glide
```

[Gen pdd climate]	
Define the initial climate parameters. Mix and match any spatial or uniform parameters. Any temporal shifts will deviate from the original parameters set here.	
global mean precipitation	(real) the mean precipitation for the model domain (myr^{-1}).
global precipitation range	(real) the yearly precipitation range across the domain (myr^{-1}).
global mean sea level temperature	(real) the mean air temperature at sea level (_C).
global sea level temperature range	(real) the yearly air temperature range at sea level (°C).
global lapse rate	(real) the rate at which temperature changes with altitude (°C).
snow threshold	(real) the air temperature at which precipitation will fall as snow (°C).
pptm file name	(string) the name of the space delimited text fie containing time and mean precipitation deviation data.
sstm file name	(string) the name of the space delimited text file containing time and mean sea level temperature deviation data.

Table B1: Config file options for generic PDD scheme.

How the Generic PDD Scheme Works

This module is effectively another layer on top of the Annual PDD scheme included with GLIMMER. The Generic PDD Scheme is used to generate some of the inputs to the Annual PDD scheme - in particular the snow fall. A description of the degree day method is provided in Reeh (1991) and in Chapter 5 of this thesis. The first step carried out by Generic PDD is to use the glimmer ts (TimeSeries) subroutines (as distributed with GLIMMER) to read any input text file containing temporal data describing shifts in mean precipitation or sea surface air temperature. This data is allocated to an array, and linear interpolation is used to calculate specific shifts for each particular model timestep. Next, the air temperature at the surface is calculated using the sea surface temperature value, a lapse rate and if available, the shift value given by the interpolation. This can be used as an input to calculate where snow falls.

The last step is to derive the snowfall pattern for the model timestep. We assume that the climate for the year varies in a sine wave pattern and we can therefore calculate (given we know the threshold temperature at which it snows) the amount of time per time step that precipitation will fall as snow, and the rate at which that snow will fall. The results of these calculations (i.e. snow and air temperature) are used in conjunction with the sea surface temperature range as inputs to the Annual PDD scheme which then returns accumulation and ablation data which is used to drive GLIMMER itself.

Fortran Code

The following pages show the code used in implementing the generic PDD model for GLIMMER.

Gen_pdd_var.def

This file defines the netCDF variables used in the generic PDD scheme.

```
#[]
#dimensions:    time, level, y1, x1
#units:
#long_name:
#data:
#factor:

# setup for code generator
[VARSET]
# prefix of the generated module
name:  gen_pdd_clim
# f90 type containing all necessary data
datatype: gen_pdd_clim_type
# module where type is defined
datamod:  gen_pdd_clim_types

[sstm]
dimensions:    time, y1, x1
units:         degree_Celcius
long_name:     mean equivalent sea-surface temperature
data:          data%sstm
coordinates:   lon lat
load:          1
hot:           1

[sstr]
dimensions:    time, y1, x1
units:         degree_Celcius
long_name:     half-range equivalent sea-surface temperature
data:          data%sstr
coordinates:   lon lat
load:          1
hot:           1

[pptm]
dimensions:    time, y1, x1
units:         meter/year
long_name:     mean annual precipitation
data:          data%pptm
coordinates:   lon lat
load:          1
hot:           1
factor:        scale2d_f1


[pptr]
dimensions:    time, y1, x1
units:         meter/year
long_name:     half-range annual precipitation
data:          data%pptr
coordinates:   lon lat
load:          1
hot:           1
factor:        scale2d_f1

[vert_lapse]
dimensions:    time, y1, x1
units:         degree_Celcius/meter
long_name:     vertical environmental lapse rate
data:          data%vert_lapse
coordinates:   lon lat
load:          1
hot:           1
factor:        1/thk0
```

```
[snow]
dimensions:     time, y1, x1
units:          meter/year
long_name:      annual accumulated snowfall
data:           data%snow
coordinates:    lon lat
factor:         scale2d_f1

[ablt]
dimensions:     time, y1, x1
units:          meter/year
long_name:      annual ice ablation
data:           data%ablt
coordinates:    lon lat
factor:         scale2d_f1

[presusurf]
# Present-day upper surface elevation
dimensions:     time,y1,x1
units:          meter
long_name:      present_surface
data:           data%presusurf
load:           1
```

Gen_pdd_clim_io.F90

Reads and writes data for the model.

```
! +++++++++++++++++++++++++++++++++++++++++++++++++++++++++++++++++
! +                                                               +
! +  ncdf_template.f90 - part of the GLIMMER ice model           +
! +                                                               +
! +++++++++++++++++++++++++++++++++++++++++++++++++++++++++++++++++
!
! Copyright (C) 2007 GLIMMER contributors - see COPYRIGHT file
! for list of contributors.
!
! This program is free software; you can redistribute it and/or
! modify it under the terms of the GNU General Public License as
! published by the Free Software Foundation; either version 2 of
! the License, or (at your option) any later version.
!
! This program is distributed in the hope that it will be useful,
! but WITHOUT ANY WARRANTY; without even the implied warranty of
! MERCHANTABILITY or FITNESS FOR A PARTICULAR PURPOSE. See the
! GNU General Public License for more details.
!
! You should have received a copy of the GNU General Public License
! along with this program; if not, write to the Free Software
! Foundation, Inc., 59 Temple Place, Suite 330, Boston, MA
! 02111-1307 USA
!
! GLIMMER is maintained by:
!
! Ian Rutt
! School of Geographical Sciences
! University of Bristol
! University Road
! Bristol
! BS8 1SS
! UK
!
! email: <i.c.rutt@bristol.ac.uk> or <ian.rutt@physics.org>
!
! GLIMMER is hosted on NeSCForge:
!
! http://forge.nesc.ac.uk/projects/glimmer/
!
! +++++++++++++++++++++++++++++++++++++++++++++++++++++++++++++++++

#define NCO outfile%nc
#define NCI infile%nc


module gen_pdd_clim_io
  !*FD template for creating subsystem specific I/O routines
  !*FD written by Magnus Hagdorn, Nick Hulton and Stewart Jamieson 2004-2007

  character(len=*),private,parameter :: hotvars = ' sstr  pptr  pptm  sstm
vert_lapse '

contains

  !*****************************************************************************
  ! netCDF output
  !*****************************************************************************
  subroutine gen_pdd_clim_io_createall(model,data,outfiles)
    !*FD open all netCDF files for output
    use gen_pdd_clim_types
    use glide_types
    use glimmer_ncdf
    use glimmer_ncio
    implicit none
    type(glide_global_type) :: model
```

```
    type(gen_pdd_clim_type), optional :: data
    type(glimmer_nc_output),optional,pointer :: outfiles

    ! local variables
    type(glimmer_nc_output), pointer :: oc

    if (present(outfiles)) then
       oc => outfiles
    else
       oc=>model%funits%out_first
    end if

    do while(associated(oc))
       if (present(data)) then
          call gen_pdd_clim_io_create(oc,model,data)
       else
          call gen_pdd_clim_io_create(oc,model)
       end if
       oc=>oc%next
    end do
  end subroutine gen_pdd_clim_io_createall

  subroutine gen_pdd_clim_io_writeall(data,model,atend,outfiles,time)
    !*FD if necessary write to netCDF files
    use gen_pdd_clim_types
    use glide_types
    use glimmer_ncdf
    use glimmer_ncio
    implicit none
    type(gen_pdd_clim_type) :: data
    type(glide_global_type) :: model
    logical, optional :: atend
    type(glimmer_nc_output),optional,pointer :: outfiles
    real(sp),optional :: time

    ! local variables
    type(glimmer_nc_output), pointer :: oc
    logical :: forcewrite=.false.

    if (present(outfiles)) then
       oc => outfiles
    else
       oc=>model%funits%out_first
    end if

    if (present(atend)) then
       forcewrite = atend
    end if

    do while(associated(oc))
#ifdef HAVE_AVG
       if (oc%do_averages) then
          call gen_pdd_clim_avg_accumulate(oc,data,model)
       end if
#endif
       call glimmer_nc_checkwrite(oc,model,forcewrite,time)
       if (oc%nc%just_processed) then
          ! write standard variables
          call gen_pdd_clim_io_write(oc,data)
#ifdef HAVE_AVG
          if (oc%do_averages) then
             call gen_pdd_clim_avg_reset(oc,data)
          end if
#endif
       end if
       oc=>oc%next
    end do
  end subroutine gen_pdd_clim_io_writeall

  subroutine gen_pdd_clim_io_create(outfile,model,data)
    use glide_types
    use gen_pdd_clim_types
    use glimmer_ncdf
    use glimmer_map_types
```

```
    use glimmer_log
    implicit none
    type(glimmer_nc_output), pointer :: outfile
    type(glide_global_type) :: model
    type(gen_pdd_clim_type), optional :: data

    integer status,varid,pos

    integer :: time_dimid
    integer :: x1_dimid
    integer :: y1_dimid

    ! defining dimensions
    status = nf90_inq_dimid(NCO%id,'time',time_dimid)
    call nc_errorhandle(__FILE__,__LINE__,status)
    status = nf90_inq_dimid(NCO%id,'x1',x1_dimid)
    call nc_errorhandle(__FILE__,__LINE__,status)
    status = nf90_inq_dimid(NCO%id,'y1',y1_dimid)
    call nc_errorhandle(__FILE__,__LINE__,status)

    NCO%vars = ' '//trim(NCO%vars)//' '
    ! expanding hotstart variables
    pos = index(NCO%vars,' hot ')
    if (pos.ne.0) then
       NCO%vars = NCO%vars(:pos)//NCO%vars(pos+4:)
       NCO%hotstart = .true.
    end if
    if (NCO%hotstart) then
       NCO%vars = trim(NCO%vars)//hotvars
    end if
    ! checking if we need to handle time averages
    pos = index(NCO%vars,"_tavg")
    if (pos.ne.0) then
       outfile%do_averages = .True.
    end if

    !     ablt -- annual ice ablation
    pos = index(NCO%vars,' ablt ')
    status = nf90_inq_varid(NCO%id,'ablt',varid)
    if (pos.ne.0) then
      NCO%vars(pos+1:pos+4) = '    '
    end if
    if (pos.ne.0 .and. status.eq.nf90_enotvar) then
       call write_log('Creating variable ablt')
       status = nf90_def_var(NCO%id,'ablt',NF90_FLOAT,(/x1_dimid, y1_dimid,
time_dimid/),varid)
       call nc_errorhandle(__FILE__,__LINE__,status)
       status = nf90_put_att(NCO%id, varid, 'coordinates', 'lon lat')
       status = nf90_put_att(NCO%id, varid, 'long_name', 'annual ice ablation')
       status = nf90_put_att(NCO%id, varid, 'units', 'meter/year')
       if (glimmap_allocated(model%projection)) then
          status = nf90_put_att(NCO%id, varid, 'grid_mapping',glimmer_nc_mapvarname)
       end if
     end if

    !     pptm -- mean annual precipitation
    pos = index(NCO%vars,' pptm ')
    status = nf90_inq_varid(NCO%id,'pptm',varid)
    if (pos.ne.0) then
      NCO%vars(pos+1:pos+4) = '    '
    end if
    if (pos.ne.0 .and. status.eq.nf90_enotvar) then
       call write_log('Creating variable pptm')
       status = nf90_def_var(NCO%id,'pptm',NF90_FLOAT,(/x1_dimid, y1_dimid,
time_dimid/),varid)
       call nc_errorhandle(__FILE__,__LINE__,status)
       status = nf90_put_att(NCO%id, varid, 'coordinates', 'lon lat')
       status = nf90_put_att(NCO%id, varid, 'long_name', 'mean annual precipitation')
       status = nf90_put_att(NCO%id, varid, 'units', 'meter/year')
       if (glimmap_allocated(model%projection)) then
          status = nf90_put_att(NCO%id, varid, 'grid_mapping',glimmer_nc_mapvarname)
       end if
     end if
```

```
    !     pptr -- half-range annual precipitation
    pos = index(NCO%vars,' pptr ')
    status = nf90_inq_varid(NCO%id,'pptr',varid)
    if (pos.ne.0) then
      NCO%vars(pos+1:pos+4) = '    '
    end if
    if (pos.ne.0 .and. status.eq.nf90_enotvar) then
       call write_log('Creating variable pptr')
       status = nf90_def_var(NCO%id,'pptr',NF90_FLOAT,(/x1_dimid, y1_dimid,
time_dimid/),varid)
       call nc_errorhandle(__FILE__,__LINE__,status)
       status = nf90_put_att(NCO%id, varid, 'coordinates', 'lon lat')
       status = nf90_put_att(NCO%id, varid, 'long_name', 'half-range annual
precipitation')
       status = nf90_put_att(NCO%id, varid, 'units', 'meter/year')
       if (glimmap_allocated(model%projection)) then
          status = nf90_put_att(NCO%id, varid, 'grid_mapping',glimmer_nc_mapvarname)
       end if
     end if

    !     presusurf -- present_surface
    pos = index(NCO%vars,' presusurf ')
    status = nf90_inq_varid(NCO%id,'presusurf',varid)
    if (pos.ne.0) then
      NCO%vars(pos+1:pos+9) = '         '
    end if
    if (pos.ne.0 .and. status.eq.nf90_enotvar) then
       call write_log('Creating variable presusurf')
       status = nf90_def_var(NCO%id,'presusurf',NF90_FLOAT,(/x1_dimid, y1_dimid,
time_dimid/),varid)
       call nc_errorhandle(__FILE__,__LINE__,status)
       status = nf90_put_att(NCO%id, varid, 'long_name', 'present_surface')
       status = nf90_put_att(NCO%id, varid, 'units', 'meter')
       if (glimmap_allocated(model%projection)) then
          status = nf90_put_att(NCO%id, varid, 'grid_mapping',glimmer_nc_mapvarname)
       end if
     end if

    !     snow -- annual accumulated snowfall
    pos = index(NCO%vars,' snow ')
    status = nf90_inq_varid(NCO%id,'snow',varid)
    if (pos.ne.0) then
      NCO%vars(pos+1:pos+4) = '    '
    end if
    if (pos.ne.0 .and. status.eq.nf90_enotvar) then
       call write_log('Creating variable snow')
       status = nf90_def_var(NCO%id,'snow',NF90_FLOAT,(/x1_dimid, y1_dimid,
time_dimid/),varid)
       call nc_errorhandle(__FILE__,__LINE__,status)
       status = nf90_put_att(NCO%id, varid, 'coordinates', 'lon lat')
       status = nf90_put_att(NCO%id, varid, 'long_name', 'annual accumulated
snowfall')
       status = nf90_put_att(NCO%id, varid, 'units', 'meter/year')
       if (glimmap_allocated(model%projection)) then
          status = nf90_put_att(NCO%id, varid, 'grid_mapping',glimmer_nc_mapvarname)
       end if
     end if

    !     sstm -- mean equivalent sea-surface temperature
    pos = index(NCO%vars,' sstm ')
    status = nf90_inq_varid(NCO%id,'sstm',varid)
    if (pos.ne.0) then
      NCO%vars(pos+1:pos+4) = '    '
    end if
    if (pos.ne.0 .and. status.eq.nf90_enotvar) then
       call write_log('Creating variable sstm')
       status = nf90_def_var(NCO%id,'sstm',NF90_FLOAT,(/x1_dimid, y1_dimid,
time_dimid/),varid)
       call nc_errorhandle(__FILE__,__LINE__,status)
       status = nf90_put_att(NCO%id, varid, 'coordinates', 'lon lat')
       status = nf90_put_att(NCO%id, varid, 'long_name', 'mean equivalent sea-surface
temperature')
       status = nf90_put_att(NCO%id, varid, 'units', 'degree_Celcius')
       if (glimmap_allocated(model%projection)) then
```

```
          status = nf90_put_att(NCO%id, varid, 'grid_mapping',glimmer_nc_mapvarname)
        end if
      end if

    !     sstr -- half-range equivalent sea-surface temperature
    pos = index(NCO%vars,' sstr ')
    status = nf90_inq_varid(NCO%id,'sstr',varid)
    if (pos.ne.0) then
      NCO%vars(pos+1:pos+4) = '    '
    end if
    if (pos.ne.0 .and. status.eq.nf90_enotvar) then
       call write_log('Creating variable sstr')
       status = nf90_def_var(NCO%id,'sstr',NF90_FLOAT,(/x1_dimid, y1_dimid,
time_dimid/),varid)
       call nc_errorhandle(__FILE__,__LINE__,status)
       status = nf90_put_att(NCO%id, varid, 'coordinates', 'lon lat')
       status = nf90_put_att(NCO%id, varid, 'long_name', 'half-range equivalent sea-
surface temperature')
       status = nf90_put_att(NCO%id, varid, 'units', 'degree_Celcius')
       if (glimmap_allocated(model%projection)) then
          status = nf90_put_att(NCO%id, varid, 'grid_mapping',glimmer_nc_mapvarname)
       end if
     end if

    !     vert_lapse -- vertical environmental lapse rate
    pos = index(NCO%vars,' vert_lapse ')
    status = nf90_inq_varid(NCO%id,'vert_lapse',varid)
    if (pos.ne.0) then
      NCO%vars(pos+1:pos+10) = '          '
    end if
    if (pos.ne.0 .and. status.eq.nf90_enotvar) then
       call write_log('Creating variable vert_lapse')
       status = nf90_def_var(NCO%id,'vert_lapse',NF90_FLOAT,(/x1_dimid, y1_dimid,
time_dimid/),varid)
       call nc_errorhandle(__FILE__,__LINE__,status)
       status = nf90_put_att(NCO%id, varid, 'coordinates', 'lon lat')
       status = nf90_put_att(NCO%id, varid, 'long_name', 'vertical environmental
lapse rate')
       status = nf90_put_att(NCO%id, varid, 'units', 'degree_Celcius/meter')
       if (glimmap_allocated(model%projection)) then
          status = nf90_put_att(NCO%id, varid, 'grid_mapping',glimmer_nc_mapvarname)
       end if
     end if

  end subroutine gen_pdd_clim_io_create

  subroutine gen_pdd_clim_io_write(outfile,data)
    use gen_pdd_clim_types
    use glimmer_ncdf
    use paramets
    use glimmer_scales
    implicit none
    type(glimmer_nc_output), pointer :: outfile
    !*FD structure containg output netCDF descriptor
    type(gen_pdd_clim_type) :: data
    !*FD the model instance

    ! local variables
    real tavgf
    integer status, varid
    integer up

    tavgf = outfile%total_time
    if (tavgf.ne.0.) then
       tavgf = 1./tavgf
    end if

    ! write variables
    status = nf90_inq_varid(NCO%id,'ablt',varid)
    if (status .eq. nf90_noerr) then
       status = nf90_put_var(NCO%id, varid, &
            (scale2d_f1)*(data%ablt), (/1,1,outfile%timecounter/))
       call nc_errorhandle(__FILE__,__LINE__,status)
    end if
```

```
  status = nf90_inq_varid(NCO%id,'pptm',varid)
  if (status .eq. nf90_noerr) then
     status = nf90_put_var(NCO%id, varid, &
          (scale2d_f1)*(data%pptm*data%delta_pp), (/1,1,outfile%timecounter/))
     call nc_errorhandle(__FILE__,__LINE__,status)
  end if

  status = nf90_inq_varid(NCO%id,'pptr',varid)
  if (status .eq. nf90_noerr) then
     status = nf90_put_var(NCO%id, varid, &
          (scale2d_f1)*(data%pptr), (/1,1,outfile%timecounter/))
     call nc_errorhandle(__FILE__,__LINE__,status)
  end if

  status = nf90_inq_varid(NCO%id,'presusurf',varid)
  if (status .eq. nf90_noerr) then
     status = nf90_put_var(NCO%id, varid, &
          data%presusurf, (/1,1,outfile%timecounter/))
     call nc_errorhandle(__FILE__,__LINE__,status)
  end if

  status = nf90_inq_varid(NCO%id,'snow',varid)
  if (status .eq. nf90_noerr) then
     status = nf90_put_var(NCO%id, varid, &
          (scale2d_f1)*(data%snow), (/1,1,outfile%timecounter/))
     call nc_errorhandle(__FILE__,__LINE__,status)
  end if

  status = nf90_inq_varid(NCO%id,'sstm',varid)
  if (status .eq. nf90_noerr) then
     status = nf90_put_var(NCO%id, varid, &
          (data%sstm+data%delta_temp), (/1,1,outfile%timecounter/))
     call nc_errorhandle(__FILE__,__LINE__,status)
  end if

  status = nf90_inq_varid(NCO%id,'sstr',varid)
  if (status .eq. nf90_noerr) then
     status = nf90_put_var(NCO%id, varid, &
          data%sstr, (/1,1,outfile%timecounter/))
     call nc_errorhandle(__FILE__,__LINE__,status)
  end if

  status = nf90_inq_varid(NCO%id,'vert_lapse',varid)
  if (status .eq. nf90_noerr) then
     status = nf90_put_var(NCO%id, varid, &
          (1/thk0)*(data%vert_lapse), (/1,1,outfile%timecounter/))
     call nc_errorhandle(__FILE__,__LINE__,status)
  end if

end subroutine gen_pdd_clim_io_write

!*****************************************************************************
! netCDF input
!*****************************************************************************
subroutine gen_pdd_clim_io_readall(data,model)
  !*FD read from netCDF file
  use gen_pdd_clim_types
  use glide_types
  use glimmer_ncio
  use glimmer_ncdf
  implicit none
  type(gen_pdd_clim_type) :: data
  type(glide_global_type) :: model

  ! local variables
  type(glimmer_nc_input), pointer :: ic

  ic=>model%funits%in_first
  do while(associated(ic))
     call glimmer_nc_checkread(ic,model)
     if (ic%nc%just_processed) then
        call gen_pdd_clim_io_read(ic,data)
     end if
```

```
    ic=>ic%next
  end do
end subroutine gen_pdd_clim_io_readall

subroutine gen_pdd_clim_io_read(infile,data,scale_vars)
  !*FD read variables from a netCDF file
  use glimmer_log
  use glimmer_ncdf
  use gen_pdd_clim_types
  use paramets
  use glimmer_scales
  implicit none
  type(glimmer_nc_input), pointer :: infile
  !*FD structure containg output netCDF descriptor
  type(gen_pdd_clim_type) :: data
  !*FD the model instance
  logical,optional :: scale_vars
  !*FD Specifies whether fields should be scaled by factors when read in.

  ! local variables
  integer status,varid
  integer up
  logical :: scale=.true.

  ! Deal with optional argument
  if (present(scale_vars)) scale=scale_vars

  ! read variables
  status = nf90_inq_varid(NCI%id,'pptm',varid)
  if (status .eq. nf90_noerr) then
     call write_log('  Loading pptm')
     status = nf90_get_var(NCI%id, varid, &
          data%pptm, (/1,1,infile%current_time/))
     call nc_errorhandle(__FILE__,__LINE__,status)
     if (scale) then
     data%pptm = data%pptm/(scale2d_f1)
     end if
  end if

  status = nf90_inq_varid(NCI%id,'pptr',varid)
  if (status .eq. nf90_noerr) then
     call write_log('  Loading pptr')
     status = nf90_get_var(NCI%id, varid, &
          data%pptr, (/1,1,infile%current_time/))
     call nc_errorhandle(__FILE__,__LINE__,status)
     if (scale) then
     data%pptr = data%pptr/(scale2d_f1)
     end if
  end if

  status = nf90_inq_varid(NCI%id,'presusurf',varid)
  if (status .eq. nf90_noerr) then
     call write_log('  Loading presusurf')
     status = nf90_get_var(NCI%id, varid, &
          data%presusurf, (/1,1,infile%current_time/))
     call nc_errorhandle(__FILE__,__LINE__,status)
  end if

  status = nf90_inq_varid(NCI%id,'sstm',varid)
  if (status .eq. nf90_noerr) then
     call write_log('  Loading sstm')
     status = nf90_get_var(NCI%id, varid, &
          data%sstm, (/1,1,infile%current_time/))
     call nc_errorhandle(__FILE__,__LINE__,status)
  end if

  status = nf90_inq_varid(NCI%id,'sstr',varid)
  if (status .eq. nf90_noerr) then
     call write_log('  Loading sstr')
     status = nf90_get_var(NCI%id, varid, &
          data%sstr, (/1,1,infile%current_time/))
     call nc_errorhandle(__FILE__,__LINE__,status)
  end if
```

```
    status = nf90_inq_varid(NCI%id,'vert_lapse',varid)
    if (status .eq. nf90_noerr) then
       call write_log('  Loading vert_lapse')
       status = nf90_get_var(NCI%id, varid, &
            data%vert_lapse, (/1,1,infile%current_time/))
       call nc_errorhandle(__FILE__,__LINE__,status)
       if (scale) then
       data%vert_lapse = data%vert_lapse/(1/thk0)
       end if
    end if

  end subroutine gen_pdd_clim_io_read

  subroutine gen_pdd_clim_io_checkdim(infile,model,data)
    !*FD check if dimension sizes in file match dims of model
    use glimmer_log
    use glimmer_ncdf
    use glide_types
    use gen_pdd_clim_types
    implicit none
    type(glimmer_nc_input), pointer :: infile
    !*FD structure containg output netCDF descriptor
    type(glide_global_type) :: model
    type(gen_pdd_clim_type), optional :: data

    integer status,dimid,dimsize
    character(len=150) message

    ! check dimensions
  end subroutine gen_pdd_clim_io_checkdim

  !*****************************************************************************
  ! calculating time averages
  !*****************************************************************************
#ifdef HAVE_AVG
  subroutine gen_pdd_clim_avg_accumulate(outfile,data,model)
    use glide_types
    use gen_pdd_clim_types
    use glimmer_ncdf
    implicit none
    type(glimmer_nc_output), pointer :: outfile
    !*FD structure containg output netCDF descriptor
    type(glide_global_type) :: model
    type(gen_pdd_clim_type) :: data

    ! local variables
    real :: factor
    integer status, varid

    ! increase total time
    outfile%total_time = outfile%total_time + model%numerics%tinc
    factor = model%numerics%tinc

  end subroutine gen_pdd_clim_avg_accumulate

  subroutine gen_pdd_clim_avg_reset(outfile,data)
    use gen_pdd_clim_types
    use glimmer_ncdf
    implicit none
    type(glimmer_nc_output), pointer :: outfile
    !*FD structure containg output netCDF descriptor
    type(gen_pdd_clim_type) :: data

    ! local variables
    integer status, varid

    ! reset total time
    outfile%total_time = 0.

  end subroutine gen_pdd_clim_avg_reset
#endif

  !*****************************************************************
  ! lots of accessor subroutines follow
```

```
!*****************************************************************************
subroutine gen_pdd_clim_get_ablt(data,outarray)
  use glimmer_scales
  use paramets
  use gen_pdd_clim_types
  implicit none
  type(gen_pdd_clim_type) :: data
  real, dimension(:,:), intent(out) :: outarray

  outarray = (scale2d_f1)*(data%ablt)
end subroutine gen_pdd_clim_get_ablt

subroutine gen_pdd_clim_set_ablt(data,inarray)
  use glimmer_scales
  use paramets
  use gen_pdd_clim_types
  implicit none
  type(gen_pdd_clim_type) :: data
  real, dimension(:,:), intent(in) :: inarray

  data%ablt = inarray/(scale2d_f1)
end subroutine gen_pdd_clim_set_ablt

subroutine gen_pdd_clim_get_pptm(data,outarray)
  use glimmer_scales
  use paramets
  use gen_pdd_clim_types
  implicit none
  type(gen_pdd_clim_type) :: data
  real, dimension(:,:), intent(out) :: outarray

  outarray = (scale2d_f1)*(data%pptm)
end subroutine gen_pdd_clim_get_pptm

subroutine gen_pdd_clim_set_pptm(data,inarray)
  use glimmer_scales
  use paramets
  use gen_pdd_clim_types
  implicit none
  type(gen_pdd_clim_type) :: data
  real, dimension(:,:), intent(in) :: inarray

  data%pptm = inarray/(scale2d_f1)
end subroutine gen_pdd_clim_set_pptm

subroutine gen_pdd_clim_get_pptr(data,outarray)
  use glimmer_scales
  use paramets
  use gen_pdd_clim_types
  implicit none
  type(gen_pdd_clim_type) :: data
  real, dimension(:,:), intent(out) :: outarray

  outarray = (scale2d_f1)*(data%pptr)
end subroutine gen_pdd_clim_get_pptr

subroutine gen_pdd_clim_set_pptr(data,inarray)
  use glimmer_scales
  use paramets
  use gen_pdd_clim_types
  implicit none
  type(gen_pdd_clim_type) :: data
  real, dimension(:,:), intent(in) :: inarray

  data%pptr = inarray/(scale2d_f1)
end subroutine gen_pdd_clim_set_pptr

subroutine gen_pdd_clim_get_presusurf(data,outarray)
  use glimmer_scales
  use paramets
  use gen_pdd_clim_types
  implicit none
  type(gen_pdd_clim_type) :: data
  real, dimension(:,:), intent(out) :: outarray
```

```
  outarray = data%presusurf
end subroutine gen_pdd_clim_get_presusurf

subroutine gen_pdd_clim_set_presusurf(data,inarray)
  use glimmer_scales
  use paramets
  use gen_pdd_clim_types
  implicit none
  type(gen_pdd_clim_type) :: data
  real, dimension(:,:), intent(in) :: inarray

  data%presusurf = inarray
end subroutine gen_pdd_clim_set_presusurf

subroutine gen_pdd_clim_get_snow(data,outarray)
  use glimmer_scales
  use paramets
  use gen_pdd_clim_types
  implicit none
  type(gen_pdd_clim_type) :: data
  real, dimension(:,:), intent(out) :: outarray

  outarray = (scale2d_f1)*(data%snow)
end subroutine gen_pdd_clim_get_snow

subroutine gen_pdd_clim_set_snow(data,inarray)
  use glimmer_scales
  use paramets
  use gen_pdd_clim_types
  implicit none
  type(gen_pdd_clim_type) :: data
  real, dimension(:,:), intent(in) :: inarray

  data%snow = inarray/(scale2d_f1)
end subroutine gen_pdd_clim_set_snow

subroutine gen_pdd_clim_get_sstm(data,outarray)
  use glimmer_scales
  use paramets
  use gen_pdd_clim_types
  implicit none
  type(gen_pdd_clim_type) :: data
  real, dimension(:,:), intent(out) :: outarray

  outarray = data%sstm
end subroutine gen_pdd_clim_get_sstm

subroutine gen_pdd_clim_set_sstm(data,inarray)
  use glimmer_scales
  use paramets
  use gen_pdd_clim_types
  implicit none
  type(gen_pdd_clim_type) :: data
  real, dimension(:,:), intent(in) :: inarray

  data%sstm = inarray
end subroutine gen_pdd_clim_set_sstm

subroutine gen_pdd_clim_get_sstr(data,outarray)
  use glimmer_scales
  use paramets
  use gen_pdd_clim_types
  implicit none
  type(gen_pdd_clim_type) :: data
  real, dimension(:,:), intent(out) :: outarray

  outarray = data%sstr
end subroutine gen_pdd_clim_get_sstr

subroutine gen_pdd_clim_set_sstr(data,inarray)
  use glimmer_scales
  use paramets
  use gen_pdd_clim_types
```

```
    implicit none
    type(gen_pdd_clim_type) :: data
    real, dimension(:,:), intent(in) :: inarray

    data%sstr = inarray
  end subroutine gen_pdd_clim_set_sstr

  subroutine gen_pdd_clim_get_vert_lapse(data,outarray)
    use glimmer_scales
    use paramets
    use gen_pdd_clim_types
    implicit none
    type(gen_pdd_clim_type) :: data
    real, dimension(:,:), intent(out) :: outarray

    outarray = (1/thk0)*(data%vert_lapse)
  end subroutine gen_pdd_clim_get_vert_lapse

  subroutine gen_pdd_clim_set_vert_lapse(data,inarray)
    use glimmer_scales
    use paramets
    use gen_pdd_clim_types
    implicit none
    type(gen_pdd_clim_type) :: data
    real, dimension(:,:), intent(in) :: inarray

    data%vert_lapse = inarray/(1/thk0)
  end subroutine gen_pdd_clim_set_vert_lapse


end module gen_pdd_clim_io
```

Gen_pdd_clim_setup.F90

Reads the config file.

```
! +++++++++++++++++++++++++++++++++++++++++++++++++++++++++++++++++
! +                                                               +
! +  gen_pdd_clim_setup.f90 - part of the GLIMMER ice model      +
! +                                                               +
! +++++++++++++++++++++++++++++++++++++++++++++++++++++++++++++++++
!
! Copyright (C) 2007 GLIMMER contributors - see COPYRIGHT file
! for list of contributors.
!
! This program is free software; you can redistribute it and/or
! modify it under the terms of the GNU General Public License as
! published by the Free Software Foundation; either version 2 of
! the License, or (at your option) any later version.
!
! This program is distributed in the hope that it will be useful,
! but WITHOUT ANY WARRANTY; without even the implied warranty of
! MERCHANTABILITY or FITNESS FOR A PARTICULAR PURPOSE. See the
! GNU General Public License for more details.
!
! You should have received a copy of the GNU General Public License
! along with this program; if not, write to the Free Software
! Foundation, Inc., 59 Temple Place, Suite 330, Boston, MA
! 02111-1307 USA
!
! GLIMMER is maintained by:
!
! Ian Rutt
! School of Geographical Sciences
! University of Bristol
! University Road
! Bristol
! BS8 1SS
! UK
!
! email: <i.c.rutt@bristol.ac.uk> or <ian.rutt@physics.org>
!
! GLIMMER is hosted on NeSCForge:
!
! http://forge.nesc.ac.uk/projects/glimmer/
!
! +++++++++++++++++++++++++++++++++++++++++++++++++++++++++++++++++

#ifdef HAVE_CONFIG_H
#include <config.inc>
#endif

module gen_pdd_clim_setup
contains
  subroutine iceclim_readconfig(iceland_clim,config)
    !*FD read gen_pdd_clim configuration
    use gen_pdd_clim_types
    use glimmer_config
    implicit none
    type(gen_pdd_clim_type) :: iceland_clim          !*FD structure holding
gen_pdd_clim data
    type(ConfigSection), pointer :: config  !*FD structure holding sections of
configuration file
    ! local variables
    type(ConfigSection), pointer :: section

    call GetSection(config,section,'Gen_pdd_climate')
    if (associated(section)) then
       write(*,*) 'Generic PDD scheme detected...'
       iceland_clim%doiceland_clim = .True.
```

```
       call GetValue(section,'pptt_phase_lag',iceland_clim%pp_tt_phase_lag)
       call GetValue(section,'snow_threshold',iceland_clim%snow_threshold)
       call GetValue(section,'global_lapse_rate',iceland_clim%global_lapse)
       call GetValue(section,'global_mean_precipitation',iceland_clim%global_pptm)
       call GetValue(section,'global_precipitation_range',iceland_clim%global_pptr)
       call GetValue(section,'global_mean_sl_temperature',iceland_clim%global_sstm)
       call GetValue(section,'global_sl_temperature_range',iceland_clim%global_sstr)
       call GetValue(section,'pptm_file_name',iceland_clim%pptm_file)    ! SSRJ
       call GetValue(section,'sstm_file_name',iceland_clim%sstm_file)    ! SSRJ
       iceland_clim%precip_ts = (iceland_clim%pptm_file .ne. '')          ! SSRJ
       iceland_clim%temp_ts = (iceland_clim%sstm_file .ne. '')                    !
SSRJ

    end if
  end subroutine iceclim_readconfig

  subroutine iceclim_printconfig(iceland_clim)
    !*FD print erosion config to log
    use glimmer_log
    use gen_pdd_clim_types
    implicit none
    type(gen_pdd_clim_type) :: iceland_clim          !*FD structure holding
gen_pdd_clim data
    ! local variables
    character(len=100) :: message

    if (iceland_clim%doiceland_clim) then
       call write_log('Gen_pdd_climate')
       call write_log('-------')
       write(message,*) 'Precipiation Temperature phase lag :
',iceland_clim%pp_tt_phase_lag
       call write_log(message)
       write(message,*) 'Snow threshold temperature : ',iceland_clim%snow_threshold
       call write_log(message)
       write(message,*) 'Global Lapse rate set to : ',iceland_clim%global_lapse
       call write_log(message)
       write(message,*) 'pptm_file_name set to : ',iceland_clim%pptm_file
       call write_log(message)
       write(message,*) 'sstm_file_name set to : ',iceland_clim%sstm_file
       call write_log(message)
       write(message,*) 'sstm_file : ',iceland_clim%precip_ts
       call write_log(message)
       write(message,*) 'pptm_file : ',iceland_clim%temp_ts
       call write_log(message)
       call write_log('')
    end if
  end subroutine iceclim_printconfig

end module gen_pdd_clim_setup
```

Gen_pdd_clim_types.F90

Sets up the model structure.

```
! +++++++++++++++++++++++++++++++++++++++++++++++++++++++++++++++++
! +                                                               +
! +  gen_pdd_clim_types.f90 - part of the GLIMMER ice model      +
! +                                                               +
! +++++++++++++++++++++++++++++++++++++++++++++++++++++++++++++++++
!
! Copyright (C) 2007 GLIMMER contributors - see COPYRIGHT file
! for list of contributors.
!
! This program is free software; you can redistribute it and/or
! modify it under the terms of the GNU General Public License as
! published by the Free Software Foundation; either version 2 of
! the License, or (at your option) any later version.
!
! This program is distributed in the hope that it will be useful,
! but WITHOUT ANY WARRANTY; without even the implied warranty of
! MERCHANTABILITY or FITNESS FOR A PARTICULAR PURPOSE. See the
! GNU General Public License for more details.
!
! You should have received a copy of the GNU General Public License
! along with this program; if not, write to the Free Software
! Foundation, Inc., 59 Temple Place, Suite 330, Boston, MA
! 02111-1307 USA
!
! GLIMMER is maintained by:
!
! Ian Rutt
! School of Geographical Sciences
! University of Bristol
! University Road
! Bristol
! BS8 1SS
! UK
!
! email: <i.c.rutt@bristol.ac.uk> or <ian.rutt@physics.org>
!
! GLIMMER is hosted on NeSCForge:
!
! http://forge.nesc.ac.uk/projects/glimmer/
!
! +++++++++++++++++++++++++++++++++++++++++++++++++++++++++++++++++

#ifdef HAVE_CONFIG_H
#include <config.inc>
#endif

module gen_pdd_clim_types
  !*FD type definition for erosion calcluations

  use glimmer_global, only : dp,sp
  use glimmer_pdd
  use glimmer_ts

  type gen_pdd_clim_type
    type(glimmer_pdd_params) :: annual_pdd !*FD Pointer to annual PDD params
    type(glimmer_tseries) :: ppts,ssts ! SSRJ

     logical :: doiceland_clim = .False.                          !*FD set to true
when gen_pdd_climate should be included
     real :: pp_tt_phase_lag = 0.                                    !*FD
phase_difference from temperature to precipitation assuming sinusoidal annual
distribution - assumes input in degrees
     real :: global_lapse = -0.008                                  !*FD use to set
global lapse rate
```

```
      real :: global_sstm = 0.                                    !*FD global mean
sea-level temperature
      real :: global_sstr = 0.                                    !*FD global sea-
level temperature range
      real :: global_pptm = 0.                                    !*FD global mean
precipitation
      real :: global_pptr = 0.                                    !*FD global
precipitation range
      real :: snow_threshold = 1.0                                !*FD temperature
at which precipitation is deemed to be snow
      character(len=50) :: sstm_file = ''
      character(len=50) :: pptm_file = ''
      logical :: precip_ts = .False.
      logical :: temp_ts = .False.
      integer :: numv = 1   ! SSRJ number of columns to be read from ts files.
      real :: delta_pp = 0.
      real :: delta_temp = 0.


      real(kind=sp),dimension(:,:),pointer :: sstm => null()      !*FD mean sea-
level temperature equivalent
      real(kind=sp),dimension(:,:),pointer :: sstr => null()      !*FD half-range
of sea-level temperature equivalent
      real(kind=sp),dimension(:,:),pointer :: pptm => null()      !*FD mean annual
precipiation
      real(kind=sp),dimension(:,:),pointer :: pptr => null()      !*FD half-range
of annual precipitation
      real(kind=sp),dimension(:,:),pointer :: snow => null()      !*FD annual
accumulated snowfall
      real(kind=sp),dimension(:,:),pointer :: ablt => null()      !*FD annual ice
ablation
      real(kind=sp),dimension(:,:),pointer :: vert_lapse => null()  !*FD local
vertical environmental lapse rate
      real(kind=sp),dimension(:,:),pointer :: presusurf => null()   !*FD present
upper surface
      logical,dimension(:,:),pointer :: landsea => null()     !*FD land / sea mask
  end type gen_pdd_clim_type

contains
  subroutine iceclim_allocate(ice_clim,numx,numy)
    !*FD allocate gen_pdd climate data
    implicit none
    type(gen_pdd_clim_type) :: ice_clim     !*FD data structure holding gen_pdd_clim
stuff
    integer, intent(in) :: numx,numy  !*FD size of arrays
    allocate(ice_clim%sstm(numx,numy))
    allocate(ice_clim%sstr(numx,numy))
    allocate(ice_clim%pptm(numx,numy))
    allocate(ice_clim%pptr(numx,numy))
    allocate(ice_clim%snow(numx,numy))
    allocate(ice_clim%ablt(numx,numy))
    allocate(ice_clim%vert_lapse(numx,numy))
    allocate(ice_clim%presusurf(numx,numy))
    allocate(ice_clim%landsea(numx,numy))
  end subroutine iceclim_allocate

  subroutine iceclim_deallocate(ice_clim)
    !*FD free memory used by erosion data structure
    implicit none
    type(gen_pdd_clim_type) :: ice_clim     !*FD data structure holding gen_pdd_clim
stuff
    deallocate(ice_clim%sstm)
    deallocate(ice_clim%sstr)
    deallocate(ice_clim%pptm)
    deallocate(ice_clim%pptr)
    deallocate(ice_clim%snow)
    deallocate(ice_clim%ablt)
    deallocate(ice_clim%vert_lapse)
    deallocate(ice_clim%presusurf)
    !deallocate(ice_clim%landsea)
  end subroutine iceclim_deallocate
end module gen_pdd_clim_types
```

Gen_pdd_climate.F90

Does the climate calculations and talks to the glimmer pdd and ts modules.

```
! +++++++++++++++++++++++++++++++++++++++++++++++++++++++++++++++
! +                                                             +
! +  gen_pdd_climate.f90 - part of the GLIMMER ice model       +
! +                                                             +
! +++++++++++++++++++++++++++++++++++++++++++++++++++++++++++++++
!
! Copyright (C) 2007 GLIMMER contributors - see COPYRIGHT file
! for list of contributors.
!
! This program is free software; you can redistribute it and/or
! modify it under the terms of the GNU General Public License as
! published by the Free Software Foundation; either version 2 of
! the License, or (at your option) any later version.
!
! This program is distributed in the hope that it will be useful,
! but WITHOUT ANY WARRANTY; without even the implied warranty of
! MERCHANTABILITY or FITNESS FOR A PARTICULAR PURPOSE. See the
! GNU General Public License for more details.
!
! You should have received a copy of the GNU General Public License
! along with this program; if not, write to the Free Software
! Foundation, Inc., 59 Temple Place, Suite 330, Boston, MA
! 02111-1307 USA
!
! GLIMMER is maintained by:
!
! Ian Rutt
! School of Geographical Sciences
! University of Bristol
! University Road
! Bristol
! BS8 1SS
! UK
!
! email: <i.c.rutt@bristol.ac.uk> or <ian.rutt@physics.org>
!
! GLIMMER is hosted on NeSCForge:
!
! http://forge.nesc.ac.uk/projects/glimmer/
!
! +++++++++++++++++++++++++++++++++++++++++++++++++++++++++++++++

#ifdef HAVE_CONFIG_H
#include <config.inc>
#endif

module gen_pdd_climate
  !*FD the main gen_pdd_climate module
  use gen_pdd_clim_types
  use gen_pdd_clim_setup
  use gen_pdd_clim_io


contains
  subroutine iceclim_initialise(ice_clim,config,model)
    !*FD initialise gen_pdd_climate model
    use glide_types
    use glimmer_config
    use paramets, only : len0,thk0
    use physcon, only : pi
    use glimmer_scales

    implicit none
```

```
    type(gen_pdd_clim_type) :: ice_clim     !*FD structure holding gen_pdd climate
data
    type(ConfigSection), pointer :: config !*FD structure holding sections of
configuration file
    type(glide_global_type) :: model       !*FD model instance

    integer i
    call glimmer_pdd_init(ice_clim%annual_pdd,config)


    ! read config for gen_pdd climate data
    call iceclim_readconfig(ice_clim,config)
    ! print config
    call iceclim_printconfig(ice_clim)
    ! create gen_pdd_climate variables
    call gen_pdd_clim_io_createall(model)
    ice_clim%pp_tt_phase_lag=ice_clim%pp_tt_phase_lag*pi/180   ! convert input phase
lag in degrees to radians
    ice_clim%global_lapse=ice_clim%global_lapse*thk0
    ice_clim%global_pptm=ice_clim%global_pptm/scale2d_f1
    ice_clim%global_pptr=ice_clim%global_pptr/scale2d_f1

    ! scale variables

    ! allocate memory
    call iceclim_allocate(ice_clim,model%general%ewn,model%general%nsn)
    ! initialise vertical lapse rate 2D field as read or default global value

    ice_clim%vert_lapse = ice_clim%global_lapse
    ice_clim%sstm = ice_clim%global_sstm
    ice_clim%sstr = ice_clim%global_sstr
    ice_clim%pptm = ice_clim%global_pptm
    ice_clim%pptr = ice_clim%global_pptr

    call gen_pdd_clim_io_readall(ice_clim,model)
    write(*,*) 'The following files were detected: '
    write(*,*) ice_clim%sstm_file
    write(*,*) ice_clim%pptm_file


    if (ice_clim%pptm_file .ne. '')  then    ! SSRJ
      call glimmer_read_ts(ice_clim%ppts,ice_clim%pptm_file,ice_clim%numv)
      write(*,*) 'precipitation timeseries read'
    end if

    if (ice_clim%sstm_file .ne. '') then
      call glimmer_read_ts(ice_clim%ssts,ice_clim%sstm_file,ice_clim%numv)
      write(*,*) 'temperature timeseries read'
    end if

  end subroutine iceclim_initialise

  subroutine iceclim_tstep(ice_clim,model,time)
    !*FD calculate mass balance for this time step
    !*Based on current surface topography so feedback to ice surface topog

    use glide_types
    use glimmer_scales
    use paramets, only : thk0
    implicit none
    type(gen_pdd_clim_type) :: ice_clim          !*FD structure holding
gen_pdd_climate data
    type(glide_global_type) :: model       !*FD model instance
    real(kind=rk) time

    ! local variables
    integer ew,ns
    real delta_pp,delta_temp,local_time
    local_time = time



    if (ice_clim%doiceland_clim) then
```

```
        !where (ice_clim%presusurf>0.0)
           ice_clim%landsea=.true.
        !elsewhere
           !ice_clim%landsea=.false.
        !end where

        if (.not. ice_clim%precip_ts) then
         ice_clim%delta_pp = 0.
        else
         call glimmer_ts_linear_scalar(ice_clim%ppts,local_time,delta_pp)
         ice_clim%delta_pp = delta_pp!/scale2d_f1
        end if

        if (.not. ice_clim%temp_ts) then
         ice_clim%delta_temp = 0.
        else
         call glimmer_ts_linear_scalar(ice_clim%ssts,local_time,delta_temp)
         !write(*,*) 'timeseries interpolated'
         ice_clim%delta_temp = delta_temp
         !write(*,*) 'timeseries assigned'
        end if

        !write(*,*) local_time,ice_clim%delta_pp,ice_clim%delta_temp

        call
surf_temps(ice_clim%sstm,ice_clim%vert_lapse,model%geometry%usrf,model%climate%artm,i
ce_clim%delta_temp)
        call snow_calc(ice_clim,model,ice_clim%delta_pp)


        call
glimmer_pdd_mbal(ice_clim%annual_pdd,model%climate%artm,ice_clim%sstr,ice_clim%snow,&
                 ice_clim%ablt,model%climate%acab,ice_clim%landsea)

        !put in a check to stop any melt below temperatures where its unlikely to get
melt.
        !do ew=1,model%general%ewn
        !  do ns=1,model%general%nsn
          !  if (model%climate%acab(ew,ns) < 0 .and. (model%climate%artm(ew,ns) -
ice_clim%global_sstr) < 0) then
          !    model%climate%acab(ew,ns) = 0
          !  end if
          !end do
        !end do

        !!do ew=1,model%general%ewn
          !!do ns=1,model%general%nsn
           !If we are at sea level then make sure that ablation can only reach a
certain amount. Ablation in this case is climatic and also calving.
            !!if ((model%climate%acab(ew,ns) < -10.0 / scale2d_f1 ) .and.
(model%geometry%usrf(ew,ns) <= 0)) then
              !!model%climate%acab(ew,ns) = -10.0 / scale2d_f1
            !!end if
          !!end do
        !!end do


    end if
    call gen_pdd_clim_io_writeall(ice_clim,model)
    !write(*,*) 'writing to netcdf...'


  end subroutine iceclim_tstep


  subroutine surf_temps(sstm,lapse,elev,surf,delta_temp)
    implicit none
    real, dimension(:,:), intent(in) :: sstm !*FD mean  sea surface equivalent
temperature
    real, dimension(:,:), intent(in) :: lapse !*FD vertical env. laspe rate
    real(dp), dimension(:,:), intent(in) :: elev !*FD surface elevation
    real, dimension(:,:), intent(out) :: surf !*FD surface temperatures
    real delta_temp
```

```
    surf=sstm+(lapse*elev)+delta_temp

  end subroutine surf_temps

  subroutine snow_calc(ice_clim,model,delta_pp)
    use physcon, only : pi
    use paramets, only : thk0
    use glimmer_scales
    use glide_types
    implicit none

    !real, dimension(:,:), intent(out) :: surf !*FD surface temperatures

    type(gen_pdd_clim_type) :: ice_clim     !*FD structure holding gen_pdd climate
data
    type(glide_global_type) :: model  !*FD model instance
    real delta_pp

    !local variables
    integer ew,ns
    real theta,t1,t2,p1,p2,pi2,snowsum,one_o_pi2

    !some angle constants
    pi2=2*pi
    p1=pi+ice_clim%pp_tt_phase_lag
    p2=pi2+ice_clim%pp_tt_phase_lag
    one_o_pi2=1./pi2

    !! just dummy for now
    !ice_clim%snow=ice_clim%pptm

    !solve for point in year when snow threshold temperature is crossed

    do ew=1,model%general%ewn
       do ns=1,model%general%nsn
          if (model%climate%artm(ew,ns)-ice_clim%sstr(ew,ns) >=
ice_clim%snow_threshold) then
             ice_clim%snow(ew,ns)=0
          else if (model%climate%artm(ew,ns)+ice_clim%sstr(ew,ns) <=
ice_clim%snow_threshold) then
             ice_clim%snow(ew,ns)=ice_clim%pptm(ew,ns)*delta_pp
          else
             !calculate number of times per year (t1,t2) when snow threshold is
crossed in angles
             theta=asin((ice_clim%snow_threshold-
model%climate%artm(ew,ns))/ice_clim%sstr(ew,ns))
             t1=p1-theta
             t2=p2+theta
             !calculate snow integral in metres*theta
             snowsum=(ice_clim%pptr(ew,ns)*(cos(t1)-cos(t2)))+((t2-
t1)*(ice_clim%pptm(ew,ns)*delta_pp))
             !convert to pp unit (metre) * years
             ice_clim%snow(ew,ns)=snowsum*one_o_pi2

          end if
          if (ice_clim%snow(ew,ns) < 0.) then
                ice_clim%snow(ew,ns) = 0.
          end if
       end do
    end do

  end subroutine snow_calc

 subroutine iceclim_finalise(ice_clim)
    !*FD finalise erosion model
    implicit none
    type(gen_pdd_clim_type) :: ice_clim          !*FD structure holding
gen_pdd_climate data
    call iceclim_deallocate(ice_clim)
  end subroutine iceclim_finalise

end module gen_pdd_climate
```

Gen_pdd_glide.F90

This file is executed to run the generic PDD scheme.

```
! +++++++++++++++++++++++++++++++++++++++++++++++++++++++++++++++
! +                                                             +
! +  gen_pdd_glide.f90 - part of the GLIMMER ice model         +
! +                                                             +
! +++++++++++++++++++++++++++++++++++++++++++++++++++++++++++++++
!
! Copyright (C) 2007 GLIMMER contributors - see COPYRIGHT file
! for list of contributors.
!
! This program is free software; you can redistribute it and/or
! modify it under the terms of the GNU General Public License as
! published by the Free Software Foundation; either version 2 of
! the License, or (at your option) any later version.
!
! This program is distributed in the hope that it will be useful,
! but WITHOUT ANY WARRANTY; without even the implied warranty of
! MERCHANTABILITY or FITNESS FOR A PARTICULAR PURPOSE. See the
! GNU General Public License for more details.
!
! You should have received a copy of the GNU General Public License
! along with this program; if not, write to the Free Software
! Foundation, Inc., 59 Temple Place, Suite 330, Boston, MA
! 02111-1307 USA
!
! GLIMMER is maintained by:
!
! Ian Rutt
! School of Geographical Sciences
! University of Bristol
! University Road
! Bristol
! BS8 1SS
! UK
!
! email: <i.c.rutt@bristol.ac.uk> or <ian.rutt@physics.org>
!
! GLIMMER is hosted on NeSCForge:
!
! http://forge.nesc.ac.uk/projects/glimmer/
!
! +++++++++++++++++++++++++++++++++++++++++++++++++++++++++++++++

#ifdef HAVE_CONFIG_H
#include <config.inc>
#endif

program gen_pdd_glide
  !*FD This is a driver to implement gen_pdd type climates
  !*FD for glide.   It uses some of the glint Degree Day routines
  use glimmer_global, only:rk
  use glide
  use glimmer_log
  use glimmer_config
  use gen_pdd_climate
  use erosion
  use paramets
  implicit none

  type(glide_global_type) :: model        ! model instance
  type(gen_pdd_clim_type) :: iceland_clim         ! erosion
  type(ConfigSection), pointer :: config  ! configuration stuff
  type(erosion_type) :: er
  character(len=50) :: fname    ! name of paramter file
  real(kind=rk) time
```

```
  integer below_sl, ew, ns, ew_sl, ns_sl


  write(*,*) 'Welcome to the custom pdd and erosion glide driver'
  write(*,*) 'Enter name of GLIDE configuration file to be read'
  read(*,*) fname

  ! start logging
  call open_log(unit=50)

  ! read configuration
  call ConfigRead(fname,config)


  ! initialise GLIDE
  call glide_config(model,config)

  call glide_initialise(model)


  call iceclim_initialise(iceland_clim,config,model)
  ! initialise gen_pdd climate
  call er_initialise(er,config,model)

  ! fill dimension variables
  call glide_nc_fillall(model)

  time = model%numerics%tstart

  do while(time.le.model%numerics%tend)

     call  iceclim_tstep(iceland_clim,model,time)

     ! alter any topg that is below zero where snow is greater than zero so
     ! that topg is no longer below zero.
     ! do this in a search radius type way so that only small areas get filled in...
     !if (time == model%numerics%tstart) then
      !!do ew=3,model%general%ewn-3
       !!do ns=3,model%general%nsn-3
                  ! if 40 % of cells in a search radius of 5 cells are below sl, then
raise them to sl + 0.1m
                  !!below_sl = 0
                  !have to look at each cell one at a time...
                  !!do ew_sl= -3,3,1
                     !!do ns_sl = -3,3,1
                         !!if ((model%geometry%usrf(ew+ew_sl,ns+ns_sl) < (0.1/thk0))
.and. &
                         !!(iceland_clim%snow(ew+ew_sl,ns+ns_sl) > 0.0) .and.
model%geometry%thck(ew+ew_sl,ns+ns_sl) > 0. &
                          !!.and. model%geometry%thck(ew,ns) == 0.) then
                             !!below_sl = below_sl + 1
                  !!end if
              !!end do
           !!end do
           !!if (below_sl >= 5) then
              !!model%geometry%topg(ew,ns) = 0.1/thk0
              !!model%geometry%usrf(ew,ns) = 0.1/thk0
              !!model%geometry%thck(ew,ns) = model%geometry%thck(ew,ns) +
model%geometry%usrf(ew,ns)
           !!end if
       !!end do
      !!end do
     !end if


     call glide_tstep_p1(model,time)
     call glide_tstep_p2(model)
     call er_tstep(er,model)
     call glide_tstep_p3(model)
     ! override masking stuff for now
     time = time + model%numerics%tinc
     !write(*,*) time
  end do
```

```
  ! finalise GLIDE
  call er_finalise(er)
  call iceclim_finalise(iceland_clim)
  call glide_finalise(model)
end program gen_pdd_glide
```

Appendix C: Scripts used to handle and generate topographies

This appendix contains scripts written in Python and AML (Arc Macro Language – for ArcGIS workstation) which were used to generate the synthetic topographies used in this thesis. In addition, the script developed to provide conversion between ArcGIS ASCII data and netCDF input data is also attached. Details are included in comments at the beginning of each script.

a2c.py

This file handles conversion from ESRIs ArcGIS ASCII format to netCDF format. It also handles projections.

```
#! /usr/bin/env python

# Stewart Jamieson (Stewart.Jamieson@ed.ac.uk) and Magnus Hagdorn, 2005 - University
of Edinburgh.
# This script reads ascii spatial data files (e.g. created in ArcGIS) and outputs a
netCDF file.

import sys, getopt,Numeric, PyCF, datetime, string, PyCF.CF_proj

def usage():
    "print short help message"

    print 'Usage: a2c.py [OPTIONS] infile outfile'
    print 'Converts ArcInfo/ArcMap ascii files to netCDF format.'
    print 'infile = input ascii file e.g. input.asc'
    print 'outfile = output netCDF file e.g. output.nc'
    print ''
    print '  -h, --help\n\tthis message'
    print '  -p, --projection\n\tname of projection file'
    print '  -e, --extras\n\tname of text file containing space delimited list
of\n\textra variables, associated ascii filenames,\n\tconversion (multiplication)
factor and a nodata alternative.\n\tyou must always give a conversion factor\n\t-
just use 1 if you do not wish to convert.'
    print '  -v, --variable\n\talternative name for input variable [default topg]'
    print '  -n, --nodata\n\tthe value you wish any NODATA value to become'
    print '  -c, --conversion\n\ta multiplication factor should you need to scale the
default variable data'
    print '  -s, --shift\n\ta shift factor to increase or decrease the default
variable'
    print '  -a, --add\n\tadd an extra variable that has a constant value [e.g.
varname/value]'
    print '  --title\n\ttitle for output netCDF file'
    print '  --institution\n\tname of institution'
    print '  --references\n\tsome references'
    print '  --comment\n\tcomment'

# get options
try:
    opts, args =
getopt.getopt(sys.argv[1:],'hp:e:v:n:c:s:a:',['help','projection=','extras=','variabl
e=','nodata=','conversion=','shift=','add=','title=','institution=','references=','co
mment='])
except getopt.GetoptError,error:
        # print usage and exit
        print error
        usage()
        sys.exit(1)

if len(args) == 2:
        inFile = args[0]
        outFile = args[1]
else:
        usage()
        sys.exit(1)


title='Ascii Topo'
institution=None
references=None
comment=None
proj = None
```

```
upper = None
source=None
inProjFile=None
extraFile=None
variable='topg'
varname='var'+ variable
origin = None
delta = None
num = None
coversion_factor = 1.0
conv_factor = 1.0
nodata_val = 1
shift = 0.0
add = None
for o,a in opts:
    if o in ('-h', '--help'):
        usage()
        sys.exit(0)
    if o in ('-p', '--projection'):
        inProjFile = a
    if o in ('-e','--extras'):
        extraFile = a
    if o in ('-v','--variable'):
        variable = a
        varname = 'var' + variable
    if o in ('-n','--nodata'):
        nodata_val = a
    if o in ('-c','--conversion'):
        conv_factor = a
    if o in ('-s','--shift'):
        shift = float(a)
    if o in ('-a','--add'):
        a = a.split('/')
        try:
          add = [a[0],a[1]]
        except:
          print 'Error, cannot parse num string'
          usage()
          sys.exit(1)
    if o == '--title':
        title = a
    if o == '--institution':
        institution = a
    if o == '--references':
        references = a
    if o == '--comment':
        comment  = a


f=open(inFile, 'r')

#read first few lines to get metadata
numx=f.readline()
numx=int(numx[string.rfind(numx,' '):])

numy=f.readline()
numy=int(numy[string.rfind(numy,' '):])

xll=f.readline()
xll=float(xll[string.rfind(xll,' '):])

yll=f.readline()
yll=float(yll[string.rfind(yll,' '):])

res=f.readline()
res=float(res[string.rfind(res,' '):])

nd=f.readline()
nd=float(nd[string.rfind(nd,' '):])

def DmsParse(pFile):
       # This parses a string from the projection file
       l = string.split(pFile.readline())
       deg = float(l[0])
```

```
        min = float(l[1])/60
        sec = float(l[2])/3600
        dms=(deg)+(min)+(sec)
        return dms


# Deal with projection information

if inProjFile == None:
  proj = None
else:
  print 'Parsing projection...'
  pFile=open(inProjFile, 'r')
  pName = pFile.readline()
  pName=pName[14:]

  pStrip = string.strip(pName)
  print pStrip
  proj = PyCF.CF_proj.DummyProj()

  if pStrip == 'ALBERS':
      proj.grid_mapping_name='albers_conical_equal_area'
      line = pFile.readline()
      while line != '':
          line = pFile.readline()
          if string.strip(line) == 'Parameters':
                  standard1=DmsParse(pFile)
                  standard2=DmsParse(pFile)
                  proj.standard_parallel = [standard1,standard2]
                  long_central=DmsParse(pFile)
                  if long_central < 0:
                          long_central = 360+long_central
                          proj.longitude_of_central_meridian = [long_central]
                  else:
                          proj.longitude_of_central_meridian = [long_central]
                  lat_proj_origin=DmsParse(pFile)
                  proj.latitude_of_projection_origin = [lat_proj_origin]
                  east=pFile.readline()
                  east=string.strip(east)
                  east_index = string.index( east, ' /* false easting (meters)', 0,
100)
                  east=east[:east_index]
                  proj.false_easting=string.atof(east)
                  north=pFile.readline()
                   north=string.strip(north)
                  north_index = string.index( north, ' /* false northing (meters)', 0,
100)
                  north=north[:north_index]
                  proj.false_northing=string.atof(north)


    elif pStrip == 'LAMBERT':
        proj.grid_mapping_name='lambert_conformal_conic'
        line = pFile.readline()
        while line != '':
            line = pFile.readline()
            if string.strip(line) == 'Parameters':
                    standard1=DmsParse(pFile)
                    standard2=DmsParse(pFile)
                    proj.standard_parallel = [standard1,standard2]
                    long_central=DmsParse(pFile)
                    if long_central < 0:
                            long_central = 360+long_central
                            proj.longitude_of_central_meridian = [long_central]
                    else:
                            proj.longitude_of_central_meridian = [long_central]
                    lat_proj_origin=DmsParse(pFile)
                    proj.latitude_of_projection_origin = [lat_proj_origin]
                    east=pFile.readline()
                    east=string.strip(east)
                    east_index = string.index( east, ' /* false easting (meters)', 0,
100)
                    east=east[:east_index]
                    proj.false_easting=string.atof(east)
```

```
                north=pFile.readline()
                 north=string.strip(north)
                north_index = string.index( north, ' /* false northing (meters)', 0,
100)
                north=north[:north_index]
                proj.false_northing=string.atof(north)


  elif pStrip == 'LAMBERT_AZIMUTHAL':
      proj.grid_mapping_name='lambert_azimuthal_equal_area'
      line = pFile.readline()
      while line != '':
          line = pFile.readline()
          if line != '':
               first = string.split(line)
               if first[0] == 'Parameters':
                       skip = pFile.readline() #skip a line as data not required
                       long_central=DmsParse(pFile)
                       if long_central < 0:
                               long_central = 360+long_central
                               proj.longitude_of_central_meridian = [long_central]
                       else:
                               proj.longitude_of_central_meridian = [long_central]
                       lat_proj_origin=DmsParse(pFile)
                       proj.latitude_of_projection_origin = [lat_proj_origin]
                       east=pFile.readline()
                       east=string.strip(east)
                       east_index = string.index( east, ' /* false easting (meters)',
0, 100)
                       east=east[:east_index]
                       proj.false_easting=string.atof(east)
                       north=pFile.readline()
                       north=string.strip(north)
                       north_index = string.index( north, ' /* false northing
(meters)', 0, 100)
                       north=north[:north_index]
                       proj.false_northing=string.atof(north)


  # Due to inconsistencies between ESRI projection files and the parameters required
by CFProj, the stereographic
  # projections may produce incorrect results so CHECK them carefully!.
  elif pStrip == 'STEREOGRAPHIC':

      line = pFile.readline()
      while line != '':
          line = pFile.readline()
          if line != '':
            first = string.split(line)
            if first[0] == 'Parameters':

              l = string.split(pFile.readline())
              type = l[0]
              if type == '2':
                  flag = 0
                  if flag == 0:
                       long_central=DmsParse(pFile)
                       lat_proj_origin=DmsParse(pFile)
                       proj.latitude_of_projection_origin = [lat_proj_origin]
                       pol_v_eq = string.split(pFile.readline()) # get whether a polar
or equatorial view.
                       pol_v_eq = pol_v_eq[0]
                       proj.false_easting=0
                       proj.false_northing=0
                       flag = 1

                  if flag == 1:
                       if pol_v_eq == 'EQUATORIAL':
                               proj.grid_mapping_name='stereographic' # type 2
stereographic projection with equatorial
                               proj.longitude_of_central_meridian = [long_central] #
long of cent projection
                               l = string.split(pFile.readline())
```

```
                                scale_factor=l[0]
                                proj.scale_factor_at_projection_origin = [scale_factor]
# scale factor
                        else:
                                proj.grid_mapping_name='polar_stereographic' # type 2
stereographic projection with north or southpole
                                proj.straight_vertical_longitude_from_pole =
[long_central]
                                #l = string.split(pFile.readline())
                                #lat_std_par = int(float(l[0]))
                                lat_std_par = DmsParse(pFile)
                                proj.standard_parallel = [lat_std_par] # lat of
standard parallel


                elif type == '1':
                    proj.grid_mapping_name='stereographic'
                    line=pFile.readline()
                    long_central=DmsParse(pFile)
                    proj.longitude_of_central_meridian = [long_central]
                    lat_proj_origin=DmsParse(pFile)
                    proj.latitude_of_projection_origin = [lat_proj_origin]
                    scale_factor=1. #defaults to 1 as Arc projection files do not
include scale factors
                    proj.scale_factor_at_projection_origin = [scale_factor]

                    east=pFile.readline()
                   east=string.strip(east)
                   east_index = string.index( east, ' /* false easting (meters)', 0,
100)
                   east=east[:east_index]
                   proj.false_easting=string.atof(east)
                   north=pFile.readline()
                   north=string.strip(north)
                   north_index = string.index( north, ' /* false northing (meters)', 0,
100)
                   north=north[:north_index]
                   proj.false_northing=string.atof(north)

                    #false_easting=string.split(string.strip(pFile.readline()))
                    #false_easting=false_easting[0]
                    #proj.false_easting=0
                    #false_northing=string.split(string.strip(pFile.readline()))
                    #false_northing=false_northing[0]
                    #proj.false_northing=0

  else:
      print 'Projection ',pStrip,' not recognized'
      print 'This program will only recognise albers equal area, lambert, lambert
azimuthal and stereographic projections.'
      sys.exit(1)


origin = [float(xll),float(yll)]
delta = [float(res),float(res)]

print 'creating output netCDF file...'
cffile = PyCF.CFcreatefile(outFile)
# global attributes
if title is not None:
    cffile.title = title
if institution is not None:
    cffile.institution = institution
if source  is not None:
    cffile.source = source
args = ''
for a in sys.argv:
    args = args + '%s '%a
cffile.history = '%s: %s'%(datetime.datetime.today(),args)
if references  is not None:
    cffile.references=references
if comment is not None:
    cffile.comment = comment
```

```
# creating dimensions
cffile.createDimension('x0',numx-1)
cffile.createDimension('x1',numx)
cffile.createDimension('y0',numy-1)
cffile.createDimension('y1',numy)
cffile.createDimension('level',1)
cffile.createDimension('time',None)
# creating variables
varx=cffile.createVariable('x0')
varx[:] = ((delta[0]*Numeric.arange(numx-
1)+(delta[0]/2))+origin[0]).astype(Numeric.Float32)
#varx[:] = (delta[0]*Numeric.arange(numx-1)).astype(Numeric.Float32)
varx=cffile.createVariable('x1')
varx[:] = ((delta[0]*Numeric.arange(numx))+origin[0]).astype(Numeric.Float32)
varlist=['varx'] #store information about which variables have already been created

vary=cffile.createVariable('y0')
vary[:] = ((delta[1]*Numeric.arange(numy-
1)+(delta[1]/2))+origin[1]).astype(Numeric.Float32)
#vary[:] = (delta[1]*Numeric.arange(numy-1)).astype(Numeric.Float32)
vary=cffile.createVariable('y1')
vary[:] = ((delta[1]*Numeric.arange(numy))+origin[1]).astype(Numeric.Float32)
varlist.append('vary')

varlevel=cffile.createVariable('level')
varlevel[0] = 1
varlist.append('level')

vartime=cffile.createVariable('time')
vartime[0] = 0
varlist.append('time')

if proj is not None:
    cffile.projection=proj

varlat=cffile.createVariable('lat')
varlist.append('lat')
varlong=cffile.createVariable('lon')
varlist.append('lon')
varname=cffile.createVariable(variable)
varlist.append(variable)



# get long/lat
longs = varlong[0,:,:]
lats = varlat[0,:,:]
for i in range(0,numy):
    longs[i,:] = varx[:]
for i in range(0,numx):
    lats[:,i] = vary[:]

lats.shape = (numx*numy,)
longs.shape = (numx*numy,)
if inProjFile != None:
       print 'Projecting file...'
       (longs,lats) = cffile.projection.Proj4.gridinv((longs,lats)) # uses the
projection method of cffile to project the file.


lats.shape = (numy,numx)
longs.shape = (numy,numx)
varlong[0,:,:] = longs[:,:].astype(Numeric.Float32)
varlat[0,:,:] = lats[:,:].astype(Numeric.Float32)


#define array for the zData
zData=Numeric.zeros((numx,numy),Numeric.Float32)

j=numy-1
for l in f.readlines():
    i=0
    for e in l.split():
```

```
        # insert each value into each array element
        e=float(e)
        if e == nd: e = float(nodata_val)
        zData[i,j]=e*float(conv_factor)+shift
        i=i+1
    j=j-1
# THIS COMMENTED OUT SECTION FIXES A PORTION OF BEDMAP AROUND THE LAMBERT BASIN,
ANTARCTICA IF SWITCHED ON.
#xcoord = 274
#ycoord = 198
#while xcoord <= 276:
#  while ycoord <= 203:
#    if xcoord == 275 and ycoord == 198:
#      zData [xcoord,ycoord] = -639
#    else:
#      zData[xcoord,ycoord] = zData[xcoord,ycoord] - 400
#    ycoord = ycoord + 1
#  xcoord = xcoord + 1
#
#xcoord = 275
#ycoord = 198
#while xcoord <= 276:
#  while ycoord <= 203:
#    if xcoord == 275 and ycoord == 198:
#      zData [xcoord,ycoord] = -639
#    else:
#      zData[xcoord,ycoord] = zData[xcoord,ycoord] - 400
#    ycoord = ycoord + 1
#  xcoord = xcoord + 1

varname[0,:,:] =  Numeric.transpose(zData[:,:]).astype(Numeric.Float32)



#add in any variables that are supposed to show constant values.
if add != None:
    addvar = str(add[0])
    addval = float(add[1])
    print addvar
    print addval
    varnew=cffile.createVariable(addvar)
    varlist.append(addvar)

    if addvar != 'eus':
       zData=Numeric.zeros((numx,numy),Numeric.Float32)
       for n in range(0,numy):
          zData[n,:] = addval
       for n in range(0,numx):
          zData[:,n] = addval
       varnew[0,:,:] =  Numeric.transpose(zData[:,:]).astype(Numeric.Float32)

    #eus (sea level change) is a cingle dimension variable, so we only assign a shift
in sea level to the cffile.
    if addvar == 'eus':
       varnew[0] = addval

# open file containing list of extra variables and their associated inputs
if extraFile != None:
  extra=open(extraFile, 'r')
  # loop here for variables listed in extraFile
  line = extra.readline()
  #print 'line',line,'line'
  while line != '':
        l = line.split()
        #print 'line = ',l
        variable = l[0]
        #if variable already exists in varlist then ignore new variable and skip to
next line
        #else parse as normal and add variable to varlist


        print 'Parsing variable',variable,'...'
        dataFile = open(l[1], 'r')
```

```
        if len(l) > 2: conversion_factor = float(l[2])

        if len(l) > 3: nodata_val = float(l[3])

        #skip metadata
        xsize=dataFile.readline()
        xsize=int(xsize[string.rfind(xsize,' '):])
        if xsize != numx:
                print 'Error in input file',l[1],'Check X dimension of all files is
same as file',inFile
                sys.exit(1)
        ysize=dataFile.readline()
        ysize=int(ysize[string.rfind(ysize,' '):])
        if ysize != numy:
                print 'Error in input file',l[1],'Check Y dimension of all files is
same as file',inFile
                sys.exit(1)
        skip=dataFile.readline()
        skip=dataFile.readline()
        skip=dataFile.readline()
        skip=dataFile.readline()

        #define array for the zData
        zData=Numeric.zeros((numx,numy),Numeric.Float32)

        j=numy-1
        for l in dataFile.readlines():
                i=0
                for e in l.split():
                        # insert each value into each array element
                        e=float(e)
                        if e == nd:
                          e = float(nodata_val)
                          zData[i,j]=e
                        else:
                          zData[i,j]=e*conversion_factor
                        i=i+1
                j=j-1

        varname = 'var' + variable
        varname=cffile.createVariable(variable)
        varlist.append(variable)
        varname[0,:,:] =  Numeric.transpose(zData[:,:]).astype(Numeric.Float32)
        line = extra.readline()
  else:
    print 'all variables parsed'
  #finish loop for extraFile here

print 'NetCDF file',outFile,'created'

cffile.close()
```

Radial_topo.py

Creates the radial valley topographies used in Chapter 2 of this thesis.

```
#! /usr/bin/env python

# Stewart Jamieson (Stewart.Jamieson@ed.ac.uk) 2005 - University of Edinburgh.
# This script creates a netCDF file with a radial valley topography.
# Additionally, it outputs a text file of x,y coordinates that lie on a circle of
# radius x, where x is user defined.


import sys,getopt, Numeric, PyCF, datetime, string, PyCF.CF_proj,RandomArray,math

def usage():
    "print short help message"

    print 'Usage: radial_topo.py [OPTIONS] outfile'
    print 'create a radial CF topography file based on Sine wave.'
    print ''
    print '  -h, --help\n\tthis message'
    print '  -c, --curve\n\tThe type of curve desired. [default: S - which is a sine
curve], other options are V \n(which is a V-shaped valley system), and U (U-shaped -
this is not properly implemented as yet).'
    print '  -d, --delta dx[/dy]\n\tNode spacing. Assume dx==dy if dy is omitted.
[default: 10000]'
    print '  -n, --num x/y\n\tGrid size. [default: 128/128]'
    print '  -s, --shift s\n\tElevational shift [default: 0]'
    print '  -w, --whitenoise w\n\tSpecifies whether white noise should be included'
    print '  -f, --frequency f\n\tFrequency of the sine wave. [default: 2]'
    print '  -a, --amplitude a[/b]\n\tSpecifies amplitude required (a) and\n\thow
ampitude scales with radius (b). [default: 1/0.02]\n\tNote: If you have a 100 m
relief topography with a /b \n\tvalue of 0.02 and you wish a 1000 m relief topography
\n\tto have the same topographic shape then you must have \n\ta /b value of 0.02 / 10
- i.e. 0.002.'
    print '  -r, --radius r\n\tRadius (no. of cells) at which xy pairs of coords
are\n\tcalculated for use in plotProfile.py [default: 50 cells]'
    print '  -t, --twist t\n\tTwist - the angle in degrees by which the topography
\n\tshould be rotated. To ensure spokes are not aligned in \n\teither 90 or 45 degree
directions, thus avoiding numerical artefacts.'
    print '  -p, --profile_out\n\tSpecifies the desired output text file for a
circular profile for use in plotProfile.py'
    print '  --title\n\t title for output netCDF file'
    print '  --institution\n\tname of institution'
    print '  --references\n\tsome references'
    print '  --comment\n\tcomment'

# get options
try:
    opts, args =
getopt.getopt(sys.argv[1:],'hc:d:n:s:f:w:a:r:t:p:',['help','curve=','delta=','num=','
shift=','frequency=','whitenoise=','amplitude=','radius=','twist=','profile_out=','ti
tle=','institution=','references=','comment='])
except getopt.GetoptError,error:
        # print usage and exit
        print error
        usage()
        sys.exit(1)

if len(args) == 1:
        outFile = args[0]
else:
        usage()
        sys.exit(1)

outProfile = None
curve = 'S'
delta = [10000.,10000.]
```

```
num = [128,128]
shift = 0.
dist = 50.
frequency = 2
noise = 0.1
namp = 0.5
amplitude = 1.
ampscale = 0.02 #this defines how amplitude is scaled with distance from the central
origin
twist = 0.
title='Sinusoidal Topo'
institution=None
references=None
comment=None
proj = None
upper = None
source=None
for o,a in opts:
    if o in ('-h', '--help'):
        usage()
        sys.exit(0)
    if o in ('-c','--curve'):
        curve = a
    if o in ('-d','--delta'):
        a = a.split('/')
        if len(a)==1:
            delta = [float(a[0]),float(a[0])]
        elif len(a)==2:
            delta = [float(a[0]),float(a[1])]
        else:
            print 'Error, cannot parse delta string'
            usage()
            sys.exit(1)
    if o in ('-n','--num'):
        a = a.split('/')
        try:
            num = [int(a[0]),int(a[1])]
        except:
            print 'Error, cannot parse num string'
            usage()
            sys.exit(1)
    if o in ('-s','--shift'):
        shift = float(a)
    if o in ('-f','--frequency'):
        frequency = float(a)
    if o in ('-w','--whitenoise'):
        noise = float(a)
    if o in ('-r','--radius'):
        dist = float(a)
    if o in ('-a','--amplitude'):
        a = a.split('/')
        if len(a)==1:
                amplitude = float(a[0])
        elif len(a)==2:
                amplitude = float(a[0])
                ampscale = float(a[1])
        else:
                print 'Error, cannot parse amplitude string'
                usage()
                sys.exit(1)
    if o in ('-t','--twist'):
        twist = float(a)
        if twist > 360:
                print 'Error - twist must be less <= 360 degrees'
                usage()
                sys.exit(1)
    if o in ('-p','--profile_out'):
        outProfile = a
    if o == '--title':
        title = a
    if o == '--institution':
        institution = a
    if o == '--references':
        references = a
```

```
    if o == '--comment':
        comment  = a

numx = num[0]
numy = num[1]
xcell=delta[0]
ycell=delta[1]
origin = [0.,0.]

print 'creating output netCDF file...'
cffile = PyCF.CFcreatefile(outFile)
# global attributes
if title is not None:
    cffile.title = title
if institution is not None:
    cffile.institution = institution
if source  is not None:
    cffile.source = source
args = ''
for a in sys.argv:
    args = args + '%s '%a
cffile.history = '%s: %s'%(datetime.datetime.today(),args)
if references  is not None:
    cffile.references=references
if comment is not None:
    cffile.comment = comment

# creating dimensions
cffile.createDimension('x0',numx-1)
cffile.createDimension('x1',numx)
cffile.createDimension('y0',numy-1)
cffile.createDimension('y1',numy)
cffile.createDimension('level',1)
cffile.createDimension('time',None)
# creating variables
varx=cffile.createVariable('x0')   .
# variables x0 and y0 must be shifted by half the delta value because they lie in the
# centre of the x1 and y1 grid. x0 and y0 are 1 less in dimension compared to x1 and
y1.
varx[:] = (delta[0]*Numeric.arange(numx-1)+(delta[0]/2)).astype(Numeric.Float32)
varx=cffile.createVariable('x1')
varx[:] = (delta[0]*Numeric.arange(numx)).astype(Numeric.Float32)

vary=cffile.createVariable('y0')
vary[:] = (delta[1]*Numeric.arange(numy-1)+(delta[1]/2)).astype(Numeric.Float32)
vary=cffile.createVariable('y1')
vary[:] = (delta[1]*Numeric.arange(numy)).astype(Numeric.Float32)

varlevel=cffile.createVariable('level')
varlevel[0] = 1

vartime=cffile.createVariable('time')
vartime[0] = 0


if proj is not None:
    cffile.projection=proj

varlat=cffile.createVariable('lat')

varlong=cffile.createVariable('lon')

vartopg=cffile.createVariable('topg')

# get long/lat
longs = varlong[0,:,:]
lats = varlat[0,:,:]
for i in range(0,numy):
    longs[i,:] = varx[:]
for i in range(0,numx):
    lats[:,i] = vary[:]

lats.shape = (numx*numy,)
longs.shape = (numx*numy,)
```

```
lats.shape = (numy,numx)
longs.shape = (numy,numx)
varlong[0,:,:] = longs[:,:].astype(Numeric.Float32)
varlat[0,:,:] = lats[:,:].astype(Numeric.Float32)


#define array for the zData
zData=Numeric.zeros((numx,numy),Numeric.Float32)
ranData=Numeric.zeros((numx,numy),Numeric.Float32)

if noise != 0.:
        ranData[:,:] = RandomArray.uniform((noise*-
1),noise,(numy,numx)).astype(Numeric.Float32)

xorigin=numx/2+1
yorigin=numy/2+1


maxrad=math.sqrt(((numx/2)**2)+((numy/2)**2))
currmax = -9999999.
currmin = 9999999.

if curve == 'S':
  j=0
  for y in zData:
        i=0
        for x in zData:
                #calculate distance to point from origin (radius)

                acoord=xorigin-i
                bcoord=yorigin-j
                r = math.sqrt((acoord**2)+(bcoord**2)) #calculate radius

                theta=math.atan2(bcoord,acoord) + twist #calculate angle

                #calculate the points position on a sine wave
                zData[i,j]=(r*math.sin(frequency*theta)) + ranData[i,j] +
((ampscale*amplitude)*(maxrad-r))

                zData[i,j]=zData[i,j]+((maxrad-r)*5) # Add a doming effect

                if zData[i,j] > currmax:
                        currmax = zData[i,j]
                if zData[i,j] < currmin:
                        currmin = zData[i,j]

                i=i+1
        j=j+1


if curve == 'V':
  j=0
  for y in zData:
        i=0
        for x in zData:
                #calculate distance to point from origin (radius)

                acoord=xorigin-i
                bcoord=yorigin-j
                r = math.sqrt((acoord**2)+(bcoord**2)) #calculate radius

                theta=math.atan2(bcoord,acoord) + (twist+(360/frequency)) #calculate
angle


                sector=360/frequency

                if theta >=0:
                        remainder=math.modf(math.degrees(theta)/sector) #modf()
function puts decimal and integer components of the division into an array.
                if theta <0:
                        remainder=math.modf((360+math.degrees(theta))/sector)
```

```
                r1 = remainder[1] #this is the fractional remainder in decimals.
                r2 = remainder[0] #this is the integer result of the division.

                circumference = math.pi*(r*2) #C=pi*diameter
                wavelength = circumference/frequency

                #get gradient of straight line between the maximum and minimum on that
sine wave at that radius

                if r2 > 0.5:

                        height = (1-r2)*(r)
                if r2 <= 0.5:
                        height = r2*(r)

                zData[i,j]=height

                zData[i,j]=zData[i,j]+((ampscale*amplitude)*(maxrad-r))+
(ranData[i,j]*0.2)+((maxrad-r)*2)# Add a doming effect and the noise

                #NOTE: THE ABOVE DOMING EFFECT ((MAXRAD-R)*5) IS THE SAME AS WHEN USED
IN SINE CURVE TOPOS. HOWEVER, IT MAY WORK BETTER WITH A SMALLER MULTIPLICATION SUCH
AS *2.

                if zData[i,j] > currmax:
                        currmax = zData[i,j]
                if zData[i,j] < currmin:
                        currmin = zData[i,j]

                i=i+1
        j=j+1

if curve == 'U':
  j=0
  for y in zData:
        i=0
        for x in zData:
                #calculate distance to point from origin (radius)

                acoord=xorigin-i
                bcoord=yorigin-j
                r = math.sqrt((acoord**2)+(bcoord**2)) #calculate radius

                theta=math.atan2(bcoord,acoord) + twist #calculate angle

                #Now calculate the points position on a straightened out version of
the sine wave

                sector=360/frequency

                if theta >=0:
                        remainder=math.modf(math.degrees(theta)/sector) #modf()
function puts decimal and integer components of the division into an array.
                if theta <0:
                        remainder=math.modf((360+math.degrees(theta))/sector)


                r1 = remainder[1] #this is the fractional remainder in decimals.
                r2 = remainder[0] #this is the integer result of the division.

                #To do this - calculate radius to this point, and calculate
circumference - divide the circumference by the frequency
                circumference = math.pi*(r*2) #C=pi*diameter
                wavelength = circumference/frequency

                #get gradient of straight line between the maximum and minimum on that
sine wave at that radius

                #use the proportion and the gradient to calculate the elevation -
assign this to the zData array.
                #sin theta = opp/adj
                #adj = sin theta * adj
```

```
                if r2 > 0.5:

                        height = (1-r2) + ((maxrad-r))
                if r2 <= 0.5:
                        height = r2 +((maxrad-r)*5)

                zData[i,j]=height

                zData[i,j]=zData[i,j]+((maxrad-r)) # Add a doming effect

                if zData[i,j] > currmax:
                        currmax = zData[i,j]
                if zData[i,j] < currmin:
                        currmin = zData[i,j]

                i=i+1
        j=j+1

newmax = -9999999. #set as an unlikely value
newmin = 9999999.
currrange=currmax-currmin

#Now rescale the range the data sould cover (i.e. to the amplitude)
j=0
for y in zData:
        i=0
        for x in zData:
                if zData[i,j] != 0:
                        acoord=xorigin-i
                        bcoord=yorigin-j
                        r = math.sqrt((acoord**2)+(bcoord**2)) #calculate radius

                        zData[i,j] = (((amplitude)/currrange)*(zData[i,j]))

                if zData[i,j] > newmax:
                        newmax = zData[i,j]
                if zData[i,j] < newmin:
                        newmin = zData[i,j]
                i=i+1
        j=j+1

#Now shift the data so that it is centreed around the 'shift' value
j=0
for y in zData:
        i=0
        for x in zData:
                if zData[i,j] != 0:
                        zData[i,j] = zData[i,j] -((amplitude*0.5)+newmin)+shift
                i=i+1
        j=j+1

#output x,y pairs for drawing profile...
if outProfile != None:
  , f=open(outProfile,'w')
    #get xy pairs for each 1 degree rotation through 360 degrees.
    deg=0
    while deg <= 360:
        x_coord=dist*math.sin(math.radians(deg)) # sine x= opp / hyp so opp = sine x *
hyp
        y_coord=dist*math.cos(math.radians(deg)) # cos x = adj / hyp etc.
        strx=str((x_coord*xcell)+(xorigin*xcell))
        stry=str((y_coord*ycell)+(yorigin*ycell))
        f.write(strx+' '+stry+'\n')
         deg=deg+1
    f.close()

vartopg[0,:,:] = Numeric.transpose(zData[:,:]).astype(Numeric.Float32)

print 'NetCDF file',outFile,'created'

cffile.close()
```

Golem2ascii.py

Converts GOLEM topographies to ArcGIS ascii files. Then use a2c.py to convert the output to netCDF for use in GLIMMER.

```
#! /usr/bin/env python

# Stewart Jamieson (Stewart.Jamieson@ed.ac.uk), 2006 - University of Edinburgh.
# This script reads a elevation file created by the GOLEM landscape evolution model
(GREG TUCKER) and outputs an ascii file.

import sys, getopt

def usage():
    "print short help message"

    print 'Usage: golem2ascii.py [options] infile outfile timeslice'
    print ''
    print 'Converts GOLEM output files into ArcInfo grid ascii file.'
    print ''
    print 'infile = input golem file e.g. golem.elev'
    print 'outfile = output ascii file e.g. golem.asc'
    print 'timeslice = timeslice required (relies on you knowing how many timeslices
were output by GOLEM to the infile - there is no specific information in the infile
that indicates how many clices are available)'
    print '  -h, --help\n\tthis message'
    #print '  -b, --border\n\tremoves a 1 cell border all the way round. Use this
option when you are using GOLEM output as input to another model from which you will
then use the result as input to GOLEM and begin the cycle again. In other words, it
will keep your domain the same rather than getting progressively larger each time you
run GOLEM'
    print '  -z, --zeros\n\tadds a specified width of border of zeros to the GOLEM
topography'
    print '  -s, --scale\n\tscale the topography by a desired multiple'


# get options
try:
    opts, args =
getopt.getopt(sys.argv[1:],'hbz:s:',['help','border','zeros','scale'])
except getopt.GetoptError,error:
        # print usage and exit
        print error
        usage()
        sys.exit(1)

if len(args) == 3:
        inFile = args[0]
        outFile = args[1]
        timeStep = args[2]
else:
        usage()
        sys.exit(1)

border_switch = 'TRUE'
flat_region = 0
scale_factor = 1.0

for o,a in opts:
    if o in ('-h', '--help'):
        usage()
        sys.exit(0)
    if o in ('-b', '--border'):
       border_switch = 'FALSE'
    if o in ('-z', '--zeros'):
       flat_region = int(a)
```

```
    if o in ('-s', '--scale'):
       scale_factor = float(a)

i = open(inFile,'r')
o = open(outFile,'w')

#read from the header of the elev file
xdim = i.readline()
ydim = i.readline()
res = i.readline()
time = i.readline()
noData = '-9999'
xcorner = '0'
ycorner = '0'


xdim = int(xdim)
ydim = int(ydim)
#add the number of flat columns and rows to the header
xdim = xdim + flat_region * 2
ydim = ydim + flat_region * 2
xdim = str(xdim)
ydim = str(ydim)

#write to the ascii header
o.write('ncols         ' + xdim + '\n')
o.write('nrows         ' + ydim + '\n')
o.write('xllcorner     ' + xcorner + '\n')
o.write('yllcorner     ' + ycorner + '\n')
o.write('cellsize      ' + res)
o.write('nodata_value  ' + noData + '\n')

xdim = int(xdim)
ydim = int(ydim)
timeStep = int(timeStep)


# Skip appropriate number of cells to get to start point of appropriate time slice.
if timeStep > 0:
  skipLines = timeStep + (((xdim - (flat_region * 2)) * (ydim - (flat_region * 2))) *
timeStep)
  for s in range(0,skipLines):
    blank = i.readline()
else:
  skipLines = 0


zLine = ''

#write the first set of blank rows.
if flat_region > 0:
  for y in range(0,flat_region):
    for x in range(0,xdim):
      zLine = zLine + ' ' + '0'
    o.write(zLine + '\n')

    zLine = ''


zLine = ''


if flat_region > 0:
  #do the reading and writing but add in the extra zeros at the start of each row.
  for y in range(0,ydim - (flat_region * 2)):
    blanks = ''
    for b in range(0,flat_region):
      blanks = blanks + ' ' + '0'
    #zLine = blanks

    for x in range(1,xdim - (flat_region * 2 - 1)):
      chunk = i.readline().strip('\n')

      if chunk != '':
```

```
        chunk = str(float(chunk) * scale_factor)

      if border_switch == 'FALSE':
        #Deal wth the first and last columns of x data (i.e. ignore them)
        if x == 0:
          zLine = zLine
        elif x == xdim - 1:
          zLine = zLine
        else:
          zLine = zLine + ' ' + chunk
      elif border_switch == 'TRUE':
        zLine = zLine + ' ' + chunk

      #Check if there is actually any data within the desired timeslice!
      if chunk == '':
        print 'Specified timeslice does not exist'
        sys.exit()

    if border_switch == 'FALSE':
      #Deal with the first and last rows of y data (i.e. ignore them)
      if y == 0:
        useless = 1
      elif y == ydim - 1:
        useless = 1
      else:
        o.write(zLine + '\n')

    elif border_switch == 'TRUE':
      o.write(blanks + zLine + blanks + '\n')
    zLine = ''

else:
  #just do the reading and writing
  for y in range(0,ydim):
    for x in range(0,xdim):
      chunk = i.readline().strip('\n')
      if chunk != '':
        chunk = str(float(chunk) * scale_factor)

      if border_switch == 'FALSE':
        #Deal wth the first and last columns of x data (i.e. ignore them)
        if x == 0:
          zLine = zLine
        elif x == xdim - 1:
          zLine = zLine
        else:
          zLine = zLine + ' ' + chunk
      elif border_switch == 'TRUE':
        zLine = zLine + ' ' + chunk

      #Check if there is actually any data within the desired timeslice!
      if chunk == '':
        print 'Specified timeslice does not exist'
        sys.exit()

    if border_switch == 'FALSE':
      #Deal with the first and last rows of y data (i.e. ignore them)
      if y == 0:
        useless = 1
      elif y == ydim - 1:
        useless = 1
      else:
        o.write(zLine + '\n')

    elif border_switch == 'TRUE':
      o.write(zLine + '\n')
    zLine = ''



#write the second set of blank rows.
if flat_region > 0:
  for y in range(0,flat_region):
```

```
    for x in range(0,xdim):
      zLine = zLine + ' ' + '0'
    o.write(zLine + '\n')
    zLine = ''

i.close()
o.close()
```

Random.aml

This script generates the random white noise topographies used in Chapter 3 of this thesis.

```
/* run this aml in GRID


&echo &off
&messages &on

&sv cellsize = [unquote [response 'Enter desired cellsize (m - default = 50)' 50]]

setcell %cellsize%

/* set window size to be 500 cells each way at resolution of 50m = 5000x5000
&ty PLEASE NOTE: THE TOPOGRAPHY MUST BE A MIMIMUM OF 5000 BY 5000 CELLS IN ORDER TO
MAINTAIN SMOOTH TRANSITIONS BETWEEN EDGES.
&sv x = [unquote [response 'enter topography x size (m - default = 5000)' 5000]]
&sv y = [unquote [response 'enter topography y size (m - default = 5000)' 5000]]
&sv x1 = [calc %x% / %cellsize%]
&sv y1 = [calc %y% / %cellsize%]

/*&sv no_of_scales = [unquote [response 'How many different frequencies should be
used? (default = 5)' 5]]
&sv amp_mult = [unquote [response 'What is the multiplication factor for amplitude as
the wavelength increases? (default = 2)' 2]]
/*&sv kernel_shape = [locase [unquote [response 'What kernel shape for smoothing?
(rectangle (default),circle)' rectangle]]]
/*&sv min_topo = [unquote [response 'Enter minimum elevation required (default=0)'
0]]
&sv max_topo = [unquote [response 'Enter maximum elevation required (default=1000)'
1000]]

setwindow 0 0 %x% %y%

&if [exists w1 -GRID] &then kill w1
w1 = rand() /*make range between -1 and 1. May have to use a standard seed - the same
each time - in order to get a single standard topography?
&if [exists w2a -GRID] &then kill w2a
w2a = w1 /* * 2 - 1
&if [exists w2b -GRID] &then kill w2b
&if [exists w2c -GRID] &then kill w2c
&if [exists w2d -GRID] &then kill w2d
&if [exists w2e -GRID] &then kill w2e
&if [exists w2f -GRID] &then kill w2f
&if [exists w2g -GRID] &then kill w2g
&if [exists w2h -GRID] &then kill w2h
&if [exists w2i -GRID] &then kill w2i


/*copy the grid 8 times and shift each one
w2b = shift(w2a,[calc 0 - %x%],0)
w2c = shift(w2a,[calc 0 - %x%],[calc 0 - %y%])
w2d = shift(w2a,[calc 0 - %x%],[calc 0 + %y%])
w2e = shift(w2a,0,[calc 0 - %y%])
w2f = shift(w2a,0,[calc 0 + %y%])
w2g = shift(w2a,[calc 0 + %x%],0)
w2h = shift(w2a,[calc 0 + %x%],[calc 0 - %y%])
w2i = shift(w2a,[calc 0 + %x%],[calc 0 + %y%])


setwindow -%x% -%y% [calc 2 * %x%] [calc 2 * %y%]

/*merge all 9 grids back together
&if [exists w2 -GRID] &then kill w2
```

```
w2 = merge(w2a,w2b,w2c,w2d,w2e,w2f,w2g,w2h,w2i)

/* smooth the topography at different wavelengths
&if [exists w3 -GRID] &then kill w3
&if [exists w4 -GRID] &then kill w4
&if [exists w5 -GRID] &then kill w5
&if [exists w6 -GRID] &then kill w6
&if [exists w7 -GRID] &then kill w7
&if [exists w8 -GRID] &then kill w8
&if [exists w9 -GRID] &then kill w9
&if [exists w10 -GRID] &then kill w10
&if [exists w11 -GRID] &then kill w11
&if [exists w12 -GRID] &then kill w12
&if [exists final_topo -GRID] &then kill final_topo
/*&if [exists w8_hs -GRID] &then kill w8_hs
/*&if [exists w9_hs -GRID] &then kill w9_hs

/*whilst increasing wanelength, also need to increase amplitude proportionally -
DONE.
/*may need to have an extra border round the data that is equal in width to the
largest focalmean window size
/*&sv naming = 3
/*&sv loop = 1
/*&do &until %loop% eq %no_of_scales%
/*      &ty focalmean radius 3
/*      w%naming% = focalmean(w[calc %naming% - 1],rectangle,3,3) * [calc %amp_mult%
** %loop%]
/*      &sv loop = [calc %loop% + 1]
/*      &ty loop %loop%
/*&end


&ty focalmean radius 3
w3 = focalmean(w2,rectangle,3,3,DATA) * %amp_mult% /*wavelength of 150m (3 cells),
and double amplitude
/*&ty focalmean radius 6
/*w4 = focalmean(w3,rectangle,6,6,DATA) * [calc %amp_mult% ** 2]
/*&ty focalmean radius 12
/*w5 = focalmean(w4,rectangle,12,12,DATA) * [calc %amp_mult% ** 3] /* This is max
wavelength used in topo experiments.
/*&ty focalmean radius 24
/*w6 = focalmean(w5,rectangle,24,24,DATA) * [calc %amp_mult% ** 4]
/*&ty focalmean radius 48
/*w7 = focalmean(w6,rectangle,48,48,DATA) * [calc %amp_mult% ** 5]
/*&ty focalmean radius 96
/*w8 = focalmean(w6,rectangle,96,96,DATA) * [calc %amp_mult% ** 6]


w9 = w3 /*+ w4 /*+ w5 /*+ w6 + w7 + w8

setwindow 0 0 %x% %y%
/* clip out the middle section
gridclip w9 w10 box 0 0 %x% %y%

&describe w10


/* add whatever below min_topo, then find out what max_topo/grid maximum is and
multiply the grid by that.
w11 = w10 + [calc 0 - %GRD$ZMIN%]
&describe w11
w12 = w11 / [calc %GRD$ZMAX% / %max_topo%]
final_topo = w12 /*  int(w12)
&describe final_topo

&if [exists w1 -GRID] &then kill w1
&if [exists w2 -GRID] &then kill w2
&if [exists w3 -GRID] &then kill w3
&if [exists w4 -GRID] &then kill w4
&if [exists w5 -GRID] &then kill w5
&if [exists w6 -GRID] &then kill w6
&if [exists w7 -GRID] &then kill w7
&if [exists w8 -GRID] &then kill w8
&if [exists w9 -GRID] &then kill w9
```

```
&if [exists w10 -GRID] &then kill w10
&if [exists w11 -GRID] &then kill w11
&if [exists w12 -GRID] &then kill w12
&if [exists w2a -GRID] &then kill w2a
&if [exists w2b -GRID] &then kill w2b
&if [exists w2c -GRID] &then kill w2c
&if [exists w2d -GRID] &then kill w2d
&if [exists w2e -GRID] &then kill w2e
&if [exists w2f -GRID] &then kill w2f
&if [exists w2g -GRID] &then kill w2g
&if [exists w2h -GRID] &then kill w2h
&if [exists w2i -GRID] &then kill w2i

&ty maximum = %GRD$ZMAX%
&ty minimum = %GRD$ZMIN%

/*w8_hs = hillshade(w8)

/*w9_hs = hillshade(w9)
```

References

Agassiz, L., 1840. Études sur les glaciers. Jent et Gassmann, Neuchatel.

Agnew, L., 2005. The Application of Glacial Modelling to Diamond Exploration in Northwest Territories and Nunavut, Canada., University of Edinburgh, Edinburgh.

Alley, R.B., 1984. A non-steady ice sheet model incorporating longitudinal stresses: application to the adjustment of interior regions of an ice sheet to changes in sea level. Report - Ohio State University, Institute of Polar Studies, 84: 100.

Alley, R.B., Baker, G.S., Lawson, D.E., Larson, G.J. and Evenson, E.B., 2003. Stabilizing feedbacks in glacier-bed erosion. Nature, 424(6950): 758-760.

Anderson, J., 1991. The Antarctic continental shelf: results from marine geological and geophysical investigations. In: R.J. Tingey (Editor), The Geology of Antarctica. Clarendon Press, Oxford, pp. 285-334.

Anderson, J. and Bartek, L.R., 1992. Cenozoic glacial history of the Ross Sea revealed by intermediate resolution seismic reflection data combined with drill site information. In: J.P. Kennett and D.A. Warnke (Editors), The Antarctic Paleoenvironment: A perspective on Global Change I. Antarctic Research Series. American Geophysical Union, Washington D.C., pp. 231-263.

Anderson, J.B., 1999. Antarctic Marine Geology. Cambridge University Press, Cambridge, 289 pp.

Anderson, J.B., Shipp, S.S., Lowe, A.L., Wellner, J.S. and Mosola, A.B., 2002. The Antarctic Ice Sheet during the Last Glacial Maximum and its subsequent retreat history: a review. Quaternary Science Reviews, 21(1-3): 49-70.

Anderson, R.S., Molnar, P. and Kessler, M.A., 2006. Features of glacial valley profiles simply explained. Journal of Geophysical Research, 111(F1): F01004 doi: 10.1029/2005JF000344.

Augustin, L. et al., 2004. Eight glacial cycles from an Antarctic ice core. Nature (London), 429(6992): 623-628.

Ballantyne, C.K., McCarroll, D., Nesje, A., Dahl, S.O. and Stone, J.O., 1998. The last ice sheet in north-west Scotland: reconstruction and implications. Quaternary Science Reviews, 17: 1149-1184.

Bamber, J.L., Layberry, R.L. and Gogineni, S., 2001. A new ice thickness and bed data set for the Greenland ice sheet 1. Measurement, data reduction, and

errors. Journal of Geophysical Research-Atmospheres, 106(D24): 33773-33780.

Bamber, J.L., Vaughan, D.G. and Joughin, I., 2000. Widespread complex flow in the interior of the Antarctic ice sheet. Science, 287(5456): 1248-1250.

Barker, P.F. and Thomas, E., 2004. Origin, signature and palaeoclimatic influence of the Antarctic Circumpolar Current. Earth-Science Reviews, 66(1-2): 143-162.

Baroni, C., Fasano, F., Giorgetti, G., Salvatore, M.C. and Ribecai, C., 2008. The Ricker Hills Tillite provides evidence of Oligocene warm-based glaciation in Victoria Land, Antarctica. Global and Planetary Change, 60: 457-470.

Baroni, C., Noti, V., Ciccacci, S., Righini, G. and Salvatore, M.C., 2005. Fluvial origin of the valley system in northern Victoria Land (Antarctica) from quantitative geomorphic analysis. Bulletin of the Geological Society of America, 117(1-2): 212.

Barrett, P.J., 1996. Antarctic palaeoenvironment through Cenozoic times - a review. Terra Antarctica, 3: 103-119.

Becquey, S. and Gersonde, R., 2003. A 0.55-Ma paleotemperature record from the subantarctic zone; implications for Antarctic Circumpolar Current development. Paleoceanography, 18(1): 14.1-14.14.

Benn, D.I. and Evans, D.J.A., 1998. Glaciers & glaciation Edition: 1. London, Arnold, United Kingdom, 734 pp.

Bindschadler, R.A. and Vornberger, P., 1998. Changes in West Antarctic Ice Sheet since 1963 from declassified satellite photography. Science, 279: 689-692.

Blunier, T. and Brook, E.J., 2001. Timing of millennial-scale climate change in Antarctica and Greenland during the last glacial period. Science, 291(5501): 109-112.

Blunier, T. et al., 1998. Asynchrony of antarctic and greenland climate change during the last glacial period. Nature, 394(6695): 739-743.

Bogen, J., 1996. Erosion rates and sediment yields of glaciers. Annals of Glaciology, 22: 48-52.

Boulton, G. and Hagdorn, M., 2006. Glaciology of the British Isles Ice Sheet during the last glacial cycle: form, flow, streams and lobes. Quaternary Science Reviews, 25(23-24): 3359-3390.

Boulton, G.S., 1974. Processes and patterns of glacial erosion. In: Coates (Editor), Glacial geomorphology. State University of New York, pp. 41-87.

Boulton, G.S., 1979. Processes of glacier erosion on different substrata. Journal of Glaciology, 23(89): 15-38.

Boulton, G.S., 1982. Subglacial processes and the development of glacial bedforms. In: R. Davidson-Arnott (Editor), Research in glacial, glacio-fluvial, and glacio-lacustrine systems. Proc. 6th Guelph symposium on geomorphology, 1980. Geo Books, pp. 1-31.

Boulton, G.S., 1996a. The origin of till sequences by subglacial sediment deformation beneath mid-latitude ice sheets. Annals of Glaciology, 22: 75-84.

Boulton, G.S., 1996b. Theory of glacial erosion, transport and deposition as a consequence of subglacial sediment deformation. Journal of Glaciology, 42(140): 43-62.

Boulton, G.S. and Clark, C.D., 1990. The Laurentide ice sheet through the last glacial cycle: the topology of drift lineations as a key to the dynamic behaviour of former ice sheets. Transactions - Royal Society of Edinburgh: Earth Sciences, 81(4): 327-347.

Boulton, G.S., Hagdorn, M. and Hulton, N.R.J., 2003. Streaming flow in an ice sheet through a glacial cycle. Annals of Glaciology, 36: 117-128.

Boulton, G.S. and Payne, A., 1992. Simulation of the European ice sheet through the last glacial cycle and prediction of future glaciation, Technical Report SKB 93-14, Swedish Nuclear Fuel and Waste Management Co.

Boulton, G.S., Smith, G.D., Jones, A.S. and Newsome, J., 1985. Glacial geology and glaciology of the last mid-latitude ice sheets. Journal - Geological Society (London), 142(3): 447-474.

Brardinoni, F. and Hassan, M.A., 2006. Glacial erosion, evolution of river long profiles, and the organisation of process domains in mountain drainage basins of coastal British Columbia. Journal of Geophysical Research, 111(F1): F01013 doi: 10.1029/2005JF000358.

Braun, J., Zwartz, D. and Tomkin, J.H., 1999. A new surface-processes model combining glacial and fluvial erosion. Annals of Glaciology, 28: 282-290.

Briner, J.P., Miller, G.H., Davis, P.T. and Finkel, R.C., 2006. Cosmogenic radionuclides from fiord landscapes support differential erosion by overriding ice sheets. Geological Society of America Bulletin, 118(3-4): 406-420.

Brocklehurst, S.H. and Whipple, K.X., 2002. Glacial erosion and relief production in the Eastern Sierra Nevada, California. Geomorphology, 42(1-2): 1-24.

Brocklehurst, S.H. and Whipple, K.X., 2004. Hypsometry of glaciated landscapes. Earth Surface Processes and Landforms, 29(7): 907-926.

Brozovic, N., Burbank, D.W. and Meigs, A.J., 1997. Climatic limits on landscape development in the Northwestern Himalaya. Science, 276: 571-574.

Budd, W.F., Keage, P.L. and Blundy, N.A., 1979. Empirical studies of ice sliding. Journal of Glaciology, 23: 157-170.

Budd, W.F., Young, N.W. and Austin, C.R., 1976. Measured and computed temperature distributions in the Law Dome ice cap, Antarctica. Journal of Glaciology, 16: 99-110.

Bueler, E., Kallen-Brown, J.A. and Lingle, C.S., 2005. Exact solutions and the verification of numerical models for ice sheets. Geophysical Research Abstracts, 7: 05241.

Caldenius, C.G., 1932. Las glaciones Cuaternarias en la Patagonia and Tierra del Fuego. Geografiska Annaler, 14: 1-164.

Clapperton, C.M., 1990. Quaternary glaciations in the southern hemisphere: an overview. Quaternary Science Reviews, 9: 299-304.

Clapperton, C.M. and Sugden, D.E., 1988. Holocene glacier fluctuations in South America and Antarctica. Quaternary Science Reviews, 7(2): 185-198.

Clark, P.U., 1994. Unstable behaviour of the Laurentide Ice Sheet over deforming sediment and its implications for climate change. Quaternary Research, 41: 19-25.

Clark, P.U., Alley, R.B. and Pollard, D., 1999. Northern Hemisphere Ice-Sheet Influences on Global Climate Change. Science, 286(5442): 1104-1111.

Clark, P.U. et al., 2006. The middle Pleistocene transition: characteristics, mechanisms, and implications for long-term changes in atmospheric PCO_2. Quaternary Science Reviews, 25(23-24): 3150-3184.

Clark, P.U. and Pollard, D., 1998. Origin of the Middle Pleistocene transition by ice sheet erosion of regolith. Paleoceanography, 13(1): 1-9.

Clarke, G.K.C., 1977. Strain heating and creep instability in glaciers and ice sheets. Reviews of Geophysics and Space Physics, 15: 235-247.

Cooper, A.K., O'Brien, P.E. and Party, L.S.S., 2001. Early stages of East Antarctic glaciation - insights from drilling and seismic reflection data in the Prydz Bay region. In: F. Florindo and A.K. Cooper (Editors), The Geologic Record of the Antarctic Ice Sheet from Drilling, Coring and Seismic Studies, Extended abstracts. Quaderna di Geofisca, pp. 41-42.

Cooper, A.K., Stagg, H. and Geist, E., 1991. Seismic stratigraphy and structure of Prydz Bay, Antarctica: implicationsfrom ODP Leg 119 drilling. In: J.B. Barron and B. Larsen (Editors), Ocean Drilling Program Leg 119, Scientific results., College Station, Texas, pp. 5-25.

Croll, J., 1867. On the excentricity of the Earth's orbit, and its physical relations to the glacial epoch. Philosophical Magazine, 33: 119-131.

Cuffey, K.M. et al., 2000. Entrainment at cold glacier beds. Geology, 28(4): 351-354.

Davis, C.H., Li, Y., McConnell, J.R., Frey, M.M. and Hanna, E., 2005. Snowfall-driven growth in East Antarctic Ice Sheet mitigates recent sea level rise. Science, 308: 1898-1901.

Davis, P.T., Briner, J.P., Coulthard, R.D., Finkel, R.W. and Miller, G.H., 2006. Preservation of Arctic landscapes overridden by cold-based ice sheets. Quaternary Research, 65(1): 156-163.

DeConto, R., Pollard, D. and Harwood, D., 2007. Sea ice feedback and Cenozoic evolution of Antarctic climate and ice sheets. Paleoceanography, 22(3).

DeConto, R.M. and Pollard, D., 2003a. A coupled climate-ice sheet modeling approach to the Early Cenozoic history of the Antarctic ice sheet. Palaeogeography, Palaeoclimatology, Palaeoecology, 198(1-2): 39-52.

DeConto, R.M. and Pollard, D., 2003b. Rapid Cenozoic glaciation of Antarctica induced by declining atmospheric CO_2. Nature, 421(6920): 245-249.

Denton, G.H. et al., 1999. Interhemispheric linkage of paleoclimate during the last glaciation. Geografiska Annaler, Series A: Physical Geography, 81(2): 107-153.

Denton, G.H. and Hughes, T.J., 1986. Global Ice-Sheet System Interlocked by Sea-Level. Quaternary Research, 26(1): 3-26.

Denton, G.H. and Hughes, T.J., 2002. Reconstructing the Antarctic Ice Sheet at the Last Glacial Maximum. Quaternary Science Reviews, 21(1-3): 193-202.

Denton, G.H., Prentice, M.L. and Burckle, L.H., 1991. Cainozoic history of the Antarctic Ice Sheet. In: R.J. Tingey (Editor), The Geology of Antarctica. Clarendon Press, Oxford, pp. 365-433.

Denton, G.H. and Sugden, D.E., 2005. Meltwater features that suggest Miocene ice-sheet overriding of the Transantarctic Mountains in Victoria Land, Antarctica. Geografiska Annaler, 87 (A)(1): 67-85.

Denton, G.H. et al., 1993a. East Antarctic ice sheet sensitivity to Pliocene climatic change from a Dry Valleys perspective. Geografiska Annaler, 75A(4): 155-204.

Denton, G.H., Wilch, T.I., Sugden, D.E., Marchant, D.R. and Hall, B.L., 1993b. East Antarctic ice sheet sensitivity to Pliocene climatic change from a dry valleys perspective. Geografiska Annaler, Series A 75, A(4): 155-204.

DePonti, A., Pennati, V., De Biase, L., Maggi, V. and Berta, F., 2006. A new fully three-dimensional numerical model for ice dynamics. Journal of Glaciology, 52(178): 365-376.

Dietrich, R. et al., 2007. Jakobshavn Isbrae, West Greenland: Flow velocities and tidal interaction of the front area from 2004 field observations. Journal of Geophysical Research-Earth Surface, 112(F3).

Ehrmann, W., Setti, M. and Marinoni, L., 2005. Clay minerals in Cenozoic sediments off Cape Roberts (McMurdo Sound, Antarctica) reveal palaeoclimatic history. Palaeogeography Palaeoclimatology Palaeoecology, 229(3): 187-211.

Engelhardt, H., Humphrey, N., Kamb, B. and Fahnestock, M., 1990. Physical conditions at the base of a fast moving Antarctic ice stream. Science, 248: 57-59.

Evans, I.S., 1969. The geomorphology and morphometry of glacial and nival areas. In: R.J. Chorley (Editor), Water, Earth and Man. Methuen, London., pp. 369-380.

Fabel, D. et al., 2004. Spatial patterns of glacial erosion at a valley scale derived from terrestrial cosmogenic ^{10}Be and ^{26}Al concentrations in rock. Annals of the Association of American Geographers, 94(2): 241.

Fabel, D. et al., 2002. Landscape preservation under the Fennoscandian ice sheets determined from in situ produced ^{10}Be and ^{26}Al. Earth and Planetary Science Letters, 201(2): 397-406.

Fairbanks, R.G., 1989. A 17,000-year glacio-eustatic sea level record: influence of glacial melting rates on the Younger Dryas event and deep-ocean circulation. Nature, 342: 637-642.

Federov, L.V., Ravich, M.G. and Hofmann, J., 1982. Geologic comparison of southeastern peninsular India and Sri Lanka with a part of East Antarctica (Enderby Land, MacRobertson Land and Princess Elizabeth Land). In: C. Craddock (Editor), Antarctic Geoscience. Proceedings of the Symposium on Antarctic Geology and Geophysics. University of Wisconsin Press, Madison, pp. 73-78.

Fisher, P., Wood, J. and Cheng, T., 2004. Where is Helvellyn? Fuzziness of multi-scale landscape morphometry. Transactions - Institute of British Geographers, 29: 106-128.

Fitzgerald, P.G. and Stump, E., 1997. Cretaceous and Cenozoic episodic denudation of the Transantarctic Mountains, Antarctica: New constraints from apatite fission track thermochronology in the Scott Glacier region. Journal of Geophysical Research-Solid Earth, 102(B4): 7747-7765.

Flowers, G.E. and Clarke, G.K.C., 2002. A multicomponent coupled model of glacier hydrology 1: theory and synthetic examples. Journal of Geophysical Research, 107.

Forbes, J.D., 1843. Travels through the Alps of Savoy and other parts of the Pennine chain with observations on the phenomena of glaciers. Adam and Charles Black, Edinburgh.

Glasser, N.F., 1995. Modelling the effect of topography on ice sheet erosion, Scotland. Geografiska Annaler, 77 A: 67-82.

Glen, J.W., 1955. The creep of polycrystalline ice. Proceedings of the Royal Society of London - Series A, 228: 519-387.

Goodfellow, B.W., Stroeven, A.P., Hättestrand, C., Kleman, J. and Jansson, K.N., 2007. Deciphering a non-glacial/glacial landscape mosaic in the northern Swedish mountains. Geomorphology, 93: 213-232.

Gough, M., Treinish, L. and al., e., 2008. NetCDF: network Common Data Form. http://www.unidata.ucar.edu/software/netcdf/.

Gow, A.J., Ueda, H.T. and Garfield, D.E., 1968. Antarctic ice sheet: preliminary result of first core hole to bedrock. Science, 161: 1011-1013.

Gregory, J.M. and Huybrechts, P., 2006. Ice-sheet contributions to future sea-level change. Philosophical Transactions of the Royal Society a-Mathematical Physical and Engineering Sciences, 364(1844): 1709-1731.

Hagdorn, M., Rutt, I. and Payne, A., 2005. GLIMMER 0.5.6 Documentation, pp. 77.

Hagdorn, M.K., 2003. Reconstruction of the Past and Forecast of the Future European and British Ice Sheets and Associated Sea-Level Change, University of Edinburgh, 199 pp.

Hall, A.M. and Glasser, N.F., 2003. Reconstructing the basal thermal regime of an ice stream in a landscape of selective linear erosion: Glen Avon, Cairngorm Mountains, Scotland. Boreas, 32(1): 191-207.

Hallet, B., 1979. A theoretical model of glacial abrasion. Journal of Glaciology, 23(89): 39-50.

Hallet, B., 1996. Glacial quarrying: A simple theoretical model. Annals of Glaciology, 22: 1-8.

Hallet, B., Hunter, L. and Bogen, J., 1996. Rates of erosion and sediment evacuation by glaciers: A review of field data and their implications. Global and Planetary Change, 12(1-4): 213-235.

Hambrey, M.J., Glasser, N.F., McKelvey, B.C., Sugden, D.E. and Fink, D., 2007. Cenozoic landscape evolution of an East Antarctic oasis (Radok Lake area, northern Prince Charles Mountains), and its implications for the glacial and climatic history of Antarctica. Quaternary Science Reviews, 26(5-6): 598-626.

Hansen, J.E., 2005. A slippery slope: How much global warming constitutes "dangerous anthropogenic interference"? Climatic Change, 68(3): 269-279.

Harbor, J.M., 1992. Numerical modeling of the development of U-shaped valleys by glacial erosion. Geological Society of America Bulletin, 104(10): 1364-1375.

Harbor, J.M., 1995. Development of glacial-valley cross sections under conditions of spatially variable resistance to erosion. Geomorphology, 14(2): 99-107.

Harbor, J.M., Hallet, B. and Raymond, C.F., 1988. A numerical model of landform development by glacial erosion. Nature, 333: 347-349.

Hay, W.W., Flogel, S. and Soding, E., 2005. Is the initiation of glaciation on Antarctica related to a change in the structure of the ocean? Global and Planetary Change, 45(1-3): 23-33.

Hays, J.D., Imbrie, J. and Shackleton, N.J., 1976. Variations in the Earth's Orbit: Pacemaker of the Ice Ages. Science, 194(4270): 1121-1132.

Hebeler, F., Purves, R.S. and Jamieson, S.S.R., In Press. Uncertainty in ice sheet modelling: the influence of topography, climate and model parameters. Journal of Glaciology.

Heusser, C.J., 1989. Southern Westerlies during the Last Glacial Maximum. Quaternary Research, 31: 423-425.

Hildes, D.H.D., Clarke, G.K.C., Flowers, G.E. and Marshall, S.J., 2004. Subglacial erosion and englacial sediment transport modelled for North American ice sheets. Quaternary Science Reviews, 23(3-4): 409-430.

Hindmarsh, R.C.A., 1996. Stability of ice rises and uncoupled marine ice sheets. Annals of Glaciology, 23: 105-115.

Hindmarsh, R.C.A., 2003. Thermomechanical coupling of ice flow with the bedrock. Annals of Glaciology, 37: 390-396.

Hindmarsh, R.C.A., 2004. A numerical comparison of approximations to the Stokes equations used in ice-sheet and glacier modeling. Journal of Geophysical Research, 109.

Hindmarsh, R.C.A., 2005. Linear stability of thermoviscous ice-sheet flow using the Stokes equations. Geophysical Research Abstracts, 7: 01189.

Hindmarsh, R.C.A., 2006. Stress gradient damping of thermoviscous ice flow instabilities. Journal of Geophysical Research, 111: B12409.

Holbourn, A., Kuhnt, W., Schulz, M. and Erlenkeuser, H., 2005. Impacts of orbital forcing and atmospheric carbon dioxide on Miocene ice-sheet expansion. Nature, 438(7067): 483-487.

Holmlund, P. and Naslund, J.O., 1994. The Glacially Sculptured Landscape in Dronning-Maud Land, Antarctica, Formed by Wet-Based Mountain-Glaciation and Not by the Present Ice-Sheet. Boreas, 23(2): 139-148.

Hubbard, A., Hein, A.S., Kaplan, M.R., Hulton, N. and Glasser, N.F., 2005. A modelling reconstruction of the late glacial maximum ice sheet and its deglaciation in the vicinity of the Northern Patagonian Icefield, South America. Geografiska Annaler, 87(2): 375-391.

Huber, M. and Nof, D., 2006. The ocean circulation in the Southern Hemisphere and its climatic impacts in the Eocene. Palaeogeography Palaeoclimatology Palaeoecology, 231: 9-28.

Hulton, N. and Mineter, M., 2000. Modelling self-organization in ice streams. Annals of Glaciology, 30: 127-136.

Hulton, N., Sugden, D., Payne, A. and Clapperton, C., 1994. Glacier modeling and the climate of Patagonia during the Last Glacial Maximum. Quaternary Research, 42(1): 1-19.

Hulton, N.R.J. and Sugden, D.E., 1995. Modelling mass balance on former maritime ice caps: a Patagonian example. Annals of Glaciology, 21: 304-310.

Hulton, N.R.J., Sugden, D.E., Bentley, M.J., Purves, R.S. and McCulloch, R.D., 2002. The Last Glacial Maximum and deglaciation in southern South America. Quaternary Science Reviews, 21(1-3): 233-241.

Hutter, K., 1983. Theoretical Glaciology. Mathematical Approaches to Geophysics. D.Reidel Publishing Company, Boston, Lancaster.

Huybrechts, P., 1986. A three-dimensional time-dependant numerical model for polar ice sheets; some basic testing with a stable and efficient finite difference scheme, Technical Report, Geografisch Intituut, Vrije Universiteit Brussel, Belgium.

Huybrechts, P., 1993. Glaciological modelling of the late Cenozoic East Antarctic ice sheet: stability or dynamism? Geografiska Annaler, Series A 75, A(4): 221-238.

Huybrechts, P. and de Wolde, J., 1999. The dynamic response of the Greenland and Antarctic ice sheets to multiple-century climatic warming. Journal of Climate, 12(8 Part 1): 2169-2188.

Huybrechts, P., Janssens, I., Poncin, C. and Fichefet, T., 2002. The response of the Greenland ice sheet to climate changes in the 21st century by interactive coupling of an AOGCM with a thermomechanical ice-sheet model. Annals of Glaciology, 35: 409-415.

Huybrechts, P. and Le Meur, E., 1999. Predicted present-day evolution patterns of ice thickness and bedrock elevation over Greenland and Antarctica. Polar Research, 18(2): 299-306.

Huybrechts, P. and Payne, T., 1996. The EISMINT benchmarks for testing ice-sheet models. Annals of Glaciology, 23: 1-12.

Huybrechts, P., Steinhage, D., Wilhelms, F. and Bamber, J., 2000. Balance velocities and measured properties of the Antarctic ice sheet from a new compilation of gridded data for modelling. Annals of Glaciology, 30: 52-60.

Huybrechts, P., Wild, M., Gregory, J. and Janssens, I., 2004. Modelling Antarctic and Greenland volume changes during the 20th and 21st centuries forced by GCM time slice integrations. Global and Planetary Change, 42(1-4): 83-105.

Iken, A. and Bindschadler, R.A., 1986. Combined measurements of subglacial water pressure and surface velocity of Finelengletscher, Switzerland: conclusions about drainage system and sliding mechanism. Journal of Glaciology, 32: 101-119.

Imbrie, J. et al., 1992. On the structure and origin of major glaciation cycles; 1, Linear responses to Milankovitch forcing. Paleoceanography, 7(6): 701-738.

IPCC, 2007. Climate Change 2007: The Physical Science Basis. Contribution of Working Group I to the Fourth Assessment Report of the IPCC.

Iverson, N.R., 1991. Potential effects of subglacial water pressure fluctuations on quarrying. Journal of Glaciology, 37: 27-36.

Jamieson, S.S.R. and Hulton, N.R.J., Submitted. The role of glacial erosion in limiting ice sheet extents. Nature Geosciences.

Jamieson, S.S.R., Hulton, N.R.J. and Hagdorn, M., 2008. Modelling landscape evolution under ice sheets. Geomorphology, 97(1-2): 91-108.

Jamieson, S.S.R., Hulton, N.R.J., Sugden, D.E., Payne, A.J. and Taylor, J., 2005. Cenozoic landscape evolution of the Lambert basin, East Antarctica: the relative role of rivers and ice sheets. Global and Planetary Change, 45(1-3): 35-49.

Jamieson, S.S.R., Sinclair, H.D., Kirstein, L.A. and Purves, R.S., 2004. Tectonic forcing of longitudinal valleys in the Himalaya: morphological analysis of the Ladakh Batholith, North India. Geomorphology, 58: 49-65.

Jamieson, S.S.R. and Sugden, D.E., 2008. Landscape evolution of Antarctica. In: A.K. Cooper et al. (Editors), Antarctica: A Keystone in a Changing World - Proceedings of the 10th International Symposium on Antarctic Earth Sciences. The National Academies Press, Washington D.C., pp. 39-54.

Kamb, B. and LaChapelle, E., 1964. Direct observation of the mechanism of glacier sliding over bedrock. Journal of Glaciology, 5: 159-172.

Kaplan, M.R., Kurz, M.D., Ackert Jr, R.P., Singer, B.S. and Douglass, D.C., 2004. Cosmogenic nuclide chronology of millennial-scale glacial advances during O-isotope stage 2 in Patagonia. Bulletin of the Geological Society of America, 116(3-4): 308-321.

Kennett, J.P., 1977. Cenozoic evolution of Antarctic glaciation, the circum-Antarctic Ocean and their impact on global palaeoceanography. Journal of Geophysical Research, 82: 3843-3860.

Kerr, A., 1993. Topography, climate and ice masses: a review. Terra Nova, 5(4): 332-342.

Kerr, A. and Huybrechts, P., 1999. The response of the East Antarctic ice-sheet to the evolving tectonic configuration of the Transantarctic Mountains. Global and Planetary Change, 23(1-4): 213-229.

Kirkbride, M. and Matthews, D., 1997. The role of fluvial and glacial erosion in landscape evolution: the Ben Ohau range, New Zealand. Earth Surface Processes & Landforms, 22: 317-327.

Kite, E.S. and Hindmarsh, R.C.A., 2007. Did ice streams shape the largest channels on Mars? Geophysical Research Letters, 34(19).

Kleman, J. and Stroeven, A.P., 1997. Preglacial surface remnants and Quaternary glacial regimes in northwestern Sweden. Geomorphology, 19(1-2): 35-54.

Kleman, J., Stroeven, A.P. and Lundqvist, J., 2007. Patterns of quaternary ice sheet erosion and deposition in fennoscandia and a theoretical framework for explanation. Geomorphology, doi: 10.1016/j.geomorph.2007.02.049.

Klocker, A., Prange, M. and Schulz, M., 2005. Testing the influence of the Central American Seaway on orbitally forced northern hemisphere glaciation. Geophysical Research Letters, 32(3).

Knight, P.G., 1999. Glaciers. Stanley Thorns, Cheltenham, 261 pp.

Lambeck, K. and Nakiboglu, S.M., 1980. Seamount loading and stress in the ocean lithosphere. Journal of Geophysical Research, 85: 6403-6418.

Lawford, R.G., 1993. Regional hydraulic response to global change in western North America. In: H.A. Mooney, E.R. Fuentes and B.I. Kronberg (Editors), Earth System Responses to Global Change: Contrasts between North and South America. Academic Press, pp. 73-99.

Lawver, L.A. and Gahagan, L.M., 2003. Evolution of Cenozoic seaways in the circum-Antarctic region. Palaeogeography Palaeoclimatology Palaeoecology, 198(1-2): 11-37.

Lawver, L.A., Royer, J.-Y., Sandwell, D.T. and Scotese, C.R., 1991. Evolution of the Antarctic continental margins. In: M.R.A. Thomson, J.A. Crame and J.W. Thomson (Editors), Geological Evolution of Antarctica: Proceedings of the Fifth International Symposium on Antarctic Earth Sciences. Cambridge University Press, Cambridge, pp. 533-539.

Layberry, R.L. and Bamber, J.L., 2001. A new ice thickness and bed data set for the Greenland ice sheet 2. Relationship between dynamics and basal topography. Journal of Geophysical Research-Atmospheres, 106(D24): 33781-33788.

Le Meur, E., Gagliardini, O., Zwinger, T. and Ruokolainen, J., 2004. Glacier flow modelling: a comparison of the shallow ice approximation and the full-stokes solution. Comptes Rendus Physique, 5(7): 709-722.

Lenton, T.M. et al., 2008. Tipping elements in the Earth's climate system. Proceedings of the National Academy of Sciences of the United States of America, 105(6): 1786-1793.

Li, Y. et al., 2005. Ice sheet erosion patterns in valley systems in northern Sweden investigated using cosmogenic nuclides. Earth Surface Processes and Landforms, 30(8): 1039-1049.

Lisiecki, L.E. and Raymo, M.E., 2005. A Pliocene-Pleistocene stack of 57 globally distributed benthic $\delta_{18}O$ records. Paleoceanography, 20(1): 1-17.

Livermore, R., Hillenbrand, C.D., Meredith, M. and Eagles, G., 2007. Drake Passage and Cenozoic climate: An open and shut case? Geochemistry Geophysics Geosystems, 8.

Løken, O.H. and Hodgson, D.A., 1971. On the submarine geomorphology along the east coast of Baffin Island. Canadian Journal of Earth Science, 8(2): 185-195.

Lunt, D.J., Valdes, P.J., Haywood, A. and Rutt, I.C., 2008. Closure of the Panama Seaway during the Pliocene: implications for climate and Northern Hemisphere glaciation. Climate Dynamics, 30(1): 1-18.

Lyell, C., 1850. Anniversary Address of the President. Quarterly Journal of the Geological Society, 6: xxvii-lxvi.

Lythe, M., Vaughan, D.G. and Consortium, B., 2001. BEDMAP: a new ice thickness and subglacial topographic model of Antarctica. Journal of Geophysical Research, 106: 11335-11352.

MacGregor, K.R., Anderson, R.S., Anderson, S.P. and Waddington, E.D., 2000. Numerical simulations of glacial-valley longitudinal profile evolution. Geology, 28(11): 1031-1034.

Mackintosh, A. et al., 2007. Exposure ages from mountain dipsticks in Mac. Robertson Land, East Antarctica, indicate little change in ice-sheet thickness since the Last Glacial Maximum. Geology, 35(6): 551-554.

Marchant, D.R., Denton, G.H., Swisher, C.C. and Potter, N., 1996. Late Cenozoic Antarctic paleoclimate reconstructed from volcanic ashes in the Dry Valleys region of southern Victoria Land. Geological Society of America Bulletin, 108(2): 181-194.

McClymont, E.L. and Rosell-Melé, A., 2005. Links between the onset of modern Walker Circulation and the mid-Pleistocene climate transition. Geology, 33: 389-392.

McClymont, E.L., Rosell-Melé, A., Haug, G. and Lloyd, J.M., In Preparation. A role for the surface ocean in the mid-Pleistocene climate transition.

McCulloch, R.D. et al., 2000. Climatic inferences from glacial and palaeoecological evidence at the last glacial termination, southern South America. Journal of Quaternary Science, 15(4): 409-417.

Mercer, J.H., 1976. Glacial history of southernmost South America. Quaternary Research, 6: 125-166.

Mercer, J.H., 1983. Cenozoic Glaciation In The Southern-Hemisphere. Annual Review Of Earth And Planetary Sciences, 11: 99-132.

Milankovitch, M., 1941. Kanon der Erdbestrahlung und seine Anwendung auf das Eiszeitproblem. Special Publication of Königliche Serbische Akademie Belgrad, 133.

Mildenhall, D.C., 1989. Terrestrial Palynology. In: P.J. Barrett (Editor), Antarctic Cenozoic History from the CIROS-1 Drillhole, McMurdo Sound. DSIR Bulletin 245, pp. 119-127.

Mishra, D.C., Sekhar, D.V.C., Raju, D.C.V. and Kumar, V.V., 1999. Crustal structure based on gravity-magnetic modelling constrained from seismic studies under Lambert Rift, Antarctica and Godavari and Mahanadi rifts, India and their interrelationship. Earth and Planetary Science Letters, 172(3-4): 287-300.

Mitchell, S.G. and Montgomery, D., 2006. Influence of a glacial buzzsaw on the height and morphology of the Cascade Range in central Washington State, USA. Quaternary Research, 65: 96-107.

Molnar, P. and England, P., 1990. Late Cenozoic uplift of mountain ranges and global climate change: Chicken or egg? Nature, 346: 29-34.

Monnereau, M., Rabinowicz, M. and Arquis, E., 1993. Mechanical Erosion and Reheating of the Lithosphere - a Numerical-Model for Hotspot Swells. Journal of Geophysical Research-Solid Earth, 98(B1): 809-823.

Montgomery, D.R., 1994. Valley incision and the uplift of mountain peaks. Journal of Geophysical Research, 99(B7): 13913-13921.

Montgomery, D.R., Balco, G. and Willett, S.D., 2001. Climate, tectonics and the morphology of the Andes. Geology, 29(7): 579-582.

Naish, T.R. et al., 2001. Orbitally induced oscillations in the East Antarctic ice sheet at the Oligocene/Miocene boundary. Nature, 413(6857): 719-723.

Naslund, J.O., 2001. Landscape development in western and central Dronning Maud Land, East Antarctica. Antarctic Science, 13(3): 302-311.

Näslund, J.O., Jansson, P., Fastook, J., Johnson, J. and Andersson, L., 2005. Detailed spatially distributed geothermal heat-flow data for modeling of basal temperatures and meltwater production beneath the Fennoscandian ice sheet. Annals of Glaciology, 40(1): 95-101.

Näslund, J.O., Rodhe, L., Fastook, J.L. and Holmlund, P., 2003. New ways of studying ice sheet flow directions and glacial erosion by computer modelling - examples from Fennoscandia. Quaternary Science Reviews, 22: 245-258.

O'Brien, P.E., Cooper, A.K., Richter, C. and al., e., 2001. Leg 188 summary: Prydz Bay-Cooperation Sea, Antarctica. Proceedings of the Ocean Drilling Program., Initial Reports 188: 1-65.

Oerlemans, J., 1982. Glacial cycles and ice-sheet modeling. Climatic Change, 4(4): 353-374.

Oerlemans, J., 1984. Numerical experiments on large-scale glacial erosion. Zeitschrift fur Gletscherkunde und Glazialgeologie, 20: 107-126.

Oerlemans, J., 2002. On glacial inception and orography. Quaternary International, 95-96: 5-10.

Oerlemans, J. et al., 1998. Modelling the response of glaciers to climate warming. Climate Dynamics, 14(4): 267-274.

Oerlemans, J. and Van Der Veen, C.J., 1984. Ice Sheets and Climate. Kluwer Academic Publishers Group., 217 pp.

Paterson, W.S.B., 1994. The physics of glaciers. 3rd edition, The physics of glaciers. 3rd edition. Pergamon, pp. 480.

Pattyn, F. and Payne, A.J., 2006. Ice Sheet Model Intercomparison Project: Benchmark Experiments for Higher-Order Ice Sheet Models (ISMIP-HOM). Geophysical Research Abstracts, 8: 04969.

Payne, A.J., 1999. A thermomechanical model of ice flow in West Antarctica. Climate Dynamics, 15(2): 115-125.

Payne, A.J. and Baldwin, D.J., 2000. Analysis of ice-flow instabilities identified in the EISMINT intercomparison exercise. Annals of Glaciology, 30: 204-210.

Payne, A.J. and Dongelmans, P.W., 1997. Self-organization in the thermomechanical flow of ice sheets. Journal of Geophysical Research 102, B6: 12219-12233.

Payne, A.J. et al., 2000. Results from the EISMINT model intercomparison: The effects of thermomechanical coupling. Journal of Glaciology, 46(153): 227-238.

Payne, A.J., Sugden, D.E. and Clapperton, C.M., 1989. Modeling the growth and decay of the Antarctic Peninsula Ice Sheet. Quaternary Research, 31(2): 119-134.

Payne, A.J., Vieli, A., Shepherd, A.P., Wingham, D.J. and Rignot, E., 2004. Recent dramatic thinning of largest West Antarctic ice stream triggered by oceans. Geophysical Research Letters, 31(23).

Pekar, S.F. and DeConto, R.M., 2006. High-resolution ice-volume estimates for the early Miocene: evidence for a dynamic ice sheet in Antarctica. Palaeogeography Palaeoclimatology Palaeoecology, 231: 101-109.

Penck, A., 1905. Glacial features in the surface of the Alps. Journal of Geology, 13: 1-19.

Perkins, S.F., 1984. Subglacial landscape in Antarctica, University of Aberdeen, Aberdeen.

Petit, J.R. et al., 1999. Climate and atmospheric history of the past 420,000 years from the Vostok ice core, Antarctica. Nature, 399(6735): 429-436.

Phillips, W.M., Hall, A.M., Mottram, R., Fifield, L.K. and Sugden, D., 2006. Cosmogenic ^{10}Be and ^{26}Al exposure ages of tors and erratics, Cairngorm Mountains, Scotland: Timescales for the development of a classic landscape of selective linear glacial erosion. Geomorphology, 73: 222-245.

Pollard, D. and DeConto, R.M., 2003. Antarctic ice and sediment flux in the Oligocene simulated by a climate-ice sheet-sediment model. Palaeogeography, Palaeoclimatology, Palaeoecology, 198(1-2): 53-67.

Pollard, D., DeConto, R.M. and Nyblade, A.A., 2005. Sensitivity of Cenozoic Antarctic ice sheet variations to geothermal heat flux. Global and Planetary Change, 49(1-2): 63-74.

Pritchard, H.D. and Vaughan, D.G., 2007. Widespread acceleration of tidewater glaciers on the Antarctic Peninsula. Journal of Geophysical Research-Earth Surface, 112(F3).

Python Software Foundation, 2008. Python 2.5.2.

Rabassa, J. and Clapperton, C.M., 1990. Quaternary glaciations of the southern Andes. Quaternary Science Reviews, 9(2-3): 153-174.

Rabassa, J. et al., 2000. Quaternary of Tierra del Fuego, southernmost South America: An updated review. Quaternary International, 67-71: 217-240.

Raine, J.I. and Askin, R.A., 2001. Terrestrial palynology of Caper Roberts drillhole CRP-3, Victoria Land Basin, Antarctica. Terra Antarctica, 8(389-400).

Raymo, M.E., 1994. The initiation of Northern Hemisphere glaciation. Annual Review Of Earth And Planetary Sciences, 22: 253-383.

Raymo, M.E., Lisiecki, L.E. and Nisancioglu, K.H., 2006. Plio-pleistocene ice volume, antarctic climate, and the global $\delta_{18}O$ record. Science, 313(5786): 492-495.

Raymo, M.E. and Ruddiman, W.F., 1992. Tectonic forcing of the late Cenozoic climate. Nature, 359: 117-122.

Reeh, N., 1991. Parameterization of melt rate and surface temperature on the Greenlandice sheet. Polarforschung, 59(3): 113-128.

Rignot, E., 2002. Mass balance of East Antarctic glaciers and ice shelves from satellite data, Annals of Glaciology, Vol 34, 2002. Annals of Glaciology, pp. 217-227.

Rignot, E. et al., 2004. Accelerated ice discharge from the Antarctic Peninsula following the collapse of Larsen B ice shelf. Geophysical Research Letters, 31(18).

Roberts, D.H. and Long, A.J., 2005. Streamlined bedrock terrain and fast ice flow, Jakobshavns Isbrae, West Greenland: implications for ice stream and ice sheet dynamics. Boreas, 34(1): 25-42.

Robin, G.d.Q., 1955. Ice movement and temperature distribution in glaciers and ice sheets. Journal of Glaciology, 2: 523-532.

Rocchi, S., LeMasurier, W.E. and Di Vincenzo, G., 2006. Oligocene to Holocene erosion and glacial history in Marie Byrd Land, West Antarctica, inferred from exhumation of the Dorrel Rock intrusive complex and from volcano morphologies. Geological Society of America Bulletin, 118(7-8): 991-1005.

Romero, H., 1985. Geografia de Chile: geografia de los climas. Instituto Geografico Militar, Santiago.

Rutt, I.C., Hagdorn, M., Hulton, N.R.J. and Payne, A.J., Submitted. The 'Glimmer' community ice sheet model. Journal of Geophysical Research.

Scholz, C.H. and Engelder, J.T., 1976. The role of asperity indentation and ploughing in rock friction - 1. Asperity creep and stick-slip. International Journal of Rock Mechanics and Mining Sciences, 13(5): 149-154.

Schweizer, J. and Iken, A., 1992. The role of bed separation and friction in sliding over an undeformable bed. Journal of Glaciology, 38: 77-92.

Sejrup, H.P. et al., 2000. Quaternary glaciations in southern Fennoscandia: Evidence from southwestern Norway and the northern North Sea region. Quaternary Science Reviews, 19(7): 667-685.

Shepherd, A., Wingham, D. and Rignot, E., 2004. Warm ocean is eroding West Antarctic Ice Sheet. Geophysical Research Letters, 31(23).

Shevenell, A.E., Kennett, J.P. and Lea, D.W., 2004. Middle Miocene Southern Ocean cooling and Antarctic cryosphere expansion. Science, 305(5691): 1766-1770.

Siegert, M.J., 2001. Ice sheets and Late Quaternary environmental change. John Wiley and Sons Ltd.

Siegert, M.J. and Glasser, N.F., 1997. Convergent flow of ice within the Astrolabe subglacial basin, Terre Adelie, East Antarctica: an hypothesis derived from numerical modeling experiments. Polar Research, 16(1): 63-72.

Singer, B.S., Ackert Jr, R.P. and Guillou, H., 2004. $^{40}Ar/^{39}Ar$ and K-Ar chronology of Pleistocene glaciations in Patagonia. Bulletin of the Geological Society of America, 116(3-4): 434-450.

Sissons, J.B., 1976. The Geomorphology of the British Isles: Scotland. Methuen, London.

Small, E.E. and Anderson, R.S., 1998. Pleistocene relief production in Laramide mountain ranges, western United States. Geology, 26(2): 123-126.

Stagg, H.M.J., 1985. The structure of Prydz Bay and MacRobertson Shelf, East Antarctica. Tectonophysics, 114: 315-340.

Stern, T.A., Baxter, A.K. and Barrett, P.J., 2005. Isostatic rebound due to glacial erosion within the Transantarctic Mountains. Geology, 33(3): 221.

Stickley, C.E. et al., 2004. Timing and nature of the deepening of the Tasmanian Gateway. Paleoceanography, 19(4): PA4027.

Stokes, C.R. and Clark, C.D., 2001. Palaeo-ice streams. Quaternary Science Reviews, 20(13): 1437.

Strahler, A.N., 1952. Hypsometric (area-altitude) analysis of erosional topography. Bulletin of the Geological Society of America, 63: 1117-1142.

Stroeven, A.P., Fabel, D., Harbor, J., Hättestrand, C. and Kleman, J., 2002a. Quantifying the erosional impact of the Fennoscandian ice sheet in the Torneträsk-Narvik corridor, northern Sweden, based on cosmogenic

radionuclide data. Geografiska Annaler, Series A: Physical Geography, 84(3-4): 275-287.

Stroeven, A.P., Fabel, D., Hättestrand, C. and Harbor, J., 2002b. A relict landscape in the centre of Fennoscandian glaciation: cosmogenic radionuclide evidence of tors preserved through multiple glacial cycles. Geomorphology, 44: 145-154.

Stumpf, A.J., Broster, B.E. and Levson, V.M., 2000. Multiphase flow of the late Wisconsinan Cordilleran ice sheet in western Canada. Geological Society of America Bulletin, 112(12): 1850-1863.

Sugden, D. and Denton, G., 2004. Cenozoic landscape evolution of the Convoy Range to Mackay Glacier area, Transantartic Mountains: Onshore to offshore synthesis. Bulletin of the Geological Society of America, 116(7-8): 840-857.

Sugden, D.E., 1978a. Glacial erosion by the Laurentide ice sheet. Journal of Glaciology, 20(83): 367-391.

Sugden, D.E., 1978b. Glacial geomorphology. Progress in Physical Geography, 2(2): 309-320.

Sugden, D.E., 1996. The East Antarctic ice sheet: unstable ice or unstable ideas? Transactions - Institute of British Geographers, 21(3): 443-454.

Sugden, D.E., Balco, G., Cowdery, S.G., Stone, J.O. and Sass Iii, L.C., 2005. Selective glacial erosion and weathering zones in the coastal mountains of Marie Byrd Land, Antarctica. Geomorphology, 67(3-4): 317-334.

Sugden, D.E., Hulton, N.R.J. and Purves, R.S., 2002. Modelling the inception of the Patagonian icesheet. Quaternary International, 95-96: 55-64.

Sugden, D.E. and John, B.S., 1976. Glaciers and Landscape. Edward Arnold, 376 pp.

Sugden, D.E. et al., 1999. Landscape development in the Royal Society Range, southern Victoria Land, Antartica: Stability since the mid-Miocene. Geomorphology, 28(3-4): 181-200.

Summerfield, M.A., 1991. Global Geomorphology. Longman, 537 pp.

Summerfield, M.A. et al., 1999. Cosmogenic isotope data support previous evidence of extremely low rates of denudation in the Dry Valleys region, southern Victoria Land, Antarctica. Geological Society Special Publication(162): 255-267.

Taylor, J. et al., 2004. Topographic controls on post-Oligocene changes in ice-sheet dynamics, Prydz Bay region, East Antarctica. Geology, 32(3): 197-200.

Tomkin, J.H., 2003. Erosional feedbacks and the oscillation of ice masses. Journal of Geophysical Research B: Solid Earth, 108(B10): ETG 12-1 - ETG 12-12.

Tomkin, J.H. and Braun, J., 2002. The influence of alpine glaciation on the relief of tectonically active mountain belts. American Journal of Science, 302(3): 169-190.

Tucker, G.E. and Bras, R.L., 1998. Hillslope processes, drainage density, and landscape morphology. Water Resources Research, 34: 2751-2764.

Tucker, G.E., Lancaster, S., Gasparini, N. and Bras, R.L., 2001. The Channel-Hillslope Integrated Landscape Development Model (CHILD). In: R.S. Harmon and W.W. Doe (Editors), Landscape Erosion and Evolution Modelling. Kluwer Academic/Plenum Publishers, New York, pp. 349-387.

Tucker, G.E. and Slingerland, R.L., 1996. Predicting sediment flux from fold and thrust belts. Basin Research, 8: 329-349.

Vaughan, D.G., Bamber, J.L., Giovinetto, M., Russell, J. and Cooper, A.P.R., 1999. Reassessment of net surface mass balance in Antarctica. Journal of Climate, 12(4): 933-946.

Veevers, J.J., 1994. Case for the Gamburtsev Subglacial Mountains of East Antarctica Originating by Midcarboniferous Shortening of an Intracratonic Basin. Geology, 22(7): 593-596.

Vimeux, F., Cuffey, K.M. and Jouzel, J., 2002. New insights into Southern Hemisphere temperature changes from Vostok ice cores using deuterium excess correction. Earth and Planetary Science Letters, 203(3-4): 829-843.

Weertman, J., 1957. On the sliding of glaciers. Journal of Glaciology, 3: 33-38.

Weertman, J., 1964. The theory of glacier sliding. Journal of Glaciology, 5: 287-303.

Whipple, K.X., Kirby, E. and Brocklehurst, S.H., 1999. Geomorphic limits to climate-induced increases in topographic relief. Nature, 401(6748): 39-43.

Whipple, K.X. and Tucker, G.E., 2002. Implications of sediment-flux-dependent river incision models for landscape evolution. Journal of Geophysical Research B: Solid Earth, 107(2): 3-1-3-20.

Wood, J., 1996. Scale-based characterisation of digital elevation models. In: D. Parker (Editor), Innovations in GIS. Taylor and Francis, pp. 256.

Zachos, J., Billups, K., Pagani, H., Sloan, L. and Thomas, E., 2001. Trends, rhythms, and aberrations in global climate 65 Ma to present. Science, 292(5517): 686-693.